ELSEVIER

Physics Reports 361 (2002) 267–417

PHYSICS REPORTS

www.elsevier.com/locate/physrep

Singular or non-Fermi liquids

C.M. Varma[a,b,1], Z. Nussinov[b], Wim van Saarloos[b,*]

[a] *Bell Laboratories, Lucent Technologies, Murray Hill, NJ 07974, USA*
[b] *Universiteit Leiden, Instituut-Lorentz, Postbus 9506, 2300 RA Leiden, Netherlands*

Received June 2001; editor: C.W.J. Beenakker

Contents

*Corresponding author. Tel.: +31-71-5275501; fax: +31-71-5275511.
E-mail address: saarloos@ilorentz.org (W. van Saarloos).
[1] Present and permanent address: Bell Laboratories, Lucent Technologies, Murray Hill, NJ 07974, USA.

PII: S0370-1573(01)00060-6

Abstract

An introductory survey of the theoretical ideas and calculations and the experimental results which depart from Landau Fermi liquids is presented. The common themes and possible routes to the singularities leading to the breakdown of Landau Fermi liquids are categorized following an elementary discussion of the theory. Soluble examples of singular or non-Fermi liquids include models of impurities in metals with special symmetries and one-dimensional interacting fermions. A review of these is followed by a discussion of singular Fermi liquids in a wide variety of experimental situations and theoretical models. These include the effects of low-energy collective fluctuations, gauge fields due either to symmetries in the Hamiltonian or possible dynamically generated symmetries, fluctuations around quantum critical points, the normal state of high-temperature superconductors and the two-dimensional metallic state. For the last three systems, the principal experimental results are summarized and the outstanding theoretical issues are highlighted.

PACS: 7.10.Ay; 71.10.Hf; 71.10.Pm; 71.27.+a

1. Introduction

1.1. Aim and scope of this paper

In the last two decades a variety of metals have been discovered which display thermodynamic and transport properties at low temperatures which are fundamentally different from those of the usual metallic systems which are well described by the Landau Fermi-liquid theory. They have often been referred to as Non-Fermi liquids. A fundamental characteristic of such systems is that the low-energy properties in a wide range of their phase diagram are dominated by singularities as a function of energy and temperature. Since these problems still relate to a liquid state of fermions and since it is not a good practice to name things after what they are not, we prefer to call them singular Fermi liquids (SFL).

The basic notions of Fermi-liquid theory have actually been with us at an intuitive level since the time of Sommerfeld: He showed that the linear low-temperature specific heat behavior of metals as well as their asymptotic low-temperature resisitivity and optical conductivity could be understood by assuming that the electrons in a metal could be thought of as a gas of non-interacting fermions, i.e., in terms of quantum mechanical particles which do not have any direct interaction but which do obey Fermi statistics. Meanwhile, Pauli calculated that the paramagnetic susceptibility of non-interacting electrons is independent of temperature, also in accord with experiments in metals. At the same time it was understood, at least since the work of Bloch and Wigner, that the interaction energies of the electrons in the metallic range of densities are not small compared to the kinetic energy. The rationalization for the qualitative success of the non-interacting model was provided in a masterly pair of papers by Landau [152,153] who initially was concerned with the properties of liquid ^{3}He. This work epitomized a new way of thinking about the properties of interacting systems which is a cornerstone of our understanding of condensed matter physics. The notion of quasiparticles and elementary excitations and the methodology of asking useful questions about the low-energy excitations of the system based on concepts of symmetry, without worrying about the myriad unnecessary details, is epitomized in Landau's phenomenological theory of Fermi liquids. The microscopic derivation of the theory was also soon developed.

Our perspective on Fermi liquids has changed significantly in the last two decades or so. This is due both to changes in our theoretical perspective, and due to the experimental developments: on the experimental side, new materials have been found which exhibit Fermi-liquid behavior in the temperature dependence of their low-temperature properties with the coefficients often a factor of order 10^3 different from the non-interacting electron values. These observations dramatically illustrate the power and range of validity of the Fermi-liquid ideas. On the other hand, new materials have been discovered whose properties are qualitatively different from the predictions of Fermi-liquid theory (FLT). The most prominently discussed of these materials are the normal phase of high-temperature superconducting materials for a range of compositions near their highest T_c. Almost every idea discussed in this review has been used to understand the high-T_c problem, but there is no consensus yet on the solution.

It has of course been known for a long time that FLT breaks down in the fluctuation regime of classical phase transitions. This breakdown occurs in a more substantial region of the phase

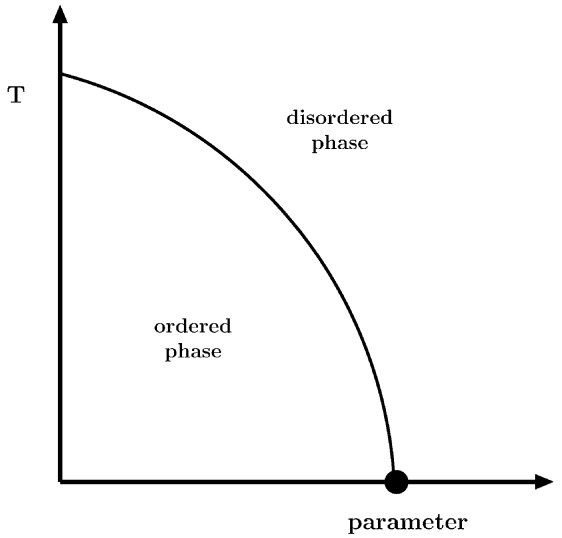

Fig. 1. Schematic phase diagram near a quantum critical point. The parameter along the x-axis can be quite general, like the pressure or a ratio of coupling constants. Whenever the critical temperature vanishes, a QCP, indicated with a dot in the figure, is encountered. In the vicinity of such a point quantum mechanical, zero-point fluctuations become very important. However, when T_c is finite, critical slowing down implies that the relevant frequency scale goes as $\omega \sim |T_c - T|^{\nu z}$, dwarfing quantum effects; the standard classical critical methodology then applies. An example of a phase diagram of this type for MnSi is shown in Fig. 34 below.

diagram around the quantum critical point (QCP) where the transition temperature tends to zero as a function of some parameter, see Fig. 1. This phenomenon has been extensively investigated for a wide variety of magnetic transitions in metals where the transition temperature can be tuned through the application of pressure or by varying the electronic density through alloying. Heavy fermions, with their close competition between states of magnetic order with localized moments and itinerant states due to Kondo effects, appear particularly prone to such QCPs. Equally interesting are questions having to do with the change in properties due to impurities in systems which are near a QCP in the pure limit.

The density–density correlations of itinerant disordered electrons at long wavelengths and low energies must have a diffusive form. In two dimensions this leads to logarithmic singularities in the effective interactions when the interactions are treated perturbatively. The problem of finding the ground state and low-lying excitations in this situation is unsolved. On the experimental side, the discovery of the metal–insulator transition in two dimensions and the unusual properties observed in the metallic state make this an important problem to resolve.

The one-dimensional electron gas reveals logarithmic singularities in the effective interactions even in a second-order perturbation calculation. A variety of mathematical techniques have been used to solve a whole class of interacting one-dimensional problems and one now knows the essentials of the correlation functions even in the most general case. An important issue is whether and how this knowledge can be used in higher dimensions.

The solution of the Kondo problem and the realization that its low-temperature properties may be discussed in the language of FLT has led in turn to the formulation and solution of impurity models with singular low-energy properties. Such models have a QCP for a particular relation between the coupling constants; in some examples they exhibit a quantum critical line. The thermodynamic and transport properties around such critical points or lines are those of local singular Fermi liquids. Although the direct experimental relevance of such models (as of one-dimensional models) to experiments is often questionable, these models, being soluble, can be quite instructive in helping to understand the conditions necessary for the breakdown of FLT and associated quasiparticle concepts. The knowledge from zero-dimensional and one-dimensional problems must nevertheless be extrapolated with care.

A problem which we do not discuss but which belongs in the study of SFLs is the quantum Hall effect problem. The massive degeneracy of two-dimensional electrons in a magnetic field leads to spectacular new properties and involves new fractional quantum numbers. The essentials of this problem were solved following Laughlin's inspired variational calculation. The principal reason for the omission is firstly that excellent papers reviewing the developments are available [213,72,111] and secondly that the methodology used in this problem is in general distinct from those for discussing the other SFLs which have a certain unity. We will however have occasions to refer to aspects of the quantum Hall effect problem often. Especially interesting from our point of view is the weakly singular Fermi liquid behavior predicted in the $\nu = \frac{1}{2}$ quantum Hall effect [118].

With less justification, we do not discuss the problem of superconductor to insulator and/or to metal transitions in two-dimensional disordered systems in the limit of zero temperature with and without an applied magnetic field. Interesting new developments in this problem with references to substantial earlier work may be found in [176,177,247]. The problem of transitions in Josephson arrays [247] is a variant of such problems.

One of the principal aspects that we want to bring to the foreground in this review is the fact that SFLs all have in common some fundamental features which can be stated usefully in several different ways. (i) They have degenerate ground states to within an energy of order $k_B T$. This degeneracy is not due to static external potentials or constraints as in, for example the spin-glass problem, but degeneracies which are dynamically generated. (ii) Such degeneracies inevitably lead to a breakdown of perturbative calculations because they generate infra-red singularities in the correlation functions. (iii) If a bare particle or hole is added to the system, it is attended by a divergent number of low-energy particle–hole pairs, so that the one-to-one correspondence between the one-particle excitation of the interacting problem and those of the non-interacting problem, which is the basis for FLT, breaks down. (iv) Since SFLs are concerned with dynamically generated degeneracies within energies of order of the measuring temperature, the observed properties are determined by quantum-mechanical to classical crossovers and in particular by dissipation in such a crossover.

On the theoretical side, one may now view Fermi-liquid theory as a forerunner of the renormalization group ideas. The renormalization group has led to a sophisticated understanding of singularities in the collective behavior of many-particle systems. It is likely that these methods have an important role to play in understanding the breakdown of FLT.

The aim of this paper is to provide a pedagogical introduction to SFLs, focused on the essential conceptual ideas and on issues which are settled and which can be expected to

survive future developments. Therefore, we will not attempt to give an exhaustive review of the literature on this problem or of all the experimental systems which show hints of SFL behavior. The experimental examples we discuss have been selected to illustrate both what is essentially understood and what is not understood even in principle. On the theoretical side, we will shy away from presenting in depth the sophisticated methods necessary for a detailed evaluation of correlation functions near QCP—for this we refer to the book by Sachdev [225]—or for an exact solution of local impurity models (see, e.g. [124,227,259]). Likewise, for a discussion of the application of quantum critical scaling ideas to Josephson arrays or quantum Hall effects, we refer to the nice introduction by Sondhi et al. [247].

1.2. Outline of the paper

The outline of this paper is as follows. We start by summarizing in Section 2 some of the key features of Landau's FLT—in doing so, we will not attempt to retrace all of the ingredients which can be found in many of the classic textbooks [208,37]; instead our discussion will be focused on those elements of the theory and the relation with its microscopic derivation that allow us to understand the possible routes by which the FLT can break down. This is followed in Section 3 by the Fermi-liquid formulation of the Kondo problem and of the SFL variants of the Kondo problem and of two interacting Kondo impurities. The intention here is to reinforce the concepts of FLT in a different context as well as to provide examples of SFL behavior which offer important insights because they are both simple and solvable. We then discuss the problem of one spatial dimension ($d=1$), presenting the principal features of the solutions obtained. We discuss why $d=1$ is special, and the problems encountered in extending the methods and the physics to $d>1$. We then move from the comforts of solvable models to the reality of the discussion of possible mechanisms for SFL behavior in higher dimensions. First we analyze in Section 5 the paradigmatic case of long-range interactions. Coulomb interactions will not do in this regard, since they are always screened in a metal, but transverse electromagnetic fields do give rise to long-range interactions. The fact that as a result no metal is a Fermi liquid for sufficiently low temperatures was already realized long ago [127]—from a practical point of view, this mechanism is not very relevant, since the temperatures where these effects become important are of order 10^{-16} K; nevertheless, conceptually this is important since it is a simple example of a gauge theory giving rise to SFL behavior. Gauge theories on lattices have been introduced to discuss problems of fermions moving with the constraint of only zero or single occupation per site. We then discuss in Section 6 the properties near a quantum critical point, taking first an example in which the ferromagnetic transition temperature goes to zero as a function of some externally chosen suitable parameter. We refer in this section to several experiments in heavy fermion compounds which are only partially understood or not understood even in principle. We then turn to a discussion of the marginal Fermi liquid phenomenology for the SFL state of copper-oxide high-T_c materials and discuss the requirements on a microscopic theory that the phenemenology imposes. A sketch of a microscopic derivation of the phenemenology is also given. We close the paper in Section 8 with a discussion of the metallic state in $d=2$ and the state of the theory treating the diffusive singularities in $d=2$ and its relation to the metal–insulator transition.

2. Landau's Fermi liquid

2.1. Essentials of Landau Fermi liquids

The basic idea underlying Landau's Fermi-liquid theory [152,153,208,37] is that of *analyticity*, i.e., that states with the same symmetry can be adiabatically connected. Simply put, this means that whether or not we can actually carry out the calculation we know that the eigenstates of the full Hamiltonian of the same symmetry can be obtained perturbatively from those of a simpler Hamiltonian. At the same time states of different symmetry cannot be obtained by "continuation" from the same state. This suggests that given a tough problem which is impossible to solve, we may guess a right simple problem. The low energy and long wavelength excitations, as well as the correlation and the response functions of the impossible problem bear a one-to-one correspondence with the simpler problem in their analytic properties. This leaves fixing only numerical values. These are to be determined by parameters, the minimum number of which is fixed by the symmetries. Experiments often provide an intuition as to what the right simple problem may be: for the interacting electrons, in the metallic range of densities, it is the problem of kinetic energy of particles with Fermi statistics. (If one had started with the opposite limit, just the potential energy alone, the starting ground state is the Wigner crystal—a bad place to start thinking about a metal!) If we start with non-interacting fermions, and then turn on the interactions, the qualitative behavior of the system does not change as long as the system does not go through (or is close to) a phase transition. Owing to the analyticity, we can even consider strongly interacting systems—the low-energy excitations in these have strongly renormalized values of their parameters compared to the non-interacting problem, but their qualitative behavior is the same as that of the simpler problem.

The heavy fermion problem provides an extreme example of the domain of validity of the Landau approach. This is illustrated in Fig. 2, which shows the specific heat of the heavy fermion compound $CeAl_3$. As in the Sommerfeld model, the specific heat is linear in the temperature at low T, but if we write $C_v \approx \gamma T$ at low temperatures, the value of γ is about a thousand times as large as one would estimate from the density of states of a typical metal, using the free electron mass. For a Fermi gas, the density of states $N(0)$ at the Fermi energy is proportional to an effective mass m^*:

$$N(0) = \frac{m^* k_F}{\pi^2 \hbar^2} , \tag{1}$$

with k_F the Fermi wavenumber. Then the fact that the density of states at the chemical potential is a thousand times larger than for normal metals can be expressed by the statement that the effective mass m^* of the quasiparticles is a thousand times larger than the free electron mass m. Likewise, as Fig. 3 shows, the resistivity of $CeAl_3$ at low temperatures increases as T^2. This also is a characteristic sign of a Fermi liquid, in which the quasiparticle lifetime τ at the Fermi surface, determined by electron–electron interactions, behaves as $\tau \sim 1/T^2$.[2] However, just as

[2] In heavy fermions, at least in the observed range of temperatures, the transport lifetime determining the temperature dependence of resistivity is proportional to the single-particle lifetime.

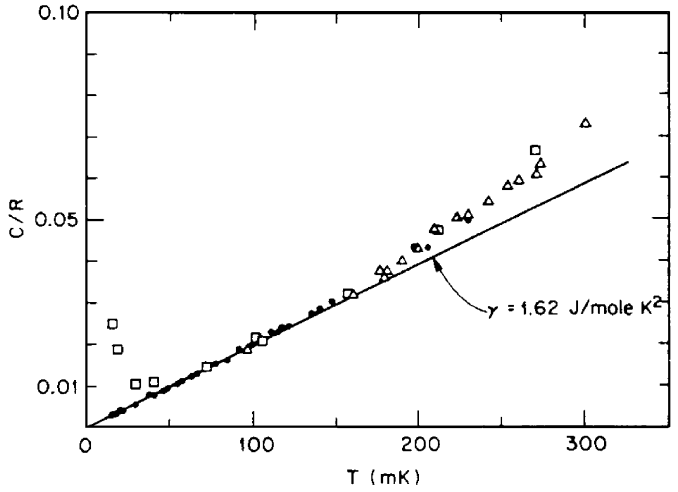

Fig. 2. Specific heat of $CeAl_3$ at low temperatures from Andres et al. [28]. The slope of the linear specific heat is about 3000 times that of the linear specific heat of, say, Cu. However, the high-temperature cut-off of this linear term is smaller than that of Cu by a similar amount. The rise of the specific heat in a magnetic field at low temperatures is the nuclear contribution, irrelevant to our discussion.

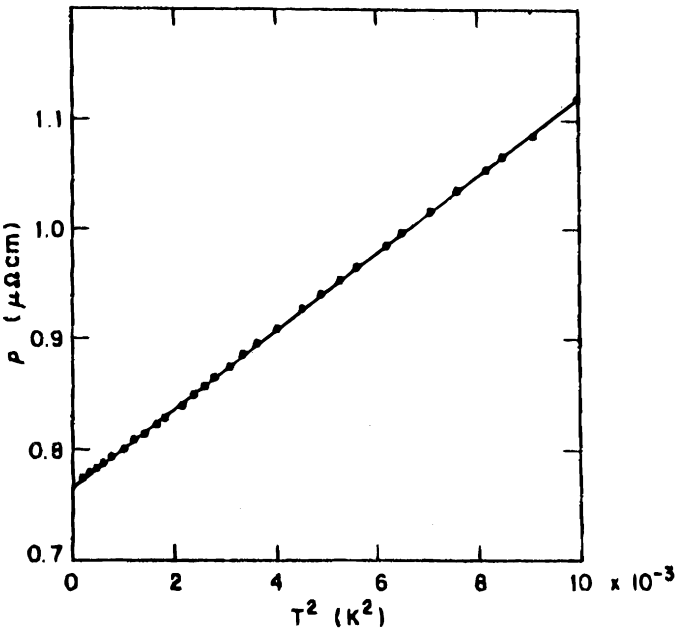

Fig. 3. Electrical resistivity of $CeAl_3$ below 100 mK, plotted against T^2. From Andres et al. [28].

the prefactor γ of the specific heat is a factor thousand times larger than usual, the prefactor of the T^2 term in the resistivity is a factor 10^6 larger—while γ scales linearly with the effective mass ratio m^*/m, the prefactor of the T^2 term in the resistivity increases for this class of Fermi liquids as $(m^*/m)^2$.

It should be remarked that the right simple problem is not always easy to guess. The right simple problem for liquid ^{4}He is not the non-interacting Bose gas but the weakly interacting Bose gas (i.e., the Bogoliubov problem [45,154]). The right simple problem for the Kondo problem (a low-temperature local Fermi liquid) was guessed [197] only after the numerical renormalization group solution was obtained by Wilson [289]. The right simple problem for two-dimensional interacting disordered electrons in the "metallic" range of densities (Section 8 in this paper) is at present unknown.

For SFLs, the problem is different: usually one is in a regime of parameters where no simple problem is a starting point—in some cases the fluctuations between solutions to different simple problems determines the physical properties, while in others even this dubious anchor is lacking.

2.2. Landau Fermi liquid and the wavefunction renormalization Z

Landau theory is the forerunner of our modern way of thinking about low-energy effective Hamiltonians in complicated problems and of the renormalization group. The formal statements of Landau theory in their original form are often somewhat cryptic and mysterious—this reflects both Landau's style and his ingenuity. We shall take a more pedestrian approach.

Let us consider the essential difference between non-interacting fermions and an interacting Fermi liquid from a simple microscopic perspective. For free fermions, the momentum states $|\mathbf{k}\rangle$ are also eigenstates of the Hamiltonian with eigenvalue

$$\varepsilon_{\mathbf{k}} = \frac{\hbar^2 k^2}{2m}. \tag{2}$$

Moreover, the thermal distribution of particles $n^0_{\mathbf{k}\sigma}$, is given by the Fermi–Dirac function where σ denotes the spin label. At $T = 0$, the distribution jumps from 1 (all states occupied within the Fermi sphere) to zero (no states occupied within the Fermi sphere) at $|\mathbf{k}| = k_{\mathrm{F}}$ and energy equal to the chemical potential μ. This is illustrated in Fig. 4.

A good way of probing a system is to investigate the *spectral function*; the spectral function $A(k,\omega)$ gives the distribution of energies ω in the system when a particle with momentum $\mathbf{k}$ is added or removed from it (remember that removing a particle excitation below the Fermi energy means that we add a hole excitation). As sketched in Fig. 5(a), for the non-interacting system, $A_0(\mathbf{k},\omega)$ is simply a δ-function peak at the energy $\varepsilon_{\mathbf{k}}$, because all momentum states are also energy eigenstates

$$A_0(\mathbf{k},\omega) = \delta(\omega - (\varepsilon_{\mathbf{k}} - \mu)) \quad \text{for } \omega > \mu\,, \tag{3}$$

$$= -\frac{1}{\pi}\mathrm{Im}\frac{1}{\omega - (\varepsilon_{\mathbf{k}} - \mu) + \mathrm{i}\delta} = -\frac{1}{\pi}\mathrm{Im}\, G^0(\mathbf{k},\omega)\,. \tag{4}$$

Here, δ is small and positive; it reflects that particles or holes are introduced adiabatically, and it is taken to zero at the end of the calculation for the pure non-interacting problem. The first step of the second line is just a simple mathematical rewriting of the delta function. In the second line the Green's function G^0 for non-interacting electrons is introduced. More generally

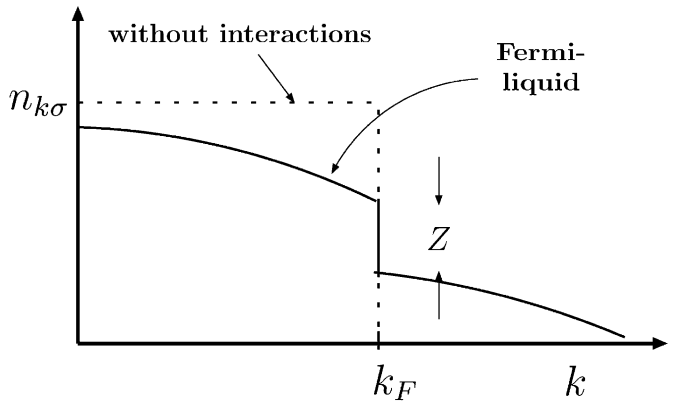

Fig. 4. Bare-particle distribution at $T=0$ for a given spin direction in a translationally invariant Fermi system with interactions (full line) and without interactions (dashed line). Note that the position of the discontinuity, i.e., the Fermi wavenumber k_F, is not renormalized by interactions.

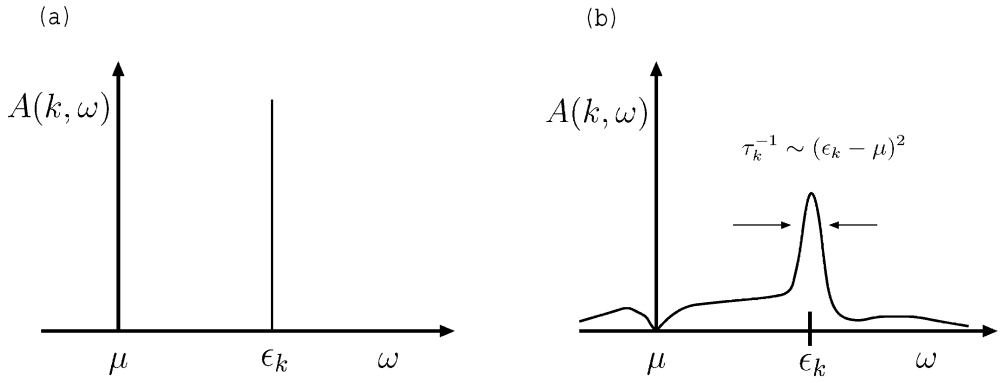

Fig. 5. (a). The non-interacting spectral function $A(k,\omega)$ at fixed k as a function of ω; (b) the spectral function of single-electron excitations in a Fermi liquid at fixed k as a function of ω. If $(1/\pi)A(k,\omega)$ is normalized to 1, signifying one bare particle, the weight under the Lorentzian, i.e., the quasiparticle part, is Z. As explained in the text, at the same time Z is the discontinuity in Fig. 4.

the single-particle Green's function $G(\mathbf{k},\omega)$ is defined in terms of the correlation function of particle creation and annihilation operators in standard textbooks [195,4,222,168]. For our present purpose, it is sufficient to note that it is related to the spectral function $A(\mathbf{k},\omega)$, which has a clear physical meaning and which can be deduced through-angle resolved photoemission experiments

$$G(\mathbf{k},\omega)=\int_{-\infty}^{\infty} \mathrm{d}x \frac{A(\mathbf{k},x)}{\omega-\mu-x+\mathrm{i}\delta\,\mathrm{sgn}(\omega-\mu)}\ . \tag{5}$$

$A(\mathbf{k},\omega)$ thus is the spectral representation of the complex function $G(k,\omega)$. Here we have defined the so-called *retarded* Green's function which is especially useful since its real and imaginary

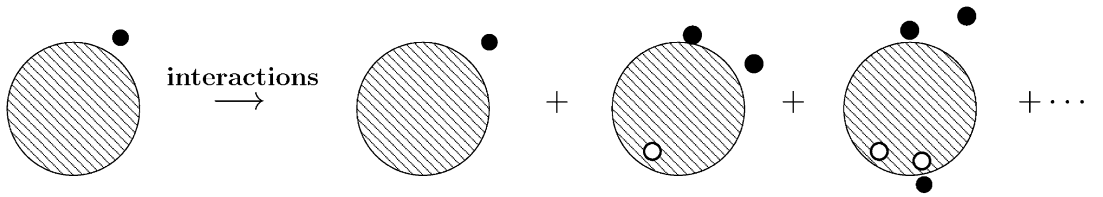

Fig. 6. Schematic illustration of the perturbative expansion (8) of the change of wavefunction as a result of the addition of an electron to the Fermi sea due to interactions with the particles in the Fermi sea.

parts obey the Kramers–Kronig relations. In the problem with interactions $G(\mathbf{k},\omega)$ will differ from $G^0(\mathbf{k},\omega)$. This difference can be quite generally defined through the single-particle self-energy function $\Sigma(\mathbf{k},\omega)$:

$$(G(\mathbf{k},\omega))^{-1} = (G^0(\mathbf{k},\omega))^{-1} - \Sigma(\mathbf{k},\omega)\ . \tag{6}$$

Eq. (5) ensures the relation between $G(\mathbf{k},\omega)$ and $A(\mathbf{k},\omega)$

$$A(\mathbf{k},\omega) = -\frac{1}{\pi}\mathrm{Im}\, G(\mathbf{k},\omega)\ . \tag{7}$$

With these preliminaries out of the way, let us consider the form of $A(\mathbf{k},\omega)$ when we add a particle to an interacting system of fermions.

Due to the interaction (assumed repulsive) between the added particle and those already in the Fermi sea, the added particle will kick particles from below the Fermi surface to above. The possible terms in a perturbative description of this process are constrained by the conservation laws of charge, particle number, momentum and spin. Those which are allowed by these conservation laws are indicated pictorially in Fig. 6, and lead to an expression of the type

$$|\psi^{N+1}_{\mathbf{k}\sigma}\rangle = Z_{\mathbf{k}}^{1/2} c^\dagger_{\mathbf{k}\sigma}|\psi^N\rangle + \frac{1}{V^{3/2}}\sum_{\mathbf{k}_1,\mathbf{k}_2,\mathbf{k}_3}\sum_{\sigma_1,\sigma_2,\sigma_3} \alpha_{\mathbf{k}_1\sigma_1\mathbf{k}_2\sigma_2\mathbf{k}_3\sigma_3} c^\dagger_{\mathbf{k}_3} c_{\mathbf{k}_2} c^\dagger_{\mathbf{k}_1}$$
$$\times\, \delta_{\mathbf{k},\mathbf{k}_1-\mathbf{k}_2+\mathbf{k}_3}\delta(\sigma;\sigma_1,\sigma_2,\sigma_3)|\psi^N\rangle + \dots\ . \tag{8}$$

Here the $c^\dagger_{\mathbf{k}}$'s and $c_{\mathbf{k}}$'s are the *bare* particle creation and annihilation operators, and the dots indicate higher-order terms, for which two or more particle–hole pairs are created and $\delta(\sigma;\sigma_1,\sigma_2,\sigma_3)$ expresses conservation of spin under vector addition. The multiple-particle–hole pairs for a fixed total momentum can be created with a continuum of momentums of the individual bare particles and holes. Therefore, an added particle with fixed total momentum has a wide distribution of energies. However, if $Z_{\mathbf{k}}$ defined by Eq. (8) is finite, there is a well-defined feature in this distribution at some energy which is in general different from the non-interacting value $\hbar^2k^2/(2m)$. The spectral function in such a case will then be as illustrated in Fig. 5(b). It is useful to separate the well-defined feature from the broad continuum by writing the spectral function

as the sum of two terms, $A(\mathbf{k},\omega)=A_{\rm coh}(\mathbf{k},\omega)+A_{\rm incoh}(\mathbf{k},\omega)$. The single-particle Green's function can similarly be expressed as a sum of two corresponding terms, $G(\mathbf{k},\omega)=G_{\rm coh}(\mathbf{k},\omega)+G_{\rm incoh}(\mathbf{k},\omega)$. Then

$$G_{\rm coh}(\mathbf{k},\omega)=\frac{Z_{\mathbf{k}}}{\omega-\tilde{\varepsilon}_{\mathbf{k}}+{\rm i}/\tau_{\mathbf{k}}}\ , \tag{9}$$

which for large lifetimes $\tau_{\mathbf{k}}$ gives a Lorentzian peak in the spectral density at the quasiparticle energy $\tilde{\varepsilon}_{\mathbf{k}}\equiv\varepsilon_{\mathbf{k}}-\mu$. The incoherent Green's function is smooth and hence for large $\tau_{\mathbf{k}}$ corresponds to the smooth background in the spectral density.

The condition for the occurrence of the well-defined feature can be expressed as the condition that the self-energy $\Sigma(\mathbf{k},\omega)$ has an analytic expansion about $\omega=0$ and $\mathbf{k}=\mathbf{k}_{\rm F}$ and that its real part is much larger than its imaginary part. One can easily see that were it not so, then expression (9) for $G_{\rm coh}$ could not be obtained. These conditions are necessary for a Landau Fermi liquid. Upon expanding $\Sigma(\mathbf{k},\omega)$ in (12) for small ω and small deviations of $\mathbf{k}$ from $\mathbf{k}_{\rm F}$ and writing it in the form (9), we make the identifications

$$\tilde{\varepsilon}_{\mathbf{k}}=\varepsilon_{\mathbf{k}}Z_{\mathbf{k}}\hat{Z}_{\mathbf{k}},\quad \frac{1}{\tau_{\mathbf{k}}}=-\,Z_{\mathbf{k}}\,{\rm Im}\,\Sigma(\mathbf{k}_{\rm F},\omega=0)\ , \tag{10}$$

where

$$Z_{\mathbf{k}}=\left(1-\frac{\partial\Sigma}{\partial\omega}\right)^{-1}_{\omega=0,\,k=k_{\rm F}},\quad \hat{Z}=\left(1+\frac{1}{v_{\rm F}}\frac{\partial\Sigma}{\partial k}\right)_{\omega=0,\,k=k_{\rm F}}\ . \tag{11}$$

From Eq. (8), we have a more physical definition of $Z_{\mathbf{k}}$: $Z_{\mathbf{k}}$ is the projection amplitude of $|\psi^{N+1}_{\mathbf{k}}\rangle$ onto the state with one bare particle added to the ground state, since all other terms in the expansion vanish in the thermodynamic limit in the perturbative expression embodied by (8):

$$Z^{1/2}_{\mathbf{k}}=\langle\psi^{N+1}_{\mathbf{k}}|c^{\dagger}_{\mathbf{k}}|\psi^{N}\rangle\ . \tag{12}$$

In other words, $Z_{\mathbf{k}}$ is the overlap of the ground state wavefunction of a system of interacting $N\pm1$ fermions of total momentum $\mathbf{k}$ with the wavefunction of N interacting particles and a bare particle of momentum $\mathbf{k}$. $Z_{\mathbf{k}}$ is called the quasiparticle amplitude.

The Landau theory tacitly assumes that $Z_{\mathbf{k}}$ is finite. Furthermore, it asserts that for small ω and $\mathbf{k}$ close to $\mathbf{k}_{\rm F}$, the physical properties can be calculated from quasiparticles which carry the same quantum numbers as the particles, i.e., charge, spin and momentum and which may be defined simply by the creation operator $\gamma^{\dagger}_{\mathbf{k},\sigma}$:

$$|\psi^{N+1}_{\mathbf{k}}\rangle=\gamma^{\dagger}_{\mathbf{k},\sigma}|\psi^{N}\rangle\ . \tag{13}$$

Close to $\mathbf{k}_{\rm F}$, and for T small compared to the Fermi energy, the distribution of the quasiparticles *is assumed to be the Fermi–Dirac distribution* in terms of the renormalized quasiparticle energies. The bare particle distribution is quite different. As is illustrated in Fig. 4, it is depleted below $\mathbf{k}_{\rm F}$ and augmented above $\mathbf{k}_{\rm F}$, with a discontinuity at $T=0$ whose value is shown in microscopic theory to be $Z_{\mathbf{k}}$. A central result of Fermi liquid theory is that close to the Fermi energy at zero temperature, the width $1/\tau_{\mathbf{k}}$ of the coherent quasiparticle peak is proportional to $(\tilde{\varepsilon}_{\mathbf{k}}-\mu)^2$ so that near the Fermi energy the lifetime is long and quasiparticles are well-defined.

Likewise, at the Fermi energy $1/\tau_{\mathbf{k}}$ varies with temperature as T^2. From the microscopic derivation of this result, it follows that the weight in this peak, $Z_{\mathbf{k}}$, becomes equal to the jump Z in $n_{\mathbf{k}\sigma}$ when we approach the Fermi surface: $Z_{\mathbf{k}} \to Z$ for $\mathbf{k} \to \mathbf{k}_{\mathrm{F}}$. For heavy fermions, as we already mentioned, Z can be of the order of 10^{-3}. However, as long as Z is non-zero, one has Fermi liquid properties for temperatures lower than about ZE_{F}. Degeneracy is effectively lost for temperatures much higher than ZE_{F} and classical statistical mechanics prevails. [3]

An additional result from microscopic theory is the so-called Luttinger theorem, which states that the volume enclosed by the Fermi surface does not change due to interactions [195,4]. The mathematics behind this theorem is that with the assumptions of FLT, the number of poles in the interacting Green's function below the chemical potential is the same as that for the non-interacting Green's function. Recall that the latter is just the number of particles in the system.

Landau actually started his discussion of the Fermi liquid by writing the equation for the deviation of the (Gibbs) free energy from its ground state value as a functional of the deviation of the quasiparticle distribution function $n(\mathbf{k},\sigma)$ from the equilibrium distribution function $n_0(\mathbf{k},\sigma)$

$$\delta n(\mathbf{k},\sigma) = n(\mathbf{k},\sigma) - n_0(\mathbf{k},\sigma) \tag{14}$$

as follows:

$$G = G_0 + \frac{1}{V}\sum_{\mathbf{k},\sigma}(\tilde{\varepsilon}_{\mathbf{k}} - \mu)\delta n_{\mathbf{k}\sigma} + \frac{1}{2V^2}\sum_{\mathbf{k}\mathbf{k}',\sigma\sigma'} f_{\mathbf{k}\mathbf{k}',\sigma\sigma'}\delta n_{\mathbf{k}\sigma}\delta n_{\mathbf{k}'\sigma'} + \cdots \tag{15}$$

Note that $(\tilde{\varepsilon}_{\mathbf{k}} - \mu)$ is itself a function of δn; so the first term contains at least a contribution of order $(\delta n)^2$ which makes the second term quite necessary. In principle, the unknown function $f_{\mathbf{k}\mathbf{k}',\sigma\sigma'}$ depends on spin and momenta. However, spin rotation invariance allows one to write the spin part in terms of two quantities, the symmetric and antisymmetric parts f^{s} and f^{a}. Moreover, for low energy and long-wavelength phenomena only momenta with $\mathbf{k} \approx \mathbf{k}_{\mathrm{F}}$ play a role; if we consider the simple case of ^{3}He where the Fermi surface is spherical, rotation invariance implies that for momenta near the Fermi momentum f can only depend on the relative angle between $\mathbf{k}$ and $\mathbf{k}'$; this allows one to expand in Legendre polynomials $P_l(x)$ by writing

$$N(0) f^{\mathrm{s,a}}_{\mathbf{k}\mathbf{k}',\sigma\sigma'} \overset{\mathbf{k}\approx\mathbf{k}'\approx\mathbf{k}_{\mathrm{F}}}{\to} \sum_{l=0}^{\infty} F^{\mathrm{s,a}}_l P_l(\hat{\mathbf{k}}\cdot\hat{\mathbf{k}}') \,. \tag{16}$$

From expression (15) one can then relate the lowest order so-called Landau coefficients F_0 and F_1^{s} and the effective mass m^* to thermodynamic quantities like the specific heat C_v, the compressibility κ, and the susceptibility χ:

$$\frac{C_v}{C_{v0}} = \frac{m^*}{m}, \quad \frac{\kappa}{\kappa_0} = (1 + F_0^{\mathrm{s}})\frac{m^*}{m}, \quad \frac{\chi}{\chi_0} = (1 + F_0^{\mathrm{a}})\frac{m^*}{m} \,. \tag{17}$$

[3] It is an unfortunate common mistake to think of the properties in this regime as SFL behavior.

Here subscripts 0 refer to the quantities of the non-interacting reference system, and m is the mass of the fermions. For a Galilean invariant system (like ^{3}He), there is a simple relation between the mass enhancement and the Landau parameter F_1^s, and there is no renormalization of the particle current $\mathbf{j}$; however, there is a renormalization of the velocity: one has

$$\mathbf{j} = \mathbf{k}/m, \quad \mathbf{v} = \mathbf{k}/m^* , \quad \frac{m^*}{m} = \left(1 + \frac{F_1^s}{3}\right) . \tag{18}$$

The transport properties are calculated by defining a distribution function $\delta n(\mathbf{k}\sigma; r, t)$ which is slowly varying in space and time and writing a Boltzmann equation for it [208,37].

It is a delightful conceit of the Landau theory that the expressions of the low-energy properties in terms of the quasiparticles in no place involve the quasiparticle amplitude $Z_{\mathbf{k}}$. In fact in a translationally invariant problem such as liquid ^{3}He, $Z_{\mathbf{k}}$ cannot be measured by any thermodynamic or transport measurements. A masterly use of conservation laws ensures that Z's cancel out in all physical properties (one can extract Z from measurement of the momentum distribution. By neutron scattering measurements, it is found that $Z \approx 1/4$ [112] for He^3 near the melting line). This is no longer true on a lattice, in the electron–phonon interaction problem [212] or in heavy fermions [265] or even more generally in any situation where the interacting problem contains more than one type of particle with different characteristic frequency scales.

2.3. Understanding microscopically why Fermi-liquid theory works

Let us try to understand from a more microscopic approach why the Landau theory works so well. We present a qualitative discussion in this subsection and outline the principal features of the formal derivation in the next subsection.

As we already remarked, a crucial element in the approach is to choose the proper non-interacting reference system. That this is possible at all is due to the fact that the number of states to which an added particle can scatter due to interactions is severely limited due to the Pauli principle. As a result, non-interacting fermions are a good stable system to perturb about; they have a finite compressibility and susceptibility in the ground state, and so collective modes and thermodynamic quantities change smoothly when the interactions are turned on. This is not true for non-interacting bosons which do not support collective modes like sound waves. So one cannot perturb about the non-interacting bosons as a reference system.

Landau also laid the foundations for the formal justification of Fermi liquid theory in two and three dimensions. The flurry of activity in this field following the discovery of high-T_c phenomena has led to new ways of justifying Fermi-liquid theory (and understanding why the one-dimensional problem is different). However, the principal physical reason, which we now discuss, remains the phase-space restrictions due to kinematical constraints.

We learned in Section 2.2 that in order to define quasiparticles, it was necessary to have a finite $Z_{\mathbf{k}_F}$, which in turn needed a self-energy function $\Sigma(\mathbf{k}_F, \omega)$ which is smooth near the chemical potential, i.e., at $\omega = 0$. Let us first see why a Fermi gas has such properties when interactions are introduced perturbatively.

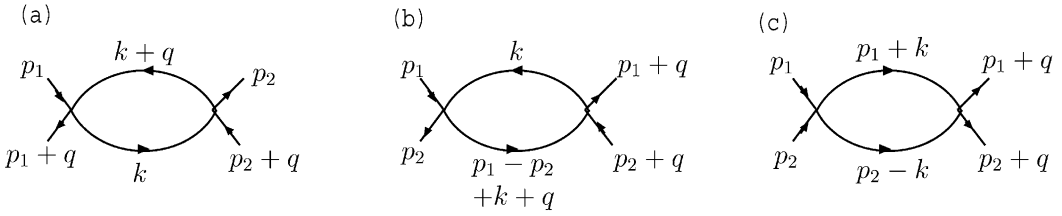

Fig. 7. The three second-order processes in a perturbative calculation of the correction to the bare interaction in a Fermi liquid.

We will explicitly consider only short-range interactions in this section, so that they can be characterized at all momentum transfers by a single parameter. Nevertheless, the essential results of Landau theory remain valid in the presence of Coulomb interactions because screening makes the interactions essentially short-ranged. The coupling constant g below may then be considered to parametrize the screened interaction.

In Fig. 7, we show the three possible processes that arise in second-order perturbation theory for the scattering of two particles with fixed initial energy ω and momentum q. Note that in two of the diagrams, Fig. 7(a) and (b) the intermediate state has a particle and a hole while the intermediate state in diagram 7(c) has a pair of particles.

We will find that, for our present purpose, the contribution of diagram 7(a) is more important than the other two. It gives a contribution

$$g^2 \sum_{\mathbf{k}} \frac{f_{\mathbf{k}+\mathbf{q}} - f_{\mathbf{k}}}{\omega - (E_{\mathbf{k}+\mathbf{q}} - E_{\mathbf{k}}) + \mathrm{i}\delta} \,. \tag{19}$$

Here, g is a measure of the strength of the scattering potential (the vertex in the diagram) in the limit of small $\mathbf{q}$. The denominator ensures that the largest contribution to the scattering comes from small scattering momenta $\mathbf{q}$: for these the energy difference is linear in $\mathbf{q}$, $E_{\mathbf{k}+\mathbf{q}} - E_{\mathbf{k}} \approx \mathbf{q}\cdot\mathbf{v}_{\mathbf{k}}$, where $\mathbf{v}_{\mathbf{k}}$ is a vector of length v_{F} in the direction of $\mathbf{k}$. Moreover, the term in the numerator is non-zero only in the area contained between two circles (for $d=2$) or spheres (for $d=3$) with their centers displaced by $\mathbf{q}$—here the phase-space restriction is due to the Pauli principle. This area is also proportional to $\mathbf{q}\cdot\mathbf{v}_{\mathbf{k}}$, and so in the small $\mathbf{q}$ approximation from diagram 7(a) we get a term proportional to

$$g^2 \frac{\mathbf{q}\cdot\mathbf{v}_{\mathbf{k}}}{\omega - \mathbf{q}\cdot\mathbf{v}_{\mathbf{k}} + \mathrm{i}\delta} \frac{\mathrm{d}f}{\mathrm{d}\varepsilon_{\mathbf{k}}} \,. \tag{20}$$

Now we see why diagram 7(a) is special. There is a singularity at $\omega = \mathbf{q}\cdot\mathbf{v}_{\mathbf{k}}$ and its value for small ω and $\mathbf{q}$ depends on which of the two is smaller. This singularity is responsible for the low-energy long-wavelength collective modes of the Fermi liquid in Landau theory. At low temperatures, $\mathrm{d}f/\mathrm{d}\varepsilon_{\mathbf{k}} = -\delta(\varepsilon_{\mathbf{k}} - \mu)$, so the summation is *restricted* to the Fermi surface. The real part of (19) therefore vanishes in the limit $qv_{\mathrm{F}}/\omega \to 0$, while it approaches a *finite* limit

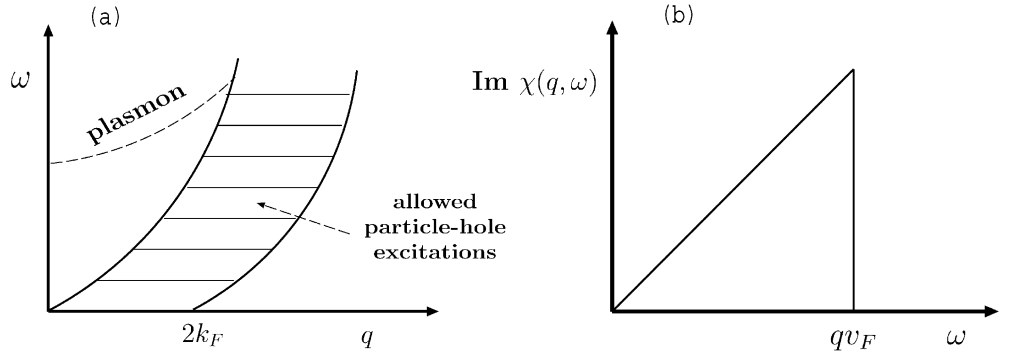

Fig. 8. (a) Restriction on allowed particle–hole excitations in a Fermi sea due to kinematics. The plasmon mode has been drawn for the case $d=3$; (b) the absorptive part of the particle–hole susceptibility (in the charge, current and spin channels) for $\omega < qv_F$ in the Fermi gas.

for $\omega \to 0$. The imaginary part in this limit is proportional to[4] ω:

$$\mathrm{Im}\,\chi(\mathbf{q},\omega) = g^2\pi N(0)\frac{\omega}{qv_F} \quad \text{for } \omega < qv_F\,, \tag{21}$$

while $\mathrm{Im}\,\chi(\mathbf{q},\omega)=0$ for $\omega > v_F q$. This behavior is sketched in Fig. 8(b). An explicit evaluation for the real part yields

$$\mathrm{Re}\,\chi(\mathbf{q},\omega) = g^2 N(0)\left[1+\frac{\omega}{qv_F}\ln\left|\frac{\omega-qv_F}{\omega+qv_F}\right|\right]\,, \tag{22}$$

which gives a constant (leading to a finite compressibility and spin susceptibility) at ω small compared to qv_F. For diagram 7(b), we get a term $\omega-(E_{\mathbf{p}_1-\mathbf{p}_2+\mathbf{k}+\mathbf{q}}-E_{\mathbf{k}})$ in the denominator. This term is always finite for general momenta $\mathbf{p}_1$ and $\mathbf{p}_2$, and hence the contribution from this diagram can always be neglected relative to the one from 7(a). Along similar lines, one finds that diagram 7(c), which describes scattering in the particle–particle channel, is irrelevant except when $\mathbf{p}_1 = -\mathbf{p}_2$, when it diverges as $\ln\omega$.

Of course, this scattering process is the one which gives superconductivity. Landau noticed this singularity but ignored its implication.[5] Indeed, as long as the effective interactions do not favor superconductivity or as long as we are at temperatures much higher than the superconducting transition temperature, it is not important for Fermi-liquid theory.

Let us now look further at the absorptive spectrum of particle–hole excitations in two and three dimensions, i.e., we examine the imaginary part of Eq. (19). When the total energy ω of the pair is small, both the particle and the hole have to live close to the Fermi surface. In

[4] This behavior implies that this scattering contribution is a marginal term in the renormalization group sense, which means that it affects the numerical factors, but not the qualitative behavior.

[5] Attractive interactions in any angular momentum channel (leading to superconductivity) are therefore marginally *relevant* operators.

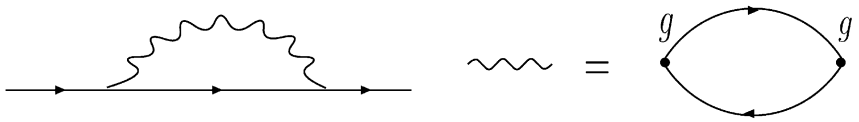

Fig. 9. The single-particle self-energy diagram in second order.

this limit, we can make any excitation with momentum $q \leqslant 2k_F$. For fixed but small values of q, the maximum excitation energy is $\omega \approx qv_F$; this occurs when $\mathbf{q}$ is in the same direction as the main momentum $\mathbf{k}$ of each quasiparticle. For q near $2k_F$, the maximum possible energy is $\omega = v_F|q - 2k_F|$. Combining these results, we obtain the sketch in Fig. 8(a), in which the shaded area in the ω–q space is the region of allowed particle–hole excitations.[6] From this spectrum, one can calculate the polarizability, or the magnetic susceptibility.

The behavior sketched above is valid generally in two and three dimensions (but as we will see in Section 4, not in one dimension). The important point to remember is that the density of particle–hole excitations decreases linearly with ω for ω small compared to qv_F. We shall see later that one way of undoing Fermi-liquid theory is to have $\omega \sim k^2$ in two dimensions or $\omega \sim k^3$ in three dimensions.

We can now use $\mathrm{Im}\,\chi(\mathbf{q},\omega)$ to calculate the single-particle self-energy to second order in the interactions. This is shown in Fig. 9 where the wiggly line denotes $\chi(\mathbf{q},v)$ which in the present approximation is just given by the diagram of Fig. 7(a).

For the perturbative evaluation of this process, the intermediate particle with energy–momentum $(\omega + v)$, $(k + q)$ is a free particle. Second-order perturbation theory then yields an imaginary part, or a decay rate,

$$\mathrm{Im}\,\Sigma(\mathbf{k},\omega) = \frac{1}{\tau(\mathbf{k},\omega)} = g^2 N(0)\left(\frac{\omega}{E_F}\right)^2 \tag{23}$$

in three dimensions for $\mathbf{k} \approx \mathbf{k}_F$. In two dimensions, the same process yields $\mathrm{Im}\,\Sigma(\mathbf{k}_F,\omega) \sim \omega^2 \ln(E_F/\omega)$.

The ω^2 decay rate is intimately related to the analytic result (22) for $\mathrm{Im}\,\chi(q,\omega)$ exhibited in Fig. (8). As may be found in textbooks, the same calculation for electron–phonon interactions or for interaction with spin waves in an antiferromagnetic metal gives $\mathrm{Im}\,\Sigma(\mathbf{k}_F,\omega) \sim (\omega/\omega_c)^3$, where ω_c is the phonon Debye frequency in the former and the characteristic zone-boundary spin-wave frequency in the latter.

The real part of the self-energy may be obtained directly or by Kramers–Kronig transformation of (23). It is proportional to ω. Therefore, if the quasiparticle amplitude Z_{k_F} is evaluated

[6] In the presence of long-range Coulomb interactions, in addition to the particle–hole excitation spectrum associated with the screened (and hence effectively short-ranged) interactions one gets a collective mode with a *finite* plasma frequency as $q \to 0$ in $d = 3$ and a $\omega \sim \sqrt{q}$ behavior in $d = 2$. The plasma mode is a high-frequency mode in which the motion of the light electrons cannot be followed by the heavy ions: screening is absent in this regime and the long-range Coulomb interactions then give rise to a finite plasma frequency in $d = 3$.

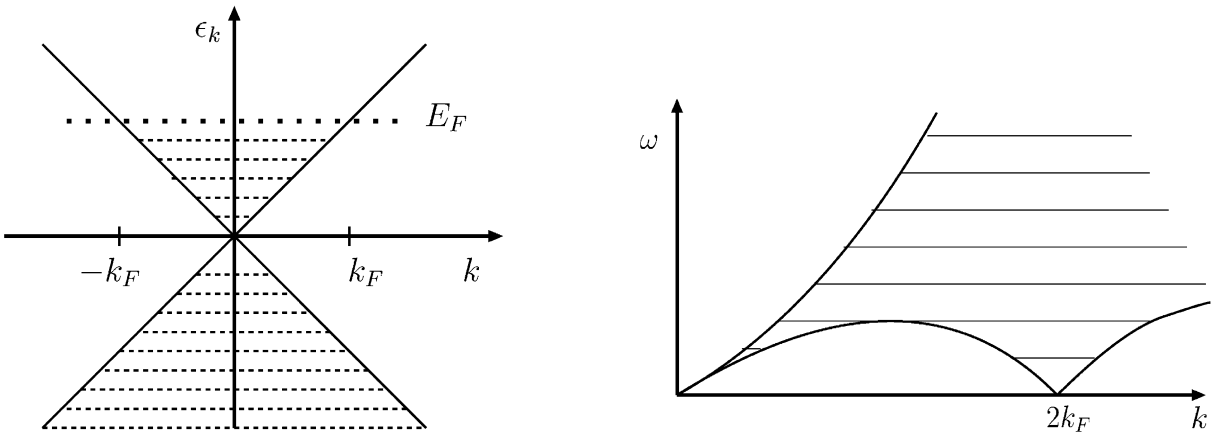

Fig. 10. Single-particle energy ε_k in one dimension, in the approximation that the dispersion relation is linearized about k_F. Note that the Fermi surface consists of just two points. The spectrum of particle–hole excitations is given by $\omega(q) = \varepsilon(k+q) - \varepsilon(k) = k_F q/m$. Low-energy particle–hole excitations are only possible for q small or for q near $2k_F$.

Fig. 11. Phase space for particle–hole excitation spectrum in one dimension compared with the same in higher dimensions, Fig. 8. For linearized single-particle kinetic energy $\varepsilon_k = \pm v_F(k - k_F)$, particle–hole excitations are only possible on lines going through $k = 0$ and $k = 2k_F$.

perturbatively [7]

$$Z_{k_F} \approx 1 - 2g^2 N(0)/E_F \ . \tag{24}$$

Thus in a perturbative calculation of the effect of interactions the basic analytic structure of the Green's function is left the same as for non-interacting fermions. The general proof of the validity of Landau theory consists in showing that what we have obtained to second order in g remains valid to all orders in g. The original proofs [4] are self-consistency arguments—we will consider them briefly in Section 2.4. They assume a finite Z in the exact single-particle Green's functions and effectively show that to any order in perturbation theory, the polarizability functions retain the analytic structure of the non-interacting theory, which in turn ensures a finite Z.

In one dimension, phase-space restrictions on the possible excitations are crucially different. [8] Here the Fermi surface consists of just two points in the one-dimensional space of momenta—see Fig. 10. As a result, whereas in $d = 2$ and 3 a continuum of low-energy excitations with finite q is possible, in one dimension at low-energy only excitations with small k or $k \approx 2k_F$ are possible. The subsequent equivalent of Fig. 8 for the one-dimensional case is the one shown in Fig. 11. Upon integrating over the momentum k with a cut-off of $\mathcal{O}(k_F)$ the contribution from

[7] This quantity has been precisely evaluated by Galitski [104] for the model of a dilute Fermi gas characterized by a scattering length.

[8] It might appear surprising that they are not different in any essential way between higher dimensions.

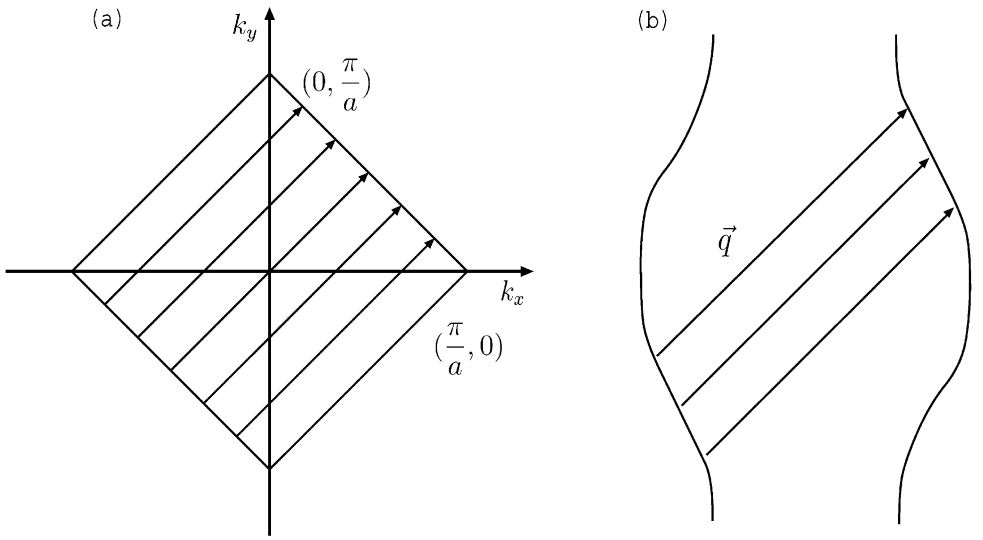

Fig. 12. (a) The nested Fermi surface obtained in a tight binding model on a square lattice with nearest-neighbor hopping; (b) a partially nested Fermi surface which leads to charge-density wave or antiferromagnetic instabilities.

this particle–hole scattering channel to $\mathrm{Re}\,\chi(q,\omega)$ is

$$\int_0^{k_F} \mathrm{d}k \frac{1}{\omega + (2k+q)v_F} \sim \ln[(\omega + qv_F)/E_F] \,. \tag{25}$$

(Note that (25) is true for both $q \ll k_F$ and $|q - 2k_F| \ll k_F$.) This in turn leads to a single-particle self-energy calculated by the process in Fig. 9 to be $\mathrm{Re}\,\Sigma(\mathbf{k}_F,\omega) \sim \omega \ln \omega$ and so $Z \sim \ln \omega$ giving a hint of trouble. The Cooper (particle–particle) channel has the same phase-space restrictions, and gives a contribution to $\mathrm{Re}\,\Sigma(k_F,\omega)$ proportional to $\omega \ln \omega$ too. The fact that these singular contributions are of the same order, leads to a competition between charge/spin fluctuations and Cooper pairing fluctuations, and in the exact calculation to power-law singularities. The fact that instead of the continuum of low-energy excitations present in higher dimensions, the width of the band of allowed particle–hole excitations vanishes as $\omega \to 0$, is the reason that the properties of one-dimensional interacting metals can be understood in terms of bosonic modes. We will present a brief summary of the results for the single-particle Green's function and correlation functions in Section 4.9.

In special cases of nesting in two or three dimensions, one can have situations that resemble the one-dimensional case. When the non-interacting Fermi surface in a tight binding model has the square shape sketched in Fig. 12(a) (which occurs for a tight-binding model with the nearest neighbor hopping on a square lattice at half-filling) a continuous range of momenta on opposite sides of the Fermi surface can be transformed into each other by one and the same wavenumber. This so-called nesting leads to log and $\log^2$ singularities for a continuous range of $\mathbf{k}$ in the perturbation theory for the self-energy $\Sigma(\mathbf{k},\omega)$. Likewise, the partially nested Fermi surface of Fig. 12(b) leads to charge density wave and antiferromagnetic instabilities. We will come back to these issues in Sections 2.6 and 6.

2.4. Principles of the microscopic derivation of Landau theory

In this section, we will sketch how the conclusions in the previous section based on second-order perturbation calculation are generalized to all orders in perturbation theory. This section is slightly more technical than the rest; the reader may choose to skip to Section 2.6.

We follow the microscopic approach whose foundations were laid by Landau himself and which is discussed in detail in excellent textbooks [197,208,37,4]. For more recent methods with the same conclusions, see [237,128]. Our emphasis will be on highlighting the assumptions in the theory so that in the next section we can summarize the routes by which the Fermi-liquid theory may break down. These assumptions are usually not stated explicitly.

The basic idea is that due to kinematic constraints, any perturbative process with n particle–hole pairs in the intermediate state provides contributions to the polarizability proportional to $(\omega/E_{\rm F})^n$. Therefore, the low-energy properties can be calculated with processes with the same "skeletal" structure as those in Fig. 7, which have only one particle–hole pair in the intermediate state. So one may concentrate on the modification of the four-legged vertices and the single-particle propagators due to interactions to all orders. Accordingly, the theory is formulated in terms of the single-particle Green's function $G(p)$ and the two-body scattering vertex

$$\Gamma(p_1, p_2, p_1 + k, p_2 - k) = \Gamma(p_1, p_2, k)\ . \tag{26}$$

Here and below we use, for the sake of brevity, p, etc. to denote the energy–momentum four vector $(\mathbf{p}, \omega)$ and we suppress the spin labels. The equation for Γ is expanded in *one of the two* particle–hole channels as [9]

$$\Gamma(p_1, p_2, k) = \Gamma^{(1)}(p_1, p_2, k) - \mathrm{i}\int \Gamma^{(1)}(p_1, q, k)G(q)G(q+k)\Gamma(q, p_2, k)\frac{d^4q}{(2\pi)^4}\ , \tag{27}$$

where $\Gamma^{(1)}$ is the irreducible part in the particle–hole channel in which Eq. (27) is expressed. In other words, $\Gamma^{(1)}$ cannot be split into two parts by cutting two Green's function lines with total momentum k. So $\Gamma^{(1)}$ includes the complete vertex in the other (often called cross-) particle–hole channel. The diagrammatic representation of Eq. (27) is shown in Fig. 13. In the simplest approximation $\Gamma^{(1)}$ is just the bare two-body interaction. Landau theory *assumes* that $\Gamma^{(1)}$ has no singularities. [10] An *assumption* is now further made that $G(p)$ does have a coherent quasiparticle part at $|\mathbf{p}| \simeq p_{\rm F}$ and $\omega \simeq 0$:

$$G(p) = \frac{Z}{\omega - \tilde{\varepsilon}_{\mathbf{p}} + \mathrm{i}\delta\,\mathrm{sgn}(\varepsilon_{\mathbf{p}})} + G_{\rm inc}\ , \tag{28}$$

---

[9] To second order in the interactions the correction to the vertex in the two possible particle–hole channels has been exhibited in the first two parts of Fig. 7.

[10] The theory has been generalized for Coulomb interactions [208,197,4].The general results remain unchanged because a screened short-range interaction takes the place of $\Gamma^{(1)}$.This is unlikely to be true in the critical region of a metal–insulator transition, because on the insulating side, the Coulomb interaction is unscreened.

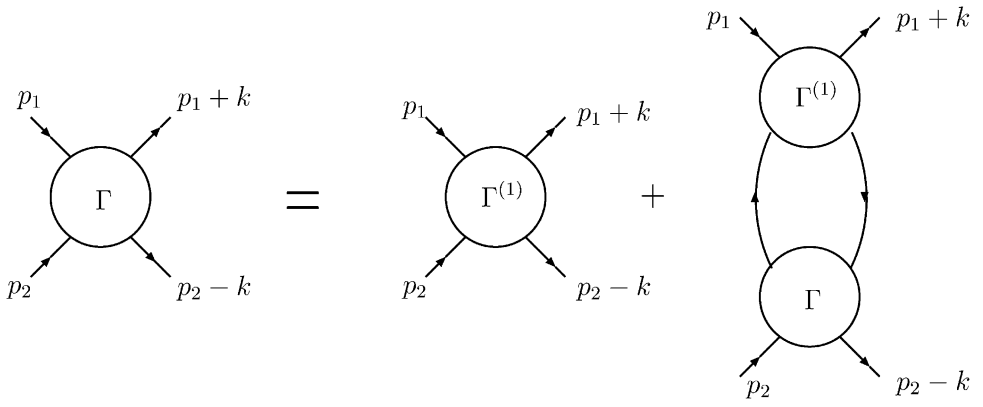

Fig. 13. Diagrammatic representation of Eq. (27).

where $\tilde{\varepsilon}_{\mathbf{p}}$ is to be identified as the excitation energy of the quasiparticle, Z its weight, and G_{inc} the incoherent non-singular part of G. (The latter provides the smooth background part of the spectral function in Fig. 5(b) and the former the sharp peak, which is proportional to the δ function for $\tilde{\varepsilon}_{\mathbf{p}} = \varepsilon_{\mathbf{p}} - \mu$.) It follows [195,4] from (28) that

$$G(q)G(q+k) = \frac{2\mathrm{i}\pi z^2}{v_{\mathrm{F}}} \frac{\mathbf{v_q} \cdot \mathbf{k}}{\omega - \mathbf{v_q} \cdot \mathbf{k}} \delta(v)\delta(|\mathbf{q}| - p_{\mathrm{F}}) + \phi(q) \tag{29}$$

for small $\mathbf{k}$ and ω, and where v and $(v+\omega)$ are frequencies of the two Green's functions. Note the crucial role of kinematics in the form of the first term which comes from the product of the quasiparticle parts of G; $\phi(q)$ comes from the scattering of the incoherent part with itself and with the coherent part and is *assumed* smooth and featureless (as it is indeed, given that G_{inc} is smooth and featureless and the scattering does not produce an infrared singularity at least perturbatively in the interaction). The vertex Γ in regions close to $\mathbf{k} \approx \mathbf{k}_{\mathrm{F}}$ and $\omega \approx 0$ is therefore dominated by the first term. The derivation of Fermi-liquid theory consists in proving that Eqs. (27) for the vertex and (28) for the Green's function are mutually consistent.

The proof proceeds by defining a quantity $\Gamma^{\omega}(p_1, p_2, k)$ through

$$\Gamma^{\omega}(p_1, p_2, k) = \Gamma^{(1)}(p_1, p_2, k) - \mathrm{i} \int \Gamma^{(1)}(p_1, q, k)\phi(q)\Gamma^{\omega}(q, p_2, k) \frac{d^4q}{(2\pi)^4} \,. \tag{30}$$

Γ^{ω} contains repeated scattering of the incoherent part of the particle–hole pairs among itself and with the coherent part, but no scattering of the coherent part with itself. Then, provided the irreducible part of $\Gamma^{(1)}$ is *smooth and not too large*, Γ^{ω} is smooth in k because $\phi(q)$ is by construction quite smooth.

Using the fact that the first part of (29) vanishes for $v_{\mathrm{F}}|k|/\omega \to 0$, and comparing (27) and (30) one can write the *forward scattering amplitude*

$$\lim_{\omega \to 0} \left[\lim_{k \to 0} \Gamma(p_1, p_2, k) \right] = \Gamma^{\omega}(p_1, p_2) \,. \tag{31}$$

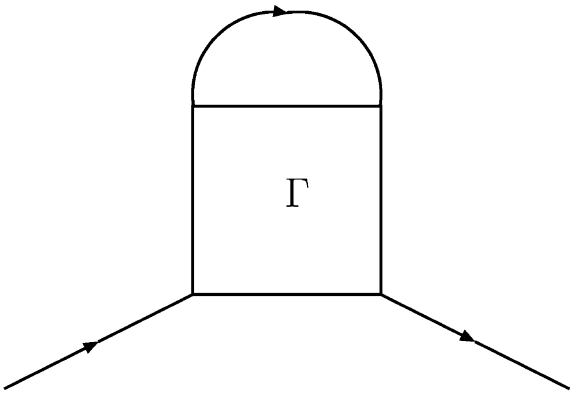

Fig. 14. Diagram for the exact single-particle self-energy in terms of the exact vertex Γ and the exact single-particle Green's function.

This is now used to write the equation for the complete vertex Γ in terms of Γ^{ω}:

$$\Gamma(p_1, p_2, k) = \Gamma^{\omega}(p_1, p_2) + \frac{Z^2 p_F^2}{(2\pi)^3 v_F} \int \Gamma^{\omega}(p_1, q)\Gamma(q, p_2, k) \frac{\mathbf{v_q} \cdot \mathbf{k}}{\omega - \mathbf{v_q} \cdot \mathbf{k}} \, d\Omega_q \,, \tag{32}$$

where in the above $|q| = p_F$ and one integrates only over the solid angle Ω_q.

Given a non-singular Γ^{ω}, a non-singular Γ is produced (unless the denominator in Eq. (32) produces singularities after the indicated integration—the Landau–Pomeranchuk singularities discussed below). The one-particle Green's function G can be expressed exactly in terms of Γ—see Fig. 14. This leads to Eq. (28) proving the self-consistency of the ansatz with a finite quasiparticle weight Z. The quantity $Z^2\Gamma^{\omega}$ is then a smooth function and goes into the determination of the Landau parameters.

The Landau parameters can be written in terms of the forward scattering amplitude. In effect, they parametrize the momentum and frequency independent scattering of the incoherent parts among themselves and with the coherent parts so that the end result of the theory is that the physical properties can be expressed purely in terms of the quasiparticle part of the single-particle Green's function and the Landau parameters. No reference to the incoherent parts needs to be made for low-energy properties. For single-component translational invariant fermions (like liquid ^{3}He) even the quasiparticle amplitude Z disappears from all physical properties. This last part is not true for renormalization due to electron–phonon interactions and in multicomponent systems such as heavy fermions. Special simplifications of the Landau theory occur in such problems and in other problems where the single-particle self-energy is nearly momentum independent [180,280,105,265,187].

As we also mentioned, the single-particle self-energy Σ can be written exactly in terms of the vertex Γ: the relation between the two is represented diagrammatically in Fig. 14. The relations between Σ and Γ are due to conservation laws which Landau theory, of course, obeys. However, the conservation laws are more general than Landau theory. It is often more convenient to express these conservation laws as relations between the self-energy and the three-point vertices, $\Lambda_{\alpha}(p\varepsilon; q\omega)$ which couple external perturbations to either the density (the fourth component,

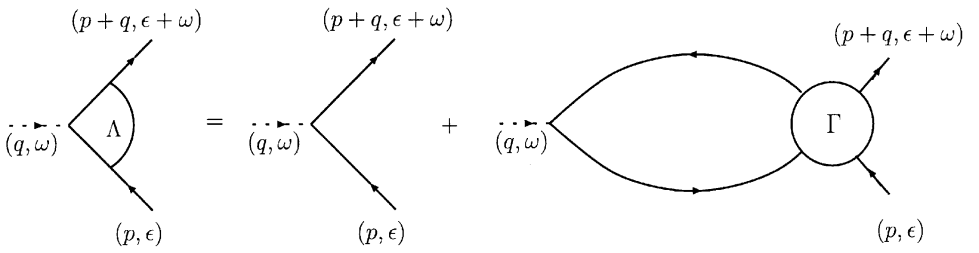

$$\Lambda \quad = \quad \lambda \quad + \quad \lambda\, G\, G\, \Gamma$$

Fig. 15. Vertex for coupling to external perturbations at energy-momentum (ω, q); λ is the bare vertex.

$\alpha = 4$) or the current density in the $\alpha = (1,2,3)$ direction. The diagrammatic representation of the equation for Λ is shown in Fig. 15. The following relations (Ward identities) have been proven for translationally invariant problems:

$$\lim\left(\frac{\omega}{q} \to 0,\ q \to 0\right) \Lambda_\alpha(\mathbf{p}\varepsilon; \mathbf{q}\omega) = \frac{p_\alpha}{m} - \frac{\partial}{\partial p_\alpha}\Sigma(\mathbf{p}, \varepsilon) \quad (\alpha = 1,2,3)\,, \tag{33}$$

$$\lim\left(\frac{\omega}{q} \to 0,\ q \to 0\right) \Lambda_4(\mathbf{p}\varepsilon; \mathbf{q}\omega) = 1 + \frac{\partial \Sigma(\mathbf{p}, \varepsilon)}{\partial \mu}\,, \tag{34}$$

$$\lim\left(\frac{q}{\omega} \to 0, \omega \to 0\right) \Lambda_\alpha(\mathbf{p}\varepsilon; \mathbf{q}\omega) = \frac{p_\alpha}{m} - \frac{\mathrm{d}}{\mathrm{d}\, p_\alpha}\Sigma(\mathbf{p}, \varepsilon) \quad (\alpha = 1,2,3)\,, \tag{35}$$

$$\lim\left(\frac{q}{\omega} \to 0, \omega \to 0\right) \Lambda_4(\mathbf{p}\varepsilon; \mathbf{q}\omega) = 1 + \frac{\mathrm{d}\Sigma(\mathbf{p}, \varepsilon)}{\mathrm{d}\varepsilon}\,. \tag{36}$$

A relation analogous to (34) is derived for fields coupling to spin for the case that interactions conserve spin. The total derivative in (35) and (36) [rather than the partial derivative in (33) and (34)] is represented such that $\mathrm{d}\Sigma/\mathrm{d}\mu$ is the variation in Σ when ε is changed to $\varepsilon + \mathrm{d}\varepsilon$ together with μ to $\mu + \mathrm{d}\mu$, and $\mathrm{d}\Sigma/\mathrm{d}\, p_\alpha$ represents the variation when the momentum $\mathbf{p}$ as well as the Fermi surface is translated by $\mathrm{d}\, p_\alpha$.

Eq. (36) is an expression of energy conservation, and Eq. (34) of particle number conservation. Eqs. (33) and (34) together signify the continuity equation. Eq. (35) represents current conservation. [11]

[11] The Ward identity Eq. (35) does not hold for an impure system where the Fermi surface cannot be defined in momentum space. Since energy is conserved, a Fermi surface can still be defined in energy space, and hence the other Ward identities continue to hold. This point is further discussed in Section 7.

In Landau theory, the right-hand sides in Eqs. (33)–(36) are expressible in terms of the Landau parameters. These relations are necessary for the derivation of the renormalization of the various thermodynamic quantities quoted in Eqs. (17) and (18) as well as the Landau transport equation. Needless to say, any theory of SFL must also be consistent with the Ward identities.

2.5. Modern derivations

The modern derivations of Fermi-liquid theory similarly start by assuming the existence of a Fermi surface. Kinematics then inevitably leads to similar considerations as above. Instead of the division into coherent and incoherent parts made in Eq. (28), the renormalization group procedures are used to systematically generate successively lower energy and small momentum Hamiltonians with excitations of particle ever closer to the Fermi surface. The calculations are carried out either in terms of fermions [237] or newly developed bosonization methods in arbitrary dimensions [128]. The end result is equivalent to Eqs. (28), (30) and (32). These methods may well turn out to be very important in finding the structure of SFLs and in systematizing them.

These derivations carry out the calculation in an arbitrary dimension d and conclude that the forward scattering amplitude is

$$\Gamma^{\omega}(p_1, p_2, k) \sim \left(\frac{k}{k_{\mathrm{F}}}\right)^{d-1} f(p_1, p_2, k)\,, \tag{37}$$

where f is a smooth function of all of its arguments. In one-dimension, the forward scattering amplitude has a logarithmic singularity, as we noted earlier.

We can rephrase the conceptual framework of Landau Fermi-liquid theory in the modern language of renormalization group theory [237]. As we discussed, in Fermi-liquid theory one treats a complicated strongly interacting fermion problem by writing the Hamiltonian $\mathscr{H}$ as

$$\mathscr{H} = \mathscr{H}_{\mathrm{simple}} + \mathscr{H}_{\mathrm{rest}}\,. \tag{38}$$

In our discussion, $\mathscr{H}_{\mathrm{simple}}$ was the non-interacting Hamiltonian. The non-interacting Hamiltonian is actually a member of a "line" of fixed-point Hamiltonians $\mathscr{H}^*$ all of which have the same symmetries but differ in their Landau parameters $F_l^{\mathrm{s,a}}$, etc. The F_l's, obtained from the forward scattering in Landau theory are associated with marginal operators and distinguish the properties of the various systems associated with the line of fixed points. Landau Fermi-liquid theory is primarily a statement regarding the domain of attraction of this line of fixed points. The theory also establishes the universal low-temperature properties due to the "irrelevant" operators generated by $\mathscr{H}_{\mathrm{rest}}$ due to scattering in channels other than the forward channel. Landau theory does not establish (at least completely) the domain of attraction of the "critical surface" bounding the domain of attraction of the Fermi liquid fixed line from those of other fixed points or lines. If $\mathscr{H}_{\mathrm{rest}}$ generates a "relevant" operator (i.e., effective interactions which diverge at low energies and temperatures) the scheme breaks down. For example, attractive interactions between fermions generate relevant operators—they presage a transition to superconductivity,

a state of different symmetry. However, if we stay sufficiently above T_c, we can usually continue using Landau theory.[12]

2.6. Routes to breakdown of Landau theory

From Landau's phenomenological theory, one can only say that the theory breaks down when the physical properties—specific heat divided by temperature,[13] compressibility, or the magnetic susceptibility—diverge or when the collective modes representing oscillations of the Fermi surface in any harmonic and singlet or triplet spin combinations become unstable. The latter, called the Landau–Pomeranchuk singularities, are indeed one route to the breakdown of Landau theory and occur when the Landau parameters $F_l^{\mathrm{s,a}}$ reach the critical value $-(2l+1)$. A phase transition to a state of lower symmetry is then indicated. The new phase can again be described in Landau theory by defining distribution functions consistent with the symmetry of the new ground state.

The discussion following Eq. (8) in Section 2.2 allows us to make a more general statement. Landau theory breaks down when the quasiparticle amplitude $Z_{\mathbf{k}}$ becomes zero; i.e., when the states $c_{\mathbf{k}}^{\dagger}|\psi^N\rangle$ and $|\psi_{\mathbf{k}}^{N+1}\rangle$ are orthogonal. This can happen if the series expansion in Eq. (8) in terms of the number of particle–hole pairs is divergent. In other words, the addition of a particle or a hole to the system creates a divergent number of particle–hole pairs in the system so that the leading term does not have a finite weight in the thermodynamic limit. From Eq. (11), which links the Z's to Σ's, this requires that the single-particle self-energy be singular as a function of ω at $k \simeq k_{\mathrm{F}}$. This in turn means that the Green's functions of SFLs contain branch cuts rather than the poles unlike Landau Fermi liquids. The weakest singularity of this kind is encountered in the borderline "marginal Fermi liquids" where[14]

$$\Sigma(k_{\mathrm{F}},\omega) \simeq \lambda\left[\omega \ln\frac{\omega_c}{\omega} + \mathrm{i}|\omega|\right] . \tag{39}$$

If a divergent number of low-energy particle–hole pairs is created upon the addition of a bare particle, it means that the low-energy response functions (which all involve creating particle–hole pairs) of SFLs are also divergent. Actually, the single-particle self-energy can be written in terms of integrals over the complete particle–hole interaction vertex as in Fig. 14. The implication is that the interaction vertices are actually more divergent than the single-particle self-energy.

---

[12] We note that in a renormalization group terminology, all Landau parameters $f_{\mathbf{k}\mathbf{k}',\sigma\sigma'}$ originating from forward scattering (i.e., zero momentum transfer), are "marginal operators" [151,237]. All other operators that determine finite temperature observable properties are "irrelevant". Thus, in a "universal" sense, condensed matter physics may be deemed to be an "irrelevant" field. So much for technical terminology!

[13] The specific heat of a system of fermions can be written in terms of integrals over the phase angle of the exact single-particle Green's function [4]. Given any singularity in the self-energy, C_v/T is never more singular than $\ln T$. This accounts for the numerous experimental examples of such behavior that we will come across.

[14] To see why this is the borderline case, note that a requisite for the definition of a quasiparticle is that the quasiparticle peak width $\tau_{\mathbf{k}}^{-1} = 2\Sigma''$ should vanish faster than linear in ω, the quasiparticle energy. Thus, $\Sigma'' \sim \omega$ is the first power for which this is not true. The $\omega \ln(\omega_c/\omega)$ term in Eq. (39) is then dictated by the Kramers–Kroning relation.

Yet another route to SFLs is the case in which the interactions generate new quantum numbers which are not descriptive of the non-interacting problem. This happens in particular in the Quantum Hall problems and in one-dimensional problems (Section 4) as well as in problems of impurity scattering with special symmetries (Section 3). In such cases, the new quantum numbers characterize new low-energy topological excitations. New quantum numbers of course imply $Z = 0$, but does $Z = 0$ imply new quantum numbers? One might wish to conjecture that this is so. However, no general arguments on this point are available. [15]

Ultimately, all breakdowns of Landau theory are due to degeneracies leading to singular low-energy fluctuations. If the characteristic energy of the fluctuations is lower than the temperature, a quasiclassical statistical mechanical problem results. On the basis of our qualitative discussion in Section 2.3 and the sketch of the microscopic derivation in Section 2.4, we may divide the various routes to breakdown of Landau theory into the following (not necessarily orthogonal) classes:

(i) *Landau–Pomeranchuk singularities*: Landau theory points to the possibility of its breakdown through the instability of the collective modes of the Fermi-surface which arise from the solution of the homogeneous part of Eq. (32). These collective modes can be characterized by the angular momentum ℓ of oscillation of the Fermi surface and whether the oscillation is symmetric "s" or antisymmetric "a" in spin. The condition for the instability derived from the condition of zero frequency of the collective modes are [208,37]

$$F_\ell^{\mathrm{s}} \leqslant -(2\ell+1), \quad F_\ell^{\mathrm{a}} \leqslant -(2\ell+1)\,. \tag{40}$$

The $\ell = 0$ conditions refer to the divergence in the compressibility and the (uniform) spin susceptibility. The former would in general occur via a first-order transition, so is uninteresting to us. The latter describes the ferromagnetic instability. No other Landau–Pomeranchuk instabilities have been experimentally identified. However, such new and exotic possibilities should be kept in mind. Thus, for example, an F_1^{s}-instability corresponds to the Fermi velocity $\to 0$, a F_2^{s} instability to a "*d-wave*-like" instability of the particle–hole excitations on the Fermi surface etc. Presumably, these instabilities are resolved by reconstruction of the Fermi surface. The microscopic interactions necessary for the Landau–Pomeranchuk instabilities and the critical properties near such instabilities have not been well investigated, especially for fermions with a lattice potential. [16]

It is also worth noting that some of the instabilities are disallowed in the limit of translational invariance. Thus, for example, time-reversal breaking states, such as the "anyon-state" [156,60] cannot be realized because in a translationally invariant problem the current operator cannot be renormalized by the interactions, as we have learnt from Eqs. (18), (33).

---

[15] It would indeed be a significant step forward if such a conjecture could be proven to be true or if the conditions in which it is true were known. One might think that this should be obvious in any given case. However, it is not so. In the SFL problems of magnetic impurities (Section 3) and in the SFL behavior of one-dimensional fermions (Section 4), a complete description of the solution was given without introducing new quantum numbers. That these problems may be discussed in such terms was only realized later, lending to the solutions additional elegance besides insight.

[16] See, however, two recent papers [116,200]. In [273] the pseudogap in the underdoped cuprates arises as a consequence of a Landau–Pomeranchuk instability.

(ii) *Critical regions of large Q-singularities*: Landau theory concerns itself only with long-wavelength response and correlations. A Fermi liquid may have instabilities at a non-zero wavevector, for example a charge-density wave (CDW) or spin-density wave (SDW) instability. Only a microscopic calculation can provide the conditions for such instabilities and therefore such conditions can only be approximately derived. An important point to note is that they arise perturbatively from repeated scattering between the quasiparticle parts of G while the scattering vertices (irreducible interactions) are regular. The superconductive instability for any angular momentum is also an instability of this kind. In general, such instabilities are easily seen in RPA and/or t-matrix calculations.

Singular Fermi liquid behavior is generally expected to occur only in the critical regime of such instabilities [117,164]. If the transition temperature T_c is finite then there is usually a stable low-temperature phase in which unstable modes are condensed to an order parameter, translational symmetry is broken, and gaps arise in part or all of the Fermi surface. For excitations on the surviving part of the Fermi surface, Fermi-liquid theory is usually again valid. The fluctuations in the critical regime are classical, i.e., with characteristics frequency $\omega_{f\ell} \ll k_B T_c$.

If the transition is tuned by some external parameter so that it occurs at zero temperature, one obtains, as illustrated already in Fig. 1, a quantum critical point (QCP). If the transition is approached at $T = 0$ as a function of the external parameter, the fluctuations are quantum-mechanical, while if it is approached as a function of temperature for the external parameter at its critical value, the fluctuations have a characteristic energy proportional to the temperature. A large region of the phase diagram near QCPs often carries SFL properties. We shall discuss such phenomena in detail in Section 6.

(iii) *Special symmetries*: The Cooper instability at $q = 0$, Fig. 7(c), is due to the "nesting" of the Fermi surface in the particle–particle channel. Usually, indications of finite-q CDW or SDW singularities are evident pertubatively from Fig. 7(a) or (b) for special Fermi surfaces, nested in some $\mathbf{q}$-direction in particle–hole channels. One-dimensional fermions are perfectly nested in both particle–hole channels and particle–particle channels (Fig. 7(a)–(c)) and hence they are both logarithmically singular. Pure one-dimensional fermions also have the extra conservation law that right going and left going momenta are separately conserved. These introduce special features to the SFL of one-dimensional fermions such as the introduction of extra quantum numbers. These issues are discussed in Section 4.9. Several soluble impurity problems with special symmetries have SFL properties. Their study can be illuminating and we discuss them in Section 3.

(iv) *Long-range interactions*: The breakdown of Landau Fermi liquid may come about through long-range interactions, either in the bare Hamiltonian through the irreducible interaction or through a generated effective interaction. The latter, of course, occurs in the critical regime of phase transitions such as discussed above. Coulomb interactions will not do for the former because of screening of charge fluctuations. The fancy way of saying this is that the longitudinal electromagnetic mode acquires mass in a metal. The latter is not true for current fluctuations or transverse electromagnetic modes which must remain massless due to gauge invariance. This is discussed in Section 5.1, where it is shown that no metal at low enough temperature is a Fermi liquid. However, the cross-over temperature is too low to be of experimental interest.

An off-shoot of an SFL through current fluctuations is the search for extra (induced) conservation laws for some quantities to keep their fluctuations massless. This line of investigation may be referred to generically as gauge theories. Extra conservation laws imply extra quantum numbers and associated orthogonality. We discuss these in Section 5.2. The one-dimensional interacting electron problem and the Quantum Hall effect problems may be usefully thought of in these terms.

(v) *Singularities in the irreducible interactions*: In all the possibilities discussed in (i)–(iii) above, the irreducible interactions $\Gamma^{(1)}$ defined after Eq. (27) are regular and not too large. As noted after Eq. (30), this is necessary to obtain a regular Γ^{ω}. When these conditions are satisfied the conceivable singularities arise only from the repeated scattering of low-energy particle–hole (or particle–particle pairs) as in Eq. (32) or its equivalent for large momentum transfers.

A singularity in the irreducible interaction of course invalidates the basis of Landau theory. Such singularities imply that the parts of the problem considered harmless perturbatively because they involve the incoherent and high-energy parts of the single-particle spectral weight as in Eq. (30) are, in fact, not so. This is also true if $\Gamma^{(1)}$ is large enough such that the solution of Eq. (30) is singular. Very few investigations of such processes exist.

How can an irreducible interaction be singular when the bare interaction is perfectly regular? We know of two examples:

In disordered metals, the density correlations are diffusive with the characteristic frequency ω scaling with q^2. The irreducible interactions made from the diffusive fluctuations and interactions are singular in $d=2$. This gives rise to a new class of SFLs which are discussed in Section 8. One finds that in this case, the singularity in the cross-particle–hole channel (the channel different from the one through which the irreducibility of $\Gamma^{(1)}$ is defined) feeds back into a singularity in $\Gamma^{(1)}$. This is very special because the cross-channel is integrated over and the singularity in it must be very strong for this to be possible.

The second case concerns the particle singularities in the irreducible interactions because of excitonic singularities. Usually, the excitonic singularities due to particle–hole between different bands occur at a finite energy and do not introduce low-energy singularities. However, if the interactions are strong enough, these singularities occur near zero frequency. In effect, eliminating high-energy degrees of freedom generates low-energy irreducible singular vertices. This only requires that the appropriate bare interactions are large compared to characteristic inter-band energies.

Consider, for example, the band structure of a solid with more than one atom per unit cell with (degenerate) valence band maxima and minima at the same points in the Brillouin zone, as in Fig. 16.

Let the conduction band be partially filled, and the energy difference between μ and the valence band below E_0 in Fig. 16 be much smaller than the attractive particle–hole interactions V between states in the valence (v) band and the conduction band (c). For any finite V, excitonic resonances form from scattering between v and c states, as in the X-ray edge problem to be discussed in Section 3.5. For large enough V, such resonances occur at asymptotically low energy so that the Fermi liquid description of states near the chemical potential in terms of irreducible interaction among the c states is invalid. The effective irreducible interactions among the low-energy states integrate over the excitonic resonance and will in general be singular if the resonance is near zero energy.

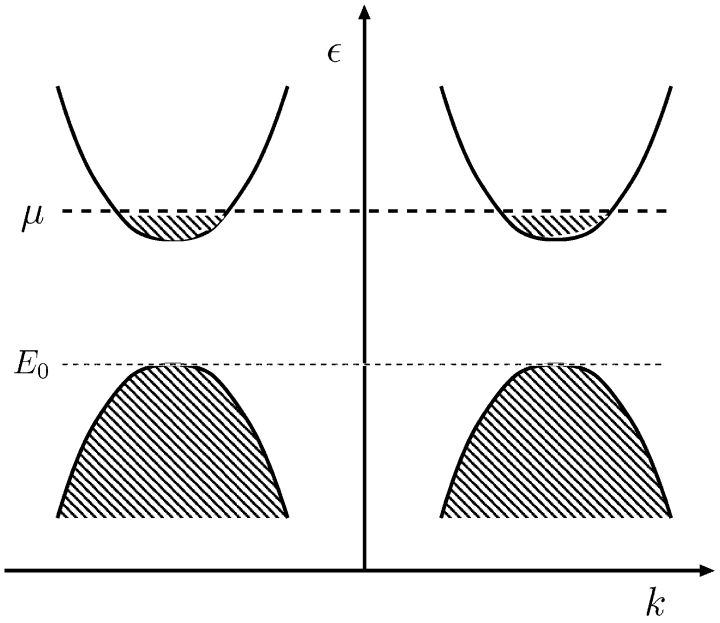

Fig. 16. A model band structure for a solid with more than one atom per unit cell. Actually in CaB_6 where excitonic singularities have been invoked to produce a ferromagnetic state [295] there are three equivalent points in the Brillouin zone where the conduction band minima and the valence band maxima occur.

Such singularities require interactions above a critical magnitude and are physically and mathematically of an unfamiliar nature. In a two-band one-dimensional model, exact numerical calculations have established the importance of such singularities [252,249].

Recently, it has been found that CaB_6 or SrB_6 with low densities of trivalent Eu or quadrivalent Ce ions substituting for (Ca, Sr) are ferromagnets [295]. The most plausible explanation [303,34,36] is that this is a realization of the excitonic ferromagnetism predicted by Volkov et al. [279]. The instability to such a state occurs because the energy to create a hole in the valence band and a particle in the conduction band above the Fermi energy goes to zero if the attractive particle–hole (interband) interactions are large enough. This problem has been investigated only in the mean field approximation. Fluctuations in the critical regime of such a transition are well worth studying.

Excitonically induced singularities in the irreducible interactions are also responsible for the Marginal Fermi-liquid state of Cu–O metals in a theory to be discussed in Section 7.

3. Local Fermi liquids and local singular Fermi liquids

In this section, we discuss a particular simple form of Fermi liquid formed by electrons interacting with a dilute concentration of magnetic impurity. Many of the concepts of Fermi-liquid theory are revisited in this problem. Variants of the problem provide an interesting array of soluble problems of SFL behavior and illustrate some of the principal themes of this article.

3.1. The Kondo problem

The Kondo problem is at the same time one of the simplest and one of the most subtle examples of the effects of strong correlation effects in electronic systems. The experiments concern metals with a dilute concentration of magnetic impurities. In the Kondo model, one considers only a single impurity; the Hamiltonian then is

$$\mathscr{H} = t \sum_{\langle ij \rangle, \alpha} c^{\dagger}_{i\alpha} c_{j\alpha} + J\mathbf{S} \cdot c^{\dagger}_{0} \sigma c_{0} \ , \tag{41}$$

where $(c_{i\alpha}, c^{\dagger}_{i\alpha})$ denote the annihilation and creation operators of a conduction electron at site i with projection α in the z-direction of spin σ. The second term is the exchange interaction between a single magnetic impurity at the origin (with spin $S = \frac{1}{2}$) and a conduction electron spin.

When the exchange constant $J > 0$, the system is a Fermi liquid. Although not often discussed, the ferromagnetic ($J < 0$) variant of this problem is one of the simplest examples of a singular Fermi liquid.

There are two simple starting points for the problem: (i) $J = 0$: This turns out to describe the unstable high-temperature fixed point.[17] The term proportional to J is a marginal operator about the high-temperature fixed point because, as discovered by Kondo [146], in a third-order perturbation calculation the effective interaction acquires a singularity $\sim J^3/t^2 \ln(t/\omega)$. (ii) $t = 0$: The perturbative expansion about this point is well behaved. This turns out to describe the low-temperature Fermi liquid fixed point. One might be surprised by this, considering that typically the bare t/J is of order 10^{+3}. But such is the power of singular renormalizations.[18]

---

[17] For the reader unfamiliar with reading a renormalization group diagram like that of Fig. 17(b) or Fig. 18, the following explanation might be helpful. The flow in a renormalization group diagram signifies the following. The original problem, with bare parameters, corresponds to the starting point in the parameter space in which we plot the flow. Then we imagine "integrating out" the high-energy scales (e.g. virtual excitations to high-energy states); effectively, this means that we consider the system at lower-energy (and temperature) scales by generating effective Hamiltonians with new parameters so that the low-energy properties remain invariant. The "length" along the flow direction is essentially a measure of how many energy scales have been integrated out—typically, as in the Kondo problem, this decrease is logarithmic along the trajectory. Thus, the regions towards which the flow points signify the effective parameters of the model at lower and lower temperatures. Fixed points towards which all trajectories flow in a neighborhood describe the universal low-temperature asymptotic behavior of the class of models to which the model under consideration belongs. When a fixed point of the flow is unstable, it means that a model whose bare parameters initially lie close to it flows away from this point towards a stable fixed point; hence it has a low-temperature behavior which does not correspond to the model described by the unstable fixed point. A fixed line usually corresponds to a class of models which have some asymptotic behavior, e.g. an exponent, which varies continuously.

[18] A particularly lucid discussion of the renormalization procedure may be found in [151]. Briefly, the procedure consists in generating a sequence of Hamiltonians with successively lower-energy cut-offs that reproduce the low-energy spectrum. All terms allowed by symmetry besides those in the bare Hamiltonian are retained. The coefficients of these terms *scale* with the cut-off. Those that decrease proportionately to the cut-off or change only logarithmically, are coefficients of marginal operators, those that grow/decrease (algebraically) are coefficients of relevant/irrelevant operators. Marginal operators are marginally relevant or marginally irrelevant. Upon renormalization, the flow is towards the strong coupling $J = \infty$ fixed point, see Fig. 17. The terms generated from $t \neq 0$ serve as irrelevant operators at this fixed point; this means that they do not affect the ground state but determine the measurable low-energy properties.

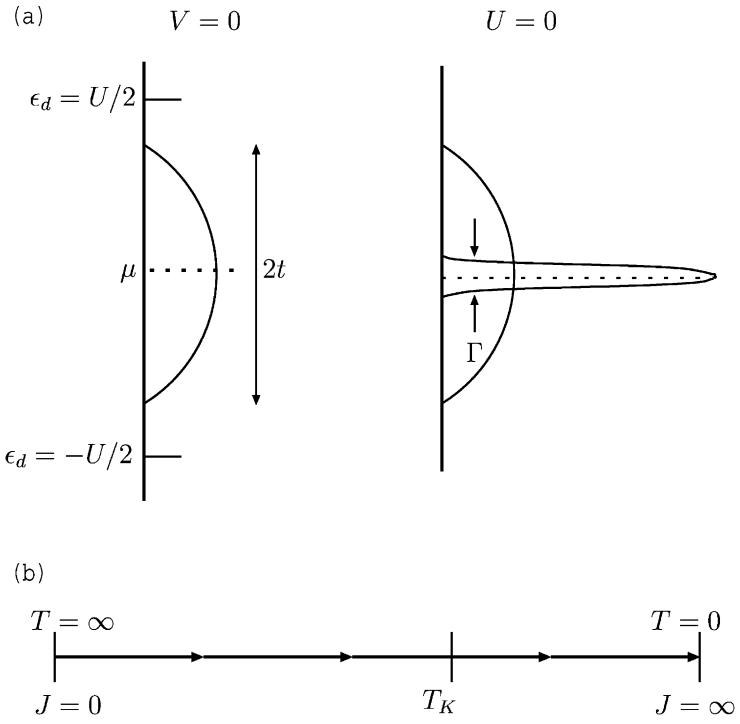

Fig. 17. (a) Hartree–Fock excitation spectrum of the Anderson model in the two limits of zero hybridization, $V=0$ and zero interaction, $U=0$; (b) renormalization group flow of the Kondo problem.

The interaction between conduction electrons and the localized electronic level is not a direct spin interaction. It originates from quantum-mechanical charge fluctuations that (through the Pauli principle) depend on the relative spin orientation. To see this explicitly, it is more instructive to consider the Anderson model [19] in which

$$\mathscr{H} = t\sum_{\langle ij\rangle} c^{\dagger}_{i\alpha}c_{j\alpha} + \varepsilon_d \sum_{\sigma} c^{\dagger}_{0\sigma}\, c_{0\sigma} + U c^{\dagger}_{0,\uparrow}c_{0,\uparrow}c^{\dagger}_{0,\downarrow}c_{0,\downarrow} + \sum_{k,\sigma}(V_k c^{\dagger}_{k,\sigma}c_{0,\sigma} + \text{h.c.})\,. \tag{42}$$

The last term in this Hamiltonian is the hybridization between the localized impurity state and the conduction electrons, in which spin is conserved. In the particle–hole symmetric case, $\varepsilon_d = -U/2$ is the one-hole state on the impurity site in the Hartree–Fock approximation and the one-particle state has the energy $U/2$.

Following a perturbative treatment in the limit $t/V, U/V \gg 1$ the Anderson model reduces to the Kondo Hamiltonian with an effective exchange constant $J_{\text{eff}} \sim (V^2/t)^2/U$.

The Anderson model has two simple limits, which are illustrated in Fig. 17:

(i) $V=0$: This describes a local moment with Curie susceptibility $\chi \sim \mu_{\text{B}}^2/T$. This limit is the correct point of departure for an investigation of the high-temperature regime. As noted one soon encounters the Kondo divergences.

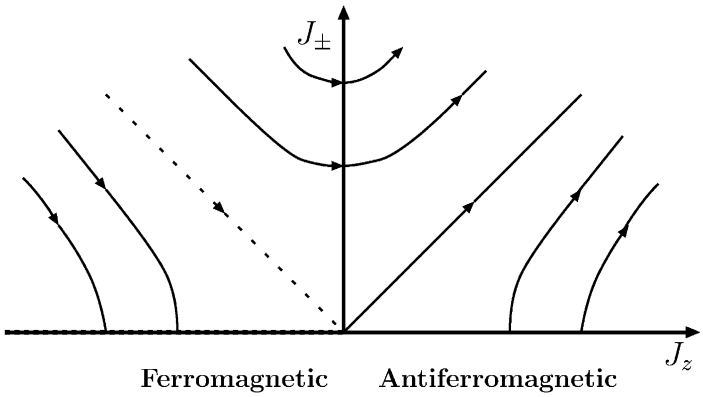

Fig. 18. Renormalization group flows for the Kondo problem, displaying the line of critical points for the "ferromagnetic" problem and the flow towards the fixed point $J_\pm^* = J_z^* \to \infty$ for the "antiferromagnetic" problem.

(ii) $U = 0$: In this limit, the impurity forms a resonance of width $\Gamma \sim V^2/t$ at the chemical potential which in the particle–hole symmetric case is half-occupied. The ground state is a spin singlet. This limit is the correct starting point for an examination of the low-temperature properties ($T \ll T_K$). A temperature independent contribution to the susceptibility and a linear contribution to the specific heat ($\sim N(0)T/\Gamma$) are contributed by the resonant state. Hence the name *local Fermi liquid*.

The conceptually tough part of the problem was to realize that (ii) is the correct stable low-temperature fixed point and the technically tough problem is to derive the passage from the high-temperature regime to the low-temperature regime. This was first done correctly by Wilson [289] through the invention of the numerical renormalization group (and almost correctly by Anderson and Yuval [22,23] by analytic methods). The analysis showed that under renormalization group scaling transformations, the ratio (J/t) increases monotonically as illustrated in Fig. 17(b)—continuous RG flows are observed from the high-temperature extreme (i) to the low-temperature extreme (ii) and a smooth crossover between the two regimes occurs at the Kondo temperature

$$T_K \sim t \exp(-t/2J) \,. \tag{43}$$

Since all flow is towards the strong-coupling fixed point, universal forms for the thermodynamic functions are found. For example, the specific heat C_v and the susceptibility χ scale as

$$C_v = T f_c(T/T_K), \quad \chi = \mu_B^2 f_\chi(T/T_K) \,, \tag{44}$$

where the f's are universal scaling functions.

An important theoretical result is that compared to a non-interacting resonant level at the chemical potential, the ratio of the magnetic susceptibility enhancement to the specific heat enhancement

$$R_W = \frac{\delta\chi/\chi}{\delta C_v/C_v} \tag{45}$$

for spin 1/2 impurities at $T \ll T_K$ is precisely 2 [289,197]. In a non-interacting model, this ratio, nowadays called the Wilson ratio, is equal to 1, since both χ and C_v are proportional to the density of states $N(0)$. Thus, the Wilson ratio is a measure of the importance of correlation effects. It is in fact the analogue of the Landau parameter F_0^a of Eq. (18).

3.2. Fermi-liquid phenomenology for the Kondo problem

Following Wilson's solution [289], Nozières [197] showed that the low-temperature properties of the Kondo problem can be understood simply through a (local) Fermi-liquid framework. This is a beautiful example of the application of the concept of analyticity and of symmetry principles about a fixed point. We present the key arguments below. For the application of this line of approach to the calculation of a variety of properties, we refer the reader to papers by Nozières and Blandin [197,198].

The properties of a local impurity can be characterized by the energy-dependent s-wave phase shift $\delta_\sigma(\varepsilon)$, which in general also depends on the spin of the conduction electron being scattered. In the spirit of Fermi-liquid theory the phase shift may be written in terms of the deviation of the distribution function $\delta n(\varepsilon)$ of conduction electrons from the equilibrium distribution

$$\delta_\sigma(\varepsilon) = \delta_0(\varepsilon) + \sum_{\varepsilon'\sigma'} \delta_{\sigma\sigma'}(\varepsilon,\varepsilon')\delta n_{\sigma'}(\varepsilon') + \cdots . \tag{46}$$

About a stable fixed point, the energy dependence is analytic near the chemical potential ($\varepsilon = 0$), so that we may expand

$$\delta_0(\varepsilon) = \delta_0 + \alpha\varepsilon + \cdots, \quad \delta_{\sigma\sigma'}(\varepsilon,\varepsilon') = \phi_{\sigma\sigma'} + \cdots . \tag{47}$$

Just as the Landau parameters are expressed in terms of symmetric and antisymmetric parts, we can write

$$\phi_{\uparrow\uparrow} = \phi_{\downarrow\downarrow} = \phi^s + \phi^a , \quad \phi_{\downarrow\uparrow} = \phi_{\uparrow\downarrow} = \phi^s - \phi^a . \tag{48}$$

Taken together, this leaves three parameters α, ϕ^s and ϕ^a to determine the low-energy properties. Nozières [197] showed that in fact there is only one independent parameter (say α which is of $\mathcal{O}(1/T_K)$, with a prefactor which can be obtained by comparing with Wilson's detailed numerical solution). To show this, note that by the Pauli principle same spin states do not interact, therefore [197]

$$\phi_{\uparrow\uparrow} = \phi^s + \phi^a = 0 . \tag{49}$$

Secondly, a shift of the chemical potential by $\delta\mu$ and a simultaneous increase in δn by $N(0)\delta\mu$ should have no effect on the phase shift, since the Kondo effect is tied to the chemical potential. Therefore according to (46) and (47)

$$[\alpha + N(0)\phi^s]\delta\mu = 0 , \quad \Rightarrow \phi^s = -\alpha/N(0) . \tag{50}$$

Thirdly, one may borrow from Wilson's solution that the fixed point has $\delta_0 = \pi/2$. This expresses that the tightly bound spin singlet state formed of the impurity spin and conduction electron spin

completely blocks the impurity site to other conduction electrons; this in turn implies maximal scattering and therefore phase shift of $\pi/2$ for the effective scattering potential [197]. In other words, it is a strong-coupling fixed-point where one conduction electron state is pushed below the chemical potential in the vicinity of the impurity to form a singlet resonance with the impurity spin. One may now calculate all physical properties in terms of α. In particular, one finds $\delta C_v/C_v = 2\alpha/(\pi VN(0))$ and a similar expression for the enhancement of χ, such that the Wilson ratio is 2.

3.3. Ferromagnetic Kondo problem and the anisotropic Kondo problem

The *ferromagnetic Kondo problem* provides us with the simplest example of SFL behavior. We will discuss this below after relating the problem to a general X-ray edge problem in which the connection to the so-called *orthogonality catastrophe* is clearer. As discussed in Section 2, orthogonality generally plays an important role in SFLs.

We start with the anisotropic generalization of the Kondo Hamiltonian, which is the proper starting model for a perturbative scaling analysis [21,100],

$$H = t\sum_{\langle ij\rangle,\sigma} c^{\dagger}_{i\sigma}c_{j\sigma} + \sum_{k,k'} [J_{\pm}(S^{+}c^{\dagger}_{k\downarrow}c_{k'\uparrow} + S^{-}c^{\dagger}_{k\uparrow}c_{k'\downarrow}) + J_z S^z(c^{\dagger}_{k,\uparrow}c_{k',\uparrow} - c^{\dagger}_{k,\downarrow}c_{k',\downarrow})] \,. \tag{51}$$

Long before the solution of the Kondo problem, perturbative renormalization group for the effective vertex coupling constants $J_{\pm}$ and J_z as a function of temperature were obtained [21,100]. The scaling relation between them is found to be exact to all orders in the $J's$:

$$(J_z^2 - J_{\pm}^2) = \text{const} \quad (J_+ = J_-) \,. \tag{52}$$

In the flow diagram of Fig. 18, we show the scaling trajectories for the anisotropic problem. In the antiferromagnetic regime, the flows continuously veer towards larger and larger $(J_{\pm}, J_z)$ values; at the attracting fixed point $(J*_{\pm}, J*_z) = (\infty, \infty)$ singlets form between the local moment and the conduction electrons.

The "ferromagnetic" regime spans the region satisfying the inequalities $J_z < 0$ and $|J_z| \geqslant J_{\pm}$. Upon reducing the bandwidth the coupling parameters flow towards negative J_z values. Observe the *line of fixed points* on the negative J_z axis. Such a *continuous line* is also seen in the Kosterlitz–Thouless transition [147] of the two-dimensional XY model. Moreover, in both problems continuously varying exponents in physical properties are obtained along these lines (in fact, the renormalization group flow equations of the Kondo model for small coupling are mathematically identical to those for the XY model). This is an instance of *a zero temperature quantum critical line*. The physics of the quantum critical line has to do with an "orthogonality catastrophe" which we describe next. Such orthogonalities are generally an important part of the physics of SFLs.

3.4. Orthogonality catastrophe

As we saw in Section 2, a Fermi-liquid description is appropriate so long as the spectrum retains a coherent single-particle piece of finite weight $Z > 0$. So if by some miracle the

evaluation of Z reduces to an overlap integral between two orthogonal wavefunctions then the system is an SFL.

In the thermodynamic ($N \to \infty$) limit, such a miracle is more generic than might appear at first sight. In fact, such an *orthogonality catastrophe* arises if the injection of an *infinitely massive particle* produces an effective finite range scattering potential for the remaining N electrons [20] (see Section 4.9). Such an orthogonality is exact only in the thermodynamic limit: The single-particle wavefunctions are not orthogonal. It is only the overlap between the ground state formed by their Slater determinants [19] which vanishes as N tends to infinity.

More quantitatively, if the injection of the additional particle produces an s-wave phase shift δ_0 for the single-particle wavefunctions (all N of them)

$$\phi(kr) = \frac{\sin kr}{kr} \to \frac{\sin(kr + \delta_0)}{kr} \tag{53}$$

then an explicit computation of the Slater determinants reveals that their overlap diminishes as

$$\langle \psi_N | \psi'_N \rangle \sim N^{-\delta_0^2/\pi^2} \, . \tag{54}$$

Here, $|\psi_N\rangle$ is the determinant Fermi sea wavefunction for N particles and $|\psi'_N\rangle$ is the wavefunction of the system after undergoing a phase shift by the local perturbation produced by the injected electron. [20]

Quite generally such an orthogonality ($Z = 0$) arises also if two N-particle states of a system possess different quantum numbers and almost the same energy. These new quantum numbers might be associated with novel topological excitations. This is indeed the case in the quantum Hall liquid where new quantum numbers are associated with fractional charge excitations. The SFL properties of the interacting one-dimensional fermions (Section 4) may also be looked at as being due to orthogonality. Often orthogonality has the effect of making a quantum many-body problem approach the behavior of a classical problem. This will be one of the leitmotifs in this review. We turn first to a problem where this orthogonality is well understood to lead to experimental consequences, although not at low energies.

3.5. X-ray edge singularities

The term X-ray edge singularity is used for the line shape for absorption in metals by creating a hole in an atomic core level and a particle in the conduction band above the chemical potential. In the non-interacting particle description of this process, the absorption starts at the threshold frequency ω_D, as sketched in Fig. 19. In this case, a Fermi edge reflecting the density of unoccupied states in the conduction band is expected to be visible in the spectrum.

---

[19] The results also hold true for interacting fermions, at least when a Fermi-liquid description is valid for both of the states.

[20] Through the Friedel sum rule, δ_0/π has a physical meaning; it is the charge that needs to be transported from infinity to the vicinity of the impurity in order to screen the local potential [80].

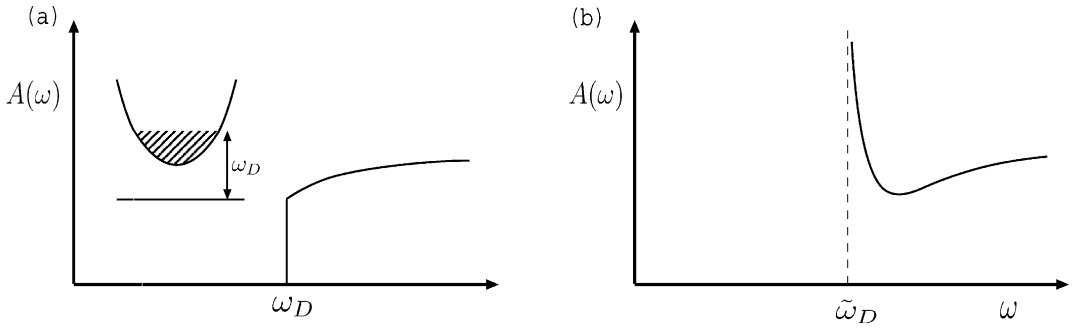

Fig. 19. Absorption line shape for transitions between a lower dispersionless level and a conduction band, (a) for zero interaction between the conduction electrons and local level, and (b) for small interaction.

However, when a hole is generated in the lower level, the potential that the conduction electrons see is different. The relevant Hamiltonian is now

$$\mathscr{H} = \varepsilon_d \left(d^\dagger d - \frac{1}{2} \right) + \sum_k \varepsilon_k c_k^\dagger c_k + \frac{1}{L} \sum_{k,k'} V(k,k') \left(c_k^\dagger c_{k'} - \frac{1}{2} \right) \left(d^\dagger d - \frac{1}{2} \right) , \tag{55}$$

where spin indices have been suppressed. The operators $(d, d^\dagger)$ annihilate or create holes in the core level, which is taken to be dispersionless. The first two terms in the Hamiltonian represent the unperturbed energies of the core hole and the free electrons. The last term depicts the screened Coulomb interaction between the conduction electrons and the hole in the core level.

As a consequence of the interactions, the line shape is quite different. This is actually an exactly solvable problem [196]. There are two kinds of effects, (a) excitonic—the particle and the hole attract, leading to a shift of the edge and a sharpening of the edge singularity—and (b) an orthogonality effect of the type just discussed above, which smoothens the edge irrespective of the sign of the interaction. This changes the absorption spectrum to that of Fig. 19(b) in the presence of interactions. The form of the singularity is [167,196]

$$A(\omega) \sim (\omega - \tilde{\omega}_{\mathrm{D}})^{-2\delta_0/\pi + \delta_0^2/\pi^2} . \tag{56}$$

The exponent δ_0^2/π^2 is a consequence of the orthogonality catastrophe overlap integral; the exponent $(-2\delta_0/\pi)$ is due to the excitonic particle–hole interactions. If the hole has finite mass, we have a problem with recoil which is not exactly solvable. Notwithstanding this, we do know the essential features of the problem. As we will discuss later in Section 4.9, recoil removes the singularity in two and three dimensions and the absorption edge acquires a characteristic width of the order of the dispersion of the hole band. If the hole moves only in one dimension, the singularity is not removed.

3.6. A spinless model with finite range interactions

A model which is a generalization of the ferromagnetic Kondo problem and in which the low-energy physics is dominated by the orthogonality catastrophe, is given by the following

Hamiltonian:

$$\mathscr{H} = \sum_{k,l} \varepsilon_k \gamma^\dagger_{k,l} \gamma_{k,l} + \frac{t}{\sqrt{L}} \sum_k (\gamma^\dagger_{k,0} d + \text{h.c.}) + \frac{1}{L} \sum_{k,k'} V_l \left(\gamma^\dagger_{k,l} \gamma_{k',l} - \frac{1}{2} \right) \left(d^\dagger d - \frac{1}{2} \right) . \tag{57}$$

The operators $(\gamma, \gamma^\dagger)$ are the annihilation and creation operators of spinless conduction electrons with kinetic energy ε_k, while as before d^+ and d create or annihilate electrons in the localized level. The local chemical potential has been set to zero ($\varepsilon_d = 0$) and the Hamiltonian is particle–hole symmetric. The new index l is an orbital angular momentum index (or a channel index). Hybridization conserves point-group symmetry, so the localized orbital hybridizes with only one channel ($l = 0$). By contrast, the impurity couples to all channels via the interaction V_l. As we are summing over all moments (k, k') this interaction is local.

This problem may be mapped onto the anisotropic Kondo model [107]. Indeed, the transformation

$$\begin{aligned} & d^\dagger \to S^\dagger , \quad d^\dagger d - \frac{1}{2} \to S_z , \\ & t \to \frac{J_\perp, 0}{\sqrt{2\pi a}} , \quad 2V_l \to \sqrt{2} J_{z,l} - 2\pi v_F (\sqrt{2} - 1) \delta_{l,0} \end{aligned} \tag{58}$$

produces

$$\mathscr{H} = \sum_{k,\sigma,l} \varepsilon_k c^\dagger_{k,\sigma,l} c_{k,\sigma,l} + \frac{1}{2} J_{\perp,0} (S^\dagger s^-_l + \text{h.c.}) + \sum_l J_{z,l} S_z s_{z,l} . \tag{59}$$

Here, a is short distance cutoff. In the resulting (anisotropic multichannel) Kondo Hamiltonian, the spin operators $\mathbf{S}$ and $\mathbf{s}_l$ portray charge excitations of the local orbital and conduction band. The spin index in the resulting Kondo Hamiltonian should now be regarded as a charge label. Physically, this mapping is quite natural. The impurity may or may not have an electron, this is akin to having spin up or spin down. Similarly, the kinetic hybridization term transforms into a spin flip interaction term of the form $(S^\dagger d^- + \text{h.c.})$. As V_l couples to the occupancy of the impurity site, we might anticipate J_z to scale with V_l. The additional correction $(-2\pi v_F(\sqrt{2} - 1)\delta_{l,0})$ originates from the subtle transformation taking the original fermionic system into an effective spin model.

This problem has been solved by renormalization group methods (see Fig. 20). But simple arguments based on the X-ray edge singularity, orthogonality and recoil give the correct qualitative physics. When $t = 0$, the problem is that of the X-ray edge Hamiltonian (with $\varepsilon_d = 0$). When t is finite, the charge at the impurity orbital fluctuates (the impurity site alternately empties and fills). This generates, in turn, a fluctuating potential. The X-ray absorption spectrum is the Fourier transform of the particle–hole pair correlator

$$\Delta(\omega) \sim \langle \gamma^\dagger(t) d(t) d^\dagger(0) \gamma(0) \rangle_\omega . \tag{60}$$

This quantity, which is none other than the hybridization correlation function, should display the X-ray edge characteristics for large frequencies ($\omega > \Delta_{\text{eff}}$) where the effect of recoil is

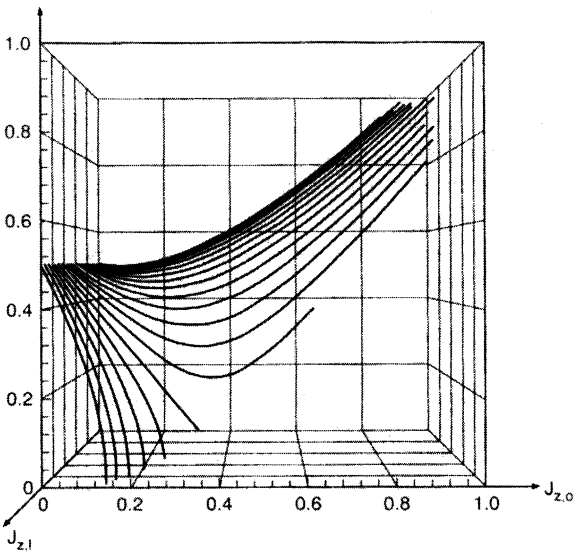

Fig. 20. The renormalization flow diagram for the model with finite range interactions according to [107]. The initial values are $J_{x,0}=0$, $J_{\perp,0}=0.5$, and $J_{x,l}$ varies from 0 to 1 in increments of 0.05. When $J_{z,l}$ becomes large enough (i.e., when V is large enough), the flow veers from the usual Kondo fixed point to a zero-hybridization ($J_{\perp,0}=0$) singular Fermi liquid.

unimportant

$$\Delta(\omega) \approx \Delta_0(\omega/W)^{\gamma}, \quad \gamma = -\frac{2\delta_0}{\pi} + \sum_l \frac{\delta_l^2}{\pi^2} \,. \tag{61}$$

The threshold frequency $\Delta_{\rm eff}$ is determined by the recoil energy. W is the bandwidth. The bare hybridization width $\Delta_0 \sim t^2/W$. The exponent in the singularity contains an excitonic shift ($-2\delta_0/\pi$) as well as an orthogonality contribution ($\sum_l \delta_l^2/\pi^2$). The recoil is cut off by $\Delta_{\rm eff}$. For frequencies $\omega < \Delta_{\rm eff}$ the electron gas becomes insensitive to the change in the potential. As the X-ray edge singularity is cut off at $\omega = O(\Delta_{\rm eff})$, self-consistency implies that

$$\Delta_{\rm eff} = \Delta(\omega = \Delta_{\rm eff}) \,. \tag{62}$$

This leads to the identification

$$\Delta_{\rm eff} = W(\Delta_0/W)^{\beta} \,, \quad \beta = 1/(1-\gamma) \tag{63}$$

so that for

$$\gamma < 1 \,, \quad \Delta_{\rm eff} \to 0 \quad \text{as } W \to \infty \,. \tag{64}$$

For $\gamma < 1$, a singular Fermi liquid emerges in which the hybridization of the localized d-orbital with the electron gas scales to zero at zero frequency. The actual value of γ determines the singular properties at low energy or temperature. In the single channel problem, such a scenario

occurs if the potential V_0 is sufficiently attractive. On mapping to the spin problem we find that this region corresponds to the singular Fermi liquid ferromagnetic Kondo problem. The scaling of the hybridization to zero corresponds, in the spin model, to $J_\pm \to 0$. In a renormalization group language, the flows impinge on the line of fixed points ($J_\perp = 0$, $J_z < 0$). In this regime, we recover, once again, a continuous set of exponents.

If the number of channels is large enough, the orthogonality catastrophe associated with the change in the number of particles on the impurity site is sufficiently strong to drive the hybridization to zero even for the case of repulsive interactions V or antiferromagnetic $J_{z,l}$.

In the singular regime various correlation functions may be evaluated [107]. For instance, the Green's function of the localized impurity

$$G_d(\tau) = -\langle T_\tau d(\tau) d^\dagger(0)\rangle \underset{\tau\to 0}{\to} \mathrm{e}^{-\sum_l (V_l/\pi v_F)^2 \ln(|\tau|+a)} . \tag{65}$$

The orthogonality induced by the fluctuation in the occupation number of the impurity site leads to the decay of the correlation function with a non-universal exponent. Owing to this orthogonality catastrophe the system behaves as a singular Fermi liquid. In the vicinity of the $t = 0$ fixed point, the self-energy due to hybridization

$$\Sigma \sim \omega^{1-\gamma} . \tag{66}$$

A line of critical points for $\gamma < 1$ is found. This bears a resemblance to the Kosterlitz–Thouless phenomenon [147]. The analogue to the emergence of vortices in the Kosterlitz–Thouless transition are instantons—topological excitations which are built of a succession of spin flips in time on the impurity site.

3.7. A model for mixed-valence impurities

We next consider a slightly more realistic model [204,240,245]

$$\begin{aligned}\mathscr{H} = &\sum_{k,\sigma,l} \varepsilon_{kl} c^\dagger_{k\sigma l} c_{k\sigma l} + \varepsilon_d n_{d,\uparrow} n_{d,\downarrow} + t \sum_\sigma (d^\dagger_\sigma c_{k\sigma 0} + \text{h.c.}) \\ &+ \sum_{k,k',l} V_{kk'l} \left(n_d - \frac{1}{2}\right) \left[\sum_\sigma c^\dagger_{k\sigma l} c_{k'\sigma l} - 1\right] .\end{aligned} \tag{67}$$

In this model, both spin and charge may be altered on the impurity site. This enhanced number of degrees of freedom implies that the states need to be specified by more quantum numbers. This also allows, a priori, for higher degeneracy. In the following, N screening channels, all of equal strength V, will be assumed. In the $U \to \infty$ limit, the spectrum of the impurity site may be diagonalized. The two lowest states are

$$\begin{aligned}&\eta^\dagger|0\rangle = |0,1\rangle \quad \text{with energy } E_\eta = -\frac{V\sqrt{N}}{4} - \frac{\varepsilon_d}{2} , \\ &\zeta^\dagger_\sigma|0\rangle = |\sigma,0\rangle \quad \text{with energy } E_\zeta = -\left[\left(\frac{\varepsilon_d}{2} - \frac{V\sqrt{N}}{4}\right)^2 + t^2\right]^{1/2} ,\end{aligned} \tag{68}$$

where in the brackets, the first entry is the charge and spin of the impurity spin and the second one is the compensating charge in the screening channels. Other states are elevated by energies $\mathcal{O}(V/\sqrt{N})$. The states satisfy the Friedel screening sum rule by having a small phase shift $\pi/2N$ in each of the N channels. The parameter V can be tuned to produce a degeneracy between the two states ($E_\eta = E_\zeta$)—the mixed valence condition. The enhanced degeneracy produces singular Fermi liquid like behavior.[21] A perturbative calculation for small ω yields a self-energy

$$\Sigma \sim [\omega \ln \omega + \mathrm{i}\omega \,\mathrm{sgn}(\omega)] + O[(\omega \ln \omega)^2] \,. \tag{69}$$

As a speculative note, we remark that this physics might be of relevance to quantum dot problems. Quantum dots are usually described in terms of the Anderson model. However, there are certainly other angular momentum channels whereby the local charge on the dot and the external environment can interact. As the external potential in the leads is varied, one is forced to pass through a potential in which this mixed valence condition must be satisfied. At this potential, the aforementioned singular behavior should be observed.

3.8. Multichannel Kondo problem

Blandin and Nozières [198] invented the multichannel Kondo problem and gave convincing arguments for its local singular Fermi liquid behavior. Since then, it has been solved by a multitude of sophisticated methods. For an overview of these and of applications of the multichannel Kondo problem, we refer to [227].

The multichannel Kondo problem is the generalization of the Kondo problem to the case in which the impurity spin has arbitrary spin S and is coupled to n "channels" of conduction electrons. The Hamiltonian is

$$\mathscr{H}_{mcK} = t \sum_{\ell=1}^{n} \sum_{i<j,\alpha} c_{i\alpha}^{(\ell)\dagger} c_{j\alpha}^{(\ell)} + \text{h.c.} + J\mathbf{S} \cdot c_0^{(\ell)\dagger} \sigma c_0^{(\ell)} \,. \tag{70}$$

Here ℓ is the channel index. Degeneracy, the key to SFL behavior, is enforced through having an equal antiferromagnetic coupling $J > 0$ in all the channels. When the couplings to the various channels are not all the same, at low enough temperatures a crossover to local Fermi-liquid behavior in the channel with the largest J_ℓ always occurs [7]. This crossover temperature is in general quite large compared to T_K because channel asymmetry is a *relevant* perturbation about the symmetric fixed point. Therefore, in comparing this theory with SFL behavior in experiments, one should ensure that one is above the crossover temperature.

The simple Kondo problem is the case $2S = 1 = n$. In this case, at low temperatures a singlet state of the impurity state and the conduction electron electrons in the appropriate channel is formed. In the general multichannel case in which $2S = n$, the physics is essentially the same, since there are exactly the right number of conduction electron channels to compensate the impurity spin at low temperatures. Thus, at low temperatures an effective spin 0 state is formed

[21] There is a singularity only in the local charge response at the impurity, not in the magnetic response. In this respect, the results of [244] are not completely correct.

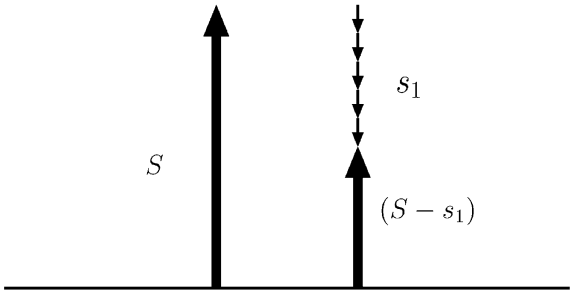

Fig. 21. In a multichannel problem, a (Hund's rule coupled) spin S is compensated by total spin s_1 $(=n/2)$ in n different conduction electron channels leaving a net uncompensated spin as shown. Alternatively exact compensation or over-compensation with special properties may arise, as discussed in the text.

again, and the properties of the *compensated Kondo problem* $2S = n$ at finite temperature is that of crossover from a weakly interacting problem above the Kondo temperature T_K to a strongly interacting problem below T_K.

The physics of the *underscreened Kondo problem* $2S > n$ is different.[22] In this case, there are not enough conduction electron spins to compensate the impurity spin. As a result, when the temperature is lowered and the effective coupling increases, only a partial compensation of the impurity spin occurs by conduction electrons with spin opposite to it. As depicted in Fig. 21, a net spin in the same direction as the impurity spin then remains at the impurity site. Since the conduction electrons with their spin in the same directions as the impurity spin can then still make virtual excitations by hopping on that site while the site is completely blocked for conduction electrons with opposite spin, a net *ferromagnetic* coupling remains between the remaining effective spin and the conduction electrons. As a result, the low-temperature physics of the underscreened Kondo problem is that of the ordinary *ferromagnetic Kondo problem*. To be more precise, the approach to the fixed point is analogous to that in the ferromagnetic Kondo problem along the boundary $J_z = -J_\pm$, because the impurity must decouple (become pseudo-classical) at the fixed point.

In the *overscreened Kondo problem* $2S < n$, there are more channels than necessary to compensate the impurity spin. At low temperatures, all n channels tend to compensate the impurity spin due to the Kondo effect. Channel democracy now causes an interesting problem. As the effective interaction J scales to stronger values, a local effective spin with direction *opposite* to the impurity spin results. This effective spin must have an effective *antiferromagnetic* interaction with the conduction electrons, since now the virtual excitations of conduction electrons with spins *opposite to the effective local spin* lower their energy. This then gives a new Kondo problem with a new effective interaction, and so on. Of course, in reality one does not get a succession of antiferromagnetic Kondo problems—the net effect is that a new stable finite-J fixed point appears. As sketched in Fig. 22, the renormalized effective interaction flows to this

[22] Since it is hard to imagine that the angular momentum states of the impurity are larger than that of the conduction electron states about the impurity, such models may be regarded to be of purely theoretical interest. See, however, Section 6.5.

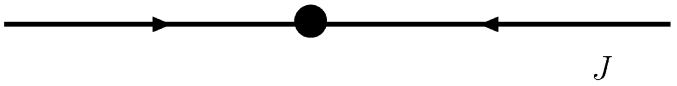

Fig. 22. Flow diagram for the degenerate over screened Kondo problem exhibiting a critical point.

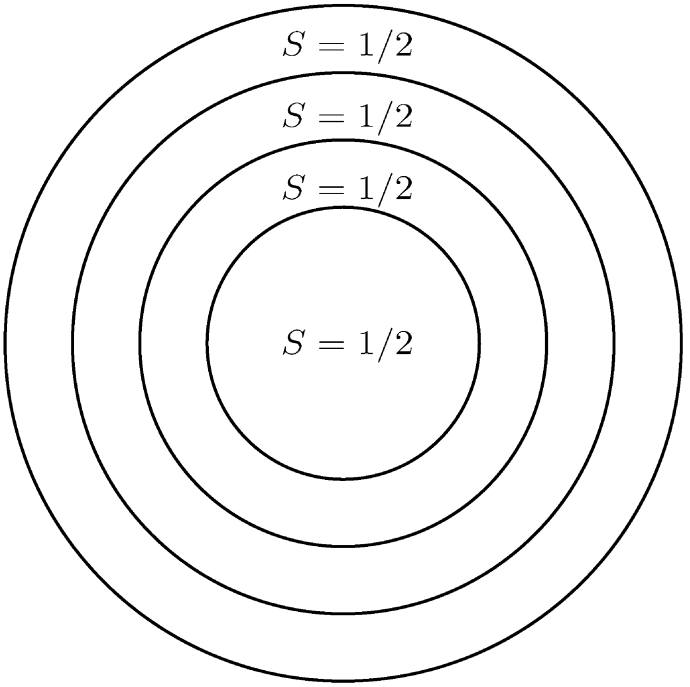

Fig. 23. Effective shells in energy space in Wilson's method. The first shell integrates over a fraction λ of the top of the band, the next shell λ of the rest, and so on. In the two-channel $S=1/2$ problem, an $S=1/2$ effective impurity is left at every stage of interpretation.

fixed point both from the strong-coupling as well as from the weak-coupling side. One can understand this intuitively from the above picture: if one starts with a large initial value of J, then in the next order of perturbation theory about it, the interaction is smaller, since in perturbation theory the effective interaction due to virtual excitations decreases with increasing J (see also Fig. 23). This means that J scales to smaller values. Likewise, if we start from small J, then initially J increases due to the Kondo scaling, but once J becomes sufficiently large, the first effect which tends to decrease J becomes more and more important. The finite-J fixed point leads to non-trivial exponents for the low-temperature behavior of quantities like the specific heat

$$\frac{C_v}{T} \propto \left(\frac{T}{T_K}\right)^{(n-2)/(n+2)} . \tag{71}$$

For $n=2$, the power-law behavior on the right-hand side is replaced by a $\ln T$ term.

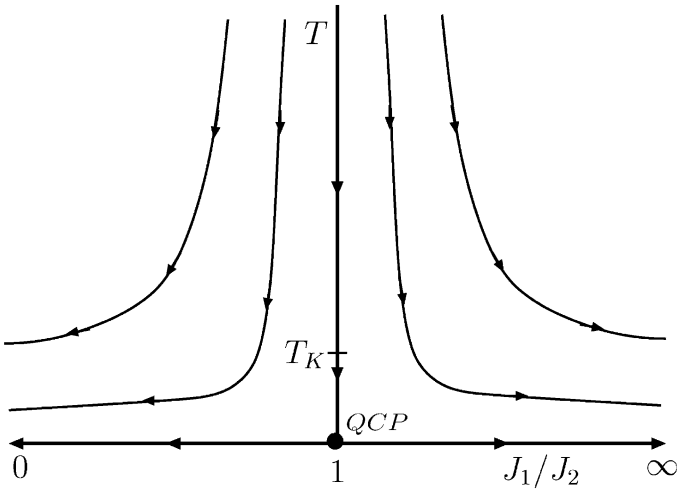

Fig. 24. Flow in temperature-anisotropy plane for the two-channel Kondo problem with coupling constant J_1 and J_2.

Another way of thinking about the problem is in the spirit of Wilson's renormalization group: Consider the problem of two channels interacting with a $S=\frac{1}{2}$ impurity. The conduction states can be expressed as linear combinations of concentric orbitals of conduction electrons around the impurity. These successive orbitals peak further and further away from the impurity. Consider first the exchange coupling of the orbitals in each of the two channels peaking at the impurity site. Each of them has $S=\frac{1}{2}$. Only one linear combination of the two channels, call it red, can couple, while the other (blue) does not. So, after the singlet with the impurity is formed, we are left with a $S=\frac{1}{2}$, color blue problem. We must now consider the interaction of this effective impurity with the next orbital and so on. It is obvious that to any order, we will be left with a spin $1/2$ problem in a color. Conformal field theory methods first showed that the ground state is left with $1/2\ln 2$ impurity. A nice application of the bosonization method [85] identifies the red and blue above as linear combinations of the fermions in the two channels so that one is purely real, the other purely imaginary. The emergence of new types of particles—the Majorana fermions in this case—often occurs at singular Fermi liquids.

As a detailed calculation confirms [7], the $J_1=J_2$ fixed point is unstable, and the flow is like that sketched in Fig. 24. This means that the $J_1=J_2$ fixed point is a quantum critical point: in the $T-J_1/J_2$ phase diagram, there is a critical point at $T=0$, $J_1/J_2=1$. Moreover, it confirms that asymmetry in the couplings is a relevant perturbation, so that the SFL behavior is unstable to any introduction of differences between the couplings to the different channels. The crossover temperature $T_\times$ below which two-channel behavior is replaced by the approach to the Kondo fixed point is [7]

$$T_\times = \mathcal{O}(T_K(\bar{J})[(J_1-J_2)/\bar{J}]^2)\,, \tag{72}$$

where $\bar{J}=(J_1+J_2)/2$.

The overscreened Kondo problem is again an example where that the SFL behavior is associated with the occurrence of degeneracy; the critical point requires degeneracy of the two orthogonal channels.

An interesting application of the two-channel Kondo problem is obtained by considering the spin label to play the role of the channel index, while the Kondo coupling is in the orbital angular momentum or crystal field states for impurities at symmetry sites in crystals [143,69,70,227]. Another possibility that has been considered is that of scattering of conduction electrons of two-level tunneling centers with different angular momentum states [302]. In this case, the tunneling model translates into a model with x and z coupling only, but this model flows towards a Kondo-type model with equal x and y spin coupling. For both types of proposed applications, one has to worry about the breaking of the symmetry, and about the question of how dilute the system has to be for a Kondo-type model to be realistic. Interesting results in the tunneling conductance of two metals through a narrow constriction, shown in Fig. 25 appear to bear resemblance to the properties expected of a degenerate two-channel Kondo effect [219,71], but this interpretation is not undisputed [290,220]. Applications to impurities in heavy fermions will be briefly discussed in Section 6.4.

3.9. The two-Kondo-impurities problem

In a metal with a finite concentration of magnetic impurities, an important question is what the (weak) interaction between the magnetic impurities does to the Kondo physics—that the effect might be substantial is already clear from the fact that the Kondo effect is seen in logarithmic corrections about the high-temperature local moment fixed point while the RKKY interaction between the moments mediated by the conduction electrons occurs as a power law correction.[23] Stated simply, $T_K \sim 1/N(0)\exp(-1/N(0)J)$ while the RKKY interaction $I \sim J^2N(0)$. The existence of mixed-valence and heavy fermion metals makes this much more than an academic question. The question of the competition between these two effects, and in particular whether long-range magnetic order can arise, was first posed by Varma [263] and by Doniach [78], who gave the obvious answer that RKKY interactions will be ineffective only when the Kondo temperature below which the local spin at each impurity is zero is much larger than the RKKY interaction I. Considering that $JN(0)$ is usually $\gg 1$, this is unlikely for $S = 1/2$ problems, but for large S, as encountered typically in rare earths and actinides, it is possible in some cases. However, the vast majority of rare earths and actinide compounds show magnetic order and no heavy fermion magnetic behavior. We will, however, only consider the $S = 1/2$ problem and work with unrealistic $JN(0)$ so that the competition between the Kondo effect and RKKY is possible.

Heavy-fermion phenomena typically occur in solids with partially filled inner shells (usually the f-shells of rare earth and actinide compounds) which hybridize very weakly with conduction electron bands formed of the outer orbitals (s, p and d) of the atoms [101,102]. They are usually

[23] Stated technically, the Kondo Hamiltonian is a marginal operator while the RKKY operator is a relevant operator about the local moment fixed point: In a perturbation calculation, the interaction produces corrections of $\mathcal{O}(1/T)$ compared to a $\ln(T)$ correction of the Kondo effect.

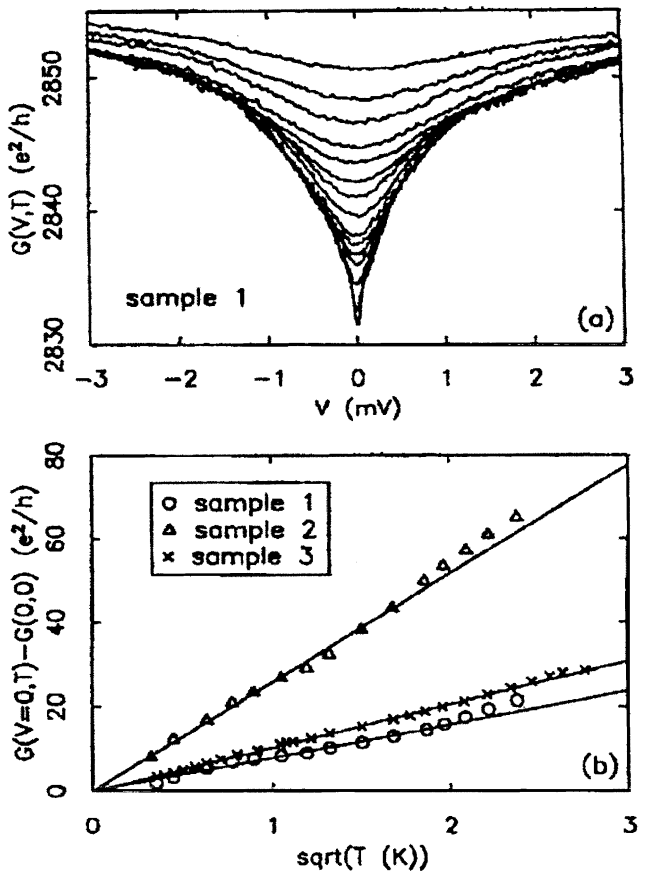

Fig. 25. (a) Differential conductance $G(V,T)$ as a function of voltage V in measurements on metal point contacts by Ralph et al. [219], for various temperatures ranging from 0.4 K (bottom curve) to 5.6 K (upper curve). Note the $\sqrt{V}$ type behavior developing as the temperature decreases; (b) the zero bias ($V=0$) conductance as a function of temperature for three different samples shows a $G(0,T)-G(0,0)\sim\sqrt{T}$ behavior. The scaling behavior as a function of voltage and temperature is consistent with two-channel Kondo behavior [219].

modelled by a *periodic array* of magnetic moments interacting locally with AFM exchange interaction with conduction electrons. The two-Kondo-impurity problem therefore serves as a first step to understanding some of the physics of heavy fermions that is not primarily associated with the occurrence of a collective phase.

In this subsection, we will summarize the results [136,137,8,9,245] for the *two-Kondo-impurity* problem: like the models we discussed above, this system also exhibits a quantum critical point at which SFL behavior is found. However, as for other impurity problems, an unrealistic symmetry must be assumed for a QCP and attendant SFL behavior.

The two-Kondo-impurity Hamiltonian is defined as

$$\mathscr{H}=t\sum_{k,\sigma}c^{\dagger}_{k\sigma}c_{k\sigma}+J[\mathbf{S}_1\cdot\sigma(r_1)+\mathbf{S}_2\cdot\sigma(r_2)]\,. \tag{73}$$

In this form, the problem has a symmetry with respect to the midpoint between the two impurity sites r_1 and r_2, and hence one can define even (e) and odd (o) parity states relative to this point. In the approximation that the k-dependence of the couplings is neglected [136], the two-Kondo-impurity Hamiltonian can then be transformed to

$$\mathscr{H} = \mathscr{H}_{\text{non-interacting}} + \sum_{kk'} (\mathbf{S}_1 + \mathbf{S}_2) \cdot [J_e c^\dagger_{k'e} \sigma c_{ke} + J_o c^\dagger_{k'o} \sigma c_{ko}]$$
$$+ \sum_{kk'} J_m (\mathbf{S}_1 - \mathbf{S}_2) \cdot [c^\dagger_{k'e} \sigma c_{ko} + c^\dagger_{k'o} \sigma c_{ke}] \,. \tag{74}$$

The coupling constants J_e, J_o, J_m are proportional to J with different numerical prefactors. The coupling between the spin and orbital channels generates an effective RKKY interaction

$$\mathscr{H}_{\text{RKKY}} = I_0(J_e, J_o, J_m) \mathbf{S}_1 \cdot \mathbf{S}_2 \tag{75}$$

between the two impurity spins, with $I_0 = 2 \ln 2 (J_e^2 + J_o^2 - 2J_m^2)$ for $t = 1$. A very important point to note is that neglecting the k-dependences of the coupling introduces particle–hole symmetry in the problem, which is generically absent.

The main results of a numerical Wilson-type renormalization group treatment of this model are the following:

(i) For ferromagnetic coupling $I_0 > 0$ or for a small antiferromagnetic coupling $I_0 > -2.24 T_K$, where T_K is the Kondo temperature of the single-impurity problem, one finds that there is a Kondo effect with

$$\langle \mathbf{S}_1 \cdot \mathbf{S}_2 \rangle \neq 0 \,, \tag{76}$$

unless I_0 is very small, $|I_0/T_K| \ll 1$. Since for uncorrelated impurity spins $\langle \mathbf{S}_1 \cdot \mathbf{S}_2 \rangle = 0$, (76) expresses that although in the RG language the RKKY interaction is an irrelevant perturbation, it is quite important in calculating physical properties due to large "corrections to scaling". Another feature of the solution in this regime is the fact that the phase shift is $\pi/2$ in *both* channels. This means that at the fixed point, the even-parity channel and the odd-parity channel have *independent* Kondo effects, each one having one electron pushed below the chemical potential in the Kondo resonance. As discussed below, this is due to particle–hole symmetry assumed in the model—without it, only the sum of the phase shifts in the two-channels is fixed.

(ii) There is no Kondo effect for $I_0 < -2.24 T_K$. In this case, the coupling between the impurities is so strong that the impurities form a singlet among themselves and decouple from the conduction electrons. There is no phase shift at the fixed point. Also, in this case, the total spin $S_{tot} = 0$, but the impurity spins become only singlet like, $\langle \mathbf{S}_1 \cdot \mathbf{S}_2 \rangle \approx -3/4$, for very strong coupling, $I_0 \ll -2.24 T_K$. So again there are important "corrections to scaling".

(iii) The point $I_0 = -2.24 T_K$ is a true critical point, at which the staggered susceptibility $\langle (\mathbf{S}_1 - \mathbf{S}_2)^2 \rangle / T$ diverges. Moreover, at this point the specific heat has a logarithmic correction to the linear T dependence, $C_v \sim T \ln T$, while the impurity spin correlation function $\langle \mathbf{S}_1 \cdot \mathbf{S}_2 \rangle$ becomes equal to $-1/4$ at this value.

Although the approximate Hamiltonian (74) has a true quantum critical point with associated SFL behavior, we stress that the analysis shows that this critical point is destroyed by any k-dependent $c^\dagger_{k'e} c_{ko}$ coupling. A coupling of this type is not particle–hole symmetric. As the approximate Hamiltonian (74) is particle–hole symmetric, these terms are not generated under

the renormalization group flow for (74). The physical two-Kondo-impurity problem (73), on the other hand, is *not* particle–hole symmetric. Therefore, the physical two-Kondo-impurity problem does *not* have a true quantum critical point—in other words, when the two-Kondo-impurity Hamiltonian (73) is approximated by (74) by ignoring *k-independent* interactions, relevant terms which destroy the quantum critical point of the latter Hamiltonian are also dropped. This has been verified by an explicit analysis retaining the symmetry breaking terms [244].

An illuminating way to understand the result for the two-impurity-Kondo problem, is to note that the Hamiltonian can be written in the following form:

$$\mathscr{H} = \begin{bmatrix} \begin{bmatrix} \mathscr{H}^{\text{even}}_{S=0} & 0 \\ 0 & \mathscr{H}^{\text{odd}}_{S=0} \end{bmatrix} & \begin{bmatrix} 0 & \mathscr{H}_{\text{mix}} \\ \mathscr{H}_{\text{mix}} & 0 \end{bmatrix} \\ \begin{bmatrix} 0 & \mathscr{H}_{\text{mix}} \\ \mathscr{H}_{\text{mix}} & 0 \end{bmatrix} & \begin{bmatrix} \mathscr{H}^{\text{even}}_{S=1} & 0 \\ 0 & \mathscr{H}^{\text{odd}}_{S=1} \end{bmatrix} \end{bmatrix}, \tag{77}$$

where $\mathbf{S} = \mathbf{S}_1 + \mathbf{S}_2$ is the total impurity spin.

In this representation, the Hamiltonian $\mathscr{H}_{\text{mix}}$ couples the $S = 0$ and 1 state, and the following interpretation naturally emerges: for large antiferromagnetic values of I_0, $\mathscr{H}_{S=0}$ is lower in energy than $\mathscr{H}_{S=1}$, while for large ferromagnetic coupling I_0, the converse is true. The two-Kondo-impurity coupling can thus be viewed as one in which by changing I_0, we can tune the relative importance of the upper left block and the lower right block of the Hamiltonian. In general, the two types of states are mixed by $\mathscr{H}_{\text{mix}}$, but at the fixed point $\mathscr{H}^*_{\text{mix}} \to 0$. This implies that there is a critical value of I_0/T_{K} where the $S = 0$ and 1 states are degenerate, and where SFL behavior occurs. At this critical value, the impurity spin is a linear combination of a singlet and triplet state with $\langle \mathbf{S}_1 \cdot \mathbf{S}_2 \rangle = -1/4$ (i.e., a value in between the singlet value $-3/4$ and the triplet value $1/4$) and the singular low-energy fluctuations give rise to the anomalous specific heat behavior.

Within this scenario, the fact that the susceptibility χ is divergent at the critical point signals that a term $\mathbf{H} \cdot (\mathbf{S}_1 - \mathbf{S}_2)$ lifts the spin degeneracy. Moreover, the leading irrelevant operators about the fixed point are all divergent at the critical point—of course, this just reflects the breakdown of the Fermi-liquid description.

The reason for $\mathscr{H}_{\text{mix}} \to 0$ is as follows. $\mathscr{H}_{\text{mix}}$ can only be generated from the last term in (74) which is particle–hole symmetric because under even–odd interchange, both the spin term and the fermion terms change sign. At the Kondo-fixed point, the leading operators must all be biquadratic in fermions. An $\mathscr{H}_{\text{mix}}$ in that case would be of the form $c^\dagger_{k\sigma\text{e}} c_{k'\sigma\text{o}}$ and such a term by itself would break particle–hole symmetry, not consistent with the last term in (74).

In the two-Kondo-impurity problem, one again encounters the essentials of degeneracy for quantum critical points and the need for (unphysical) constraints to preserve the singularity. Once again, new types of quantum numbers can be invoked in the excitations about the QCP.

From the point of view of understanding actual phenomena for problems with a moderate concentration of impurities or in reference to heavy fermion compounds, the importance of the solution to the two-Kondo-impurity problem is the large correction to scaling found in the Wilson-type solution away from the special symmetries required to have a QCP. These survive

quite generally and must be taken into account in constructing low-energy effective Hamiltonians in physical situations.

4. SFL behavior for interacting fermions in one dimension

We have already noted the unique phase-space restrictions for scattering of fermions in one dimension. For low-energy processes, one may confine attention to one-particle states in the vicinity of the two Fermi-points, $\pm k_F$. These two points are always nested for particle–hole scattering (both in the singlet and the triplet spin-channels) and lead to singularities in the appropriate correlation functions. The upper cut-off singularities is the bandwidth, just as the Cooper singularity in the particle–particle channel. The competition between these singularities lead to rather unique low-energy correlation functions in one dimension.

The simplicity due to the sharp restriction in phase space allows a thorough analysis of the one-dimensional problem. A variety of elegant mathematical techniques, including exact solutions in certain non-trivial limits, have been employed to analyze the problem of interacting electrons in one dimension. There are also various different ways of thinking about the one-dimensional problem, each of which provides insight into the general problem of singular Fermi liquids. We shall touch on these different aspects without going into the details of the technical steps leading to their derivation. To get a flavor for the mathematical nature of the results and their differences from Fermi liquids, we will present the derivation of the diagonalizable form of the Hamiltonian as well as exhibit the principal thermodynamic properties and correlation functions. Detailed reviews of the technical steps in the various solutions as well as numerical calculations may be found in [113,246]. We also discuss the special aspects of the one-dimensional problem and the methods and whether the results can be extended to higher dimensions.

We first present the Hamiltonian and the $T = 0$ "phase diagram" (obtainable by perturbative RG) which identifies the principal singularities for various coupling constants in the problem. This will be followed by a presentation of some of the results of the exact solution of the simplified model known as the Tomonaga–Luttinger model as well as the more general model for special values of the coupling constants (along the so-called "Luther–Emery" line [163]).

Since in one dimension, hard core bosons and spinless fermions cannot go around each other, special features in their statistics may be intuitively expected. A special feature of one-dimensional physics is that the low-energy excitations can be described by either fermions or bosons. The bosonic description of the Tomonaga–Luttinger model is especially attractive and will be presented below.

A related distinctive feature of one-dimensional physics is that single-particle as well as multiple-particle correlation functions are expressible in terms of independent charge and spin excitations, which, in general, propagate with different velocities.[24] This feature has been shown

[24] Even a Fermi liquid displays distinct energy scales for charge and spin (particle–hole) fluctuations because of the difference in the Landau parameters in the spin-symmetric and spin-antisymmetric channels. The phrase spin–charge separation should therefore be reserved for situations, as in one dimension, where the single-particle excitations separate into objects which carry charge alone and which carry spin alone.

to arise due to extra conservation laws in one dimensions [51,179]. As we shall discuss, an extension of charge–spin separation to higher dimensions is unlikely because there are no such conservation laws.

The one-dimensional singularities may also be seen as a manifestation of the orthogonality catastrophe [20] that we discussed in Section 3.4. We shall see that this feature disappears in higher dimension due to the effects of recoil.

Some cases where the one-dimensional models solved are experimentally realized include the edge states of quantum Hall liquids and quasi-one-dimensional organic and inorganic compounds [83,84]. In the latter case, the asymptotic low-energy properties are, however, unlikely to be those of the one-dimensional models because of the inevitable coupling to the other dimensions which proves to be a relevant perturbation. Nonetheless, data on carbon nanotubes [74] discussed in Section 4.11 show clear evidence of one-dimensional interacting electron physics. Several one-dimensional spin chains problems can also be transformed into problems of one-dimensional fermions [225].

4.1. The one-dimensional electron gas

In this section, we shall outline the special features of the one-dimensional problem which make it soluble and show its singular properties. As it often happens, solubility implies finding the right set of variables in terms of which the Hamiltonian is expressed as a set of harmonic oscillators.

In one dimension, the "Fermi surface" is reduced to the two Fermi points $k = \pm k_F$. At low energies, particles may move only to the right or to the left with momenta of almost fixed magnitude $k \simeq rk_F$ (belonging, to either the right ($r = 1$) or to the left ($r = -1$) moving branch).

Due to the constrained character of one-dimensional motion, the phase space for collisions between particles is severly limited compared to higher dimensions. Let us start off by an inspection of the possible collisions. By energy and lattice momentum conservation alone, all the low-energy scattering processes may be classified into four interactions. These interactions are schematically illustrated in Fig. 26.

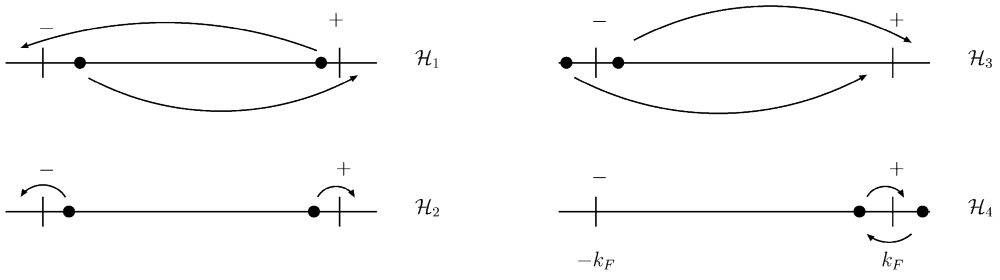

Fig. 26. Pictorial representation of the low-energy interaction terms in the one-dimensional problem. After [181]. The "+" and "−" points are a shorthand for the two Fermi points $k = k_F$ and $(-k_F)$, respectively.

By observing this small set of allowed processes we note that the general Hamiltonian describing the low-energy dynamics may be split into four parts

$$\mathscr{H} = \mathscr{H}_0 + \mathscr{H}_{\text{forward}} + \mathscr{H}_{\text{backward}} + \mathscr{H}_{\text{Umklapp}} \,. \tag{78}$$

In Eq. (78) $\mathscr{H}_0$ is the free electron Hamiltonian

$$\mathscr{H}_0 = \sum_k \varepsilon_k c_k^\dagger c_k \,. \tag{79}$$

The other three terms describe the interactions depicted in Fig. 26.

The Umklapp process ($\mathscr{H}_{\text{Umklapp}}$), denoted conventionally by $\mathscr{H}_3$ as in Fig. 26, describes interactions in which the lattice momentum is conserved yet plain momentum is not: i.e., $k_1^{\text{in}} + k_2^{\text{in}} = k_1^{\text{out}} + k_2^{\text{out}} + G$ with $G \neq 0$ a non-vanishing reciprocal lattice "vector" (a scalar in this one-dimensional case). From Fig. 26, we note that such a process can occur only in the special case when $4k_F$ is very close to a reciprocal lattice "vector". It follows that except for half-filling of the one-dimensional band, such a process cannot occur. So, in general, one needs to study only forward ($\mathscr{H}_2$ or $\mathscr{H}_4$) processes or backwardscattering ($\mathscr{H}_1$) processes. Note that $\mathscr{H}_{\text{forward}}$ describes interactions with small momentum transfer and $\mathscr{H}_{\text{backward}}$ momentum transfer close to $2k_F$.

We will now introduce a few simplifying assumptions which form the backbone of all *Luttinger liquid* treatments of the one-dimensional problem:

(1) In Eq. (79), ε_k may be expanded about the two Fermi points to produce the linear dispersion

$$\varepsilon_r(k) = v_F(rk - k_F) + E_F \tag{80}$$

with v_F and E_F denoting the Fermi velocity and the Fermi energy, respectively. As before, $r = \pm 1$ is the right/left branch index.

(2) The band cutoff is taken to be infinite. These assumptions lead us to focus attention on a simplified system in which there are two independent flavors of particles (right and left movers) each of which has a linear dispersion relation with unbounded momentum and energy. The simplified energy spectrum is shown in Fig. 10: an infinite "sea" of unphysical (negative energy) states below the usual Fermi sea. The added infinity of unphysical states with $\varepsilon_k < 0$ have a negligible physical effect (as they are far removed from the chemical potential, they enable the problem to be tractable mathematically).

First we explain how the one-dimensional Hamiltonian can be expressed equivalently in terms of Bosonic variables. Define the charge-density operators ρ_r and the spin-density operators S_r for the two branches, $r = \pm$, by

$$\rho_r = \Sigma_{\sigma=\pm1} \psi_{r,\sigma}^\dagger \psi_{r,\sigma}, \quad S_r^z = \tfrac{1}{2} \Sigma_{\sigma,\sigma'} \psi_{r,\sigma}^\dagger \tau_{\sigma,\sigma'}^z \psi_{r,\sigma'} \,, \tag{81}$$

where τ^z is a Pauli matrix. The Fourier transform of the particle-density operators is

$$\rho_{r,\sigma}(q) = \sum_k c_{r,\sigma,k+q}^\dagger c_{r,\sigma,k} = \rho_{r,\sigma}^\dagger(-q) \,. \tag{82}$$

A pivotal point is that, within the stated assumptions, these Fermi bilinears may be explicitly shown to obey Bose commutation relations.[25]

We will soon see that these density operators are not merely bosonic but that, in the linear-band approximation, they may also be viewed as raising and lowering operators which reduce the Hamiltonian Eq. (78) to a simple quadratic (oscillator) form.

With our first assumption, we may linearize ε_k about the two Fermi points for low-energy processes; the energy of a particle–hole pair created by $\rho_{r,\sigma}(q)$:

$$\varepsilon_{r,k+q} - \varepsilon_{r,k} = rv_{\mathrm{F}}q \tag{83}$$

is *independent of* k in a Luttinger liquid. (This step cannot be implemented in higher dimensions.) In other words, states created by $\rho_{r,\sigma}(q)$ are linear combinations of individual electron–hole excitations all of which have the same energy and are therefore eigenstates of $\mathscr{H}_0$. It follows that for $q > 0$, the bosonic $\rho_{r=+,\sigma}(q)$ $[\rho_{r=-,\sigma}(q)]$ is a raising [lowering] operator. The kinetic energy $\mathscr{H}_0$ may be expressed in terms of the density operators

$$\mathscr{H}_0 = \frac{2\pi v_{\mathrm{F}}}{L}\sum_{r=\pm}\sum_{q>0}\rho_{r,\sigma}(rq)\rho_{r,\sigma}(-rq)\ . \tag{84}$$

Upon separating the densities on a given branch into charge and spin pieces

$$\rho_{r\sigma}(x) = \tfrac{1}{2}[\rho_r(x) + \sigma S^z_r(x)]\ , \tag{85}$$

the *free Hamiltonian* may be expressed as a sum in the spin and charge degrees of freedom

$$\mathscr{H}_0 = \sum_r \mathscr{H}_0[\rho_r] + \sum_r \mathscr{H}_0[S^z_r]\ . \tag{86}$$

It follows that in the non-interacting problem, spin and charge have identical dynamics and propagate in unison. Once interactions are introduced, the electron will "*fractionalize*" and spin and charge dynamics will, in general, differ.

We now turn to a closer examination of the various interaction terms in the Hamiltonian. The part describing the forward scattering (small momentum transfer) events $\rightarrow (k_{\mathrm{F}},\sigma;k_{\mathrm{F}},\sigma')$ may be further subdivided (as shown) into the processes $(k_{\mathrm{F}},\sigma;-k_{\mathrm{F}},\sigma') \rightarrow (k_{\mathrm{F}},\sigma;-k_{\mathrm{F}},\sigma')$ and $(k_{\mathrm{F}},\sigma;k_{\mathrm{F}},\sigma')$, respectively

$$\mathscr{H}_{\text{forward}} = \mathscr{H}_2 + \mathscr{H}_4 \tag{87}$$

---

[25] Explicitly, for the right movers the only non-vanishing commutation relations read $[\rho_{r=+1,\sigma}(-q),\rho_{r=+1,\sigma}(q)] = \sum_k (n_{k-q} - n_k)$. By invoking the last of the stated Luttinger liquid assumptions, we find that $\sum_k(n_{k-q} - n_k) = \sum_{k>k_0}(n_{k-q} - n_k) = \sum_{k_0-q\leqslant k\leqslant k_0} n_k = Lq/2\pi$. Here, k_0 is a high momentum cut-off which is taken to infinity at the end of the calculation. Similar relations are found for the left movers ($r = -1$). Taken together, we find the operators $\rho_{r,\sigma}(q)$ to be unnormalized Bose operators: $[\rho_{r,\sigma}(q),\rho_{r',\sigma'}] = \delta_{\sigma,\sigma'}\delta_{r,r'}\delta_{q+q',0}(rqL/2\pi)$.

with

$$\mathscr{H}_2 = \frac{1}{L}\sum_q \sum_{\sigma\sigma'} g_2^{\sigma\sigma'} \rho_{+,\sigma}(q)\rho_{-,\sigma'}(-q)\ , \tag{88}$$

$$\mathscr{H}_4 = \frac{1}{2L}\sum_q \sum_{\sigma\sigma'} g_4^{\sigma\sigma'} [\rho_{+,\sigma}(q)\rho_{+,\sigma'}(-q) + \rho_{-,\sigma}(q)\rho_{-,\sigma'}(-q)]\ . \tag{89}$$

The operators $\rho_{r,\sigma}$ involve a creation and annihilation operator on the same branch. Let us further define also operators ρ_σ^r formed from bilinears of fermions on opposite branches

$$\rho_\sigma^r = \sum_k c^\dagger_{r,\sigma,k} c_{-r,\sigma,k+q}\ . \tag{90}$$

In terms of these, the Hamiltonian describing backscattering interactions (the scattering event $(+k_F,\sigma;-k_F,\sigma') \to (-k_F,\sigma;k_F,\sigma')$ and its reverse) becomes

$$\mathscr{H}_{\text{backwards}} = \mathscr{H}_1 = g_1 \sum_q \sum_{\sigma\sigma'} g_1^{\sigma\sigma'} \rho_\sigma^+(q)\rho_{\sigma'}^-(-q) \tag{91}$$

and the Umklapp term reads

$$\mathscr{H}_{\text{umklapp}} = \frac{1}{2L}\sum_q \sum_{\sigma\sigma'} g_3^{\sigma\sigma'} [\rho_\sigma^+(q)\rho_{\sigma'}^+(-q) + \rho_\sigma^-(q)\rho_{\sigma'}^-(-q)]\ . \tag{92}$$

The behavior of $g_i^{\sigma,\sigma'}(q)$ in momentum space translates into corresponding real-space couplings. If the couplings $\{g_i(q)\}$ are momentum independent constants, then the corresponding real-space interactions are local and describe contact collisions. Unless otherwise stated, this is the case that we shall consider.

In all these expressions, the coupling constants may be spin-dependent

$$g_i^{\sigma\sigma'} = g_{i\parallel}\delta_{\sigma\sigma'} + g_{i\perp}\delta_{\sigma-\sigma'}\ . \tag{93}$$

As the terms $H_{1\parallel}$ and $H_{2\parallel}$ describe the same process, we may set $g_{1\parallel} = 0$ with no loss of generality. As already mentioned, Umklapp processes are important only when $4k_F$ is a reciprocal lattice vector so that all scattering particles may be near the Fermi points. The condition for spin rotation invariance $[\mathscr{H}, \vec{S}] = 0$ reduces the number of independent coupling constants further

$$g_{2\perp} - g_{1\perp} = g_{2\parallel} - g_{1\parallel}\ . \tag{94}$$

On examining all four possible interactions, we note that the forward scattering $\mathscr{H}_2$ and $\mathscr{H}_4$ break no symmetries but that $\mathscr{H}_1$ and $\mathscr{H}_3$ may; The latter leads to qualitatively new properties. Backscattering breaks the $SU(2)_L \otimes SU(2)_R$ symmetry of spin currents for each of the individual left–right moving fronts. Gaps (or condensates) are usually associated with broken symmetries, and this case is no exception: A spin gap $\Delta_s > 0$ is dynamically generated when these interactions (i.e., an attractive backscattering (H_1) process $(+k_F,\sigma;-k_F,\sigma') \to (-k_F,\sigma;k_F,\sigma')$).

Similarly, the Umklapp process (H_3) breaks the conservation of individual charge currents; a charge gap $\Delta_c > 0$ is associated with this broken Galilean invariance. The gaps open up only if the interactions are attractive. On a formal level, Umklapp breaks independent right and

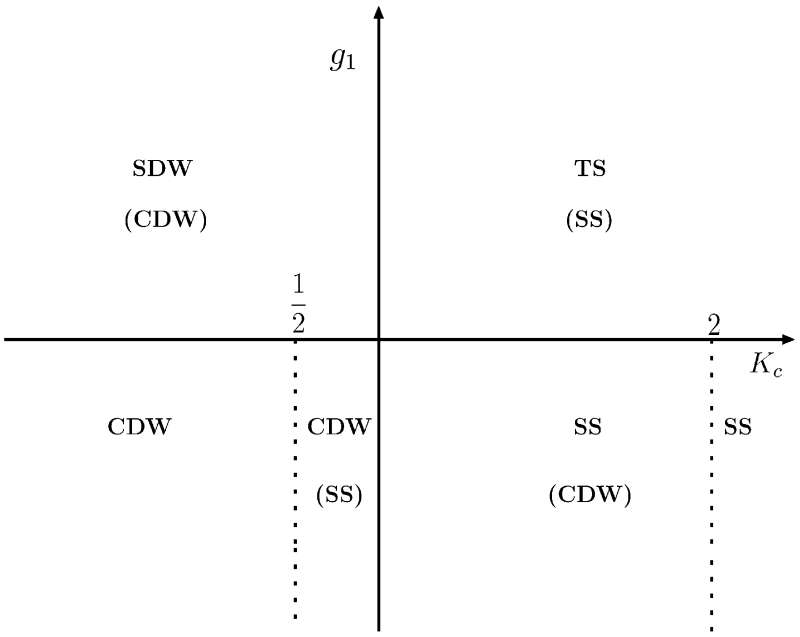

Fig. 27. Phase diagram for one-dimensional interacting fermions in the (K_c, g_1) plane with $g_{1\|} = 0$ in Eq. (93) and K_c given by Eq. (103). *SDW* and (*CDW*) in the upper left quadrant indicates that both the spin density wave susceptibility and the charge-density wave susceptibility diverge as $T \to 0$, but that the spin-density wave susceptibility diverges a factor $\ln^2 T$ faster than the charge-density wave susceptibility—see Eq. (112). Other sectors are labeled accordingly. From [233].

left $(U(1)_L \otimes U(1)_R)$ charge conservation symmetry leaving the system with only a single $U(1)$ symmetry.

We shall later show in Section 4.7 how unbroken $U(1)_L \otimes U(1)_R$ and $SU(2)_L \otimes SU(2)_R$ symmetries (in models without Umklapp or backscattering) allow independent left–right conservation laws with interesting consequences.

Before discussing the exact solutions to sub-classes of the above general model, it is good to obtain physical insight through a "phase diagram" obtained by the perturbative renormalization group flow equations [246,233]. Due to the limitation of phase space, the one-dimensional problem is subject to all manners of competing singularities. In one dimension, there are no truly ordered phases of course, but at $T = 0$ correlation functions diverge and one may say that there is algebraic long-range order. One may thus determine a "phase diagram" according to which susceptibilities diverge as $T \to 0$: the one associated with singlet superconductivity (*SS*), triplet superconductivity (*TS*), a charge-density wave (*CDW*) at $2k_F$, and a spin-density wave (*SDW*) at $2k_F$. The expressions for these susceptibilities are given in Eq. (112) below, and the resulting "phase diagram" is shown in Fig. 27.[26]

[26] It is a useful exercise (left to the reader) to see how Fig. 27 corresponds to the intuitive notions of what kind of interaction, short- or long-range, in singlet or triplet channel, favors which instability. These notions are transferrable to higher dimensions.

4.2. The Tomonaga–Luttinger model

With forward scattering alone in (78) and after linearizing the kinetic energy, we obtain the Tomonaga–Luttinger (T–L) model. In terms of fermion field operators $\psi_{r,\sigma}(x)$ and $\psi^{\dagger}_{r,\sigma}(x)$, and density and spin operators $\rho_r(x)$ and $S^z_r(x)$ in real space, the T–L model is

$$\mathscr{H}^{\mathrm{T-L}} = \int \mathrm{d}x \left[-v_{\mathrm{F}} \sum_{r,\sigma=\pm} r\psi^{\dagger}_{r,\sigma} \mathrm{i}\partial_x \psi_{r,\sigma} + \frac{1}{2} \sum_{r=\pm} g_{2,c}\rho_r(x)\rho_{-r}(x) \right] + \sum_{r=\pm} g_{4,c}\rho_r(x)\rho_r(x) + 2\sum_{r=\pm} g_{2,s} S^z_r(x) S^z_{-r}(x) + g_{4,s} S^z_r(x) S^z_r(x) \,, \tag{95}$$

where

$$g^c_i = \frac{g_{i\parallel} + g_{i\perp}}{2}, \quad g^s_i = \frac{g_{i\parallel} - g_{i\perp}}{2} \,. \tag{96}$$

Note that the $g_{2,s}$ term is the only term which breaks $SU(2)$ spin symmetry. The T–L model is exactly solvable. After all, as previously noted, the (Dirac-like) kinetic energy Hamiltonian $\mathscr{H}_0$ is also quadratic in the density operators. So the Hamiltonian is readily diagonalized by a Bogoliubov transformation whereupon the Hamiltonian becomes a sum of two *independent* (harmonic) parts describing non-interacting charge- and spin-density waves: the charge- and spin-density waves are the collective eigenmodes of the system.

The simplest way to solve the TL model and to explicitly track down these collective modes is via the bosonization of the electronic degrees of freedom.[27] The bosonic representation of the fermionic fields proceeds by writing [113,193,225]

$$\psi_{r,\sigma}(x) = \lim_{a\to 0} \frac{\exp[\mathrm{i}r(k_{\mathrm{F}}x + \Phi_{r\sigma}(x))]}{\sqrt{2\pi a}} F_{r\sigma} \,, \tag{97}$$

where a is a short distance regulator. $\Phi_{r\sigma}(x)$ satisfies

$$[\Phi_{r\sigma}(x), \Phi^{\dagger}_{r',\sigma'}(x')] = -\mathrm{i}\pi\delta_{r,r'}\delta_{\sigma,\sigma'}\,\mathrm{sign}(x - x') \,. \tag{98}$$

The so-called Klein factors[28] $F_{r\sigma}$ are chosen such that the proper fermionic anticommutation relations are reproduced. The exponential envelope $\exp[\mathrm{i}\Phi_{r\sigma}(x)]$ represents the slow bosonic collective degrees of freedom which dress the rapidly oscillating part $F_{r\sigma}\exp[\mathrm{i}k_{\mathrm{F}}x]$ describing the energetic particle excitations near the Fermi points.

---

[27] The reader should be warned that many different conventions abound in the literature.

[28] The Klein factors connect states differing by one electron. When the thermodynamic limit is taken in a gapless system, there is, for all practical purposes (the computation of correlation functions), no differences between states containing N and $N \pm 1$ particles. However, when gaps open up, giving rise to finite correlation lengths, caution must be exercised when dealing with these operators. The literature contains several examples of calculations which were later discovered to be incorrect, precisely due to this subtlety.

The slowly varying fields Φ may be written in terms of the bosonic fields $\phi_{c,s}$ and their conjugate momenta $\partial_x\theta_{c,s}$

$$\Phi_{r,\sigma} = \sqrt{\pi/2}[(\theta_c - r\phi_c) + \sigma(\theta_s - r\phi_s)] \,. \tag{99}$$

In terms of the new variables, the familiar charge and spin densities are

$$\rho(x) = \sum_r \rho_r(x) = \sqrt{\frac{2}{\pi}}\partial_x\phi_c, \quad S^z(x) = \sum_r S^z_r(x) = \sqrt{\frac{1}{2\pi}}\partial_x\phi_s \,. \tag{100}$$

In the $(\theta_{c,s}, \phi_{c,s})$ representation, the Tomonaga–Luttinger Hamiltonian becomes a sum of two decoupled sets of oscillators describing the gapless charge and spin density wave eigenmodes

$$\mathscr{H}^{\mathrm{T-L}} = \int \mathrm{d}x \sum_{v=c,s} \frac{v_v}{2}\left[K_v(\partial_x\theta_v)^2 + \frac{(\partial_x\phi_v)^2}{K_v}\right] \equiv \mathscr{H}_s^{\mathrm{T-L}} + \mathscr{H}_c^{\mathrm{T-L}} \,. \tag{101}$$

The velocities of the collective charge and spin modes are easily read off by analogy to a harmonic string

$$v_{c,s} = \sqrt{\left(v_{\mathrm{F}} + \frac{g_4^{c,s}}{\pi}\right)^2 - \left(\frac{g_2^{c,s}}{\pi}\right)^2} \,. \tag{102}$$

Likewise, the moduli determining the power-law decay of the correlations are

$$K_{c,s} = \sqrt{\frac{\pi v_{\mathrm{F}} + g_4^{c,s} - g_2^{c,s}}{\pi v_{\mathrm{F}} + g_4^{c,s} + g_2^{c,s}}} \,. \tag{103}$$

In Section 4.7, we shall show how the above expressions for the spin and charge density wave velocities simply follow from the conservation of left and right moving particles in the T–L model.

As previously noted, the charge and spin velocities are degenerate in the non-interacting model. When interactions are introduced, the charge and spin velocities (v_c and v_s) as well as the energy to create spin and charge excitations (v_s/K_s and v_c/K_c, respectively) become different. The charge constant K_c is less than 1 for repulsive interactions, which elevates the energy of the charge excitations, while K_c is greater than 1 for attractive interactions.

4.3. Thermodynamics

As evident from (101) the contributions of the independent charge and spin modes must appear independently in most physical quantities.

The specific heat coefficient is found to be

$$\gamma/\gamma_0 = \frac{v_{\mathrm{F}}}{2}\left(\frac{1}{v_c} + \frac{1}{v_s}\right) \,, \tag{104}$$

where $\gamma = \gamma_0$ for the non-interacting system.

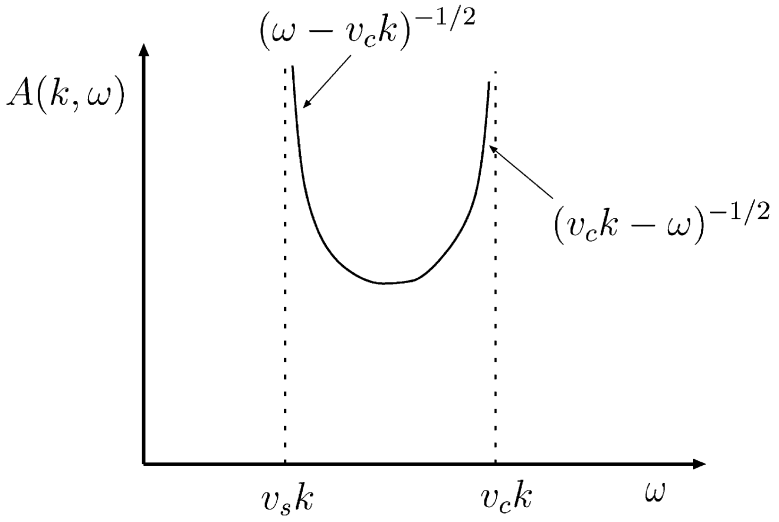

Fig. 28. The zero-temperature spectral function $A(k,\omega) = \mathrm{Im}\{G^{<}_{r=+1}(k,\omega)\}$ as a function of ω for the case ($g_2 = 0,\ g_4 \neq 0$)—the "one-branch Luttinger liquid" in which the spin and charge velocities differ but for which the correlation exponents retain their canonical value $K_c = 1$ according to (103). In the figure $v_c > v_s$ and $k > 0$ are assumed. Note the inverse square root singularities. This is a consequence of $K_c = 1$ which makes $\gamma_c = 0$. After Voit [278].

The spin susceptibility and the compressibility are also readily computed from (101)

$$\chi_0 = v_F/v_s, \quad \kappa/\kappa_0 = v_F K_c/v_c \ , \tag{105}$$

where χ_0 and κ_0 are the susceptibility and compressibility of the non-interacting gas. The Wilson ratio, already encountered in our discussion of the Kondo problem in Section 3.2,

$$R_W = \frac{\chi/\chi_0}{\gamma/\gamma_0} = \frac{2v_c}{v_c + v_s} \tag{106}$$

deviates from its Fermi-liquid value of unity by an amount dependent on the relative separation between the spin and charge velocities.

4.4. One-particle spectral functions

We display the calculated zero temperature spectral functions of the T–L model [278] in order to point out the differences from the Landau Fermi-liquid discussed in Section 2

$$\begin{aligned} A(k,\omega) &\approx (\omega - v_c(k - k_F))^{2\gamma_c - 1/2} |\omega - v_c(k - k_F)|^{\gamma_c - 1/2} \quad (v_c > v_s) \ , \\ A(k,\omega) &\approx (\omega - v_s(k - k_F))^{\gamma_c - 1/2} |\omega - v_s(k - k_F)|^{2\gamma_c - 1/2} \quad (v_c < v_s) \ . \end{aligned} \tag{107}$$

These spectral functions are sketched in Fig. 28 for the case $g_2 = 0$ and in Fig. 29 for the general case. Note that unlike the single quasiparticle pole in $A(k,\omega)$ in a Landau Fermi liquid, $A(k,\omega)$

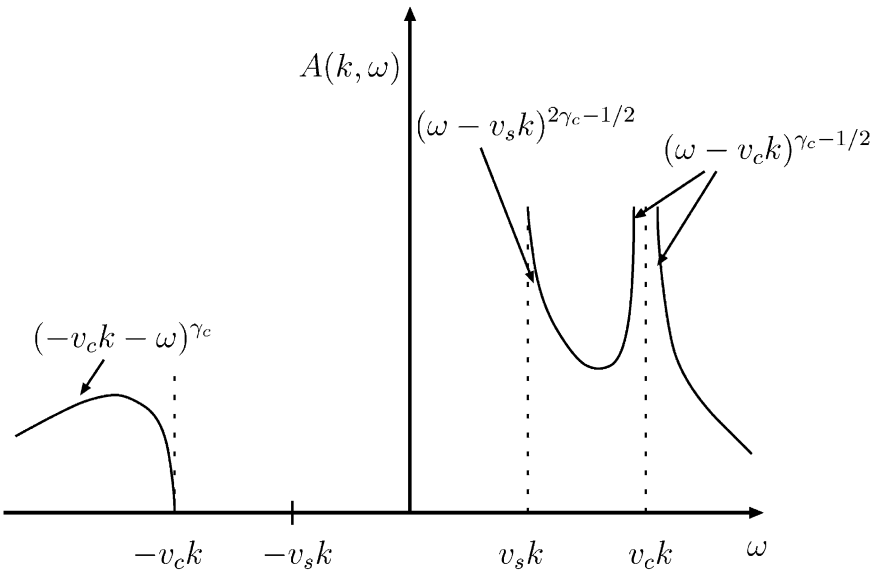

Fig. 29. The generic ($g_2 \neq 0$, $g_4 \neq 0$) zero-temperature spectral function. Note the broader range of non-trivial singularities near $v_s k$ and $\pm v_c k$. Here both the effect of spin–charge velocity difference and the emergence of non-trivial exponents is visible. After Voit [277,278].

in a Lutinger liquid is smeared with a *branch cut* extending from the spin mode excitation energy to the charge mode excitation energy. These branch cuts split into two in an applied magnetic field, see Fig. 30. Note also the important difference for the case shown in Fig. 28, that $g_2 = 0$, when the left and right branches are orthogonal, from the general case shown in Fig. 29. These results are exact for small ω and small $|k - k_F|$.

Another manifestation of the SFL behavior is the behavior of the momentum distribution function derived from $A(k,\omega)$ by integrating over ω:

$$n_k \sim n_{k_F} - const \times \mathrm{sign}(k - k_F)|k - k_F|^{2\gamma_c} , \tag{108}$$

where

$$\gamma_{c,s} = \tfrac{1}{8}(K_{c,s} + K_{c,s}^{-1} - 2) . \tag{109}$$

In contrast to a Fermi liquid, the expression for n_k does not exhibit a step-like discontinuity at the Fermi points. The exponent $2\gamma_c$ is *non-universal* (as usual, an outcome of a line of critical points).

The single-particle density of states obtained from $A(k,\omega)$ by integrating over k:

$$N(\omega) \approx |\omega|^{2\gamma_c} \tag{110}$$

vanishes at the Fermi surface.

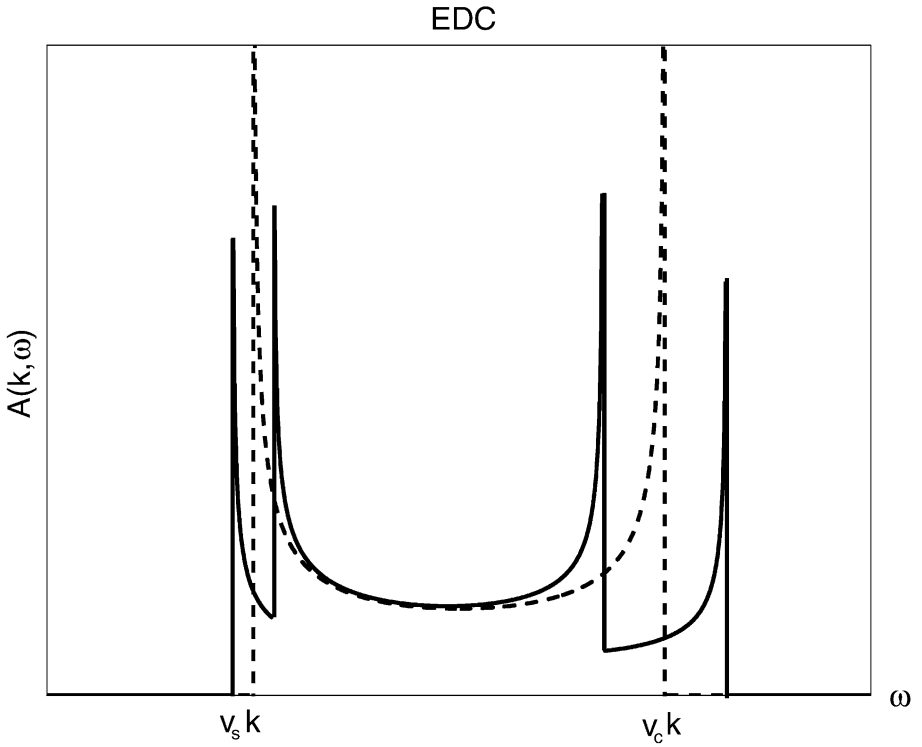

Fig. 30. The energy distribution curve (the spectrum $A(k,\omega)$ at fixed k) as a function of ω in the presence of a magnetic field. The dashed line is the zero-field result of Fig. 28. The magnitude of the Zeeman splitting is enhanced with respect to $(v_c - v_s)k$ for clarity. From Rabello and Si [218].

The spectral function $A(k,0)$, at the chemical potential, has also been calculated as a function of temperature. Representative plots are shown in Fig. 31. These are to be contrasted with the delta-function in a Landau Fermi liquid.

The reader will further note that in Fig. 31, the energy distribution curves are much broader than the momentum distribution curves. This is a general occurrence in one-dimensional systems and is a consequence of the fact that an injected electron of momentum and energy (k,ω) disintegrates (while conserving energy and momentum) into two independent spin and charge excitations having energies $\omega_{c,s} = v_{c,s}|k|$.

4.5. Correlation functions

Since the Hamiltonian is separable in charge and spin and as ψ is a product of independent charge and spin degree of freedom, all real-space correlation functions are products of independent charge and spin factors. We show the most important correlation functions in the illustrative examples below, and refer for a summary of the various exact expressions to [202].

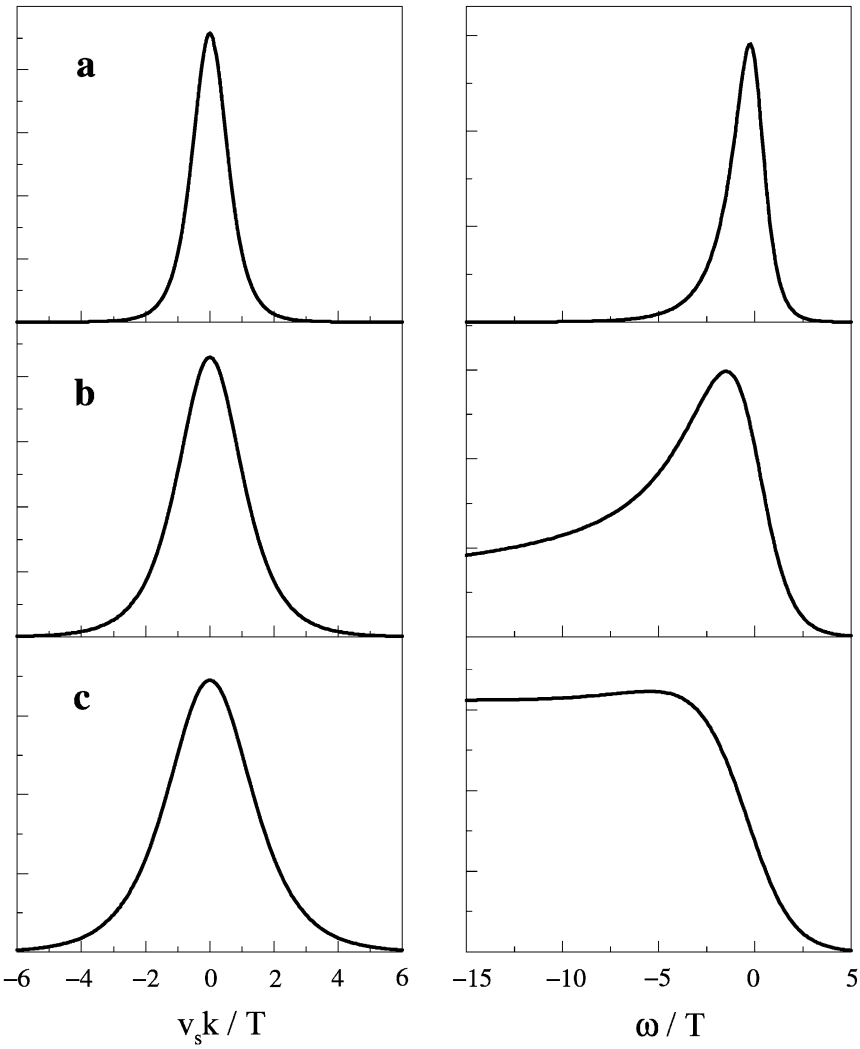

Fig. 31. (Left panel) Momentum distribution curves at $\omega = 0$ (i.e., the spectrum at fixed $\omega = 0$ as a function of k) for a spin rotationally invariant Tomonaga–Luttinger liquid, plotted as a function of $v_s k/T$; (right panels) energy distribution curves at $k = 0$ (the spectrum at fixed $k = 0$) as a function of ω/T. In both panels, $v_c/v_s = 3$ and $\gamma_c = 0$ in (a), $\gamma_c = 0.25$ in (b), and $\gamma_c = 0.5$ in (c). From Orgad [202].

Sometimes, the Bosonization method in its elegance obscures the underlying physics of these correlation functions. The genesis of the power-law dependence of the correlations exhibited below is the nesting in both charge and spin particle–hole channels and the Cooper channel. The logarithmic singularities evident in the simplest calculation turn into power laws on summing the singularities exactly. To obtain the exact values of the exponents one requires an exact method, for example Bosonization.

The most important feature of the large distance behavior of the charge and spin correlators is their algebraic decay at zero temperature

$$\langle\rho(x)\rho(x')\rangle \simeq \frac{K_c}{(\pi(x-x'))^2} + B_{1,c}\frac{\cos(2k_F(x-x'))}{|x-x'|^{1+K_c}}\ln^{-3/2}|x-x'| + B_{2,c}\frac{\cos(4k_F(x-x'))}{|x-x'|^{4K_c}} + \cdots$$

$$\langle\vec{S}(x)\cdot\vec{S}(x')\rangle \simeq \frac{1}{(\pi(x-x'))^2} + B_{1,s}\frac{\cos(2k_F(x-x'))}{|x-x'|^{1+K_c}}\ln^{1/2}|x-x'| + \cdots \quad (111)$$

at asymptotically long distances and $K_s = 1$. For not very repulsive interactions, so that $K_c < 1$, the $2k_F$ fluctuations are dominant. We have previously seen that such a CDW/SDW instability may arise due to the special $2k_F$ nesting wavevector in one dimension.[29] The amplitudes $\{B_{i,c}\}$ and $\{B_{i,s}\}$ are non-universal while the exponents are determined by the stiffness of the free charge and spin fields.

While the above expressions are for $K_s = 1$, in the general case $K_s \neq 1$, the spin correlator decays asymptotically with the exponent $(K_s + K_c)$.

At non-zero temperatures, it is found that the Fourier transforms of these correlation functions scale as

$$\chi_{CDW} \approx T^{K_c-1}|\ln T|^{-3/2}, \quad \chi_{SDW} \approx T^{K_c-1}|\ln T|^{1/2},$$
$$\chi_{SS} \approx T^{K_c-1}|\ln T|^{-3/2}, \quad \chi_{TS} \approx T^{K_c-1}|\ln T|^{1/2}. \quad (112)$$

The "phase diagram" shown in Fig. 27 is of course consistent with the dominant singularities of (112). The reader will note that the quantities on the left-hand side of Eq. (112) differ from those on the right-hand side by a factor of $|\ln T|^{-2}$, but that if any quantity on the right-hand side diverges, then so does its counterpart (with the same power of T). The dominant and the subdominant divergences are marked in each sector of the phase diagram depicted in Fig. 27, with the subdominant behavior indicated between brackets.

These results also lead, in principle, to clear experimental signatures. X-rays, which couple to the charge density waves, should peak at low temperatures with intensities given by

$$I_{2k_F} \sim T^{K_c}, \quad I_{4k_F} \sim T^{2K_c-1}. \quad (113)$$

The NMR probe couples to the spin degrees of freedom and the theoretically computed nuclear relaxation time scales as

$$T_1 \sim T^{-K_c}. \quad (114)$$

[29] We also show a $4k_F$ modulation of the charge-density correlation which arises due to Umklapp scattering near half-filling, i.e, $4k_F =$ a reciprocal vector. If instead of point contact interactions (q independent couplings g_i) we augment the system by additional long-range Coulomb interactions via $\int dx\,dx' V(x-x')\partial_x\phi_c\partial'_x\phi_c$ with a Coulomb like kernel $V(x) \sim [x^2+d^2]^{-1/2}$ then singular density correlations at $4k_F$ are triggered. This is of course related to the physics of Wigner crystallization. Owing to the one-dimensional character of the system no true long-range order can be found; however, the $4k_F$ component of the charge–charge correlations decays in an extremely slow fashion $\sim (\exp[-A\sqrt{\ln x}])$ (slower than algebraic).

4.6. The Luther–Emery model

The Luther–Emery model extends the Tomonaga–Luttinger Hamiltonian by including the backscattering interactions parametrized by $\mathscr{H}_1$, which scatter from $(+k_F,\sigma;-k_F,\sigma')$ to $(-k_F,\sigma;k_F,\sigma')$ and vice versa. The Umklapp processes ($\mathscr{H}_3$) continue to be discarded.

The backscattering term

$$\mathscr{H}_1 = \int \mathrm{d}x\, g_1 \sum_{r=\pm1} \psi^\dagger_{r,\sigma=+1}\psi^\dagger_{-r,\sigma=-1}\psi_{r,\sigma=-1}\psi_{-r,\sigma=1} \tag{115}$$

written in terms of the bosonic variables introduces a non-trivial sine-Gordon like interaction [113]

$$\mathscr{H}_s = \int \mathrm{d}x\, \frac{v_s}{2}\left[K_s(\partial_x\theta_s)^2 + \frac{(\partial_x\phi_s)^2}{K_s}\right] + \frac{2g_1}{(2\pi a)^2}\cos(\sqrt{8\pi}\phi_s) \tag{116}$$

with rescaled values of the spin and charge velocities and stiffness constants.[30] When $g_1 > 0$ (repulsive interactions), g_1 is renormalized to zero in the long wavelength limit. Since along the RG flow trajectories $K_s - 1 \approx g_1/(\pi v_s)$, this means that K_s renormalizes to 1. The physics corresponding to this case is in the Tomonaga–Luttinger model that we just discussed.

When symmetry breaking backscattering interactions are attractive and favorable ($g_1 < 0$) the Tomonaga–Luttinger $SU(2)_L \otimes SU(2)_R$ symmetry is broken and an associated spin gap opens up. On a more formal level, the non-trivial cosine term in Eq. (116) leads to different minimizing values of the spin field ϕ_s dependent on the sign of g_1. Consequently, when the backscattering interactions are attractive, a spin gap of magnitude

$$\Delta_s \sim \frac{v_s}{a}\left[\frac{g_1}{2\pi^2 v_s}\right]^{1/(2-2K_s)} \tag{117}$$

opens up. The attractive backscattering leads to the formation of bound particle–hole pairs which form a CDW. The spin correlation length is then finite

$$\xi_s = \frac{v_s}{\Delta_s}\,. \tag{118}$$

In the spin gapped phase,[31] the Hamiltonian can be conveniently expressed in terms of new *refermionized* spin fields $\Psi_r(x)$.

$$\Psi_r = F_r \exp[-\mathrm{i}\sqrt{\pi/2}(\theta_s - 2r\phi_s)]\,. \tag{119}$$

Luther and Emery observed that at the point $K_s = 1/2$, the Hamiltonian in terms of these new spin fields becomes that of non-interacting free fermions having a mass gap $\Delta_s = g_1/(2\pi a)$.

$$\mathscr{H}_s = \int \mathrm{d}x \sum_{r=\pm1} [-\mathrm{i}v_s r\Psi^\dagger_r\partial_x\Psi_r + \Delta_s\Psi^\dagger_r\Psi_{-r}] \tag{120}$$

---

[30] If Umklapp scattering were included (it is *not* in the present section), then an analogous term $2g_3/(2\pi a)^2\cos(\sqrt{8\pi}\phi_c)$ would be generated. The spin and charge fields then take similar roles for the backscattering ($\mathscr{H}_1$) and Umklapp ($\mathscr{H}_3$) interactions.

[31] Gaps in the charge spectrum also develop when Umklapp scattering is relevant.

leading to the spin excitation spectrum

$$E_s = \sqrt{\Delta_s^2 + v_s^2(k - k_F)^2} \ . \tag{121}$$

We will now discuss how the spin gap may fortify both superconductivity and the $2k_F$ charge-density wave order.

When expressed in terms of Bose operators, the superconducting gap operator

$$\Delta_{SC} = \psi^\dagger_{r=-1,\sigma=+1}\psi^\dagger_{r=1,\sigma=-1} + \psi^\dagger_{r=1,\sigma=+1}\psi^\dagger_{r=-1,\sigma=-1} \tag{122}$$

turns, as all correlators do, into a product of the spin and charge degrees of freedom. For Δ_{SC}, the relevant product is amongst the cosine of the spin field ϕ_s and an exponential of the θ_c operator (i.e., the field *dual to the charge field*). Thus the cosine of the spin field plays the role of the amplitude. It follows that when spin fluctuations are frozen (by opening a gap), superconducting correlations may be consequently enhanced. The appearance of the dual field θ_c in an expression for the superconducting gap Δ_{SC} should come as no surprise as superconducting (phase) and charge (number operator) order are conjugate and dual to each other.

According to Eq. (112), in the presence of a spin gap, the superconducting susceptibility scales as

$$\chi_{SC} \sim \Delta_s T^{(1/K_c)-2} \ . \tag{123}$$

The $2k_F$ charge density wave order

$$\rho_{r2k_F} = \sum_\sigma \psi^\dagger_{r,\sigma}\psi_{-r,\sigma} \tag{124}$$

is associated, as it must, with the charge field ϕ_c (in lieu of its dual θ_c). Consequently, a computation shows that

$$\chi_{CDW} \sim \Delta_s T^{K_c-2} \ . \tag{125}$$

Note that the appearance of K_c in the exponent by contrast to the appearance of $1/K_c$ in χ_{SC} associated with the dual charge field θ_c. This is once again a part of the old maxim that "*CDW* (*or number*) *ordering is conjugate and dual to superconducting* (*or phase*) *order*" in action.

In conclusion: The charge field or its dual (the phase field) may condense, under the umbrella of the spin gap, to a $2k_F$ charge density wave or to a superconducting gap.

This completes our compendium of the essential properties of one-dimensional interacting fermions. We will now critically examine the results from several different points of views.

4.7. Spin–charge separation

As in many other physical problems, the availability of an exact solution to the one-dimensional electron gas problem is intimately linked to the existence of additional conservation laws or symmetries. One may attack the Luttinger liquid problem by looking for its symmetries.

The $U(1)_L \otimes U(1)_R$ symmetry present in the absence of Umklapp scattering may be exhibited by considering the effect of the separate left and right rotations by angles $\Gamma_{L,R}$ on the fermion variables

$$\psi_{L\sigma}(x,t) \to e^{i\Gamma_L}\psi_{L\sigma}(x,t), \quad \psi_{R\sigma}(x,t) \to e^{i\Gamma_R}\psi_{R\sigma}(x,t) \,. \tag{126}$$

All of the currents are trivially invariant under this transformation as the $\psi^\dagger$ fields transform with opposite phases. Physically, this corresponds to the conservation of the number and net spin of left and right moving particles.

As discussed by Metzner and Di Castro [179], these separate conservation laws for the left and right moving charge and spin currents lead to Ward identities which enable the computation of the single-particle correlation functions.

In the absence of Umklapp scattering, charge is conserved about each individual Fermi point. The net total charge density $\rho \equiv \rho_+ + \rho_-$ and charge density asymmetry $\tilde{\rho} \equiv \rho_+ - \rho_-$ in the Tomonaga–Luttinger Hamiltonian satisfy the continuity equations

$$\partial_\tau \rho = [\mathscr{H}, \rho] = -qj, \quad \partial_\tau \tilde{\rho} = [\mathscr{H}, \tilde{\rho}] = -q\tilde{j} \,, \tag{127}$$

where

$$j(q) = u_c[\rho_+ - \rho_-], \quad \tilde{j} = \tilde{u}_c[\rho_+ + \rho_-] \tag{128}$$

and where the velocities are given by

$$u_c = v_F + \frac{g_4^c - g_2^c}{\pi}, \quad \tilde{u}_c = v_F + \frac{g_4^c + g_2^c}{\pi} \,. \tag{129}$$

These results follow straightforwardly from the form of $\mathscr{H}^{T-L}$ in combination with the fact that the only non-zero commutator is

$$[\rho_{r,\sigma}(q), \rho_{r',\sigma'}(-q')] = \delta_{qq'}\delta_{rr'}\delta_{\sigma\sigma'}\left(\frac{qL}{2\pi}\right) \,. \tag{130}$$

Let us illustrate simply how many of the results derived via bosonization may also be directly computed by employing these conservation laws. The existence of gapless charge modes is a direct consequence of the right–left charge conservation laws. The two first-order continuity equations given above lead to

$$[\partial_\tau^2 + u_c\tilde{u}_c q^2]\rho = 0 \tag{131}$$

from which we can read off a linear charge dispersion mode

$$\omega = v_c|q| \tag{132}$$

with velocity $v_c = \sqrt{u_c\tilde{u}_c}$, in agreement with the earlier result (102). Thus, collective charge excitations propagate with a velocity v_c. A similar relation may be found for the spin velocity v_s which in general is different from v_c. This *spin–charge separation* also becomes clear from

the explicit form of the expectation values of the charge and spin densities

$$\langle 0|\psi_r(x_0)\rho_r(x,t)\psi_r^\dagger(x_0)|0\rangle = \delta(x - x_0 - rv_c t)\ ,$$
$$\langle 0|\psi_r(x_0)S_r^z(x,t)\psi_r^\dagger(x_0)|0\rangle = \delta(x - x_0 - rv_s t)\ , \tag{133}$$

where $|0\rangle$ denotes the ground state.

The separate right–left conservation laws cease to hold if (backscattering) impurities are present. Accordingly, as shown by Giamarchi and Schulz, [108] spin–charge separation then no longer holds.

4.8. Spin–charge separation in more than one dimension?

Spin–charge separation in one dimension requires extra conservation laws. Can something analogous occur in more than one dimension? No extra conservation laws are discernible in the generic Hamiltonians in two dimension, although such Hamiltonians can doubtless be constructed. Are there conditions in which generic Hamiltonians become dynamically equivalent to such special Hamiltonians (because the unwelcome operators are "irrelevant")? No definite answers to these questions are known. In Section 5.2 and later in this section we shall briefly review some interesting attempts towards spin–charge separation in higher dimensions. First we present qualitative arguments pointing out the difficulty in this quest.

There is a simple caricature given by Schulz [233] for qualitatively visualizing charge–spin separation for a special one-dimensional case: the $U \to \infty$ Hubbard model. This model is characterized (at half-filling) by the algebraic decay of spin-density correlations, which at short distances appear as almost antiferromagnetic alignments of spins. Let us track the motion of a hole introduced into an antiferromagnetically ordered chain. The hole is subject to only the lattice kinetic term which enables it to move by swapping with a nearby spin.

An initial configuration will be

$$\ldots \Downarrow\Uparrow\Downarrow\Uparrow\Downarrow\ O\ \Downarrow\Uparrow\Downarrow\Uparrow\Downarrow \ldots \tag{134}$$

After one move the configuration is

$$\ldots \Downarrow\Uparrow\Downarrow\Uparrow\ O\ \Downarrow\Downarrow\Uparrow\Downarrow\Uparrow\Downarrow \ldots \tag{135}$$

After two additional moves to the left the configuration reads

$$\ldots \Downarrow\Uparrow\ O\ \Downarrow\Uparrow\Downarrow\Downarrow\Uparrow\Downarrow\Uparrow\Downarrow \ldots \tag{136}$$

Thus the initial hole surrounded by two spins of the same polarization has broken into a charge excitation ("holon" or "chargon" — a hole surrounded by antiferromagnetically aligned spins) and a spin excitation ("spinon") composed of two consecutive parallel spins in an antiferromagnetic environment. The statistics of the localized spinons and holons in this model must be such that their product is fermionic.

The feasibility of well-defined spin and charge excitations hinges on the commuting nature of the right and left kinetic (hopping) operators $T_{\text{Right}}, T_{\text{Left}}$ which are the inverse of each other.

Any general term of the form

$$(T_{\mathrm{Left}})^{n_1^{\mathrm{Left}}}(T_{\mathrm{Right}})^{n_1^{\mathrm{Right}}}(T_{\mathrm{Left}})^{n_2^{\mathrm{Left}}}(T_{\mathrm{Right}})^{n_2^{\mathrm{Right}}}\ldots=(T_{\mathrm{Left}}T_{\mathrm{Right}})^{N_{\mathrm{R}}}T_{\mathrm{Left}}^{N_{\mathrm{L}}-N_{\mathrm{R}}}=I\times T_{\mathrm{Left}}^{N_{\mathrm{L}}-N_{\mathrm{R}}}\ , \quad (137)$$

where $N_{\mathrm{R,L}}=\sum_i n_i^{\mathrm{R,L}}$. We have just shown that terms of the form $T_{\mathrm{L}}^{n_{\mathrm{L}}}$ lead to a representation of the sort depicted above which gives rise to spin–charge separation and therefore our result holds for the general perturbative term. The proof of spin–charge separation for the one-dimensional electron gas rests on the existence of separate conservation laws for the left and right moving domain walls, as a result of the fact that the operators T_{Right} and T_{Left} commute.

Such a simple "proof" cannot be extended to higher dimensions. In higher dimensions this suggestive illustration for spin–charge separation is made impossible by the non-commuting (frustrating) nature of the permutation operators $T_{\mathrm{Up}}, T_{\mathrm{Down}}, T_{\mathrm{Right}}, T_{\mathrm{Left}},\ldots$ Moreover, even if the exchange operators commuted we would be left with terms of the form $T_{\mathrm{Left}}^{n_{\mathrm{Left}}}T_{\mathrm{Up}}^{n_{\mathrm{Up}}}$ which when acting on the single hole state will no longer give rise to states that may be seen as a direct product of localized holon and spinon like entities.

Let us simply illustrate this by applying a sequence of various exchanges on the planar state $|\psi\rangle$:

$$\begin{array}{ccccccccc} - & + & - & + & - & + & - & + \\ + & - & + & - & + & - & + & - \\ - & + & - & + & - & + & - & + \\ + & - & + & 0 & + & - & + & - \\ - & + & - & + & - & + & - & + \end{array}\ , \quad (138)$$

where $+$ and $-$ denote up and down spins, respectively. By applying $T_{\mathrm{Down}}T_{\mathrm{Right}}^2T_{\mathrm{Up}}T_{\mathrm{Left}}^2$ we arrive at $|\psi'\rangle$

$$\begin{array}{ccccccccc} - & + & - & + & - & + & - & + \\ + & - & + & - & + & - & + & - \\ - & - & + & + & - & + & - & + \\ + & + & - & 0 & + & - & + & - \\ - & + & - & + & - & + & - & + \end{array} \quad (139)$$

a state which obviously differs from $T_{\mathrm{Down}}T_{\mathrm{up}}T_{\mathrm{Right}}^2T_{\mathrm{Left}}^2|\psi\rangle=|\psi\rangle$. Unlike the one-dimensional case, damage is not kept under check. Note the extended domain wall neighboring the hole, enclosing a 2×2 region of spins of the incorrect registry. Note also that the hole is now surrounded by a pair of antiferromagnetically aligned spins along one axis and ferromagnetically aligned spins along the other. A path closing on itself does not lead to the fusion of the "holon" and "spinon" like entities back into a simple hole. As the hole continues to further explore both dimensions, damage is continuously compounded. The state $T_{\mathrm{Down}}^2T_{\mathrm{Right}}T_{\mathrm{Down}}T_{\mathrm{Right}}T_{\mathrm{Up}}^3T_{\mathrm{Left}}^2|\psi\rangle=|\tilde{\psi}\rangle$ contains a string of eight spins of incorrect orientation surrounded by a domain wall whose perimeter is 16 lattice units long

$$\begin{array}{ccccccccc} - & - & + & + & - & + & - & + \\ + & + & - & + & + & - & + & - \\ - & - & - & + & - & + & - & + \\ + & + & - & 0 & + & - & + & - \\ - & + & - & + & - & + & - & + \end{array}\ . \quad (140)$$

As seen, the moving electron leaves a string of bad magnetic bonds in its wake. The energy penalty of such a string is linear in its extent. It is therefore expected that this (magnetic string) potential leads, in more than one dimension, to a confining force amongst the spin and charge degrees of freedom. As this caricature for the *single hole* makes clear, the notion of localized "spinons" and "holons" is unlikely to hold water for the $U \to \infty$ Hubbard model in more than one dimension. The well-defined SFL solutions for special models with nested Fermi-surface in two dimensions should, however, be noted [96].

A certain form of spin–charge separation in two dimensions may be sought in the very special *hole aggregates* (or stripes) that have been detected in some of the cuprates [257] and the nickelates [59]. Here, holes arrange themselves along lines which concurrently act as antiferromagnetic domain walls (i.e., behave like holons) in the background spin texture. Charge and spin literally separate and occupy different regions of space. In effect, the two-dimensional material breaks up into one-dimensional lines with weak inter-connections.[32] Related behavior is also found in numerical work [174] in the so-called, t'–t–J model.[33] An important question for such models is the extent to which the interconnections between stripes are "irrelevant"—i.e., the coupled chains problem, which we briefly allude to in Section 4.10.

4.9. Recoil and the orthogonality catastrophe in one dimension and higher

Here we show how the SFL behavior in one dimension is intimately tied to the issue of orthogonality which we discussed in Sections 2.2 and 3.4. This line of thinking is emphasized by Anderson [20,24] who has also argued that this line of reasoning gives SFL behavior in two dimensions for arbitrary small interactions.

We consider the effect of interactions through the explicit computation of our old friend from Section 2.2, the quasiparticle weight

$$Z_k^{1/2} = \langle \psi_k^{N+1} | c_k^\dagger | \psi^N \rangle \ . \tag{141}$$

As we have seen, this indeed vanishes in all canonical one-dimensional models. Consider the model [50] of a Hamiltonian describing N fermions interacting with an injected particle via a delta function potential

$$H = -\frac{1}{2m}\sum_{i=1}^{N}\frac{\partial^2}{\partial x_i^2} - \frac{1}{2m}\frac{\partial^2}{\partial x_0^2} + U\sum_{i=1}^{N}\delta(x_i - x_0) \ . \tag{142}$$

---

[32] This observation has led to a line of thought which is of some interest in the context of the issues discussed here. If one focusses on the quantum mechanics of a single line of holes by formulating it as a quantum-mechanical lattice string model [87], the string traces out a two-dimensional world sheet in space–time. Quantum-mechanical particles in one dimension, on the other hand, trace out world lines in space–time. It is claimed that one can recover most of the power-law correlation functions of one-dimensional interacting fermions from the classical statistical mechanics of fluctuating lines, and along these lines approach stripe formation as some form of spin–charge separation in two dimensions [300].

[33] In this paper it was further observed that the kinetic motion of single holes may scramble the background spin environment in such a way that, on average, the holes may become surrounded by antiferromagnetically ordered spins on all sides (i.e., both along the horizontal and along vertical axis)—this is claimed to be a higher dimensional generalization of the holons encountered so far.

The calculation for the small s-wave phase shifts for all single-particle states $\{\phi_i(x_i)\}$ is relatively straightforward. The quasiparticle weight Z reduces to an overlap integral between two $(N+1)$-particle Slater determinants, and one finds

$$Z \sim N^{-2(\delta_F/\pi)^2} \tag{143}$$

with

$$\delta_F = -\tan^{-1}[Uk_F/2]\,. \tag{144}$$

In the thermodynamic limit $Z=0$ and no quasiparticles exist. As we see, the scattering phase shifts must conspire to give rise to anomalous behavior (exponents) for the electronic correlation function in such a way that they lead to a vanishing density of states at the Fermi level. We have already given explicit expressions for the anomalous exponent(s) under the presence of general scattering terms.

As indicated in Sections 2 and 3, an identically vanishing overlap integral between two $(N+1)$ particle states could be a natural outcome of the emergence of additional quantum numbers labeling orthogonal states. These states could correspond to different topological excitation sectors (e.g. solitons). Each quantum number corresponds to some conserved quantity in the system. In the one-dimensional electron gas this may be derived as we saw as a consequence of separate conservation law for left and right movers.

An illustrative example of how singular Fermi liquid behavior due to orthogonality of the wavefunction is robust in one dimension but easily destroyed in higher dimensions, is provided by the X-ray edge singularity problem, already discussed in Section 3.5. As sketched in Fig. 19, we consider the transition of an electron from a deep core level to the conduction band through absorption of a photon. This problem is essentially the same as that of optical absorption in degenerate semiconductors, and from this point of view it is natural to analyze, following Nozières [199], the effect of dispersion in the hole band, the analogue of the deep level state. For optical absorption in a semiconductor, the transition conserves momentum; hence in the absence of final state interactions, the threshold absorption is associated with the transition indicated with the arrowed line in Fig. 19, and absorption starts discontinuously above the threshold energy ω_D provided that the hole mass is infinite. For finite hole mass, the threshold gets rounded on the scale of the dispersion of the hole band. However, in one dimension, the edge singularity *does survive* because low-energy electron–hole excitations in one dimension have momenta only near 0 and near $2k_F$ (see Fig. 10); electron–hole pairs cannot carry away arbitrary momenta. This is seen in the following calculation [199].

Assume a simple featureless final state potential V, and consider first the case without recoil. The relevant quantity to calculate is the transient propagator for the scatterer

$$G(t) = \langle 0|d\,e^{i\mathscr{H}t}d^\dagger|0\rangle \tag{145}$$

as the spectrum is the Fourier transform of $G(t)$. In (145), the potential V is turned on at time 0 and turned off at time t. In a linked cluster expansion, we may write $G(t)=e^{C(t)}$, where $C(t)$ is the contribution of a single closed loop. In lowest order perturbation theory, $C(t)$ becomes

$$C(t) = \int_0^t d\tau \int_0^t d\tau' V^2 g(0,\tau-\tau')g(0,\tau'-\tau)\,, \tag{146}$$

where $g(0,\tau)$ is the free conduction electron propagator at the origin. For large times, one has $g(0,\tau) \approx -\mathrm{i}N(0)/\tau$, and when this is used in (146) one immediately find that for large times

$$C(t) = V^2 N(0)^2 \ln t, \quad \Rightarrow \quad G(t) \propto 1/t^n \,, \tag{147}$$

where

$$n = V^2 N(0)^2 = \delta^2/\pi^2 + 1 \tag{148}$$

is the phase shift exponent due to the orthogonality effect, compare Eq. (56). A power-law decay of $G(t) \sim 1/t^n$ at long times corresponds to power-law dependence $\sim (\omega - \omega_\mathrm{D})^{n-1} = (\omega - \omega_\mathrm{D})^{\delta^2/\pi^2}$ just above the absorption edge.

If we now take into account the recoil effect, then the dispersion of the lower band implies that the hole in this band can hop from site to site. The propagator $G(t)$ is then obtained as a sum over all trajectories $R(\tau)$ of the scattering hole which begin and end at $R = 0$. For a given history, we can extend the above analysis to lowest order by replacing the propagator $g(0,\tau)$ by $g(\rho,\tau)$, where $\rho(\tau) = R(\tau) - R(\tau')$. For positive time difference, we can then write

$$g(\rho,\tau) = \sum_{k>k_\mathrm{F}} \mathrm{e}^{\mathrm{i}\varepsilon_k \tau - \mathrm{i}\mathbf{k}\cdot\rho} \,. \tag{149}$$

For small hopping rates and large times, the integration over the modulus is dominated by the energy term, and this yields a term proportional to $-1/\tau$ as in the recoilless case. The trajectory of the hole enters through the average $\overline{\exp(-\mathrm{i}\mathbf{k}\cdot\rho)}^{\mathrm{FS}}$ over the Fermi sphere. A simple calculation yields

$$\overline{\exp(-\mathrm{i}\mathbf{k}\cdot\rho)}^{\mathrm{FS}} = \begin{cases} \cos(k_\mathrm{F}\rho), & d=1 \,, \\ J_0(k_\mathrm{F}\rho), & d=2 \,, \\ \dfrac{\sin(k_\mathrm{F}\rho)}{k_\mathrm{F}\rho}, & d=3 \,. \end{cases} \tag{150}$$

In order to calculate the large time behavior of the Green's function, we finally have to average the square of this result over the distribution function of the trajectories ρ for large times. Using the large-ρ behavior of the expressions found above, one then finds [199] that for large times

$$g^2(\rho,\tau) \approx N^2(0)\tau^{-2} \left\langle \left(\overline{\exp(-\mathrm{i}\mathbf{k}\cdot\rho)}^{\mathrm{FS}} \right)^2 \right\rangle_\rho = \begin{cases} \frac{1}{2}N^2(0)/\tau^2, & d=1 \,, \\ \propto \ln \rho_\mathrm{typ}(\tau)/(\rho_\mathrm{typ}(\tau)\tau^2), & d=2 \,, \\ \propto 1/(\rho_\mathrm{typ}^2(\tau)\tau^2), & d=3 \,, \end{cases} \tag{151}$$

where ρ_typ is the typical distance the hole trajectory moves away from the origin in time τ. In one dimension, we see that g^2 still falls off as $1/\tau^2$ and hence in analogy to (147) that $G(t)$ has power-law long time behavior: in the presence of recoil, an edge singularity persists but the exponent n is now only half of that in the absence of dispersion of the lower state (a consequence of the averaging over ρ).

Since $\rho_{\rm typ}(\tau)$ grows diffusively as $\tau^{1/2}$ for large τ, the integrand in the expression (146) for $C(t)$ converges faster than $1/t^2$, and hence $C(t)$ converges to a finite limit for large times. The singular X-ray edge effect is washed out in two and three dimensions due to the recoil.

If the above argument is extended to arbitrary dimension by analytically continuing the angular average over the Fermi surface to continuous dimensions, one finds that the orthogonality and concomitant singular behavior is destroyed for any dimension $d > 1$. Nevertheless, the subdominant behavior of the integrals will contain non-integer powers of time, and this gives rise to subdominant non-analytic terms in the spectrum for non-integer d. This behavior is completely in agreement with an analysis of the dimensional crossover from Luttinger liquid behavior to Fermi-liquid behavior as a function of dimension [51].

4.10. Coupled one-dimensional chains

The two coupled chain problem has been thoroughly considered [90,95,159,232,33,194] following earlier perturbative RG calculations [264] on a related model. The two-chain or ladder is especially interesting both theoretically and experimentally. In general inter-chain coupling is a relevant parameter, changing the behavior qualitatively. In the model of coupled Luttinger chains, the weight of the massless bosons characteristic of one dimension goes down with the number of chains. The general lesson to be drawn is that inter-chain coupling is always a relevant parameter, but that for a small number of coupled chains special features of the one-dimensional problem persist. In the passage to two dimension by increasing the number of chains to thermodyanmic values, features of the one-dimensional problem such as charge–spin separation are lost. Specifically for models in which the one-chain problem can be bosonized, the approach to two dimension by increasing the number of chains appears to lead to a Fermi liquid in two dimensions.

The two-chain problem presents some interesting new features. One of them is the "d-wave" type superconductivity and the other is the presence of phases of "orbital antiferromagnetism" for some range of parameters [203,173].

4.11. Experimental observations of one-dimensional Luttinger liquid behavior

There has, of course, been a long-standing interest to observe the fascinating one-dimensional Luttinger liquid-type SFL behavior experimentally, but the possibility of clear signatures has arisen only in the last few years. The clearest way to probe for Luttinger liquid behavior is to measure the tunneling into the one-dimensional system. Associated with the power-law behavior (110) in one dimension, one has a power-law behavior for the single-electron tunneling amplitude into the wire. For fixed voltage, this leads to a differential conductance $\mathrm{d}I/\mathrm{d}V \sim V^{\alpha}$, with the exponent α determined by the charge stiffness K_c, the geometry, and the band structure. Hence, from the measurement of the tunneling as a function of temperature or voltage, α and thus K_c can be extracted. Recent experiments on resonant tunneling [32] of small islands embedded in one-dimensional quantum wires in semiconductors, grown with a so-called cleaved edge overgrowth method, do indeed yield a power-law temperature behavior of the conductance [106] which is consistent with Luttinger liquid behavior, but the value of the exponent is substantially different from the one expected theoretically.

It has recently also been realized that nature has been kind enough to give us an almost ideal one-dimensional wire to study one-dimensional electron physics: the wavefunctions of carbon nanotubes turn out to be coherent over very large distances [74]. Although the circumference of the nanotubes is rather large, due to the band structure of the graphite-like structure the conduction in nanotubes can be described in terms of two gapless one-dimensional bands. Moreover, it was realized by Kane et al. [141] that due to the special geometry the backscattering in nanotubes is strongly suppressed, so that they are very good realizations of the Tomonaga–Luttinger model of Section 4.2, with an interaction constant K_c which is determined by the Coulomb energy on a cylinder. Their calculation based on this idea gives a value $K_c \approx 0.2$.

Fig. 32 shows recent nanotube data [211] which confirm the predictions by Kane et al. [141]: the differential conductance $\mathrm{d}I/\mathrm{d}V$ is found to vary as V^{α} as a function of the bias voltage at low but fixed temperatures, or as T^{α} as a function of temperature at fixed bias. For tunneling into the bulk of a carbon nanotube, the relevant density of states

$$N_{\mathrm{bulk}}(\omega) \sim \omega^{\alpha_{\mathrm{bulk}}} \quad \text{with } \alpha_{\mathrm{bulk}} = \gamma_c \,. \tag{152}$$

The fact that the exponent here is only half the value attained in the simple Luttinger Liquid—see Eq. (110)—is due to the fact that there are *two* Luttinger Liquid-like bands present in the carbon nanotubes.[34] Only one linear combination of the two associated charge modes attains a non-trivial stiffness $K_c \neq 1$ [141].

By contrast, at the tips of the nanotubes, surplus electronic charge can propagate in only one direction and, as a consequence, the tunneling is more restricted

$$N_{\mathrm{tip}}(\omega) \sim \omega^{\alpha_{\mathrm{tip}}} \quad \text{with } \alpha_{\mathrm{tip}} = (K_c - 1)/4 \,. \tag{153}$$

By Fermi's golden rule, the relevant exponents for (tip–tip) or (bulk–bulk) tunneling are $\alpha_{\mathrm{t-t}} = (K_c - 1)/2$ and $\alpha_{\mathrm{b-b}} = 2\gamma_c$, respectively. Bulk–bulk tunneling is achieved by arranging the nanotubes according to the crossing geometry depicted in the inset of Fig. 32 above. By

[34] The electrostatic charging energy depends only on the symmetrized band mode, which in bosonic variables can be written as $\theta_{c,+} = (\theta_{c,\mathrm{band}=1} + \theta_{c,\mathrm{band}=2})/\sqrt{2}$. The essential reason that exponents can change depending on the number of bands is that the normalization factor $1/\sqrt{2}$ in this bosonic variable enters in the exponent when the electron variables are written in terms of the bosonic modes, as discussed in Section 4.2. A simple way to illustrate the halving of the exponents in the context of the various results we have discussed is by considering the difference between the spinful Luttinger liquid that we have discussed and the spinless Luttinger liquid (a system only having charge degrees of freedom): the spinful model has a density of states exponent which is half of the spinless one. A calculation proceeds along the following lines: for the spinful case, the relevant Green's function is $G_{\mathrm{R}\sigma=+1}(x,t) = \langle \mathrm{e}^{\mathrm{i}(\Phi_{c\mathrm{R}}(x,t)+\Phi_{s\mathrm{R}}(x,t))/\sqrt{2})} \mathrm{e}^{-\mathrm{i}(\Phi_{c\mathrm{R}}(0,0)+\Phi_{s\mathrm{R}}(0,0))/\sqrt{2})} \rangle$. Note the factor $1/\sqrt{2}$ in the exponent, coming from the projection onto the proper bosonic variables. This expected value can be written as $G_{\mathrm{R}\sigma=+1}(x,t) = \langle \mathrm{e}^{\mathrm{i}\Phi_{c\mathrm{R}}(x,t)/\sqrt{2}} \mathrm{e}^{-\mathrm{i}\Phi_{c\mathrm{R}}(0,0)/\sqrt{2}} \rangle \langle \mathrm{e}^{\mathrm{i}\Phi_{s\mathrm{R}}(x,t)/\sqrt{2}} \mathrm{e}^{-\mathrm{i}\Phi_{s\mathrm{R}}(0,0)/\sqrt{2}} \rangle$, which with the aid of the results of Section 4.4 becomes $G_{\mathrm{R}\sigma=+1}(x,t) = \frac{1}{|x-v_c t|^{1/2}} \frac{1}{|x^2-v_c^2 t^2|^{\gamma_c}} \times \frac{1}{|x-v_s t|^{1/2}} \frac{1}{|x^2-v_s^2 t^2|^{\gamma_s}}$. From this result, one immediately obtains the density of states $N(\omega) = \int \mathrm{d}t G(x=0,t) \mathrm{e}^{\mathrm{i}\omega t}$. A simple integration then yields $N(\omega) = [v_c^{-2\gamma_c} v_s^{-2\gamma_s}] \int \mathrm{d}t\, t^{-1} t^{-2(\gamma_c+\gamma_s)} \mathrm{e}^{\mathrm{i}\omega t} \sim \omega^{2(\gamma_c+\gamma_s)}$. Since K_s renormalizes to 1 for repulsive interactions (see the remark just after (116)), one usually has $\gamma_s = 0$ and so in this case, the density of states exponent is simply $2\gamma_s$. This is precisely (110). Now consider what one gets for the spinless Luttinger liquid. In this case, neither the bosonic spin modes *nor the projection factor* $1/\sqrt{2}$ are present in the above expression for G. This results in a spatial decay with an exponent $2\gamma_c$ instead of γ_c, and hence an exponent $4\gamma_c$ in the density of states. In other words, for $\gamma_s = 0$ the density of states exponent in the spinful case is half of what it is in the spinless case. The same mechanism is at work in the nanotubes.

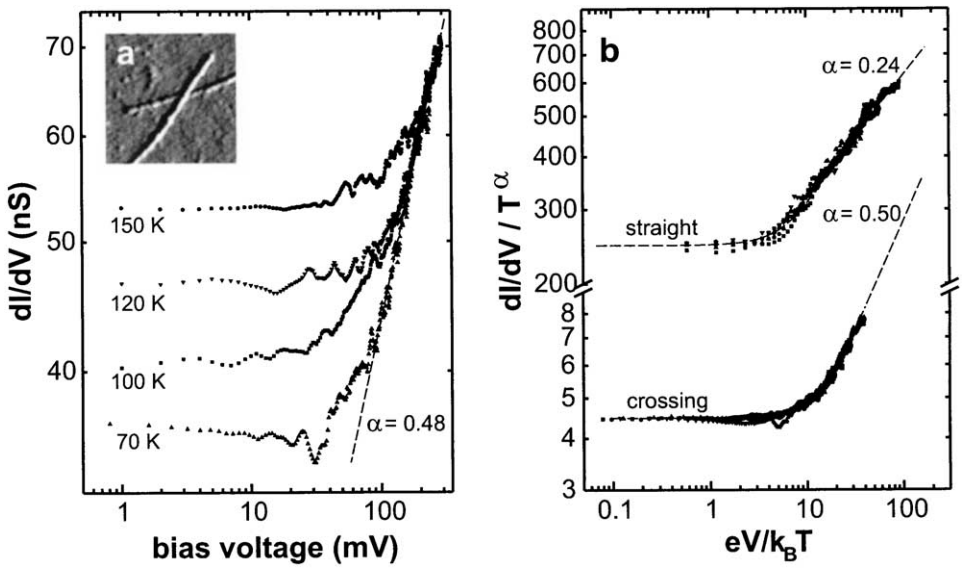

Fig. 32. Differential conduction dI/dV measured by Postma et al. [211] for carbon nanotubes. At low voltages or temperatures, Coulomb blockade effects dominate, but at higher temperatures or bias voltages, one probes the one-dimensional SFL behavior. Panel (a) shows the differential conductance as a function of bias voltage for various temperatures (note that these temperatures are relatively high, reflecting the fact that the electronic energy scales of the nanotubes is high). The effective exponent α for the large V behavior is 0.48; since these data are for tunneling between two nanotubes, $\alpha = 2\gamma_c$, so $\gamma_c \approx 0.24$ and $K_c \approx 0.27$. The predicted value is $K_c \approx 0.2$ [141]. The data in panel (b) show the differential conductance as a function of temperature at fixed bias for two nanotubes which cross, as well as for a single nanotube with a bend.

extracting the value of the charge stiffness K_c from each of the independent measurements of α_{t-t}, α_{b-b} for the two different geometries, a single consistent stiffness $K_c \approx 0.27$ was found [211], in good agreement with theoretical prediction.

The data shown in Fig. 32 corroborate the predicted scaling $dI/dV \sim V^{\alpha}$ over about one decade at voltages larger than a few $k_B T$. The problem in obtaining data over a larger range is that at a fixed temperature one has a crossover to linear behavior at small voltages due to thermal effects, while when performing measurements at fixed voltage as a function of temperature, Coulomb blockade effects reduce the conductance at low T to a value where they beset probing the intrinsic Luttinger liquid effects. Nevertheless, other datasets exhibit scaling over a range of up to three decades in V, and moreover, all experiments in different sample layouts with a variety of contact and defect structures yield a similar Luttinger stiffness around 0.23. In conclusion, therefore, taken together experiments on nanotubes yield very good experimental evidence for Luttinger liquid behavior.

Other, older, canonical realizations of Luttinger liquids include the Quantum Hall edge states. These represent a chiral spinless Luttinger liquid. Here, low-lying energy states can only prevail at the edge of the sample, and, concurrently, disperse linearly about the Fermi energy. Edge states can attain macroscopic linear (perimeter) extent, and the tunneling experiments between such states [182,114] have observed several features predicted theoretically [287,140]. We refer

the interested reader to the review articles by Schulz et al. [233] and Fisher and Glazman [98] for further details.

We note here recent ingenious experiments [76] which demonstrate, in effect (among other things) the separate conservation of left and right going electrons in a one-dimensional wire by showing that a separate chemical potential can be ascribed to the left-going electrons and to the right-going electrons. These may set the stage for the observation of spin–charge separation as well.

5. Singular Fermi-liquid behavior due to gauge fields

5.1. SFL behavior due to coupling to the electromagnetic field

Almost 30 years ago, Holstein et al. [127] (see also Reizer [221]) showed that the coupling of electrons to the electromagnetic fields gives rise to SFL behavior. Since the typical temperatures where the effects become important are of the order of 10^{-15} K, the effect is not important in practice. However, the theory is of considerable general interest.

If we work in the Coulomb gauge in which $\nabla \cdot \mathbf{A} = 0$ for the electromagnetic $\mathbf{A}$ field, then the transverse propagator D_{ij}^0 in free space is given by

$$D_{ij}^0(\mathbf{k},\omega) = \langle A_i A_j \rangle(\mathbf{k},\omega) = \frac{\delta_{ij} - \hat{k}_i \hat{k}_j}{c^2 k^2 - \omega^2 - \mathrm{i}\varepsilon} , \tag{154}$$

where ε is an infinitesimal positive number. The interaction of the electrons with the electromagnetic field is described by the coupling term

$$\mathbf{j} \cdot \mathbf{A} + \rho A^2 , \tag{155}$$

where $\mathbf{j}$ is the electron current operator and ρ the density operator.

Quite generally in the Coulomb gauge, one finds from perturbation theory, or phenomenologically from the Maxwell equations, that the electromagnetic propagator in a metal can be written as

$$D_{ij}^{-1} = (D_{ij}^0)^{-1} - M(\delta_{ij} - \hat{k}_i \hat{k}_j)^{-1} . \tag{156}$$

The perturbative diagrammatic expansion of M is indicated in Fig. 33. The first term leads to a term proportional to the density while the second term is the first correction due to particle–hole excitations. In formulas, these terms yield

$$M(k,\omega) = \frac{4\pi\alpha}{m} \left(n + \frac{1}{m} \int \frac{\mathrm{d}^d p}{(2\pi)^d} \frac{[p^2 - (\mathbf{p} \cdot \hat{\mathbf{k}})^2][f_{p-k/2} - f_{p+k/2}]}{\omega - (\varepsilon_{p-k/2} - \varepsilon_{p+k/2})} \right) . \tag{157}$$

Here n is the electron density, and $\alpha = 1/137$ is the fine structure constant. For $\omega/k \to 0$, the two terms combined yield

$$M(k,\omega) \approx \frac{3\pi\alpha n}{m} \left[4 \left(\frac{\omega}{k v_{\mathrm{F}}} \right)^2 + 2\mathrm{i} \frac{\omega}{k v_{\mathrm{F}}} \right] . \tag{158}$$

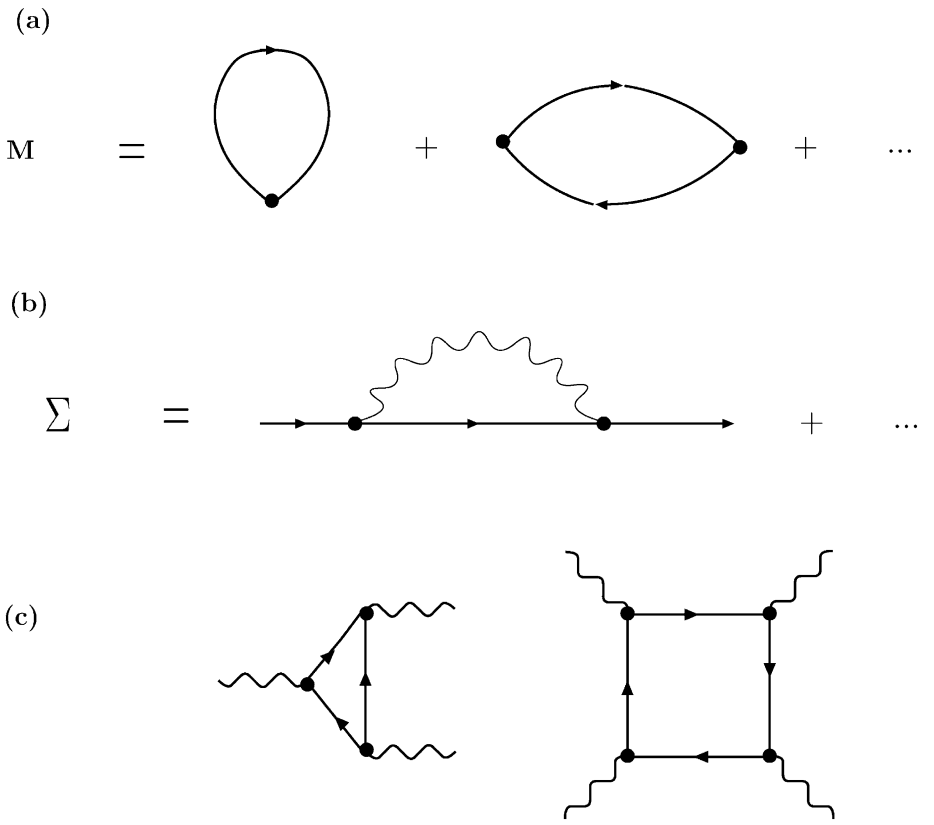

Fig. 33. (a) The diagrams for M; (b) the diagram for the self-energy from the discussion of the SFL effect arising from the coupling of the electrons to the electromagnetic gauge fields; (c) anharmonic interaction of fluctuations such as (c) are non-singular in the SFL problem of coupling of the electrons in metals to electromagnetic fields.

At small frequencies, for the propagator D this yields

$$D_{ij}(\mathbf{k},\omega) \approx \frac{\delta_{ij} - \hat{k}_i\hat{k}_j}{\mathrm{i}6\pi\alpha n\dfrac{\omega}{mkv_{\mathrm{F}}} + c^2k^2 - \mathrm{i}\varepsilon}\,, \tag{159}$$

which corresponds to an overdamped mode with dispersion $\omega \sim k^3$.

Before discussing how such a dispersion gives SFL behavior in three dimensions, it is instructive to point out that although (159) was obtained perturbatively, Maxwell's equations ensure that the field propagator must generally be of this form at low frequencies and momenta. Indeed, for a metal we can write the current $\mathbf{j}$ as $\mathbf{j} = \sigma(k,\omega)\mathbf{E}$; if we combine this with the Maxwell equation $\nabla \times \mathbf{H} = \mathbf{j} + \partial\mathbf{E}/\partial t$ we easily find that the general form of the propagator is

$$D_{ij}(\mathbf{k},\omega) = \frac{\delta_{ij} - \hat{k}_i\hat{k}_j}{4\mathrm{i}\pi\mu\omega\sigma(\mathbf{k},\omega) + c^2k^2}\,. \tag{160}$$

Here, μ is the diamagnetic permeability. For pure metals, the low-frequency limit is determined by the anomalous skin effect [5] and $\sigma(\mathbf{k},0) \sim k^{-1}$. According to expression (160), this $1/k$ behavior then implies that the dispersion at small frequencies generally goes as $\omega \sim k^3$ for a pure metal. For dirty metals, considering the fact that $\sigma(k,0)$ approaches a finite limit σ_0 at small wavenumbers, according to (160), there is a crossover to a behavior $\omega \sim k^2$ at small wavenumbers.

Gauge invariance of the theory requires that the photon cannot acquire a mass (a finite energy in the limit $k \to 0$) in the interaction process with the electrons, and hence the form of Eq. (159) remains unchanged. Thus the anharmonic corrections to the photon propagator due to processes such as those shown in Fig. 33(c) do not change the form of Eq. (159). The self-energy of the electrons due to photon exchange, Fig. 33(b), may now be calculated with confidence given the small coupling constant in lowest order. The leading contribution in $d=3$ is

$$\Sigma(k_F,\omega) \sim \alpha(\omega \ln \omega + i\omega \,\mathrm{sgn}\,\omega) \,. \tag{161}$$

The momentum dependence, on the other hand, is *non-singular* as a function of $k - k_F$.

The non-analytic behavior of the self-energy as a function of frequency implies that the resistivity of a pure metal in $d=3$ is proportional to $T^{5/3}$ at low temperatures. [35]

The simplicity and strength of the above example lies in the fact that the theory has no uncontrolled approximations, and the gauge-invariance of the photon field dictates the low-energy low-momentum behavior of the photon propagator $D_{ij}(\mathbf{k},\omega)$. Moreover, vertex corrections are not important because the Migdal theorem is valid [209] when the frequency of fluctuations is very small compared to their momenta, as in $\omega \sim q^3$.

However, the SFL behavior as a result of the coupling to the electromagnetic field is not relevant in practice. This can most easily be argued as follows. For a Fermi gas, the entropy per particle is

$$\frac{S}{N} = \frac{\pi^2 m k_B^2 T}{\hbar^2 k_F^2} \,, \tag{163}$$

while for the entropy for the electrons interacting with the electromagnetic field one finds from the above results [127]

$$\frac{S}{N} \approx \frac{2\pi^2 \alpha\mu}{3} \frac{k_B^2 T}{\hbar c k_F} \ln\left(\frac{\omega_0}{T}\right) \tag{164}$$

with

$$\omega_0 = \frac{c\varepsilon_F}{\alpha\mu v_F} \,. \tag{165}$$

---

[35] This follows from the fact that in the quasielastic approximation, the transport relaxation rate τ_{tr}^{-1} is related to the single-particle relaxation rate $\tau^{-1}(\theta)$ due to scattering through an angle θ near the Fermi surface

$$\tau_{tr}^{-1} = \int d\Omega (1 - \cos(\theta)) \tau^{-1}(\theta) \,. \tag{162}$$

For small T, $\omega \sim k^3 \sim T$, and hence the characteristic angle of scattering, $\theta \sim (k/k_F) \sim (T/E_F)^{1/3}$ is small. Upon expanding $(1 - \cos\theta) \simeq \theta^2/2$, one finds that the effective transport scattering rate goes as $\int d^3k \, k^2 f(k^3/T) \sim T^{5/3}$.

Upon comparing these two results, one concludes that the SFL effects start to become important for temperatures

$$k_B T \lesssim \omega_0 e^{-3m^* c/2\alpha\mu\hbar^2 k_F} . \tag{166}$$

Since the numerical factor in the exponent is typically of order $10^5\ \mu^{-1}$ for ordinary metals, the temperature range one finds from this is of order 10^{-15} K for values of μ of order unity, according to this estimate. Note, however, that for pure ferromagnetic metals μ can be as large as 10^4. Possibly, in some ferromagnets, the effects can become real.

5.2. Generalized gauge theories

The example of coupling to the electromagnetic field identifies one possible theoretical route to SFL behavior, but as we have seen that the crossover temperatures that one estimates for this scenario are too small for observable physical properties. The smallness of the estimated crossover temperature is essentially due to the fact that the coupling to the electromagnetic field is determined by the product $\alpha v_F/c$, where $\alpha = 1/137$ and typically $v_F/c = \mathcal{O}(10^{-2})$. Motivated by this observation, many researchers have been led to explore the possibility of obtaining SFL effects from coupling to different, more general gauge bosons which might be generated dynamically in strongly correlated fermions. For a recent review with references to the literature, see [158,192,193]. The hope is that if one could consistently find such a theory in which the small factor $\alpha v_F/c$ arising in the electromagnetic theory is replaced by a term of order unity, realistic crossover temperatures might arise. Much of the motivation in this direction comes from Anderson's proposal [24] of spin–charge separation and resonating valence bonds in the high-temperature superconductivity problem which we discuss in Section 7.

The essence of approaches along these lines is most easily illustrated by considering electrons on a lattice in the case in which strong on-site (Hubbard-type) repulsions forbid two electrons to occupy the same site. Then, each site is either occupied by an electron with an up or down spin, or by a hole. If we introduce fictitious fermionic creation and annihilation operators $f^\dagger$ and f for the electrons and fictitious bosonic hole creation and annihilation operators $b^\dagger$ and b for the holes, we can express the constraint that there can only be one electron or one hole on each lattice site by

$$\sum_{\alpha=1}^{2} f_{i\alpha}^\dagger f_{i\alpha} + b_i^\dagger b_i = 1 \quad \text{for each } i . \tag{167}$$

With this convention, the real electron field $\psi_{i\alpha}$ can be written as a product of these fermion and boson operators

$$\psi_{i\alpha} = f_{i\alpha} b_i^\dagger . \tag{168}$$

This expresses the fact that given constraint (167), a real fermion annihilation at a site creates a hole. This way of writing the electron field may be motivated by the physics of the one-dimensional Hubbard model: there a local excitation may indeed be expressed in terms of a charged spinless holon and an uncharged spinon. In general, in a transformation to boson and fermion operators as in (168) there is some freedom as to with which operator we associate the charge and with which the spin.

Whenever we split a single electron operator into two, as in (168), then there is a gauge invariance, as the product is unchanged by the transformation

$$f_{i\alpha}(t) \to e^{i\lambda(t)} f_{i\alpha}(t), \quad b_i(t) \to e^{i\lambda(t)} b_i(t) . \tag{169}$$

We can promote this invariance to a dynamical gauge symmetry by introducing a gauge field **a** and writing the Hamiltonian in the continuum limit as

$$\mathscr{H} = \int d\mathbf{r} \sum_{\sigma} f_{\sigma}^{\dagger} \left(-\frac{i\nabla + \mathbf{a}}{2m_f} \right)^2 f_{\sigma} + (\phi - \mu_f) f_{\sigma}^{\dagger} f + \int d\mathbf{r}\, b^{\dagger} \left(-\frac{i\nabla + \mathbf{a}}{2m_b} \right)^2 b + (\phi - \mu_b) b_{\sigma}^{\dagger} b . \tag{170}$$

Here, ϕ is a Lagrange multiplier field which is introduced to implement constraint (167). Note that the **a** field enters in much the same way in the Hamiltonian as the electromagnetic field usually does—indeed, a change in the individual f's and b's by a space-dependent phase factor as in (169) can be reabsorbed into a change of **a**. Note also the presence of the chemical potentials μ_f and μ_b to enforce that for a deviation of the (average) density n from one per site, the density of holes is $1 - n$ and of fermions is n.

The next step in the theory is to find the fluctuation propagator for the **a** field, as a function of μ_f and μ_b. For finite μ_f and negative μ_b (bosons uncondensed), the fluctuation propagator is similar to that of the previous section but with $(\alpha v_F/c)$ replaced by a term of $\mathcal{O}(1)$. Spinon and holon self-energies can now be calculated and composition laws [134] are derived to relate physical correlation functions to correlation functions of spinons and holons.

Unfortunately, this very attractive route has turned out to be less viable than had been hoped. It is not clear whether the difficulties are purely technical; they are certainly formidable. The essential reason is that while photons have no mass and are not conserved, and hence cannot Bose condense, in a gauge theory obtained by introducing additional bosons, the bosons generally *can and will* Bose condense because they do have a chemical potential. Bose condensation leads to a mass term in the propagator for the gauge fields. The singularities in the fermions due to the gauge fields then disappear. It is the analogue of the fact that superconductivity leads to the Meissner effect—there the emergence of the superconducting field breaks gauge invariance and leads to the expulsion of the magnetic field from the superconductor. The latter effect can also be thought of as being due to the generation of a mass term for the gauge fields.

Several variants of these ideas have been proposed with and without attempts to suppress the unphysical condensation through fluctuations [188]. The trouble is that such fluctuations tend to bind the spinons and holons and the happy situation in one dimension where they exist independently—being protected by (extra) conservation laws, see Section 4.9—is hard to realize. As usual, it appears that the introduction of new quantum numbers requires new symmetries.

Interesting variants using the idea of spin–charge separation have recently appeared [235,188].

In passing, we note that the idea to split an electron operator into a boson and fermion operator, as in (167), is not limited to gauge theories like the ones discussed in this section. In the form used here, where the boson is carrying the hole charge, such theories are usually

known as slave-boson approaches. Now, the Heisenberg spin one-half problem can also be formulated as a hard-core boson problem, and higher-order spins can be formulated in terms of so-called Schwinger bosons [31]. However, since one generally has some freedom in introducing slave variables for interacting electron problems, mixed variants also exist. For example, the t–J-model can be rewritten in terms of a model with Schwinger bosons carrying the spins and spinless slave fermions carrying the charge [31].

6. Quantum critical points in fermionic systems

As mentioned in Section 1, quantum critical behavior is associated with the existence of a $T = 0$ phase transition; of course, in practice one can only experimentally study the behavior at non-zero temperatures, but in this sense, the situation is no different from ordinary critical phenomena: one never accesses the critical point itself, but observes the critical scaling of various experimentally accessible quantities in its neighborhood.

In practice, the most common situation in which one observes a quantum critical point is the one sketched in Fig. 1, in which there is a low-temperature ordered state—a ferromagnetic state, antiferromagnetic state or charge-density wave-ordered state, for instance—whose transition temperature to the disordered state or some other ordered state goes to zero upon varying some parameter. In this case, the quantum critical point is then *also* the end point of a $T = 0$ ordered state. However, sometimes the "ordered" state really only exists *at* $T = 0$, for example in metal–insulator transitions and in quantum Hall effect transitions [247,212]. A well-known example of this case in spin models is in two-dimensional antiferromagnetic quantum Heisenberg models with "quantumness" as a parameter g [56], which do not order at any finite temperature, but which show genuine ordered phases at $T = 0$ below some value $g < g_c$.

Although the question concerning the origin of the behavior of high-temperature superconductors is not settled yet, there are strong indications, discussed in the next section, that much of their behavior is governed by the proximity to a quantum critical point.

One of the first formulations of what we now refer to as quantum critical behavior was due to Moriya [189,190] and Ramakrishnan [186] who did an RPA calculation for a model of itinerant fermions with a Stoner-type instability to a ferromagnetic state. In modern language, their approach amounts to a $1/N$ expansion. Various other important contributions were made [38,79]. The standard more modern formulation now, which we will follow, is due to Hertz [123]. A nice introduction can be found in the article by Sondhi et al. [247], and for a detailed expose, we refer to the book by Sachdev [225]. See also the review by Continento [67].

6.1. Quantum critical points in ferromagnets, antiferromagnets, and charge-density waves

A clear example of quantum critical behavior, and actually one for which one can compare with theoretical predictions, is summarized in Figs. 34–37. The figures show various data from [254] on the magnetic compound MnSi [205,206,160,170,254]. Fig. 34 shows that for low pressures and temperatures, this compound exhibits a magnetic phase whose transition temperature T_c vanishes as the pressure is increased up to $p_c = 14.8$ kbar. This value of the pressure then identifies the quantum critical point. Fig. 35 shows that when the same data are plotted as $T_c^{4/3}$

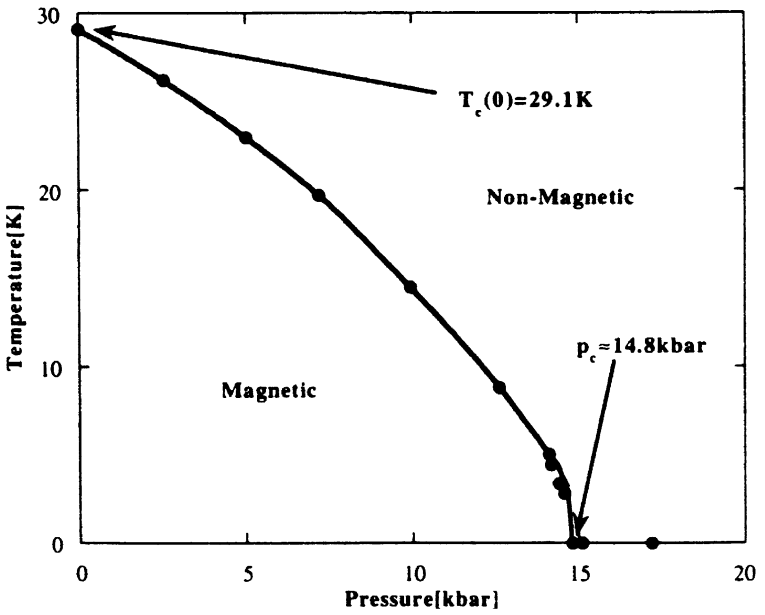

Fig. 34. Magnetic phase diagram as a function of pressure of MnSi [205,206,254]. From [254].

versus pressure, the data fall nicely on a straight line except close to the critical pressure. This observed scaling of $T_c^{4/3}$ with $p - p_c$ away from p_c is in accord with the behavior predicted by the theory discussed below. Actually, the transition is weakly first order near p_c; so a very detailed verification of the theory is not possible.

Fig. 36 shows data for the temperature dependence of $\rho - \rho_0$ near p_c, where ρ_0 is the residual low-temperature resistivity. In the presence of a field of 3 T, one observes the usual $\rho - \rho_0 \sim T^2$ Fermi-liquid scaling, but at zero field the results are consistent with $\rho - \rho_0 \sim T^{5/3}$ behavior predicted by the theory. However, if we write the low-temperature resistivity behavior as

$$\rho = \rho_0 + AT^{\theta} \tag{171}$$

then both the residual resistivity ρ_0 and the amplitude A are found to show a sharp peak at p_c as a function of pressure — see Fig. 37. This behavior is not understood nor is the fact that the exponent θ does not appear to regain the Fermi-liquid value of 2 for significant values of $p > p_c$ (at $H = 0$) and in a temperature regime where the theory would put the material in the quantum-disordered Fermi-liquid regime.

6.2. Quantum critical scaling

Before discussing other experimental examples of quantum critical behavior, it is expedient to summarize some of the essential quantum critical scaling ideas.

As is well known, at a finite temperature transition, the critical behavior is classical and we can use classical statistical mechanics to calculate the correlation functions. This is so

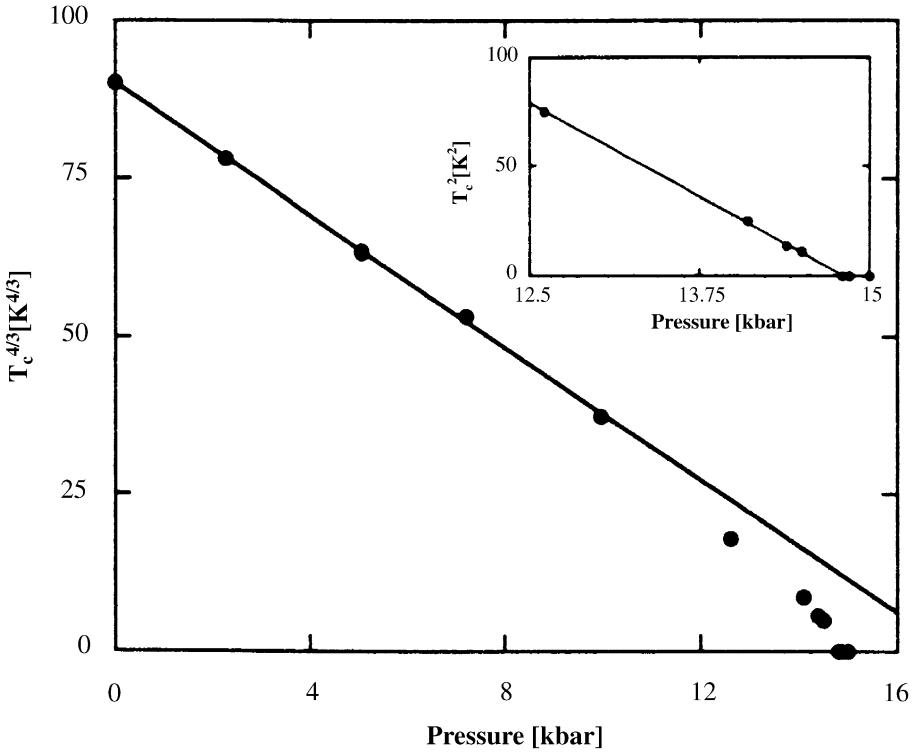

Fig. 35. Power-law dependence of the Curie temperature as a function of pressure for MnSi. From [254].

because due to critical slowing down, the characteristic time scale τ diverges with the correlation length,

$$\tau \sim \xi^z \,. \tag{172}$$

Near a critical point the correlation length ξ diverges as

$$\xi \sim |T - T_c|^{-\nu} \,. \tag{173}$$

The combination of these two results shows that critical slowing down implies that near any finite temperature critical point the characteristic frequency scale ω_c goes to zero as

$$\omega_c \sim |T - T_c|^{\nu z} \,. \tag{174}$$

Therefore, near any phase transition $\omega_c \ll T_c$, and as a result the phase transition is governed by classical statistical physics; the Matsubara frequencies are closely spaced relative to the temperature, the thermal occupation of bosonic modes is large and hence classical, etc.

In classical statistical mechanics, the dynamics is *slaved* to the statics; usually, the dynamical behavior is adequately described by time-dependent Landau-Ginzburg type of equations or Langevin equations which are obtained by building in the appropriate conservation laws and equilibrium scaling behavior [117]. At a quantum critical point, on the other hand, the dynamics must be determined a priori from the quantum-mechanical equations of motion.

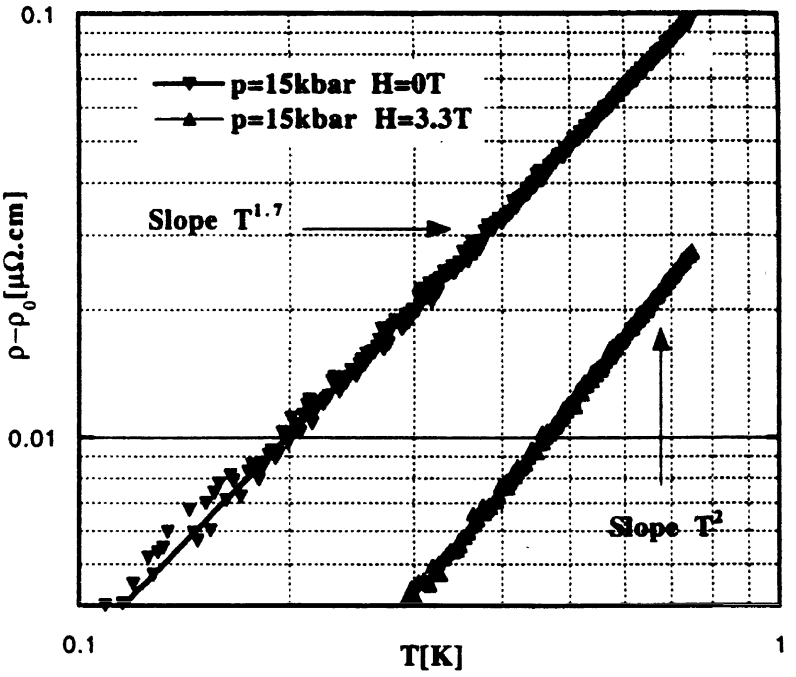

Fig. 36. T-dependence of $(\rho(T)-\rho_{T=0})$ near the critical pressure p_c with and without an external magnetic field. From [254].

The general scaling behavior near a $T=0$ quantum critical point can, however, be discussed within the formalism of dynamical scaling [117,164], just as near classical critical points. Consider for example the susceptibility for the case of MnSi that we considered above. The scaling ansatz for the singular part of the susceptibility

$$\chi(k,\omega,p)=\langle MM\rangle(k,\omega,p) \tag{175}$$

implies that near the critical point where the correlation length and time-scale diverge, the zero-temperature susceptibility χ is a universal function of the scaled momentum and frequency

$$\chi(k,\omega,p)=\xi^{-d_M}\,\Upsilon(k\xi,\omega\xi_t)\,, \tag{176}$$

where now

$$\xi\sim|p-p_c|^{-\nu},\quad \xi_t\equiv\tau=\xi^z\,. \tag{177}$$

This is just like the classical scaling with $T-T_c$ replaced by $p-p_c$. The reason for writing ξ_t instead of τ is that in quantum statistical calculations, the "timewise" direction becomes like an additional dimension, so that ξ_t plays the role of a correlation "length" in this direction. However, the time-direction has both a long-time cutoff given by $1/k_BT$ and a short-time cutoff

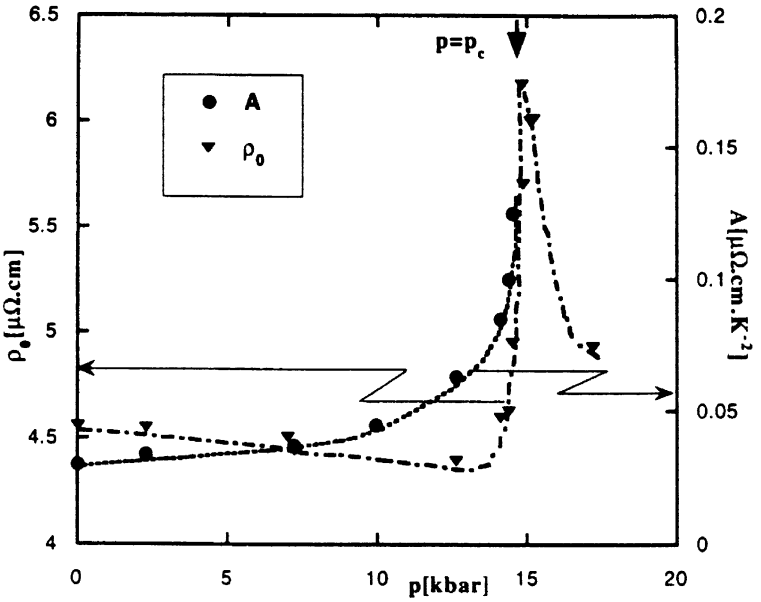

Fig. 37. Evolution of ρ_0 and A under pressure, when the temperature dependence of the resistivity is fitted to $(\rho = \rho_0 + AT^2)$. From [254].

given by the high-energy cutoff in the problem—exchange energy or Fermi energy, whichever is smaller in the ferromagnetic problem. The short-time cutoff has its analog in the spatial scale. The long-time cutoff, which determines the crossover from classical to quantum behavior, plays a crucial role in the properties discussed below. The crucial point is that when $z \neq 1$, there is an anisotropic scaling between the spatial and time-wise directions, and as we shall discuss below, this implies that as far as the critical behavior is concerned, the effective dimensionality of the problem is $d + z$, not $d + 1$.

The exponent d_M in (176) reflects that a correlation function like χ has some physical dimension which often is inevitably related to the spatial dimension. The dependence of critical properties on spatial dimensions must be expressible purely in terms of the divergent correlation length ξ. Often, d_M is fixed by dimensional considerations (in the language of field theory, it is then given by the "engineering dimension" of the field), but this may not be true in general. It must be so, however, if χ is a correlation function of a conserved quantity. [36]

Let us now address the finite temperature scaling, taking again the case of MnSi as an example. The various regimes in the $T-p$ diagram discussed below are indicated in Fig. 38.

[36] E.g. if we consider the free energy *per unit volume* at a classical transition, the energy scale is set by $k_B T$, and $d_M = d$; likewise, if we consider the surface tension of an interface, whose physical dimension is energy per unit surface area, $d_M = d - 1$.

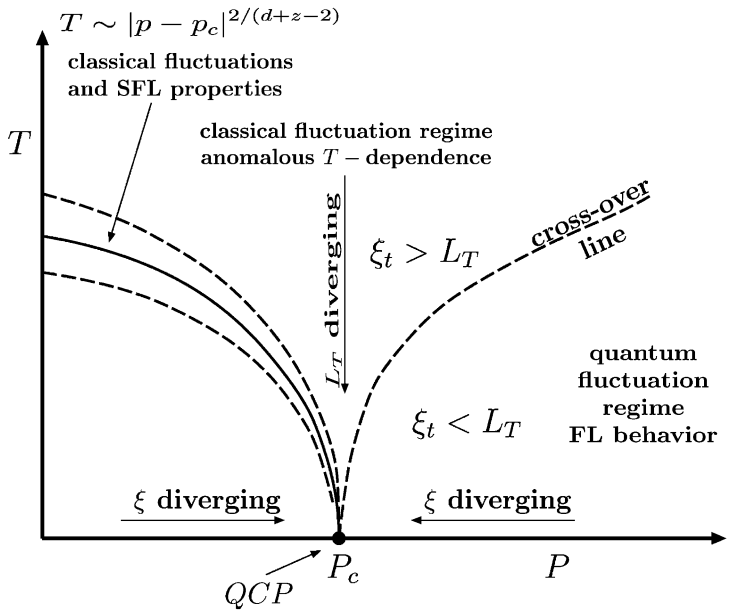

Fig. 38. Generic phase diagram and crossovers for quantum critical points with the various regimes indicated. ξ is the correlation length at $T = 0$; L_T is the "thermal length" given in Eq. (178).

To distinguish these regimes it is necessary to define an additional quantity, the thermal length

$$L_T \equiv \frac{\hbar}{k_B T} \,. \tag{178}$$

L_T corresponds dimensionally to a time-scale. It marks the crossover between phenomena at long time scales which can be treated essentially classically from those on a shorter scale which are inherently quantum mechanical. Whenever $\xi_t < L_T$, the correlation length and time are finite and quantum mechanics begins to dominate. This is the regime on the right in the figure. Fermi-liquid behavior is expected in this regime. However, if one approaches the critical point ($T = 0$, $p = p_c$) from above along the vertical line, then L_T diverges but so does ξ_t. Moreover, ξ_t diverges faster than L_T since z is usually larger than 1. This means that the characteristic fluctuation energy and temperature are similar. So the behavior is quasiclassical throughout each correlated region down to zero temperature (In a path integral formulation [247,225] one considers the model on a infinite strip whose width is finite in the timewise direction and equal to L_T. Hence, for $\xi_t > L_T$ the model is fully correlated across the strip in this direction). This regime is therefore characterized by anomalous T dependence in the physical quantities up to some ultra-violet cutoff. It is important to stress that this so-called "quantum critical scaling behavior"[37] is expected in the observable properties in the complete region between the dashed

[37] The term is somewhat problematic; it refers to the quasiclassical fluctuation regime around a quantum critical point.

lines joining together at $T=0$, $p=p_c$ up to the high temperature scale in the problem, which is usually several times larger than the highest transition temperature to the ordered phase as a function of p. So SFL is observable over a whole range of parameter p for temperatures between the left and right crossover lines.

If one approaches the line of phase transitions to the ordered phase, which is marked with a solid line in the figure, one has a region with SFL properties dominated by classical fluctuations close to the transition. Millis [183] has corrected Hertz's results [123] on this point, and has found that the critical temperature of the phase transition scales as $T_c \sim |p - p_c|^{z/(d+z-2)}$. Estimates of the classical critical region are also given. Results along similar lines may also be found in [66,67].

If we include both the temperature and the parameter p, the scaling ansatz for the imaginary part of χ becomes

$$\chi''(k,\omega,p,T) \sim \xi^{-d_M}\,\Upsilon_1\left(k\xi, \omega\xi^z, \frac{\omega}{T}\right) . \tag{179}$$

This can be rewritten in other forms depending on which experiment is being analyzed. For example, the above form is especially suitable for analysis as a function of $(p - p_c)$. For analyzing data as a function of temperature, we may instead rewrite

$$\chi''(k,\omega,p,T) = L_T^{-d_M/z}\,\Upsilon_2\left(kL_T^{1/z}, \omega L_T, \frac{L_T}{\xi_t}\right) \tag{180}$$

and for analyzing data as a function of frequency

$$\chi''(k,\omega,p,T) = T^{-d_M/z}\,\Upsilon_3\left(\frac{k}{T^{1/z}}, \frac{\omega}{T}, \frac{1}{T\xi_t}\right) . \tag{181}$$

Moreover, the scaling of the free energy $\mathscr{F}$ can be obtained from the argument that it is of the order of the thermal energy $k_B T$ per correlated volume ξ^d. Moreover, since L_T acts as a finite cutoff for ξ_t in the timewise direction, we then get the scaling

$$\mathscr{F} \sim T\xi^{-d} \sim T(\xi_t)^{-d/z} \sim T^{1+d/z} . \tag{182}$$

By differentiating twice, this also immediately gives the specific heat behavior at low temperatures. In writing the above scaling forms, we have assumed that no "dangerously irrelevant variables" exist, as these could change ω/T scaling to ω/T^{Δ} scaling.[38]

In order to get the critical exponents and the crossover scales, one has to turn to a microscopic theory. The theory for this particular case of the quantum critical point in MnSi is essentially

[38] "Dangerously irrelevant variables" are irrelevant variables which come in as prefactors of scaling behavior of quantities like the free energy [97]. Within the renormalization group scenario, the hyperscaling relation $d\nu = 2-\alpha$ is violated above the upper critical dimension because of the presence of dangerously irrelevant variables. Presumably, dangerously irrelevant variables are more important than usually at QCPs, since the effective fluctuation dimension is above the upper critical dimension for $d=3$ and $z>1$. Some examples are discussed in [225].

a random phase approximation and proceeds along the following lines: (i) one starts with a model of interacting fermions; (ii) an ordering field $M(k,\omega)$ is introduced; (iii) one assumes that the fermions can be eliminated near the critical point to get a free energy in terms of M of the form

$$\mathscr{F} = \int \mathrm{d}\omega \int \mathrm{d}^d k \chi^{-1}(k,\omega)|M(k,\omega)|^2 + \int \mathrm{d}\{\omega\} \int \mathrm{d}\{k\} VM(k_1,\omega_1)M(k_2,\omega_2)M(k_3,\omega_3)M(k_4,\omega_4) \times \delta(\omega_1+\omega_2+\omega_3+\omega_4)\delta(k_1+k_2+k_3+k_4) + \cdots . \quad (183)$$

Note that this is essentially an extension of the usual Landau–Ginzburg–Wilson free energy to the frequency domain. Indeed, from here on one can follow the usual analysis of critical phenomena, treating the frequency ω on an equal footing with the momentum k.

The important result of such an analysis is that the effective dimension as far as the critical behavior is $d+z$, *not* $d+1$ as one might naively expect. Since $z \geqslant 1$ in all known examples, the fact that the effective dimension is larger or equal than $d+1$ reflects the fact that the correlation "length" ξ_t in the timewise direction grows as ξ^z, i.e., at least as fast as the spatial correlation length.[39] Moreover, the fact that $z \geqslant 1$ implies that the effective dimension of a $d=3$ dimensional problem is always larger or equal than four. Since the upper critical dimension above which mean field behavior is observed equals four for most critical phenomena, one thus arrives immediately at the important conclusion that most quantum critical points in three dimensions should exhibit classical fluctuations with mean field scaling exponents! It also implies that the critical behavior can typically be seen over a large parameter or temperature range—the question of the width of the critical region, which normally is determined by the Ginzburg criterion, does not arise. On the other hand, questions concerning the existence of dangerously irrelevant variables, due for example to the scaling of the parameters V in Eq. (183), do arise.

In order to judge the validity and generality of these results, it is important to keep in mind that they are derived *assuming* that the coefficients of the M^2, M^4 terms are analytic functions of k, ω and the pressure p, etc. This is completely in line with the usual assumption of analyticity of the bare coupling parameters in a renormalization group approach. This assumption may well be violated—in fact none of the impurity models discussed earlier can be treated along these lines: the fermions cannot be integrated out there, and if one attempts to apply the above procedure, one finds singular contributions to the bare coupling parameters. Later on we shall discuss a three-dimensional experimental example where this assumption appears to be invalid. Secondly, it is inherently an expansion about the non-magnetic state, which cannot apply in the ordered phase: In the ordered phase with non-zero magnetization, $M \neq 0$, there is a gap for some momenta in the fermionic spectra. This gap cannot be removed perturbatively.

[39] This has important consequences for a scaling analysis of numerical data, aimed at determining the critical behavior. For it implies that the finite size scaling has to be done *anisotropically*, with the anisotropy depending on the exponent z which itself is one of the exponents to be determined from the analysis.

In a *ferromagnet*, the ground state susceptibility on the disordered side is given by

$$\chi^{-1}(k,\omega) = \left[(p - p_c) + k^2 + \frac{i\omega}{k v_F} \right] . \tag{184}$$

In the first two terms, we recognize the usual mean field type behavior with a correlation length that diverges as $\xi \sim (p - p_c)^{1/2}$, hence the critical exponent $\nu = 1/2$. The last term, which describes Landau damping of the spin wave modes, is very special here as it arises from fluctuations of magnetization, a quantity which is conserved (commutes with the Hamiltonian). Therefore, the characteristic damping rate must approach zero as $k \to 0$. Since at the critical point (184) leads to a damping $\omega \sim k^3$, the critical exponent $z = 3$. According to the theory described above, the critical behavior at the quantum critical point ($T = 0, p = p_c$) is therefore of the mean field type for any physical dimension $d \geqslant 1$, since the effective dimension $d + z \geqslant 4$ (with only logarithmic corrections to mean field theory when $d = 1$).

The scattering of electrons off the long-wavelength spin waves is dominated by small angle scattering, and it is easy to calculate the resulting dominant behavior of the self-energy of the electrons. Near the critical point, the behavior of χ is very similar to the electromagnetic problem that we discussed in Section 5. Analogously, one also finds SFL behavior here: in $d = 3$, $\Sigma(k_F, \omega) \sim \omega \ln \omega + i|\omega|$ while in $d = 2$ one obtains $\Sigma(k_F, \omega) \sim \omega^{2/3} + i|\omega|^{2/3}$. Furthermore, for the resistivity one finds in three dimensions $\rho \sim T^{5/3}$—this is consistent with the behavior found in MnSi in the absence of a field, see Fig. 36. Moreover, as we mentioned earlier, according to the theory, near the critical point T_c should vanish as $|p - p_c|^{z/(d+z-2)}$; with $d = z = 3$ this yields $T_c \sim |p - p_c|^{3/4}$. As we saw in Fig. 35, this is the scaling observed over a large range of pressures, except very near p_c. $ZrZn_2$ [115] is an example in which the ferromagnetic transition is shifted to $T = 0$ under pressure continuously. The properties are again consistent with the simple theory outlined. There is, however, trouble on the horizon [161]. The asymptotic temperature dependence for $p > p_c$ is not proportional to T^2, as expected. We will return to this point in Sections 6.4.

For *antiferromagnets* or *charge density waves* the critical exponents are different. In these cases, the order parameter is not conserved, and the inverse susceptibility in these cases is of the form

$$\chi^{-1}(k,\omega) = \left[(p - p_c) + (k - k_0)^2 + \frac{i\omega}{\Gamma} \right] , \tag{185}$$

where k_0 is the wavenumber of the antiferromagnetic or charge-density wave order. From this expression we immediately read off the mean field exponents $z = 2$ and $\nu = 1/2$. Since the effective dimension $d + z$ is above the upper critical dimension for $d = 3$, the mean field behavior is robust in three dimensions. In $d = 2$, on the other hand, the effective dimension $d + z = 4$ is *equal to* the upper critical dimension, and hence one expects logarithmic corrections to the mean field behavior. Indeed, in two dimensions one finds for the self-energy [126] $\Sigma(\hat{\mathbf{k}}_F, \omega) \sim \omega \ln \omega + i|\omega|$ (only) for those $\hat{\mathbf{k}}_F$ from which spanning vectors to other regions of the Fermi surface separated by $\mathbf{k}_0$ can be found; the resistivity goes as $\rho(T) \sim T^2 \ln T$ in this case. However, if several bands cross the Fermi surface, as often happens in heavy fermions, Umklapp-type scattering may enforce the same temperature dependence in the resistivity as in the single-particle self-energy,

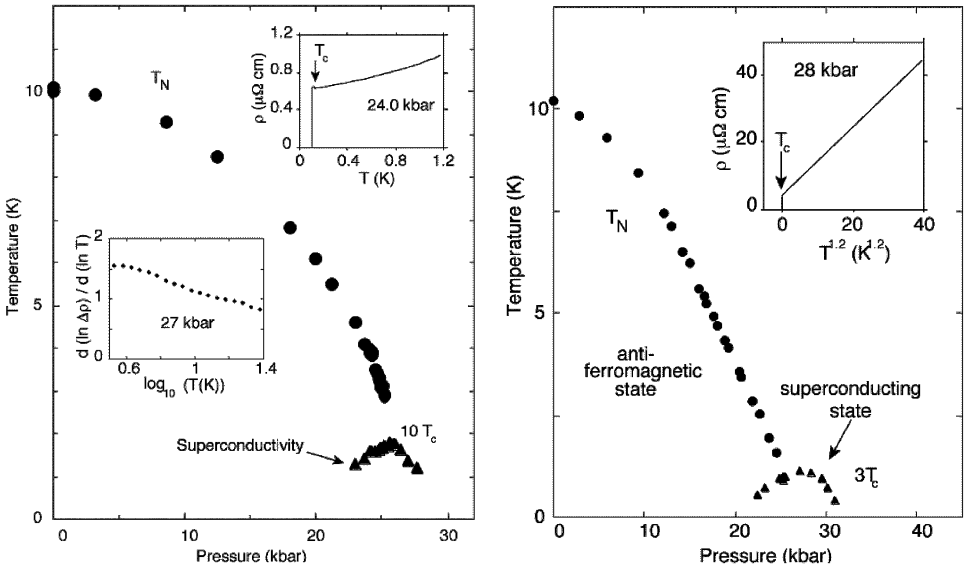

Fig. 39. (Left panel) Temperature–pressure phase diagram of high-purity single-crystal $CeIn_3$. A sharp drop in the resistivity consistent with the onset of superconductivity below T_c is observed in a narrow window near p_c the pressure at which the Néel temperature T_N tends to absolute zero. (upper inset) This transition is complete even below p_c itself. (lower inset). Just above p_c, where there is no Néel transition, a plot of the temperature dependence of $d(\ln \Delta\rho)/d(\ln T)$ is best able to demonstrate that the normal state resistivity varies as $T^{1.6\pm0.2}$ below about 3 K. $\Delta\rho$ is the difference between the normal state resistivity and its residual value (which is calculated by extrapolating the normal state resistivity to absolute zero). For clarity, the values of T_c have been scaled by a factor of ten. (right panel) Temperature–pressure phase diagram of high-purity single-crystal $CePd_2Si_2$. Superconductivity appears below T_c in a narrow window where the Néel temperature T_N tends to absolute zero. The inset shows that the normal state a-axis resistivity above the superconducting transition varies as $T^{1.2\pm0.1}$ over nearly two decades in temperature. The upper critical field B_{c2} at the maximum value of T_c varies near T_c at a rate of approximately $-6T/K$. For clarity, the values of T_c have been scaled by a factor of three, and the origin of the inset has been set at 5 K below absolute zero. Both plots are from Mathur et al. [170].

except at some very low crossover temperature. The physical reason for this dependence despite the fact that the soft modes are at large momentums (and therefore vertex corrections do not change the temperature dependence of transport relaxation rates) is that the set of $\hat{\mathbf{k}}_F$ usually covers a small portion of the Fermi surface.

Fig. 39 shows the phase diagram of two compounds that order antiferromagnetically at low temperatures. The first one, $CeIn_3$, is a three-dimensional antiferromagnet. A superconducting phase intervenes at very low temperatures (note the different scale on which the transition to the superconducting phase is drawn), covering the region around the quantum critical point at a pressure of about 26 kbar. At this pressure, the normal state resistivity is found to vary as $\rho(T) \sim T^{1.6\pm0.2}$ which is consistent with the theoretical prediction that at a quantum critical point dominated by antiferromagnetic fluctuations the resistivity should scale as $\rho \sim T^{1.5}$. The right panel in Fig. 39 shows the phase diagram and resistivity data of the three-dimensional antiferromagnet $CePd_2Si_2$; the data in this case are best fitted by $\rho \sim T^{1.2}$; this is consistent with the theoretical prediction $\rho \sim T^{1.25}$ which results if one has a $(\mathbf{k}-\mathbf{k}_0)^4$ dispersion around

the AFM vector $\mathbf{k}_0$ in one direction and the usual $(\mathbf{k}-\mathbf{k}_0)^2$ dispersion in the other two. However, no independent evidence for such dispersion is available yet. In both these cases, part of the region of superconductivity, in a region bounded by a line emanating from the QCP and going on to the transition line from the antiferromagnetic to the normal state, is expected to be antiferromagnetic as well.

These two compounds are also of interest because the phase diagram bears a resemblance to the phase diagram of the high-T_c copper-oxide based superconductors in which the conduction electron density is the parameter varied—see Fig. 49. Unlike the heavy fermion compounds where the ordered phase is antiferromagnetic, the order in copper-oxides near the QCP is not AFM. Its nature is in fact unknown. In the heavy fermion compounds, superconductivity promoted by antiferromagnetic fluctuations is expected to be of the d-wave variety [187] as it is in the high-T_c copper-oxide compounds.

6.3. Experimental examples of SFL due to quantum criticality: open theoretical problems

We have discussed the observed quantum critical behavior in some system which is largely consistent with the simple RPA-like theoretical predictions. There are, however, quite a few experimentally observed signatures of singularities near QCPs, especially in heavy fermion compounds, which are not understood theoretically by the simple RPA theory of the previous subsection. In this section, we present some prominent examples of these.

RPA-type theories work when the dissipation of fluctuations is given very simply. The failures below show that dissipation in the quantum to classical crossover regime in actual physical systems is quite often much more interesting; it has singularities not anticipated in RPA. The difficulties are almost certainly not just mathematical. While dissipation in classical mechanics is intoduced *ex cathedra*, in quantum problems we need to understand it in a fundamental way.

The experimental observations fall into two general categories, in both of which the low-temperature resistivity does not obey the power laws expected of Fermi liquids: Compounds in which resistivity decreases from its limit at $T=0$ and those in which it increases. In both cases, the C_v/T is singular for $T\to 0$. It is reasonable to associate the former with the behavior due to impurities and the latter with the QCP properties of the pure system. However, as we discussed in Section 3.9, the QCP due to impurities requires tuning to special symmetries unlikely to be realized experimentally. As we will discuss, the effect of impurities without any special symmetries but coupling to the order parameter is expected to be quite different near the QCP of the pure system compared to far from it. Under some circumstances, it is expected to be singular and may dominate the observations.

We start with experiments in the second category. Figs. 40–42 show several datasets for the heavy fermion compound $CeCu_{6-x}Au_x$ for various amounts of gold. This compound exhibits a low-temperature paramagnetic phase for $x<0.1$ and a low-temperature antiferromagnetic phase for $x>0.1$. The specific heat data of Fig. 40 and the resistivity data of Fig. 42 show that while without Au, i.e., in the paramagnetic regime, the behavior is that of a heavy Fermi-liquid metal, the alloy near the quantum critical composition $CeCu_{5.9}Au_{0.1}$ exhibits a specific heat with an anomalous

$$C_v \sim T\ln T \tag{186}$$

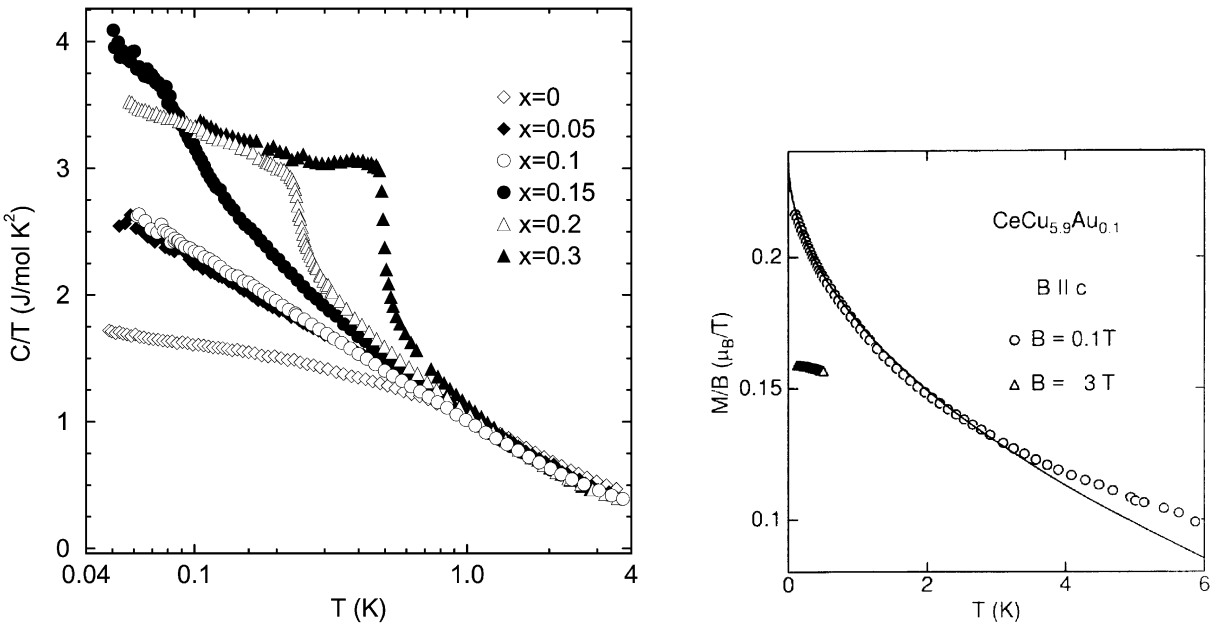

Fig. 40. The specific heat C/T of $CeCu_{6-x}Au_x$ versus $\log T$. From Löhneysen et al. [282–284].

Fig. 41. Susceptibility data for $CeCu_{5.9}Au_{0.1}$. From Löhneysen et al. [285].

over a temperature range of almost two decades. At the same composition, the resistivity shows a linear temperature dependence, and the susceptibility data in Fig. 41 which have been fitted to a deviation from a constant as $T \to 0$ varying as a $\sqrt{T}$ cusp. The anomalous behavior is replaced by Fermi-liquid properties by both a magnetic field and increasing the substitution of copper by gold or by application of pressure [44,281]. The compound $YbRh_2S_2$ seems to have similar properties [258]. Related properties have also been found in U_2Pt_2In [88,89] and in $UPt_{3-x}Pd_x$ [75], UBe_{13}, $CeCu_2Si_2$, $CeNi_2Ge_2$ [250]. The SFL properties observed at the Mott insulator-to-metal transition in $BaVS_3$ [99] are also of related interest. A good example of an antiferromagnetic QCP in itinerant electrons is in the alloy series $Cr_{1-x}V_x$ for which the magnetic correlations have been measured [122].

None of the quantum critical properties of the CeCuAu compounds is consistent with any of the models that we have discussed. Information on the magnetic fluctuation spectra for $CeCu_{5.9}Au_{0.1}$ is available through neutron scattering experiments [229,251]. The data shown in Fig. 43 show rod-like peaks, indicating that the spin fluctuations are almost two-dimensional at this composition. The neutron scattering data can be fitted by an expression for the spin susceptibility of the form

$$\chi^{-1}(k,\omega) = C[f(\delta k) + (-i\omega + aT)^{\alpha}] \tag{187}$$

with a function f which is consistent with an effectively two-dimensional scattering

$$f(\delta k) = b(\delta k_{\perp})^2 + c(\delta k_{\parallel})^4 \,. \tag{188}$$

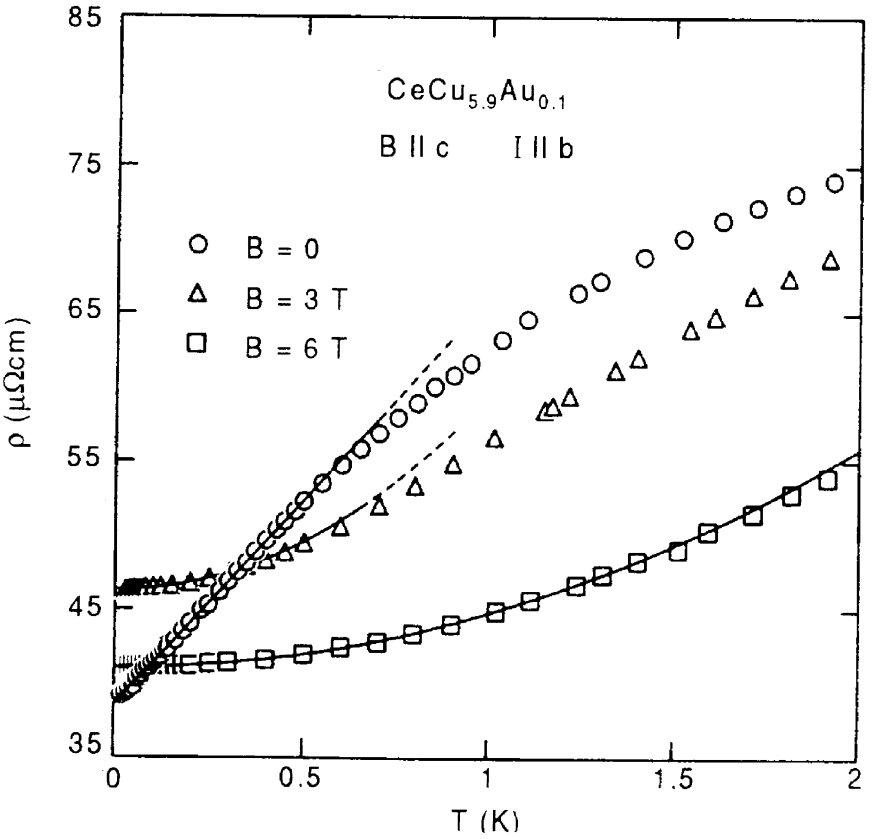

Fig. 42. Resistivity data for $CeCu_{5.9}Au_{0.1}$. From Löhneysen et al. [285].

$\delta k_{\|}$ and $\delta k_{\perp}$ are the deviations from the AFM Bragg vector parallel and perpendicular to the c-axis in these (nearly) orthorhombic crystals. Further

$$a \approx 1, \quad \alpha = 0.74 \pm 0.1 \, . \tag{189}$$

At present, there is no natural leeway for this anomalous exponent α within known theoretical frameworks. However, if one accepts this particular form of χ as giving an adequate fit, then the observed specific heat follows: at the critical composition, we expect the scaling relation

$$\mathscr{F} \sim T\xi_{\perp}^{-(d-1)}\xi_{\|}^{-1} \sim TT^{(d-1)\alpha/2}T^{\alpha/4} \sim T^{1+(d-1/2)\alpha/2} \, , \tag{190}$$

which immediately gives $C_V \sim \mathrm{d}^2\mathscr{F}/\mathrm{d}T^2 \sim T$ for $\alpha = 4/5$. A better calculation [229,230] provides the logarithmic multiplicative factor. Even the measured uniform magnetic susceptibility is consistent with the above form of $\chi(q,\omega)$.

The observed resistivity does not follow directly from the measured χ; a further assumption is required. The assumption that works is that fermions couple to the fluctuations locally, as in

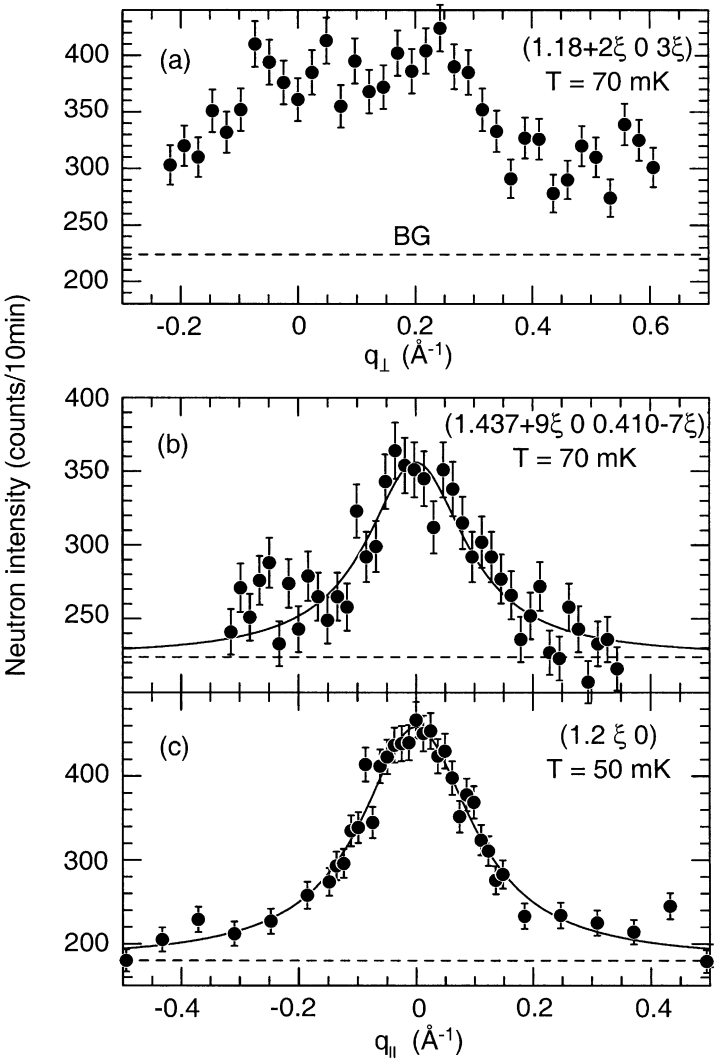

Fig. 43. Neutron scattering data for $CeCu_{5.9}Au_{0.1}$, a compound which is close to a QCP. The figure shows q-scans along three different crystallographic directions, from top to bottom in the a, b and c directions for $\hbar\omega = 0.1$ meV. The figures show that there is only a weak q-dependence along the rods ($q_\perp$), while transverse scans ($q_{\|}$) show well-defined peaks with nearly the same line width. From Stockert et al. [251].

an effective Hamiltonian $\sim c^{\dagger}_{i,\sigma'} c_{i,\sigma} S_{i,\sigma,\sigma'}$. Then if the measured fluctuation spectra are that of some localized spins S_i, the single-particle self-energy is that due to the exchange of bosons with propagator proportional to

$$\sum_k \chi(\mathbf{k},\omega) \sim \ln(\omega) + \mathrm{i}\,\mathrm{sgn}(\omega)\,. \tag{191}$$

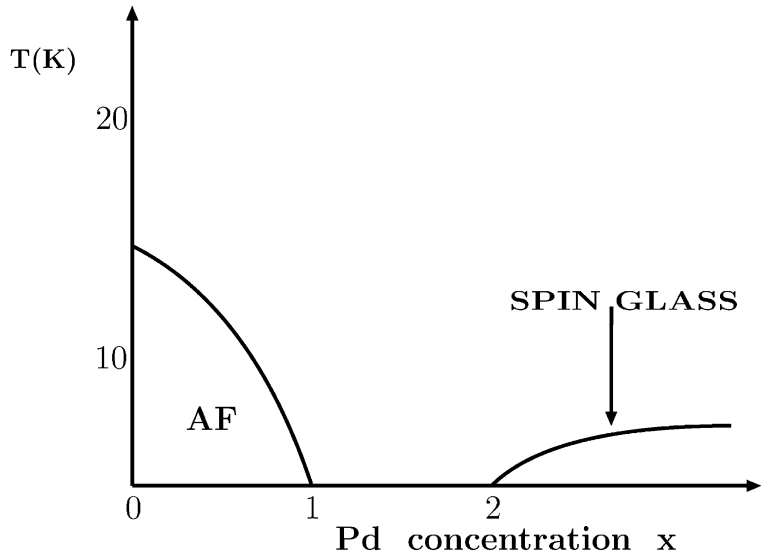

Fig. 44. The phase diagram of $UCu_{5-x}Pd_x$. At low dopings and temperatures, the system is in an antiferromagnetic phase. In the undoped sample ($x=0$): $T_N=15$ K with a magnetization $\mu \simeq 1\mu_B$. For doping $x=1$ and 1.5 the specific heat $C_v/T \sim T$ (for $x=1$) while displaying weak logarithmic characteristics for $x=1.5$. Similarly, the susceptibility $\chi(T) \sim \ln T$ and $\chi \sim T^{-0.25}$ (for $x=1$, 1.5, respectively). Courtesy of M. C. Aronson.

This ensures that the single-particle relaxation rate as well as the transport relaxation rate[40] is proportional to T. A major theoretical problem is why the non-local or "recoil" terms in the interaction of itinerant fermions are irrelevant — i.e., why is the effective Hamiltonian not

$$\Sigma_{k,q} c^{\dagger}_{k+q,\sigma} c_{k,\sigma'} (S_q + S^{\dagger}_{-q})_{\sigma',\sigma} \,, \tag{192}$$

or, in other words, why has momentum conservation been legislated away?

The singularity of χ also raises the question whether the anharmonic processes, Fig. 33(c), which are benign and allow the elimination of fermions in the RPA theory, give singular contributions to χ. Also, can fermions really be eliminated in calculating the critical behavior? At a more mundane level, what is the form of the microscopic magnetic interactions in the problem which lead to the observed two-dimensional nature of the correlations?

As an example in the second category, in Fig. 44 we show the phase diagram of some of the resistivity data of the heavy fermion compound $UCu_{5-x}Pd_x$. There are several other compounds in this category also; for a review we refer to [169,171]. For a theoretical discussion of the scaling properties of some of this class of problems see [27].

For $x < 1$, there is an (antiferromagnetic) ordered state at low temperatures, while for $x > 2$, a spin-glass phase appears. At first sight, one would therefore expect possible SFL behavior *only* near the critical composition $x=1$ and near $x=2$. The remarkable observation, however,

[40] In this calculation, the $\delta k_{\|}^4$ dispersion is neglected entirely, so that the problem is two dimensional. The inclusion of this term changes the result to $T^{5/4}$.

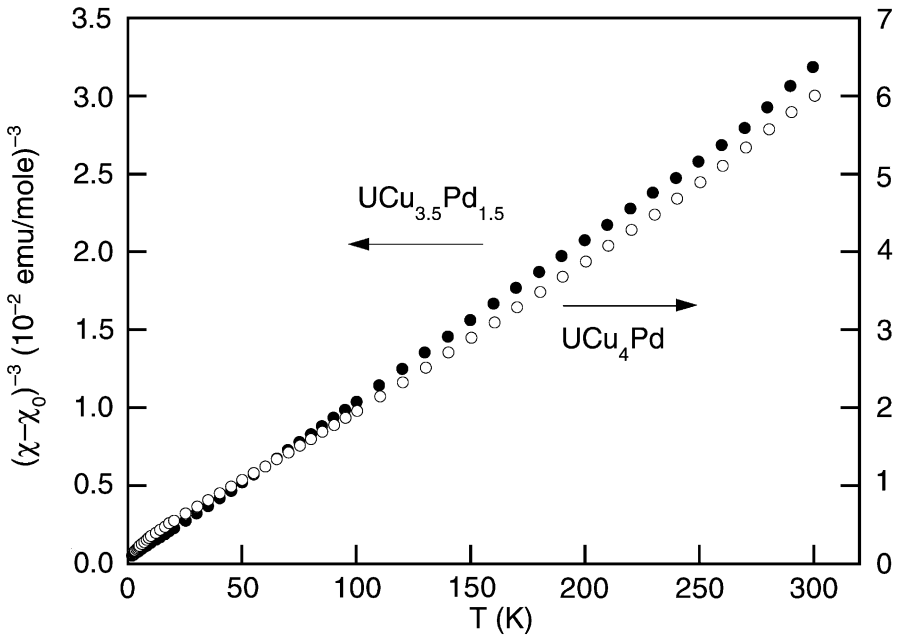

Fig. 45. The temperature dependence of the static susceptibility of $\chi(T)$ for both UCu_4Pd and $UCu_{3.5}Pd_{1.5}$, showing that for both compounds, $\chi(T)$ has a low temperature divergence as $T^{-1/3}$. The measuring field is 1 T. From Aronson et al. [29,30].

is that over a whole range of intermediate compositions, one observes anomalous behavior of the type [29,30]

$$\rho = \rho_0 - BT^{1/3}, \quad \chi \sim T^{-1/3} . \tag{193}$$

The data for χ that show this power-law behavior for $UCu_{3.5}Pd_{1.5}$ and UCu_1Pd are shown in Fig. 45. Note that the anomalous scaling is observed over a very large temperature range, and that it is essentially the same for the compound with $x = 1$ which as Fig. 44 shows is a good candidate for a composition close to a QCP, and the compound with $x = 1.5$ which is right in the middle of the range where there is no phase transition. The fact that this is genuine scaling behavior is independently confirmed [29,30] from the fact that the frequency-dependent susceptibility, measured by neutron scattering, shows a very good collapse of the data with the scaling assumption [41]

$$\chi''(\omega, T) = T^{-1/3}\, \Upsilon\left(\frac{\omega}{T}\right) . \tag{194}$$

Again, none of this behavior finds a clear explanation in any of the well-studied models. One is tempted to use the critical points of impurity models (see for example [70] and references therein), but runs into the difficulty of having to tune to special symmetries. The ideas of critical

[41] We note that this as well as the result for χ in CeCuAu are examples of an anomalous dimension, as the engineering dimension of the susceptibility χ is $1/energy$—see the remark made just after Eq. (177).

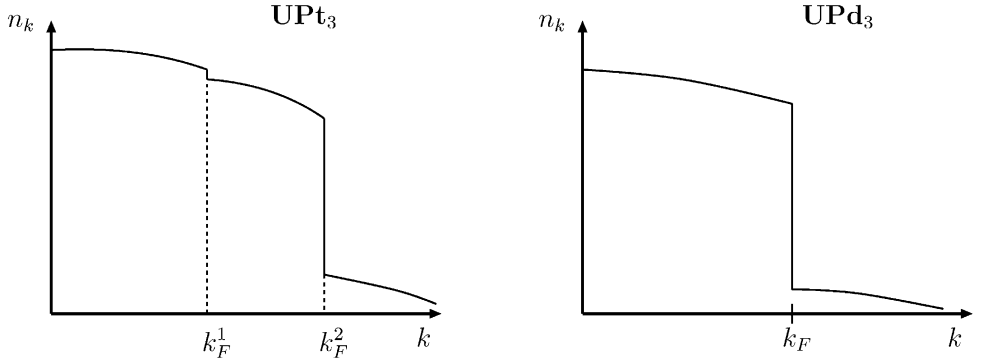

Fig. 46. Schematic occupation number function n_k for UPt_3 and for UPd_3.

points of metallic spin-glasses (see for example [224,234]), although theoretically appealing, are also not obviously applicable over such a wide range of composition. It must be mentioned however, that NMR does show clear evidence of the inhomogeneity in the singular part of the magnetic fluctuations in several heavy fermion compounds [42]. This has inspired models of varying sophistication (see [185] and references therein, and also [55]) in which the Kondo temperature itself has an inhomogeneous distribution. It is possible to fit the properties with reasonable distributions but there is room for a deeper examination of the theoretical issues related to competition of disorder, Kondo effects and magnetic interactions between the magnetic moments.This point is reinforced by recent measurements of local magnetic fluctuation spectra through μ-relaxation measurements [165]. Singular fluctuations are observed with a power law in agreement with (194). What is new is that the fluctuations are deduced to be independent of spatial location, indicating that they are a collective property and cannot be attributed to inhomogeneous local scales such as the Kondo temperatures.

6.4. Special complications in heavy fermion physics

In heavy fermion compounds, there is often an additional complication that besets treating a QCP as a simple antiferromagnetic transition coupled to itinerant electrons. Often, such materials exhibit magnetic order of the f-electrons (with magnetic moments of $\mathcal{O}(1\mu_B)$ per f-electron). Thus, such materials have local moments in the ordered phase; so the disappearance of the (anti)ferromagnetic order at a quantum critical point is accompanied by a metal–insulator transition of the f-electrons. This means that the volume of the Fermi surface changes in the transition.

We may illustrate the above scenario by comparing UPt_3, a heavy fermion compound with effective mass of the order of 100, with UPd_3, an "ordinary" metal with effective mass of $\mathcal{O}(1)$ in which the f-electrons are localized. A schematic summary of the momentum occupation n_k for the two cases is shown in Fig. 46: in the former n_k is shown with two discontinuities, one small $\mathcal{O}(10^{-2})$ representing the large renormalization in the effective mass of "f-electrons" while the other is close to 1 representing the modest renormalization of s- and d-electrons. The other case, representative of UPd_3 has just one Fermi surface with a jump in n_k close

to 1. The Fermi surface in the former encloses the number of electrons equal to the sum of the f and s–d electrons while the latter includes only the s–d electrons. This is consistent with de Haas-van Alphen measurements as well as the band structure calculations of the two compounds; but the band structure calculation must be carried out with the f-electrons assumed as being itinerant in the former and as part of the localized core in the latter. The magnetic transitions in heavy fermion compounds (with ordered moment of $\mathcal{O}(1\mu_B)$) occurs through the conversion of itinerant f-electrons to localized electrons. So the Fermi surface on the two sides of the transition must switch between the two schematic representations in Fig. 46. The problem couples the "metal–insulator transition" of the f-electrons to the magnetic fluctuations—those of itinerant electrons on one side and of interacting local moments on the other. The fluctuations of the metal–insulator transition and the Fermi surfaces is an important part of the problem. Some theoretical work with these ideas in mind is available [242]. Another possible approach is to generate an effective Hamiltonian for the heavy fermion lattice from a pairwise sum of the effective Hamiltonian deduced from the two Kondo impurity problems discussed in Section 3.9 and study its instabilities. The two impurity problems contain the rudiments of some of the essential physics.

In connection with the data in $CeCu_{6-x}Au_x$, we have discussed two important puzzles: the non-trivial exponent d_M/z measured by $\chi(k,\omega)$, and the coupling of fermions to the local fluctuations alone for transport properties. In the other category (impurity-dominated), the first puzzle reoccurs; the second puzzle may be explained more easily since the measured fluctuation spectrum $\chi(k,\omega)$ is in fact k-independent. Both puzzles reoccur in the SFL phenomena in the cuprate compounds to be discussed in Section 7.

6.5. Effects of impurities on quantum critical points

As is well known, randomness can have an important effect on classical phase transitions. Two classes of quenched disorder are distinguished: First, impurities coupling quadratically to the order parameter [121] or, equivalently, impurities which may be used to define a local transition temperature $T_c(r)$; the second class concerns impurities coupling linearly to the order parameter [131]. The so-called Harris criterion, for the first class, tells us that the disorder is relevant, i.e., changes the exponents or turns the transition to a crossover, if the specific heat exponent α of the pure system is positive or, equivalently, if

$$d\nu - 2 < 0\,. \tag{195}$$

For application to QCP phenomena, the value of ν to be used is different in the quantum fluctuation regime and the quasiclassical regime.[42] For the latter, ν should be defined by the correlation length $\xi \sim (T - T_c)^{-\nu_1}$ for a fixed $(p - p_c)$ while in the former, near $T = 0$ it should be defined by $\xi \sim (p - p_c)^{-\nu_2}$. Accordingly, the effect of disorder depends on the direction from which one approaches the QCP. Similarly, the celebrated Imry-Ma argument [131] for linearly coupled disorder can be generalized to QCPs.

[42] Actually, the Harris criterion is derived in the form (195) for ν and d, *not* in terms of the exponent α. This is particularly important at QCPs, since as we discussed in Section 6.2 for QCPs, one is often *above* the upper critical dimension where the hyperscaling relation $d\nu - 2 = \alpha$ breaks down.

In problems of fermions, additional effects of disorder arise because the vertices coupling the impurity to the fermions can be renormalized due to the singularity in the fluctuation of the pure system [271]. Not too much work has been done along these lines. A simple example is the effect of magnetic impurities near a ferromagnetic transition [155]. The growth of the magnetic correlation length converts a single-channel Kondo effect to a multichannel Kondo effect with a regime in which the singularities discussed in Section 3.8 for the degenerate multichannel Kondo effect may be realized without tuning any parameters [166]. This may be relevant to the deviations from the predictions of the pure case discussed here in the properties near the QCP in MnSi. Extensions of these ideas to antiferromagnetic and other QCPs would be quite worthwhile.

7. The high-T_c problem in the copper-oxide-based compounds

About 10^5 scientific papers have appeared in the field of high-T_c superconductors since their discovery in 1987. For reviews, see the Proceedings [175] of the latest in a series of Tri-annual Conferences or [110]. Although no consensus on the theory of the phenomena has been arrived at, the intensive investigation has resulted in a body of consistent experimental information. Here, we emphasize only those properties which are common to all members of the copper-oxide family and in which singular Fermi-liquid properties appear to play the governing role.

The high-T_c materials are complicated, and many fundamental condensed matter physics phenomena play a role in some or other part of their phase diagram. As we shall see, the normal state near the composition of the highest T_c shows convincing evidence of being a weak form of an SFL, a marginal Fermi liquid. Since the vertices coupling fermions to the fluctuations for transport in the normal state and those for Cooper pairing through an exchange of fluctuations can be derived from each other, the physics of SFL and the mechanism for superconductivity in the cuprates are intimately related.

7.1. Some basic features of the high-T_c materials

A wide variety of Cu–O containing compounds with different chemical formulae and different structures belong to the high-T_c family. The common chemical and structural features are that they all contain two-dimensional stacks of CuO_2 planes which are negatively charged with neutralizing ions and other structures in between the planes. The minimal information about the structure in the Cu–O planes and the important electronic orbitals of the copper and oxygen atoms is shown in Fig. 47. The structure of one of the simpler compounds $La_{2-x}Sr_xCuO_4$ is shown in Fig. 48(a) with the CuO_2 plane shown again in Fig. 48(b). For $x=0$ the CuO_2 plane has a negative charge of $-2e$ per unit cell which is nominally ascribed to the $Cu^{2+}(O^{2-})_2$ ionic configuration. Since O^{2-} has a filled shell while Cu^{2+} has a hole in the three-dimensional shell, the Cu–O planes have a half-filled band according to the non-interacting or one-electron model. However, at $x=0$, the compound is an antiferromagnetic insulator with $S=1/2$ at the copper sites. This is well known to be characteristic of a Mott-type insulator in which the electron–electron interactions determine the ground state. Actually [297,266,267], copper-oxide compounds at $x=0$ belong to the charge-transfer sub-category of Mott-insulators. However, at $x=0$, the ground state and low-energy properties of all Mott-insulators are *qualitatively*

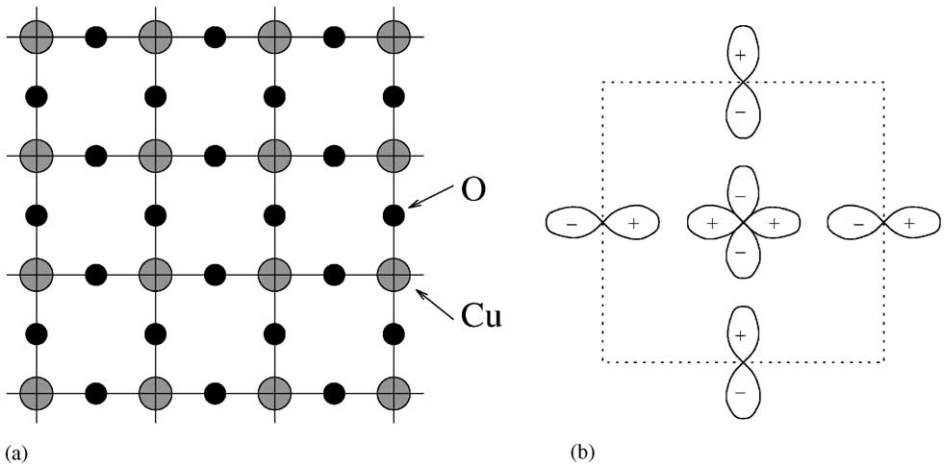

Fig. 47. (a) Schematic structure of the copper-oxide *ab*-planes in La_2CuO_4. Ba or Sr substitution for La in the parent compound La_2CuO_4 introduces holes in the CuO_2 planes. The structure of other high T_c materials differs only in ways which do not affect the central issues, e.g. it is oxygen doping in $YBa_2Cu_3O_{6+x}$ that provides planar holes. The magnetic moments of the planar copper atoms are ordered antiferromagnetically in the ground state of the undoped compounds. From [135]. (b) The "orbital unit cell" of the Cu–O compounds in the *ab* plane. The minimal orbital set contains a $d_{x^2-y^2}$ orbital of Cu and p_x and a p_y orbital of oxygen per unit cell.

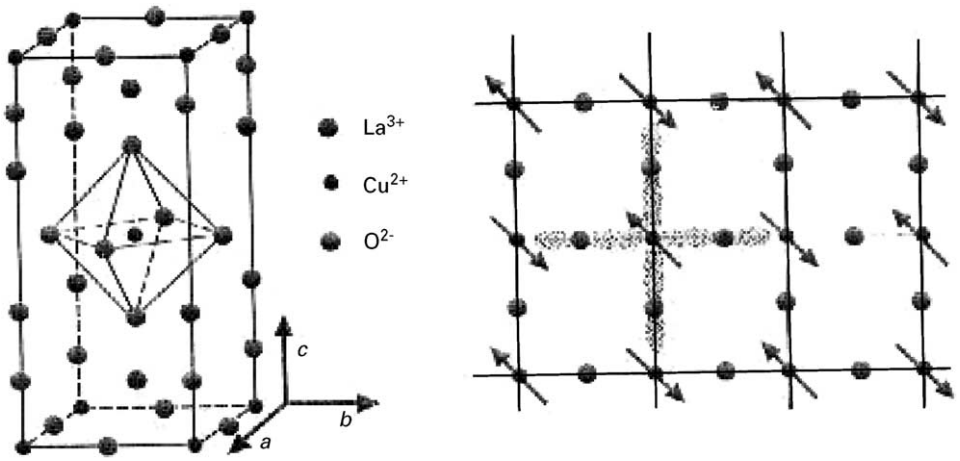

Fig. 48. (left) The crystal structure of La_2CuO_4. From [201]. Electronic couplings along the *c* direction are weak; (right) schematic of the CuO_2 plane. The arrows indicate the alignment of spins in the antiferromagnetic ground state of La_2CuO_4. Speckled shading indicates oxygen p_σ orbitals; coupling through these leads to a superexchange in the insulating state.

the same. By substituting divalent Sr for the trivalent La in the above example, "holes" are introduced in the copper-oxide planes with density x per unit cell.

Fig. 49 is the generic phase diagram of the Cu–O compounds in the T–x plane. In the few compounds with electron doping which have been synthesized properties vary with doping density in a similar way.

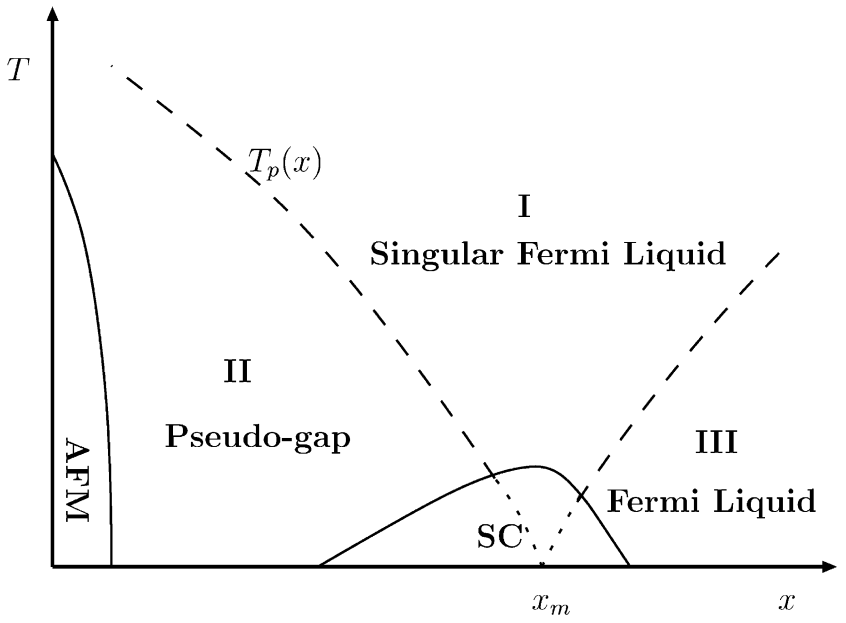

Fig. 49. Generic phase diagram of the cuprates for hole doping. The portion labeled by AFM is the antiferromagnetic phase, and the dome marked by SC is the superconducting phase. Crossovers to other characteristic properties are marked and discussed in the text. A low-temperature "insulating phase" in Region II due to disorder has not been shown.

Antiferromagnetism disappears for x typically less than 0.05 to be replaced by a superconducting ground state starting at somewhat larger x. The superconducting transition temperature is peaked for x typically between 0.15 and 0.20 and disappears for x typically less than 0.25. We will define x_m to be the density for maximum T_c. Conventionally, copper-oxides with $x < x_m$ are referred to as underdoped, with $x = x_m$ as optimally doped and with $x > x_m$ as overdoped. Superconductivity is of the "d-wave" singlet symmetry.

The superconducting region in the T–x plane is surrounded by three distinct regions: a region marked (III) with properties characteristic of a Landau Fermi liquid, a region marked (I) in which (marginally) SFL properties are observed and a region marked (II) which is often called the *pseudo-gap* region whose correlations in the ground state still remain a matter of conjecture. The *topology* of Fig. 49 around the superconducting region is that expected around a QCP. Indeed, it resembles the phase diagram of some heavy fermion superconductors (see e.g. Fig. 39) except that region II has no long-range antiferromagnetic order—the best experimental information is that, generically, spin rotational invariance as well as (lattice) translational invariance remains unbroken in the passage from (I) to (II) in the Cu–O compounds.

The quantity $\gamma(T) \equiv C_v(T)/T$ and the magnetic susceptibility $\chi(T)$, which are temperature independent for a Landau Fermi liquid begin to decline rapidly [162] in the passage from region I to region II, which we will call $T_p(x)$, but without any singular feature. However, the transport properties—resistivity, nuclear relaxation rate (NMR), etc.—show sharper change in their temperature dependence at $T_p(x)$. The generic deduced electronic contribution to the specific heat for overdoped, optimally doped and underdoped compounds is shown in Fig. 50.

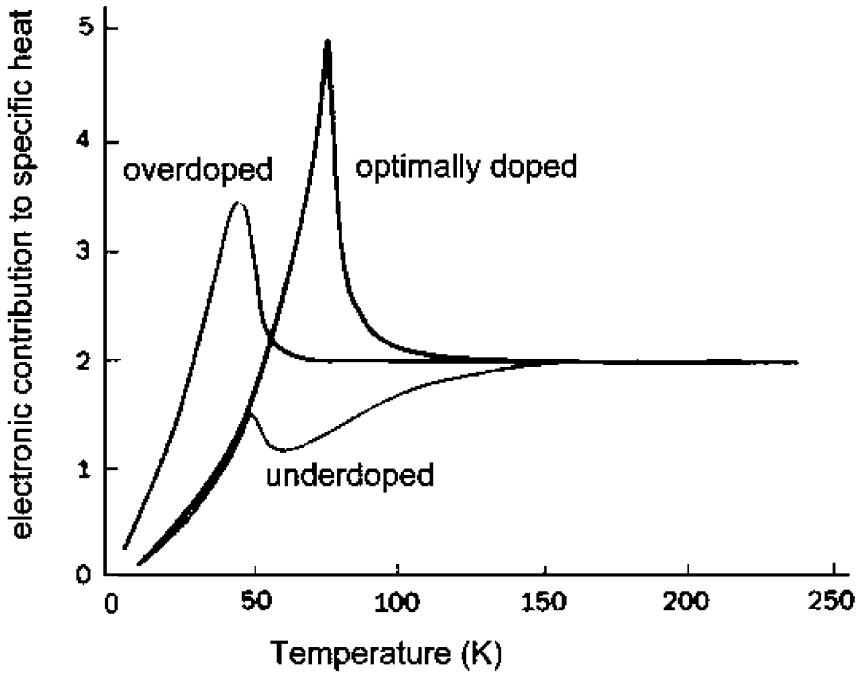

Fig. 50. The electronic contribution to the specific heat as a function of temperature for underdoped, optimally doped and overdoped samples of $Y_{0.8}Ca_{0.2}Ba_2Cu_3O_{7-x}$. For optimally doped and overdoped samples, the heat capacity remains constant as the temperature is lowered, then shows the characteristic features at the superconducting transition temperature T_c and rapidly approaches zero in the superconducting state. For underdoped samples, however, the heat capacity starts to fall well above T_c as the temperature is reduced, and there is only a small peak at T_c indicating much smaller condensation energy than the optimal and overdoped compounds [162]. From [35].

The generic behavior for an underdoped compound for the resisitivity, nuclear relaxation rate and Knight shift—proportional to the uniform susceptibility—is shown in Fig. 51. Angle resolved photoemission (ARPES) measurements show a diminution of the electronic density of states starting at about $T_p(x)$ with a four-fold symmetry: no change along the (π,π) directions and maximum change along the $(\pi,0)$ directions. The magnitude of the anisotropic "pseudo-gap" is several times $T_p(x)$.

It is important to note that given the observed change in the single-particle spectra, the measured specific heat and the magnetic susceptibility in the pseudo-gap region are consistent with the simple calculation using the single-particle density of states alone. Nothing fancier is demanded by the data, at least in its present state. Moreover, the transport properties as well as the thermodynamic properties at different x can be collapsed to scaling functions with the same $T_p(x)$ as a parameter [291].

7.2. Marginal Fermi liquid behavior of the normal state

Every measured transport property in Region I is unlike that of a Landau Fermi liquid. The most commonly measured of these is the dc resistivity shown for many different compounds at

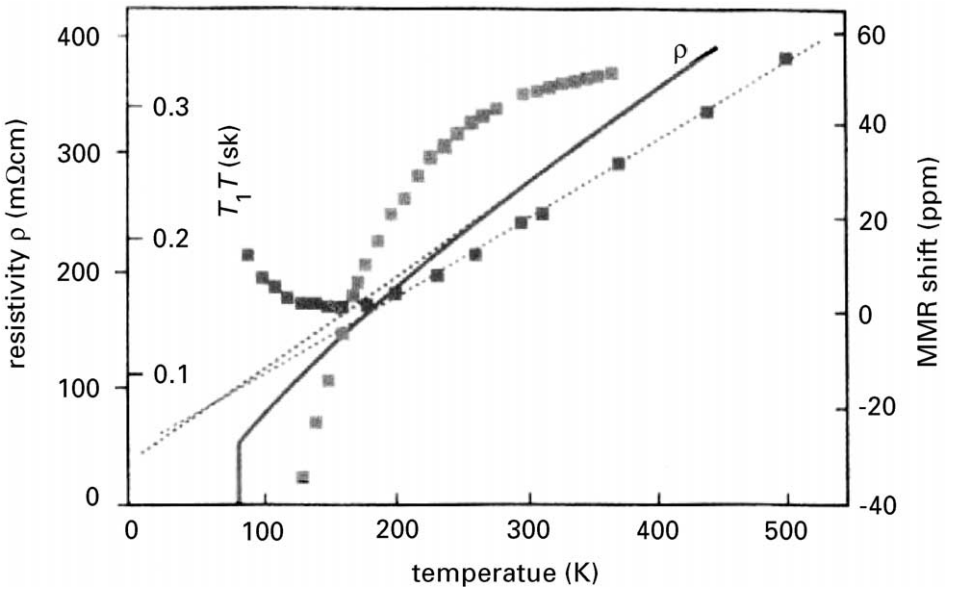

Fig. 51. Signatures of the pseudo-gap in various transport properties for the underdoped compound $YBa_2Cu_4O_8$. At high temperatures, the resistivity (solid line) decreases linearly with temperature. In the pseudogap region, it drops faster with temperature before falling to zero at the superconducting transition temperature (about 85 K). Similarly, the NMR relaxation time displays characteristics of the optimum doped compounds above about 200 K (squares on dashed line) but deviates strongly from it in the pseudogap region. The NMR shift (top squares) also deviates from the temperature-independent behavior (not shown) below the inset of the pseudogap. Note that the pseudogap expresses itself as a sharper change with temperature in the transport properties compared to the equilibrium properties—specific heat and magnetic susceptibility [46,293,10]. From [35].

the "optimum" composition in Fig. 52 including one with $T_c \approx 10$ K. The resistivity is linear from near T_c to the decomposition temperature of the compound. As shown in Fig. 51, in the "under-doped" region, the departure from linearity commences at a temperature $\sim T_p(x)$ marked in Fig. 49. Similarly, the crossover into region (III) shown in Fig. 49 is accompanied by Fermi-liquid-like properties. Wherever measurements are available, every other measured transport property shows similar changes.

The different measured transport properties study the response of the compounds over quite different momentum and energy regions. For example, the Raman scattering studies the long-wavelength density and current response at long wavelength but over a range of frequencies from low $\mathcal{O}(1\,\mathrm{cm}^{-1})$ to high, $\mathcal{O}(10^4\,\mathrm{cm}^{-1})$. On the other hand, nuclear relaxation rate T_1^{-1} depends on the magnetic fluctuations at very low frequencies but integrates over all momenta, so that the short-wavelength fluctuations dominate. In 1989, it was proposed [268,269] that a single hypothesis about the particle–hole excitation spectra captures most of the diverse transport anomalies. The hypothesis is that the density as well as magnetic fluctuation spectrum has an absorptive part with the following property:

$$\chi''(q,\omega)\begin{cases} = -\chi_o''\omega/T & \text{for } \omega \ll T\,, \\ = -\chi_o''\ \mathrm{sgn}(\omega) & \text{for } \omega_c \gg |\omega| \gg T\,. \end{cases} \tag{196}$$

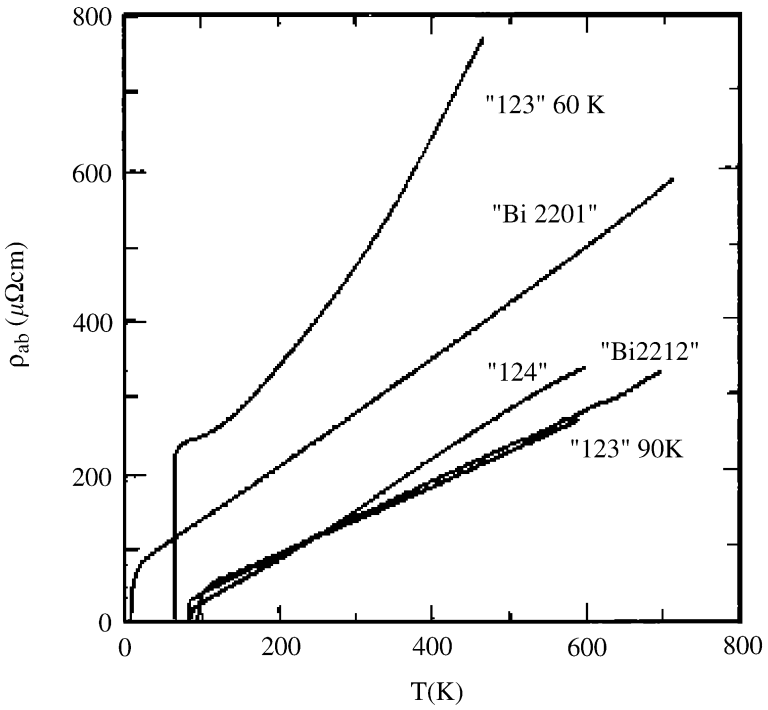

Fig. 52. Resistivity as a function of temperature for various high-temperature superconductors. From [39].

Here χ_o'' is the order of the bare single-particle density of states $N(0)$ and ω_c is an upper cutoff. The fluctuation spectrum is assumed to have only a weak momentum dependence, except at very long wavelength, where a q^2 dependence is required for fluctuations of conserved quantities like density or spin (in the absence of spin–orbit interactions). A form which implements these requirements for the conserved quantities, with a rather arbitrary crossover function to get the different regimes of ω/T, is

$$\chi''(\mathbf{q},\omega) \sim \frac{-xq^2}{\omega(\omega^2+\pi^2x^2)} \quad \text{for } v_F q \ll \sqrt{\omega x}\,, \tag{197}$$

where $x=\omega$ for $\omega/T \ll T$ and $x=T$ for $\omega/T \gg 1$.

Using the Kramers–Kronig relations, one deduces that the real part of the corresponding correlation functions has a $\log(x)$ divergence at all momenta except the conserved quantities where the divergence does not extend to $v_F q \geqslant x$. Thus compressibility and magnetic susceptibility are finite. (Aside from the contributions encapsulated in the approximate forms (196) or (197), an analytic background fluctuation spectrum of the Fermi liquid form is of course also present.)

The spectral function (196) is unlike that of a Landau Fermi liquid discussed in Section 2, which always displays a scale—the Fermi-energy, Debye-frequency, or spin-wave energy, etc.—obtained from parameters of the Hamiltonian. Such parameters have been replaced by T. As we have discussed in Section 6, this scale-invariance of (196) is characteristic of fluctuations in the

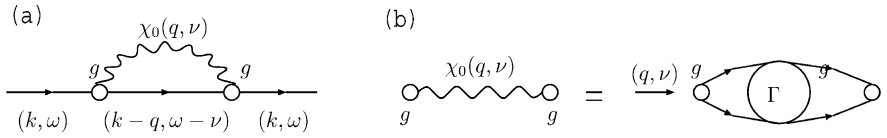

Fig. 53. (a) Diagram for the singular contribution to the one-particle self-energy with the fluctuating $\chi(q,\nu)$. g's are the vertices which in microscopic theory [270] is shown to have important momentum dependence, but which gives negligible momentum dependence to the self-energy. (b) For $\chi_0(q,\nu)$ which is momentum independent, a total vertex Γ may sometimes be usefully defined, which has the same frequency dependence as Eq. (198) and which is also q-independent. The lines are the exact single-particle Green's functions.

quasiclassical regime of a QCP. Eq. (196) characterizes the fluctuations around the QCP: comparing with Eq. (179), the exponent $d_M/z = 0$ and $1/z = 0$. These are equivalent to the statement that the momentum dependence is negligibly important compared to the frequency dependence. This is a very unusual requirement for a QCP in an itinerant problem: the spatial correlation length plays no role in determining the frequency dependence of the critical properties.

The experimental results for the various transport properties for compositions near the optimum are consistent in detail with Eq. (196), supplemented with the elastic scattering rate due to impurities (see later). We refer the reader to the original literature for the details. The temperature independence and the frequency independence in Raman scattering intensity up to ω of $\mathcal{O}(1\,\mathrm{eV})$ directly follows from (197). Eq. (197) also gives a temperature independent contribution to the nuclear relaxation rate T_1^{-1} as is observed for Cu nuclei. The transport scattering rates have the same temperature dependence as the single-particle scattering rate. The observed anomalous optical conductivity can be directly obtained by using the continuity equation together with Eq. (197), or by first calculating the single-particle scattering rate and the transport scattering rate. The single-particle scattering rate is independently measured in ARPES experiments and provides the most detailed test of the assumed hypothesis.

To calculate the single-particle scattering rate, assume to begin with a constant coupling matrix element g for the scattering of particles by the singular fluctuations. We shall return to this point in the section on microscopic theory. Then provided there is no singular contribution to the self-energy from particle–particle fluctuations, the graph in Fig. 53 represents the singular self-energy exactly. It is important to note that for this to be true, Eq. (197) is to be regarded as the exact (not irreducible) propagator for particle–hole fluctuations; it should not be iterated.

The self-energy $\Sigma(\mathbf{q},\omega)$ can now be evaluated straightforwardly to find a singular contribution

$$\Sigma(\omega,q) \approx g^2(\chi_o'')^2\left(\omega\ln\frac{x}{\omega_c} - \mathrm{i}\frac{\pi}{2}x\right) \tag{198}$$

for $x \ll \omega_c$ and $v_F|(q-k_F)| \gg \omega_c$. The noteworthy points about (198) are:

(1) The single-particle scattering rate is proportional to x rather than to x^2 as in Landau Fermi liquids.
(2) The momentum independence of the single-particle scattering rate.

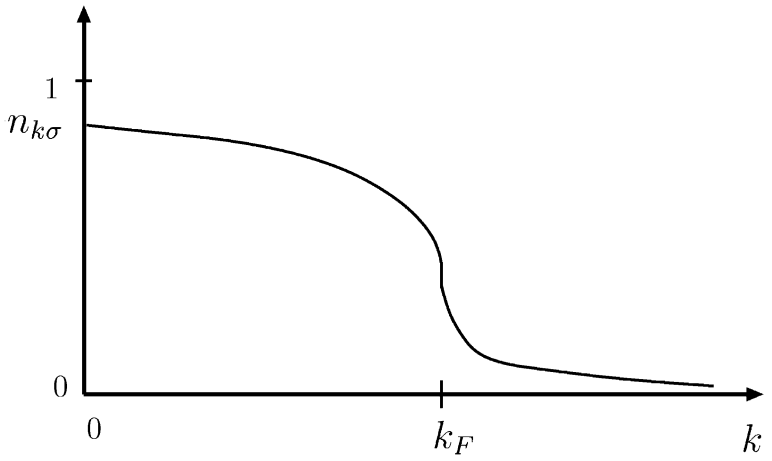

Fig. 54. The $T=0$ distribution of bare particles in a marginal Fermi liquid. No discontinuity exists at k_F but the derivative of the distribution is discontinuous.

(3) The quasiparticle renormalization amplitude

$$Z=\left(1-\lambda\ln\frac{x}{\omega_c}\right)^{-1} \tag{199}$$

scales to zero logarithmically as $x\to 0$. Hence the name marginal Fermi liquid.

(4) The single-particle Green's function

$$G(\omega,q)=\frac{1}{\omega-(\varepsilon_q-\mu)-\Sigma(q,\omega)} \tag{200}$$

has a branch cut rather than a pole. It may be written as

$$\frac{Z(x)}{\omega-(\tilde{\varepsilon}_q-\tilde{\mu})-i/\tilde{\tau}}\,, \tag{201}$$

where $\tilde{\varepsilon}_q$ is the renormalized single-particle energy

$$\tilde{\varepsilon}_q-\tilde{\mu}=Z(\varepsilon_q-\mu)\approx Z\mathbf{v}_F\cdot(\mathbf{q}-\mathbf{k}_F) \tag{202}$$

for small $|q-k_F|$. Also, $\tilde{\tau}^{-1}(x)=Z\,\mathrm{Im}\,\Sigma(\omega)$, and the effective Fermi velocity $\tilde{v}_F=Zv_F$ has a frequency and temperature-dependent correction.

(5) The single-particle occupation number has no discontinuity at the Fermi surface, but its derivative does, see Fig. 54. So the Fermi surface remains a well-defined concept both in energy and in momentum space.

The predictions of (200) have been tested in detail in ARPES measurements only recently. ARPES measures the spectral function

$$A(q,\omega)=-\frac{1}{\pi}\frac{\Sigma''(q,\omega)}{[\omega-(\varepsilon_q-\mu)-\Sigma'(q,\omega)]^2+[\Sigma''(q,\omega)]^2}\,. \tag{203}$$

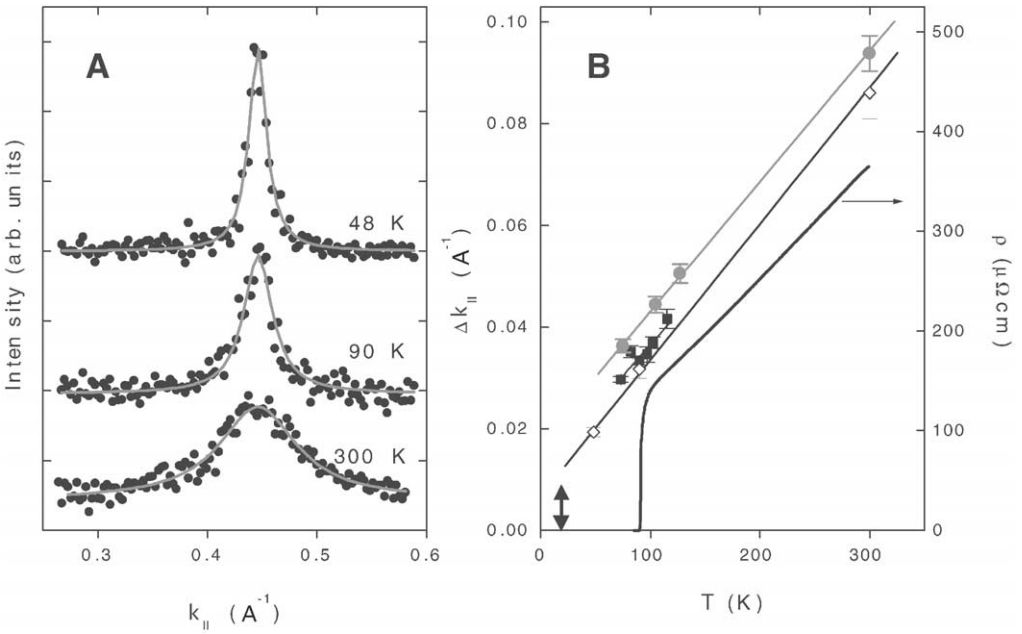

Fig. 55. (a) Momentum distribution curves for different temperatures. The solid lines are Lorentzian fits; (b) momentum widths of MDCs for three samples (circles, squares, and diamonds). The thin lines are T-linear fits which show consistency with Eq. (203) and the MFL hypothesis. The resistivity (solid black line) is also shown. The double-headed arrow shows the momentum resolution of the experiment. From Valla et al. [261].

In ARPES experiments, the energy distribution curve at fixed momentum (EDC) and the momentum distribution curve at fixed energy (MDC) can both be measured. It follows from Eq. (203) that if Σ is momentum independent perpendicular to the Fermi surface, then an MDC scanned along $\mathbf{k}_{\perp}$ for $\omega \approx \mu$ should have a Lorentzian shape plotted against $(\mathbf{k} - \mathbf{k}_{\mathrm{F}})_{\perp}$ with a width proportional to $\Sigma''(\omega)/v_{\mathrm{F}}(\hat{\mathbf{k}})$. For a marginal Fermi liquid (MFL), this width should be proportional to x. The agreement of the measured line shape to a Lorentzian and the variation of the width with temperature are shown in Fig. 55. The Fermi velocity $v(\hat{\mathbf{k}})$ is measured through the EDC with the conclusion that it is independent of $\hat{\mathbf{k}}$ to within the experimental errors. Further data from the same group shows that the temperature dependence is consistent with linearity all around the Fermi surface [262] with a coefficient independent of $\hat{\mathbf{k}}$ although the error bars are huge near the $(\pi, 0)$ direction. Besides the MFL contribution, there is also a *temperature independent* contribution to the width which is strongly angle-dependent, to which we will soon turn. The ambiguity of the temperature (and frequency) dependence near the $(\pi, 0)$ direction is removed by the EDC measurements. In Fig. 56, the EDCs at the Fermi surface in the (π, π) direction and the $(\pi, 0)$ directions are shown together with a fit to the MFL spectral function with a constant contribution added to Σ''. EDCs have the additional problem of an energy-independent experimental background. This has also been added in the fit. In both directions, Σ'' has a contribution proportional to ω with the same coefficient within

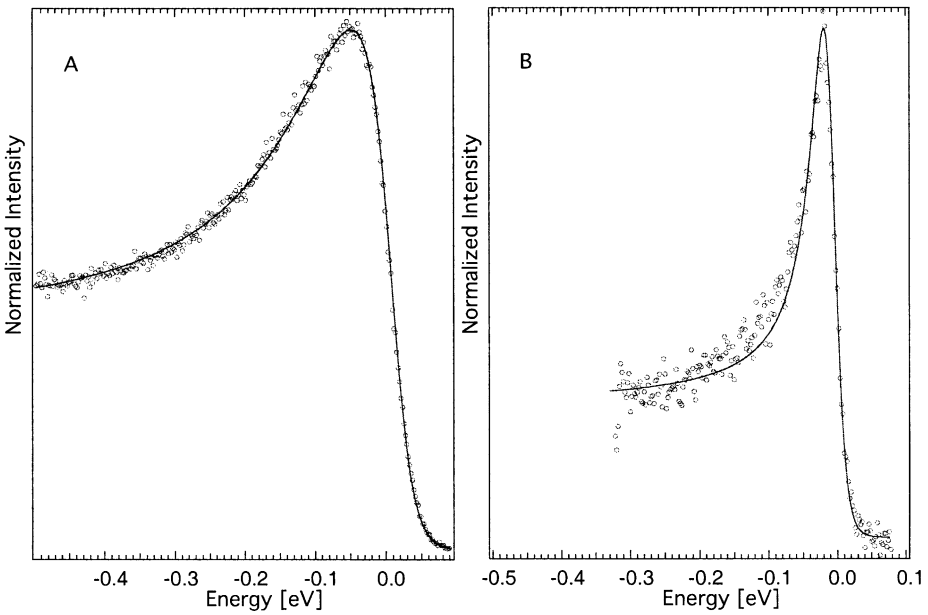

Fig. 56. Fits of the MFL self-energy $\Gamma + \lambda\hbar\omega$ to the experimental data, according to (204). Estimated uncertainties are $\pm 15\%$ in Γ and $\pm 25\%$ in λ. (a) A scan along the (1,0) direction, $\Gamma = 0.12$, $\lambda = 0.27$; (b) a scan along the (1,1) direction, $\Gamma = 0.035$, $\lambda = 0.35$. From Kaminsky and co-workers [139].

the experimental uncertainty. Fig. 57 presents the self-energy for the fit at 13 different points on the Fermi surface, showing that the inelastic part is proportional to ω and independent of momentum.

In summary, the ARPES experiments give that

$$\Sigma''(k,\omega;T) \cong \Gamma(\hat{k}_F) + \Sigma''_{MFL}(\omega,T)\,. \tag{204}$$

The (ω,T)-independent contribution $\Gamma(\hat{\mathbf{k}}_F)$ can only be understood as due to impurity scattering [2]. Its dependence on $\hat{\mathbf{k}}_F$ can be understood by the assumption that in well-prepared samples, the impurities lie between the Cu–O planes and therefore only lead to small angle scattering of electrons in the plane. The contribution $\Gamma(\hat{\mathbf{k}}_F)$ at $\hat{\mathbf{k}}_F$ then depends on the forward scattering matrix element and the local density of states at $\hat{\mathbf{k}}_F$ which increase from the (π,π) direction to the $(\pi,0)$ direction. This small angle contribution has several very important consequences: (i) relative insensitivity of residual resistivity to disorder, (ii) relative insensitivity of d-wave superconductivity transition temperature to the elastic part of the single-particle scattering rate [142], and (iii) most significantly, relative insensitivity to the anomalous Hall effect and magneto resistance. Such anomalous magneto-transport properties follow from a proper solution of the Boltzmann equation including both small angle elastic scattering and angle independent MFL inelastic scattering [275].

The momentum independence of the inelastic part of Σ'' is crucial to the SFL properties of the cuprates. Since the inelastic scattering to all angles on the Fermi surface is the same, i.e., s-wave scattering, the vertex corrections to transport of vector quantities like particle current and energy current are zero. It follows that the momentum transport scattering rate measured in

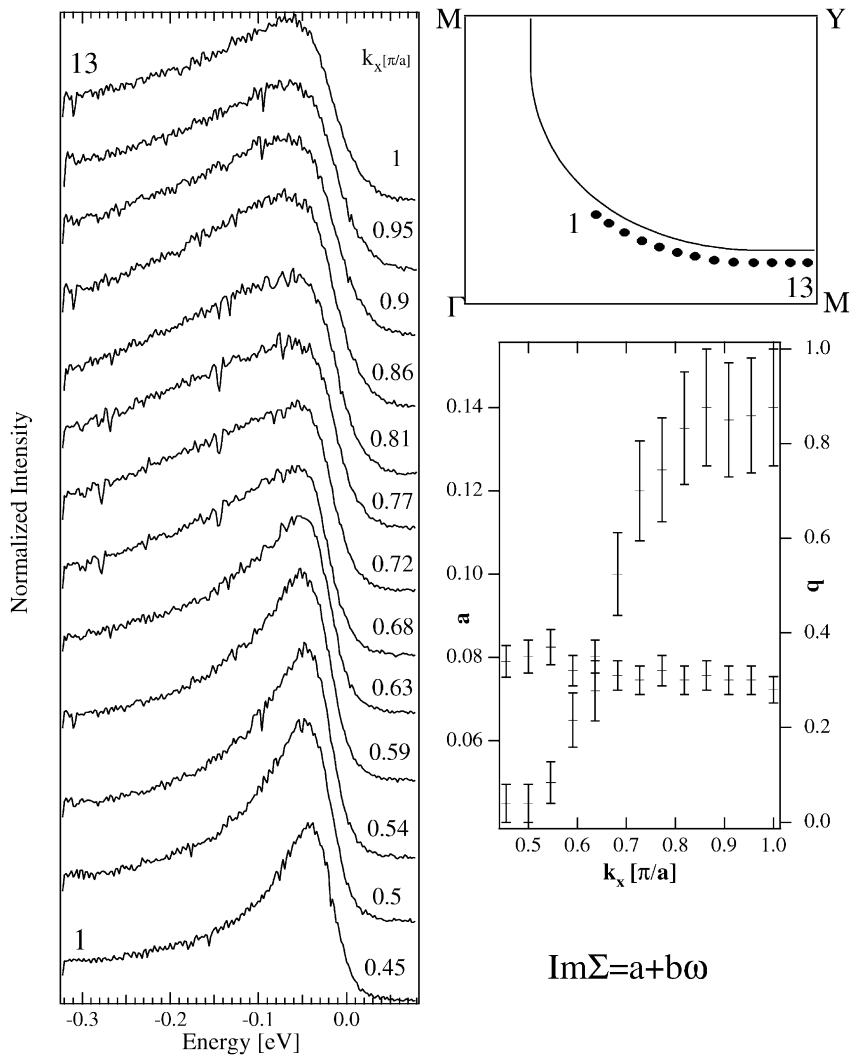

Fig. 57. The left panel shows the energy distribution curves measured in optimally doped Bi2212 perpendicular to the Fermi-surface at 13 points shown in the top-right panel. Each of these is fitted to the Marginal Fermi-liquid self-energy plus a frequency independent scattering contribution, i.e., with $\mathrm{Im}\,\Sigma(\omega,\hat{k}_F)=a(\hat{k}_F+b\omega)$, with fits of the quality shown in Fig. 56. The variation of the fitting parameters a and b on the 13 points is shown in the bottom-right panel. The parameter b is seen to be independent of direction to within experimental error while a increases by about a factor of 4 in going from the (π,π) direction to the $(\pi,0)$ direction. (Figure courtesy of A. Kaminsky and J.C. Campuzano, presented at Proceedings of the International Conference on Spectroscopy of Novel Superconductors, Chicago, May 13–17, 2000). Similar results may be found in the work by Valla et al. [262].

resistivity or optical conductivity and the energy transport rate measured in thermal conductivity have the same (ω,T) dependence as the single-particle scattering rate $1/\tau(\omega,T)$.

Recently far-infrared conductivity measurements [68] have been analyzed and shown to be consistent with $1/\tau(\omega,T)$ deduced from MFL including the logarithmic corrections.

As already discussed no singular correction to the magnetic susceptibility is to be expected on the basis of (196). However, the specific heat should have a logarithmic correction so that

$$\gamma(T) = \gamma_0[1 + \lambda \ln(\omega_c/T)] \,. \tag{205}$$

Such a logarithmic correction has not yet been deciphered in the data presumably because the electronic specific heat in the normal state is less than $\mathcal{O}(10^{-2})$ of the total measured specific heat and must be extracted by a subtraction procedure which is not sufficiently accurate.

7.3. General requirements in a microscopic theory

The MFL self-energy, Eq. (198), has been verified in such detail in its $(\omega, T, \mathbf{q})$ dependence that it is hard to see how any theory of CuO compounds can be relevant to the experiments without reproducing it (or a very close approximation to it) in Region I of the phase diagram of Fig. 49. Such a scale-invariant self-energy is characteristic of the quasiclassical regime of a QCP and indeed the topological features of the phase diagram are consistent with there being a QCP at x_c near the composition for the highest T_c (Alternatively, a QCP in the overdoped region where T_c vanishes is predicted in some approaches, like in [235]). To date, no method has been found to obtain Eq. (197) except through the scale-invariant form of fluctuations which is momentum independent ($z \approx \infty$) as in Eq. (196).

A consistent and applicable microscopic theory of the copper-oxides must show a QCP with fluctuations of the form (197). This is a very unusual requirement for a QCP in a homogeneous extended system for at least two reasons. First, the fluctuations must have a negligible $\mathbf{q}$-dependence compared to the frequency dependence, i.e., $z \approx \infty$ and second, the singularity in the spectrum should just have logarithmic form; i.e., there should be no exponentiation of the logarithm giving rise to power laws. Such singularities do arise, as we discussed in Section 3, in models of isolated impurities under certain conditions but they disappear when the impurities are coupled; recoil kills the singularities. The requirement of negligible q/ω dependence runs contrary to the idea of critical slowing down in the fluctuation regime of the usual transitions, in which the frequency dependence of the fluctuations becomes strongly peaked at zero frequency because the spatial correlation length diverges.

Another crucial thing to note is that any known QCP (in more than one dimension) is the end of a line of continuous transitions at $T = 0$. Region II (at least at $T = 0$) must then have a broken symmetry (this includes part of Region III, which is also superconducting). The experiments appear to exclude any broken translational symmetry or spin-rotational symmetry for this region[43] although as discussed in Section 7.1, a sharp change in transport properties is observed along with a four-fold symmetric diminution of the ARPES intensity for low energies at $T \approx T_p(x)$. If there is indeed a broken symmetry, it is of a very elusive kind; experiments have not yet found it.

[43] A new lattice symmetry due to lattice distortions or antiferromagnetism, if significant, would change the fermi surface because the size of the Brillouin zone would decrease. This would be visible both in ARPES measurements as well as in hall effect measurements.

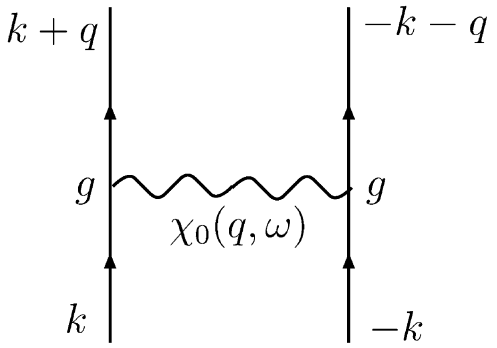

Fig. 58. The Cooper-pair vertex and the normal state self-energy, Fig. 53, are intimately related.

A related question is how a momentum independent $\chi(\mathbf{q},\omega,T)$ can be the fluctuation spectrum of a transition which leads to an anisotropic state as in Region II. Furthermore, how can such a spectrum lead to an anisotropic superconducting state? After all, it is unavoidable that $\chi(\mathbf{q},\omega,T)$ of Eq. (197) which determines the inelastic properties in Region I may also be responsible for the superconductive instability. After all, the process leading to the normal self-energy, Fig. 53, the superconductive self-energy, and the Cooper pair vertex, Fig. 58, are intimately related. Given $\mathrm{Im}\,\chi(\mathbf{q},\omega,T)$, the effective interaction in the particle–particle channel is

$$V_{\mathrm{pair}}(\mathbf{k},\mathbf{k}\pm\mathbf{q}) = g^2\,\mathrm{Re}\,\chi(\mathbf{q},\omega)\,. \tag{206}$$

$\mathrm{Re}\,\chi(\mathbf{q};\omega)$ is negative for all q and for all $-\omega_c \leqslant \omega \leqslant \omega_c$. So we do have a mechanism for superconductive pairing in the Cu–O problem given by the normal state properties just as the normal state self-energy and transport properties of, say, Pb tell us about the mechanism for superconductivity in Pb. In fact, given that the normal state properties give that the upper cut-off frequency is of $\mathcal{O}(10^3)$ K and that the coupling constant $\lambda \sim g^2N(0)$ is of $\mathcal{O}(1)$, the correct scale of T_c is obtained. The important puzzle is, how can this mechanism produce d-wave pairing given that $\chi(\mathbf{q},\omega)$ is momentum independent. How can one obtain momentum independent inelastic self-energy in the normal state and a d-wave superconducting order parameter from the same fluctuations?

In the next section, we summarize a microscopic theory which attempts to meet these requirements and answer some of the questions raised.

7.4. Microscopic theory

There is no consensus on even the minimum necessary model Hamiltonian to describe the essential properties in the phase diagram, Fig. 49, of the CuO compounds. It is generally agreed that, since other transition metal compounds do not share the properties of CuO compounds, a model Hamiltonian with some rather special features is called for. Two such features are:

(A) They are two-dimensional with an insulating antiferromagnetic ground state and spin $S = 1/2$ per unit cell at half-filling. Although not unique, this feature is rare. If this is the

determining feature, a two-dimensional Hubbard model is adequate [24]. Even this model is not soluble in $d = 2$.

(B) The copper oxides are the extreme limit of charge transfer compounds [297] in which charge fluctuations in the metallic state occur almost equally on oxygen and copper. Then the longer-range ionic interactions, which in magnitude are comparable to the on-site interactions, have a crucial role to play in the low-energy dynamics in the metallic state through excitonic effects. A model with both Cu and O orbitals, hopping between them, and the excitonic interactions besides the on-site repulsions is then required [266,267]. This is of course even harder to deal with than the Hubbard model.

Numerous attempts have been made using one or the other such models to obtain SFL behavior. We briefly discuss the motivations for the pursuit of model (A) before summarizing in a little more detail the only attempt to obtain the phenomenological fluctuation spectrum of Eq. (196), and which relies on a model of type (B).

7.4.1. The doped Hubbard model

The investigations of the copper-oxide problem from this point of view ask some valid and deep questions [24]. How does a low concentration of holes move through the spin configurations in a two-dimensional model with double occupancy strictly prohibited?[44] In Section 4.8, we have sketched the difficulties of connecting to the same problem in one dimension when the ground state at zero doping is an antiferromagnet. In fact, analytic [228] and numerical [172] answers to the question for a single hole show the spectral weight of a heavy particle with an incoherent part composed of multiple spin-wave polaronic cloud. Simply extrapolated (a dangerous thing to do), a Fermi liquid is expected. The larger zero-point fluctuations of the $S = 1/2$ model, compared to a large-spin model only change the relative weight of the coherent and the incoherent parts. However, more subtle possibilities must be considered. The antiferromagnetic ground state of a Heisenberg $S = 1/2$ model (or the undoped non-degenerate Hubbard model) in two dimensions is close in energy to a singlet ground state. A possible description of such a state is as a linear combination on the basis of singlet-bonds of pairs of spins. As noted earlier, such itinerant bond states have been termed resonating valence bonds [25] (by analogy to the ground state of benzene like molecules). The massive degeneracy of the singlet bond-basis raises interesting possibilities. If the quantum fluctuations of spins were (significantly) larger than allowed by $S = 1/2$, such states would indeed be the ground state, as they are in the one-dimensional model or two-dimensional models with additional frustrating interactions [6]. It is possible that by doping with holes in the $S = 1/2$ Heisenberg model, the additional quantum fluctuations induce a ground state and low-lying excitations which utilize the massive degeneracy of RVB states. Especially intriguing is the fact that resonating valence ground state may be looked up on as the projection of the BCS ground state to a fixed number of particles [24]. Furthermore, in the normal state this line of reasoning is likely to lead to an SFL.

---

[44] Questions of this type have a long history in the field of correlated electron systems going back to the classic work of Nagaoka [191] on the ferromagnetism induced by the motion of one hole in a half-filled infinitely repulsive Hubbard model.

A specific proposal incorporating the RVB idea [144] relies on the ground state of the half-filled model to be localized dimers. Then defects in this state due to deviation from half-filling can plausibly support excitations which are charged spinless bosons. Further work on this idea may be found in [225,188]. Related ideas were put forth in [82,236].

These are a very attractive set of ideas and no proof exists that they are disallowed. We have already considered an implementation of these ideas in Section 5.2 on generalized gauge theories. As discussed, controlled calculations using these ideas are hard to come by. Moreover, what theoretical results do exist do not correspond in a persuasive way to the experimental results on the copper-oxide materials.

One should take special note here of the idea of Anyon superconductivity which besides being a lovely theoretical idea, is founded on the solution to a well-defined model, and has clear experimental predictions. Laughlin and collaborators [156,138,91] found a specific model with long-range four-spin interactions for which his quantum hall wavefunction is the ground state. Therefore, time-reversal and parity are spontaneously broken in this state. This state is superconducting. The predicted time-reversal broken properties have not been observed experimentally [248].

An alternative idea from the microscopic characterization of these materials as doped Hubbard models is that a dilute concentration of holes in the Hubbard model is likely to phase separate or form ordered one-dimensional charge-density wave/spin-density wave structures [298,299,86]. There exists both empirical [257] and computational [288] support for this idea at least for a very dilute concentration of holes. For concentrations close to optimum compositions these structures appear in the experiment to exist only at high energies with short correlation lengths and times and small amplitudes in the majority of copper–oxygen compounds. Their relation to SFL properties is again not theoretically or empirically persuasive.

7.4.2. The excitonic interactions model

This relies on a model of type (B). A brief sketch of the calculations leading to a QCP and an MFL spectrum is given here. We refer the reader to [266,268,275] for details.

At half-filling, the ground state and the low-lying excitations of such models are identical to the Hubbard model. However, important differences can arise in the metallic state. Consider the one-electron structure of such models. The O–O hopping in the lattice structure with $d_{x^2-y^2}$ orbitals in Cu and p_x, p_y orbitals on O, as shown in Fig. 47, produces a weakly dispersing "non-bonding" band while the Cu–O hopping produces "bonding" and "anti-bonding" bands—see Fig. 59. We need consider only the filled non-bonding band and the partially filled anti-bonding bands shown in Fig. 59.

In the mean field approximation, such an electronic structure together with the on-site interaction and the ionic interactions is unstable to an unusual phase provided the latter, summed over the nearest neighbors, is of the order or larger than the bandwidth. In this phase, translational symmetry is preserved but time-reversal symmetry and the four-fold rotation symmetry about the Cu sites is broken. The ground state has a current pattern, sketched in Fig. 60, in which each unit cell breaks up into four plaquettes with currents in the direction shown. The variation of the transition temperature with doping x is similar to the line $T_p(x)$ in Fig. 38, so that there is a QCP at $x = x_c$. Experiments have been proposed to look for the elusive broken symmetry sketched in Fig. 60 [274].

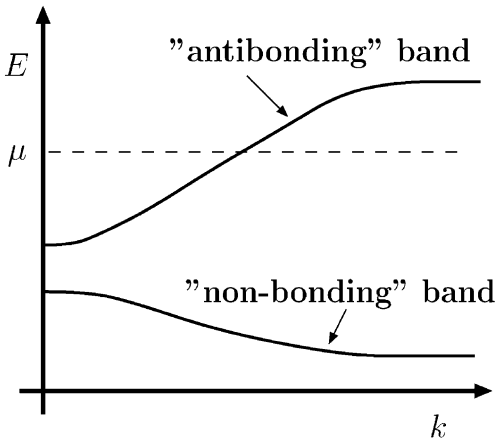

Fig. 59. Three bands result from the orbitals shown in Fig. 47(b) in a one-electron calculation; two of these are shown. The chemical potential lies in the "anti-bonding" band and is varied by the doping concentration. The other band shown is crucial for the theory using excitonic effects as in [270].

The long-range interactions in the model also favor other time-reversal breaking phases which also break translational invariance. This is known from calculations on ladder models [203]. Such states have also been proposed for copper-oxide compounds [148,128,58].

Our primary interest here is how the mechanism of transition to such a phase produces the particular SFL fluctuation spectrum (197) in Region I of the phase diagram. The driving mechanism for the transition is the excitonic singularity, due to the scattering between the states of the partially filled conduction band c and the valence band v of Fig. 59. This scattering is of course what we considered in Sections 3.5 and 4.9 for the problem of X-ray edge singularities for the case that the interband interaction V in Eq. (55) is small and the valence band is dispersionless (i.e., the no recoil case). Actually, the problem is exactly soluble for the no-recoil case even for large V [65]. For large enough V, the energy to create the exciton, ω_{ex}, is less than the v–c splitting Δ. The excitonic line shape is essentially the one sketched in Fig. 19(b) and given by Eq. (56) for $\omega > \omega_{ex}$, but δ is now the phase shift modulo π which is the value required to pull a bound state below Δ. The excitonic instability arises when $\omega_{ex} \to 0$.

The effect of a finite mass or recoil on the excitonic spectra is to smoothen the edge singularity on the scale of the valence band dispersion between $k = 0$ and $k = k_F$. The phase shift δ or the interaction energy V no longer determines the low-energy shape of the resonance. V does determine its location. The low-energy fluctuation spectra is determined by the following argument. Let us concentrate on $q = 0$ which is obviously where $\mathrm{Im}\,\chi_{ex}(\mathbf{q}, \omega)$ is largest. The absorptive part of a particle–hole spectra must be odd in frequency

$$\mathrm{Im}\,\chi(\mathbf{q}, \omega) = -\,\mathrm{Im}\,\chi(\mathbf{q}, -\omega)\,. \tag{207}$$

As V increases, $\mathrm{Im}\,\chi_{ex}(0, \omega)$ must shift its weight towards zero-frequency as shown in Fig. 61. Let us continue to denote by $|\omega_{ex}|$ the characteristic energy of the maximum in $\mathrm{Im}\,\chi$. For $|\omega|$ small compared to $|\omega_{ex}|$, $\mathrm{Im}\,\chi(0, \omega) \sim \omega$ while for $|\omega|$ large compared to $|\omega_{ex}|$, it is very slowly

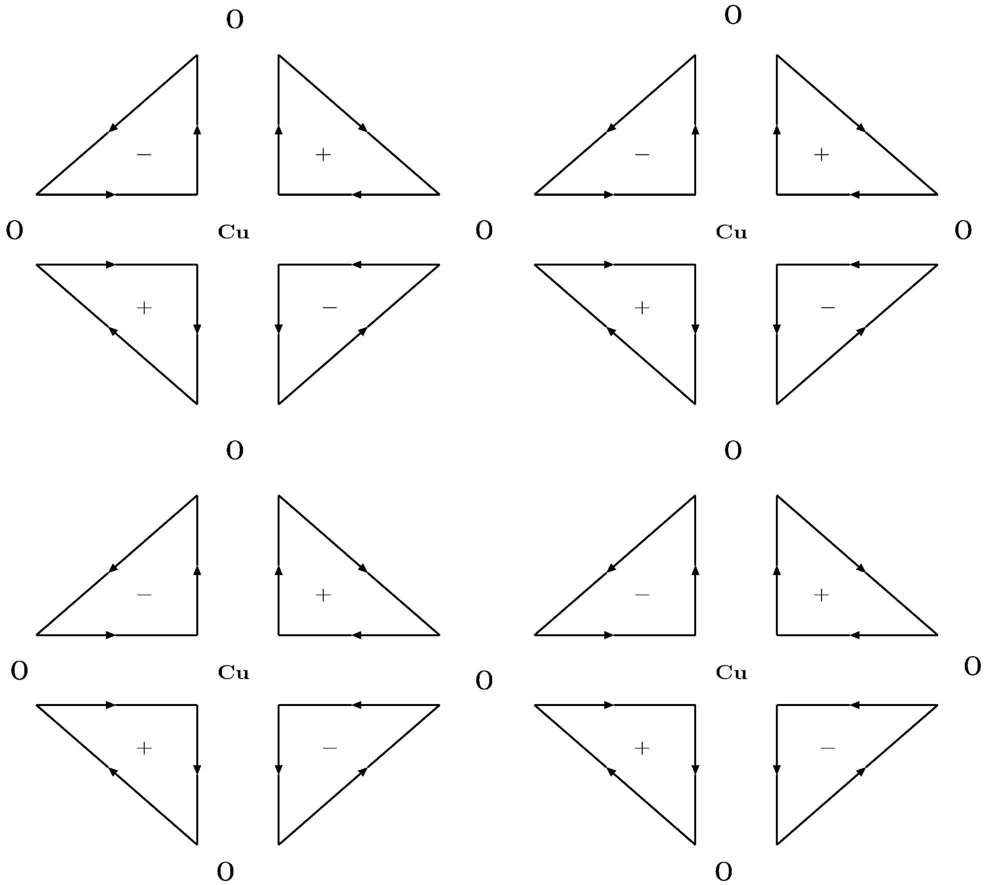

Fig. 60. One of the possible current patterns in the time-reversal breaking phase predicted for Region II of the phase diagram.

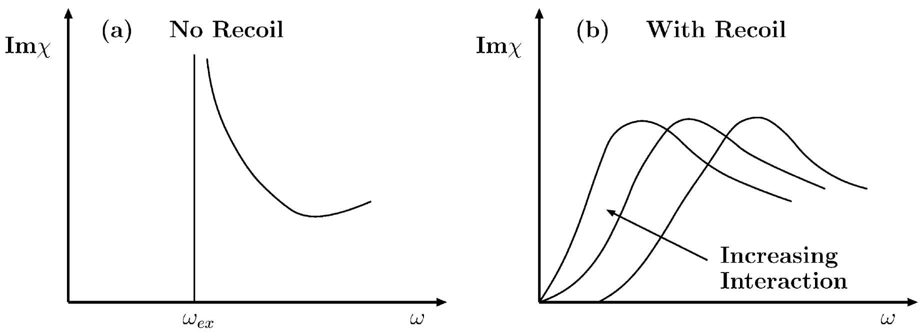

Fig. 61. Sketch of the development of the particle–hole spectra in the microscopic model for the cuprates.

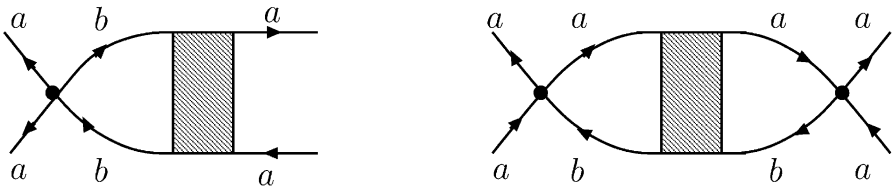

Fig. 62. Singularity of interaction Γ_{aaaa} between states "a" near the chemical potential generated by the excitonic singularity between the states "a" of the conduction band and states "b" of the valence band. The excitonic singularity is indicated by the shaded block.

varying up to a cut-off ω_c on the scale of the Fermi energy. Then by the Kramers–Kronig relation, to leading order

$$\mathrm{Re}\,\chi(0,\omega) \sim \ln(\omega_c/\max(\omega_x,\omega))\ . \tag{208}$$

For any finite $|\omega_{\mathrm{ex}}|$, $\mathrm{Re}\,\chi$ is finite and there is no instability. Only for $|\omega_{\mathrm{ex}}| \to 0$, i.e. $\mathrm{Im}\,\chi(0,\omega) \to \mathrm{sgn}\,\omega$, $\mathrm{Re}\,\chi(0,\omega)$ is singular $\sim \ln|\omega|$ and there is an instability. Thus in an excitonic instability of a Fermi sea with a dispersive valence band, the zero-temperature spectrum has the form $\chi(\omega,0) \sim \ln|\omega| + \mathrm{i}\,\mathrm{sgn}\,\omega$ at the instability. Given a parameter p such that the instability occurs only at p_c, i.e., $\omega_{\mathrm{ex}}(p \to p_c) \to 0$, the generalization for finite temperature T and momentum q and $p \neq p_c$ is

$$\chi(\mathbf{q},\omega) = \left[\left(\frac{\mathrm{i}\omega}{\max(\omega,T,\omega_{\mathrm{ex}}(p))} + \ln\frac{\omega_c}{\max(\omega,T,\omega_{\mathrm{ex}}(p))}\right)^{-1} + a^2q^2 + (p_c(T) - p)\right]^{-1}\ . \tag{209}$$

Here, ω_c is the cut-off frequency of $\mathcal{O}(\Delta)$. Since the binding energy is $\mathcal{O}(1\,\mathrm{eV})$, the size of the exciton, a, is of the order of the lattice constant. The $\mathbf{q}$ dependence of (209) is negligible compared to the frequency dependence. The exponent z is effectively infinite. At $p \approx p_c$, to logarithmic accuracy, the above expression (209) is identical to the phenomenological hypothesis (197).

The effective low-energy interaction for states near the chemical potential, which is sketched in Fig. 62, is singular when the excitonic resonance is at low frequency. Here is an example of the mechanism mentioned under (v) in Section 2.6 where the irreducible interaction obtained by integrating over non-perturbed high-energy states is singular. This is, of course, only possible when the interactions represented by the shaded block in Fig. 62 are large enough.

In relation to some of the questions raised about the phenemenology at the end of the last subsection, the momentum dependence of the vertex coupling the low-energy fermions to the fluctuations in Figs. 53 and 58 has been evaluated [273]. It is non-local with a form depending

on the wavefunctions of the conduction and valence bands and the leading result is

$$g(k,k') \sim (\sin(k_x a/2)\sin(k'_x a/2) - \sin(k_y a/2)\sin(k'_y a/2)) \,. \tag{210}$$

Note that at $(k-k')=0$ this is proportional to $[\cos(k_x a)-\cos(k_y a)]$. This is intimately related to the d-wave current distribution in the broken-symmetry phase predicted for Region (II), shown in Fig. 60. Eq. (210) is such that when the diagram of Fig. 53 is evaluated, the intermediate state momentum integration makes the self-energy depend very weakly on the incoming momentum. But when the pairing kernel of Fig. 58 is evaluated, it is momentum dependent and exhibits attraction in the d-wave channel.

Similarly, as has been shown [273], the vertex of Eq. (210) leads to an anisotropic state with properties of the pseudo-gap state of Region II below a temperature $T_p(x)$. The principal theoretical problem remaining with this point of view is that a transition of the Ising class occurs at $T_p(x)$ at least in mean field theory. This would be accompanied by a feature in the specific heat unlike the observations. [45]

The microscopic theory reviewed above reproduces the principal features of the phase diagram Fig. 49 of the copper-oxide superconductors, and of the SFL properties. It also gives a mechanism for high-temperature superconductivity of the right symmetry. Further confidence in the applicability of the theory to the cuprates will rest on the observation of the predicted current pattern of Fig. 60 in Region II of the phase diagram. [46]

8. The metallic state in two dimensions

The distinction between metals and insulators and the metal–insulator transition has been a central problem in condensed matter physics for seven decades. Despite the accumulated theoretical and empirical wisdom acquired over all these years, the experimental observation made in 1995 of a metal–insulator transition in two dimensions [149] was a major surprise and is a subject of great current controversy. The theoretical work in the 1980s [11,92–94,157,14] on disordered interacting electrons pointed to a major unsolved theoretical problem in two dimensions. Infrared singularities were discovered in the scattering amplitudes which scaled to strong coupling where the theory is uncontrolled (The situation is similar to that after the singularities in the one- or two-loop approximations in the Kondo problem were discovered, revealing a fascinating problem without providing the properties of the asymptotic low-temperature state). However, the problem was not pursued and the field lapsed till the new experiments came along.

The 1980s theoretical work shows that this problem naturally belongs as a subject in our study of singular Fermi liquids. We will first summarize the principal theoretical ideas relevant to the problem before the 1995 experiments. We then briefly summarize the principal results of these and subsequent experiments. Reviews of the experiments have appeared in [3,16,17].

---

[45] One might appeal to disorder to round off the transition, but this appears implausible quantitatively. More likely, the nature of the transition is strongly affected by the fluctuation spectra of the form of Eq. (196) and is unlikely to be of the Ising class.

[46] As already mentioned in Section 2.6, ferromagnetism in some compounds has an excitonic origin. The dynamics near such a transition should also exhibit features of the edge-singularity as modified by recoil.

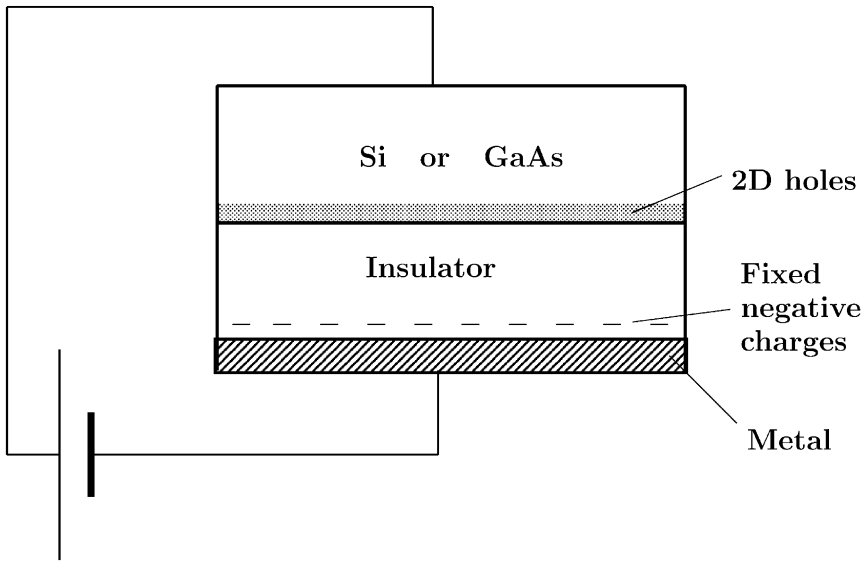

Fig. 63. Sketch of a MOSFET. Holes (or electrons) are trapped at the interface of the semiconductor and the insulator due to the band gap difference between them, the dipole layer and the applied electric field. Two-dimensional electrons (holes) may also be found by layered structures (heterostructures) of semiconductors with different band gaps such as GaAs and AlGaAs.

There are two types of theoretical problems raised: the nature of the metallic state and the mechanism of the metal–insulator transition. We will address the former and only briefly touch on the latter.

8.1. The two-dimensional electron gas

We consider an electron gas with a uniform positive background with no complications arising from the lattice structure—this is how the many-electron problem was originally formulated: the Jellium model. This situation is indeed realized experimentally in MOSFETS (and heterostructures) in which an insulator is typically sandwiched between a metallic plate and a semiconductor—see Fig. 63. By applying an electric field, a two-dimensional charge layer accumulates on the surface of the semiconductor adjacent to the insulator, whose density can simply be changed by varying the field strength (For details see [26].). Similar geometries have been used to observe the quantum Hall effects and the metal–insulator transition by varying the density.

Typically we will be interested in phenomena when the average inter-electron distance is $\mathcal{O}(10) - \mathcal{O}(10^2)$ nm. The thickness of the insulating layer is typically more than 100 nm, so that the positive (capactive) charge on the insulator provides a uniform background to a first approximation. In Si samples, surface roughness is the principal source of disorder at high densities, while at low densities (in the regime where the transition takes place) ionized impurity scattering dominates due to the fact that there is much less screening. In GaAs, remote

impurity scattering dominates, and this scattering is mostly small angle. This is the main reason that the mobility in these samples is large.

Neglecting disorder, the problem is characterized by r_s, defined as the ratio of the potential energy to the kinetic energy

$$r_s = \frac{me^2}{4\pi\varepsilon\hbar^2\sqrt{\pi n}} \,. \tag{211}$$

Here n is the electron density, m the band mass, and ε the background static dielectric constant. We can also write

$$\pi r_s^2 a_0^2 = \frac{1}{n} \,, \tag{212}$$

which expresses that r_s is the radius of the circle whose area is equal to the area per conduction electron, measured in units of the Bohr radius a_0. For a two-valley band structure, as on the (110) surface of Si, the kinetic energy is reduced and r_s is twice that defined by Eqs. (211) and (212).

For $r_s \ll 1$, (the dense electron limit) the kinetic energy dominates and metallic behavior is expected. For $r_s \gg 1$, the potential energy dominates and a crystalline state (Wigner crystal) is expected. The best current numerical estimates place the transition to the crystalline state at $r_{sc} \approx 37$ [253]. The entropy at the transition is tiny, indicating that the radial distribution function for the liquid state at low densities is similar to that of the crystal for distances up to a few times $r_s a_0$.

It is important to note for our subsequent study that magnetism is always lurking close by. Reliable numerical calculations show that the magnetic state in the Wigner crystal near the critical density is determined by multiple-particle exchanges [47]. On the metallic side, the energy of the ferromagnetic state is only a few percent above the unpolarized metallic or crystalline states for $r_s \approx r_{sc}$ [253]. Disorder is expected to make the metal–insulator state continuous. On the insulating side at $T \to 0$, the disordered Wigner crystal is expected to be glassy and have low-energy properties of a Coulomb glass [239]. On the metallic side fluctuations in the local density of electrons might be expected to lead to locally polarized magnetic states or possibly to some unusual frustrated magnetic states [57]. The perturbative calculations with disorder and interactions, already alluded to [92–94,54] also hint at the formation of magnetic moments in the metallic state. It is the interplay of such magnetic fluctuations with itinerancy which is one of the principal theoretical problem in understanding the metallic state.

8.2. Non-interacting disordered electrons: scaling theory of localization

Detailed reviews on the material in this section may be found in [256,157,14,133].

The concept of localization of non-interacting electrons for strong enough disorder was invented in 1958 by Anderson [18]. In one dimension, all electronic states are localized for arbitrarily small disorder while in three dimension a critical value of disorder is required. That $d = 2$ is the marginal dimension in the problem was discovered through the scaling theory of localization.

The conceptual foundations for the scaling theory of localization were laid by Thouless and co-workers [255,256] and by Abrahams et al. [1], and were developed formally by Wegner [286]. Abrahams et al. [1] also made predictions which could be tested experimentally. Thouless noted first of all that the *conductance* G of a hypercube of volume L^{D} in any dimension d is dimensionless when expressed in units of (e^2/h), thus defining a scale independent quantity

$$g = G/(e^2/h) \, . \tag{213}$$

Next, he argued that g for a box of linear size $2L$ may be obtained from the properties of a box of size L and the connection between the two of them. The conductance of a box of size L itself increases with the transition amplitude t between energy levels in the two boxes and decreases with the characteristic width of the distribution of the energy levels in the boxes $\Delta W(L)$ due to the disorder

$$g(L) \approx f\left(\frac{\Delta t(L)}{\Delta W(L)}\right) \, . \tag{214}$$

For weak-Gaussian disorder, the bandwidth may be expected to be proportional to the square root of the number of impurities in the box, so $\Delta W(L) \sim L^{d/2}$. The transition amplitude t is obtained by the hopping between near-neighbors near the surface of the boxes of size L. It is therefore proportional to the surface area L^{d-1}. Thus [47]

$$g(L) = f(L^{(d-2)/2}) \, . \tag{215}$$

Now, in three dimensions the conductivity should approach a constant for large L (Ohm's law!), and hence the conductance should scale as L. This implies that the scaling function $f(x)$ should go for large L as $f(x) \sim x^2$. Note that for $d > 2$ the g therefore increases with increasing L while for $d < 2$ the large L behavior is determined by the small argument behavior of the scaling function; clearly $d = 2$ is the marginal dimension.

In a very influential paper, Abrahams et al. [1] analyzed the β-function of the RG flow

$$\beta(g) \equiv d(\ln g)/d(\ln L) \tag{216}$$

and showed by a perturbative calculation in $1/g$ that

$$\beta(g) = (d-2) - \frac{1}{\pi^2}\frac{1}{g} \, , \tag{217}$$

where the first part comes from Eq. (215) with $f(x) \sim x^2$.

For small enough g (i.e., for large disorder) we expect exponential localization $g(L) \sim \mathrm{e}^{-L/\zeta}$, where ζ is the localization length, so that $\beta(g) \sim (-L/\zeta)$. The smooth connection between the perturbative result (217) for large g and the exponentially localized solution at small g is shown in Fig. 64. While for $d = 3$ (or any $d > 2$), a critical disorder g_c is required for localization, for $d = 2$ states are asymptotically localized for any disorder for non-interacting fermions. The

[47] This line of reasoning of course breaks down when we include electron–electron interactions.

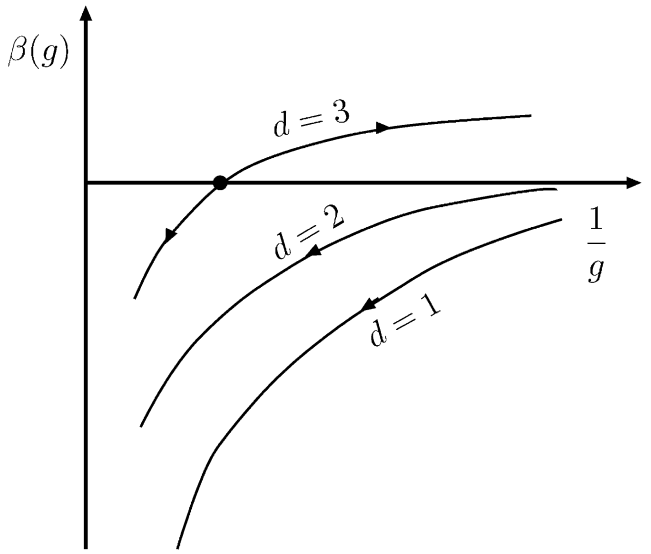

Fig. 64. The scaling function for non-interacting electrons with disorder deduced by Abrahams et al. [1].

characteristic value of the localization length in $d=2$ is estimated from the perturbative solution:

$$g(L) = g_0 - \frac{1}{\pi^2} \ln\left(\frac{L}{\ell}\right) , \tag{218}$$

where g_0 is the dimensionless conductance at $L \approx \ell$. In conventional Boltzmann transport theory $g_0 = (e^2/2\pi\hbar)k_F\ell$. The localization length ζ is of the order of the value of L at which the correction term is of order g_0, so that

$$\zeta \approx \ell \exp\left(\frac{\pi}{2} k_F \ell\right) . \tag{219}$$

At $T \to 0$, the sample size of a sample with $k_F\ell \gg 1$ has to be very large indeed for weak localization to be observable.

The theory described above must be modified at finite temperatures due to inelastic scattering. If the inelastic scattering rate is much less than the elastic scattering rate, $\tau_{in}^{-1} \ll \tau^{-1}$, localization effects are cut-off at a length scale $L_{Th}(T)$, the Thouless length scale

$$L_{Th} = (D\tau_{in})^{1/2} , \tag{220}$$

where $D = (v_F^2\tau/d)$ is the (Boltzmann) diffusion constant. However, as noted by Altshuler et al. [12,13], the correct scale for the cut-off is τ_ϕ^{-1}, the phase breaking rate. In an individual collision the energy change ΔE may be such that the phase changes only by a very small amount, $\tau_{in}\Delta E \ll 2\pi$. The phase breaking time is then longer and is shown to be given by $\tau_\phi \sim (\Delta E \tau_{in})^{-2/3}\tau_{in}$. The $T=0$ theory with the "phase length"

$$L_\phi = (D\tau_\phi)^{1/2} \tag{221}$$

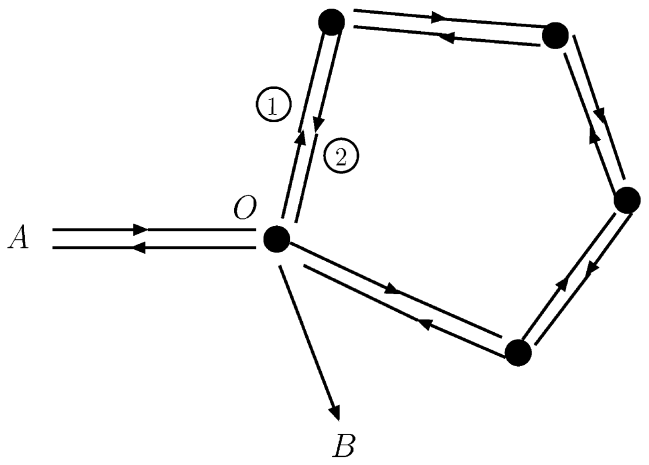

Fig. 65. Interfering (time-reversed) parts in elastic scattering off a fixed set of impurities. The probability for the particle to arrive at B is reduced because of the enhanced probability for the particle to arrive back at A, as a result of interference.

replacing L then gives the finite temperature scaling behavior to which experiments may be compared.

The characteristic temperature T_x at which weak-localization effects become prominent may be estimated in a manner similar to (218)

$$T_x \tau_\phi(T_x) = \exp(-\pi k_F \ell) \, . \tag{222}$$

This expression puts useful bounds on the temperatures required to observe weak localization.

Eq. (217) is derived microscopically by considering repeated backward scattering between impurities. It can also be derived by considering quantum interference between different paths to go from one point A to another B [41]. The total probability Ω for this process is

$$\Omega = \left| \sum_i a_i \right|^2 = \sum_i |a_i|^2 + \sum_{i \neq j} a_i^* a_j \, , \tag{223}$$

where a_i is the amplitude of the ith path. The second term in Eq. (223) is non-zero only for classical trajectories which cross, for example at the point O in Fig. 65. The probability of finding a particle at the point O is increased from $2|a_i|^2$ to

$$|a_1|^2 + |a_2|^2 + 2 \operatorname{Re} a_1^* a_2 = 4|a_1|^2 \tag{224}$$

because the two paths are mutually time-reversed. Increasing this probability of course leads to a decrease in the probability of the particle to arrive at B, and hence to a decrease in the conductivity.

This argument makes it clear as to why the interfering paths must be shorter than the phase relaxation rate due to inelastic processes and why magnetic impurities or a magnetic field which

introduces phase shift between two otherwise time-reversed paths suppress weak localization. In two dimensions [14]

$$\sigma(H,T)-\sigma(O,T)=\frac{e^2}{2\pi^2\hbar}\left[\psi\left(\frac{1}{2}+\frac{1}{x}\right)+\ln x\right]\ , \tag{225}$$

where ψ is the digamma function and

$$x=4L_\phi^2 eH/\hbar c\equiv(L_\phi/L_H)^2\ . \tag{226}$$

The quantity in brackets in (225) is equal to $x^2/24$ for $x\to 0$ and to $\ln(x/4)-\gamma$ for $x\to\infty$.

Spin–orbit scattering preserves time-reversal symmetry but spin is no longer a good quantum number. The spins are rotated in opposite directions in the two self-intersecting paths of Fig. (65) if the impurities are spin–orbit scatters [125,14,157]. This has been shown to lead to an average overlap of the spinfunction of $-\frac{1}{2}$ (because a rotation by 2π of wavefunction of a spin 1/2 particle leads to a wavefunction of opposite sign). The correction to the β-function of Eq. (217) due to this effect is

$$\frac{1}{2\pi^2}\frac{1}{g}\ . \tag{227}$$

This effect tends to an *enhancement* of the conductivity.

8.3. Interactions in disordered electrons

Fermi liquid theory for interacting electrons survives in three dimensions in the presence of a dilute concentration of impurities [43]. Some noteworthy differences from the pure case are:

(1) Owing to the lack of momentum conservation, the concept of a Fermi surface in momentum space is lost but it is preserved in energy space, i.e., a discontinuity in particle occupation as a function of energy occurs at the chemical potential. The momentum of particles may be defined after impurity averaging. General techniques for calculating impurity-averaged quantities are well developed; see for example [4,43]. Here and subsequently in this chapter the self-energies, vertices, etc. refer to their form after impurity averaging.

(2) In the presence of impurities, the density–density correlation (and spin-density correlation, if spin is conserved) at low frequencies and small momentum must have a diffusive form (this is required by particle-number conservation and the continuity equation)

$$\pi(q,\omega)=\kappa\frac{Dq^2}{\mathrm{i}\omega+Dq^2},\quad q\ll\ell^{-1}\quad\text{and}\quad\omega\ll\tau^{-1}\ . \tag{228}$$

Here $\kappa=\mathrm{d}n/\mathrm{d}\mu$ is the compressibility and D is the diffusion constant. For non-interacting electrons, $D=\frac{1}{3}v_\mathrm{F}^2\tau$. Interactions renormalize D and κ [43]. In the diagrammatic representation used below, the diffusive propagator is shown by a cross-hatched line connecting a particle and a hole line as in Fig. 66.

(3) Owing to statement 1, the *impurity-averaged* single-particle spectral function at a fixed $\mathbf{k}$ is spread out over an energy Γ, so that for frequencies within a range Γ of the chemical

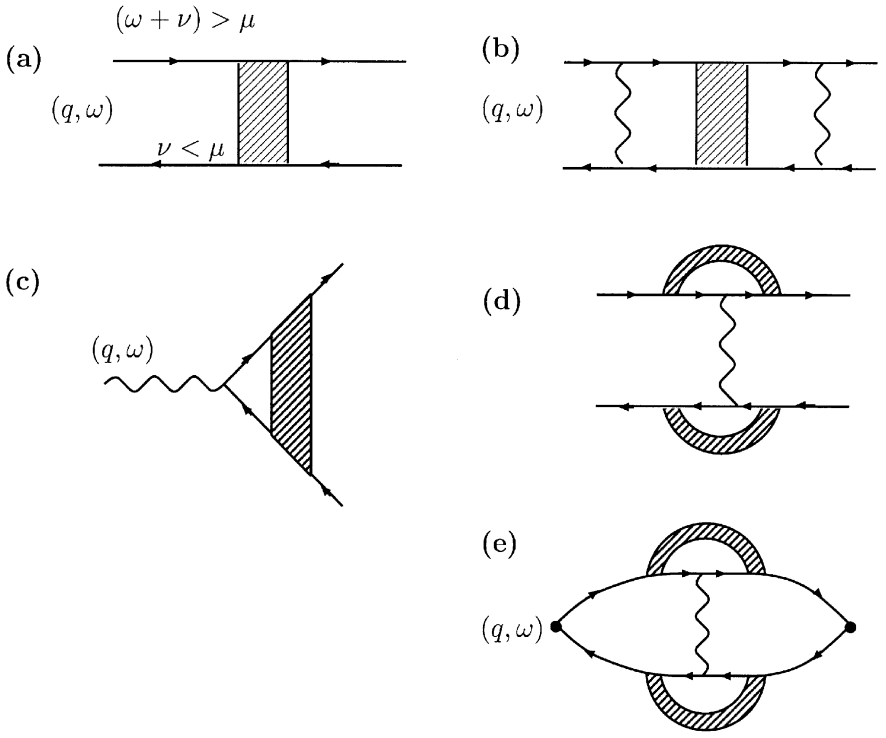

Fig. 66. Elementary processes important in the problem of two-dimensional disordered interacting electrons and referred to in the text. (a) Representation of the diffusion propagator due to impurity scattering vertices and corresponding self-energy. The particle lines and hole lines should be on opposite sides of the chemical potential. (b) Singular second-order interactions. (c) Singular vertex in the density channel (and in the spin-density channel for the spin-conserving problem). (d) Singular (irreducible) first-order interactions. (e) Elementary singular polarization propagator.

potential, it has both a hole part (for $\omega<\mu$) and a particle part (for $\omega>\mu$). This is an important technical point in microscopic calculations.

(4) The Ward identities relating the coupling of vertices to external perturbations change for the coupling to unconserved quantities (for the pure case they are given in Section 2.6). For example, no Ward identity can be derived for the vertex needed for the conductivity calculation, i.e., $\mathrm{Lim}_{\omega\to0}\,\mathrm{Lim}_{q\to0}\,\Lambda_\alpha^{\mathrm{impure}}$, because current is not conserved.

$$\lim_{q\to0}\lim_{\omega\to0}\Lambda_\alpha^{\mathrm{impure}}=\frac{k_\alpha}{m}-\frac{\partial\Sigma(k,\omega)}{\partial k_\alpha} \tag{229}$$

holds because after impurity averaging momentum is conserved. However, microscopic calculations show that, at least when Fermi-liquid theory is valid (cf. Section 2.4),

$$\lim_{\omega\to0}\lim_{q\to0}\Lambda_\alpha^{\mathrm{impure}}=\lim_{q\to0}\lim_{\omega\to0}\Lambda_\alpha^{\mathrm{impure}}\ . \tag{230}$$

Indeed, if this were not so, one would not get a finite dc conductivity at $T=0$ for a disordered metal in $d=3$. An argument for this is as follows: Normally, we calculate the conductivity by first taking the limit $q \to 0$ and then the limit $\omega \to 0$, as on the left-hand side of (230). In practice, however, even when we apply a homogeneous field to a system, the electrons in a disordered medium experience a field which varies on the scale of the distance between the impurities, and so the physically relevant limit is the one on the right-hand side of (230), where the limit $\omega \to 0$ is taken first. But the validity of (230) appears not to extend to the case of singular Fermi liquids, at least for the present case where the singularities are q-dependent. This is one of the important difficulties in developing a consistent theory for disordered interacting electrons in $d=2$.

The diffusive form of the density correlation function and spin-density correlation is the culprit of the singularities which arise due to interactions in two dimensions. For example, the elementary effective vertex in Fig. 66 due to a bare frequency independent short-range interactions in two dimensions is

$$v^2 \int_0^{\ell^{-1}} \mathrm{d}q\, q \left(\frac{1}{\mathrm{i}\omega + Dq^2} \right) \approx v^2 N(0) \ln(\omega\tau) \,. \tag{231}$$

The singularity arises because $\pi(\omega,q) = f(\omega/Dq^2)$. Recall that for pure electrons $\pi(\omega,q) = f(\omega/v_{\mathrm{F}}q)$ leading to a logarithmic singularity for the second-order vertex in one dimension and regular behavior in higher dimensions. Similarly, $\pi(\omega,q) = f(\omega/q^3)$ leads to a logarithmic singularity in the second-order vertex in three dimensions, as we saw in Section 5.1 on SFLs due to gauge interactions.

Note that in Eq. (231) and other singular integrals in the problem have ultra-violet cutoffs at $q \approx \ell^{-1}$ and $\omega \approx \tau^{-1}$ since the diffusive form is not applicable at shorter length scales or time scales. It also follows that Boltzmann transport theory is valid at temperatures larger than τ^{-1}.

Actually, even the first-order interaction dressed by diffusion fluctuations is singular. Consider first the diffusion correction to the vertex shown in Fig. 15

$$\frac{\Lambda}{\Lambda_0} = \frac{1}{\tau}(\mathrm{i}\omega + Dq^2)^{-1} \,, \tag{232}$$

provided $\varepsilon < 0, \varepsilon - \omega > 0$ or vice versa. The restriction is a manifestation of point (3) and arises because in the diffusion process, only intermediate states with one line above (particle) and the other below (hole) the chemical potential contribute as they alone define the physical density. This leads to the first-order *irreducible* interaction and the polarization graph shown in Fig. 67 to be logarithmically singular.

For the small q of interest for singular properties, one need consider interactions only in the s-wave channel. One then has two interaction parameters, one in the singlet channel and the other in the triplet channel.

Consider the problem with Coulomb interactions. Then the effective interaction in the singlet channel sums the polarization bubbles connected by Coulomb interactions. Using (228) for the polarization bubble, it is shown [14] that for small momentum transfer the interaction in the

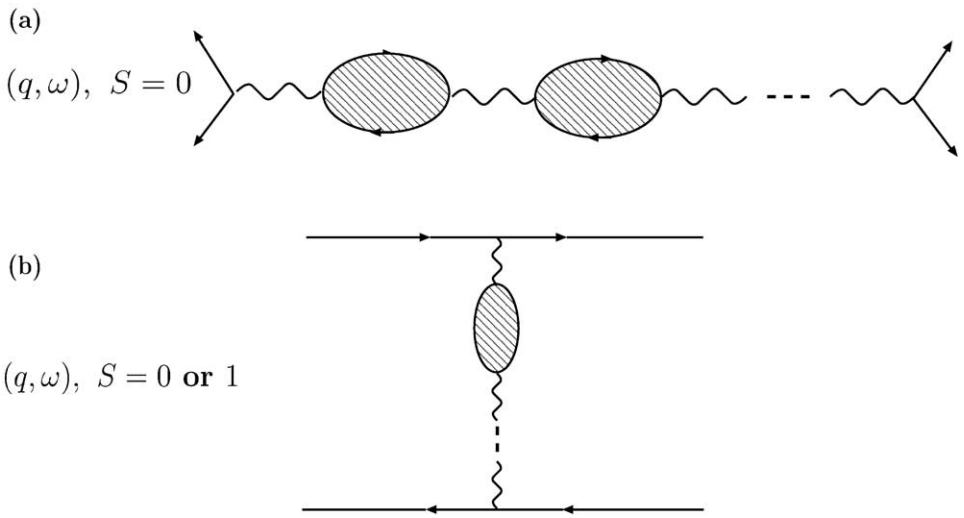

Fig. 67. Effective interactions can be split into singlet and triplet channels. In the singlet-only channel (a), the density–density interaction is screened by the Coulomb interaction and is universal at long wavelengths. In the triplet channel and in the singlet channel for large momentum, the screened density–density interaction appears only in the cross channel and is therefore non-universal.

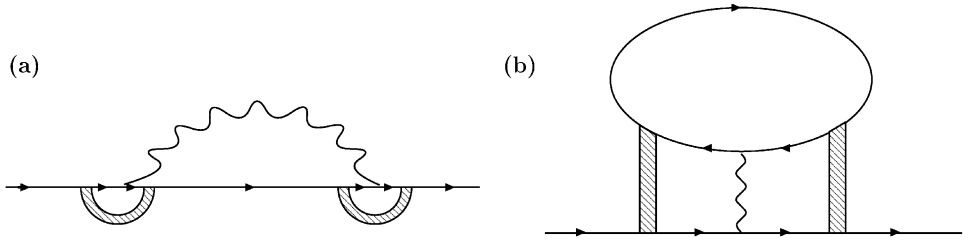

Fig. 68. Simplest processes contributing to the singular self-energy. (a) Exchange process; (b) Hartree process.

spin singlet ($S=0$) channel, Fig. 67, becomes

$$V_{\text{singlet}} = 2\kappa\ . \tag{233}$$

In the non-interacting limit $\kappa = N(0)$, independent of density. Consider now the ladder-type interactions illustrated in Fig. 68. These involve both the singlet and the triplet interactions. The momentum carried by the interaction lines is, however, to be integrated over. Therefore, the triplet interactions do not have a universal behavior, unlike the singlet interactions.

Altshuler, Aronov and collaborators [14] (see also [103]) calculated the logarithmic corrections to first order in the interactions for various physical quantities. To these one can add the contribution already discussed due to weak localization. The corrections to the single-particle density of states, the specific heat and the conductivity over the non-interacting values

are, respectively:

$$\frac{\delta N}{N} = \frac{1}{4\pi\varepsilon_F\tau}\ln|\omega\tau|\left|\ln\left|\frac{\omega}{\tau(Ds^{-2})^2}\right|\right| , \tag{234}$$

$$\frac{\delta C}{C} = \frac{1}{\pi\varepsilon_F\tau}\left(1-\frac{3}{2}F\right)\ln|T\tau| , \tag{235}$$

$$\frac{\delta\sigma}{\sigma} = \frac{1}{4\pi^2}\left(2-\frac{3}{2}F\right)\ln|T\tau| . \tag{236}$$

The compressibility has no logarithmic corrections. In these equations, s is the screening length and F is a parameter which is of the order of the dimensionless interaction r_s.

The first terms in (235) and (236) are due to exchange processes and the second due to the Hartree processes. The exchange process, of which the contribution to the self-energy is shown in Fig. 66, use the interaction in the singlet channel; hence the universal coefficient. The second contribution uses both the triplet and the (large part of the q) singlet interactions. In first order of interaction, the difference in signs of the two processes is natural. In pure systems, the Hartree process does not appear as it involves the $q=0$ interaction alone which is exactly canceled by the positive background. For disordered systems, due to the fluctuation in the (ground state) density, a first-order Hartree process, Fig. 68 contributes.

In the presence of a magnetic field, the $S_z = \pm 1$ parts of the triplet interactions acquire a low-energy cut-off. Therefore, the logarithmic correction to the resistivity is suppressed leading to negative magnetoresistance proportion to $F(H/kT)^2$ for small H/kT but $g\mu_B H \gg \tau_{so}^{-1}, \tau_s^{-1}$ where τ_{so}^{-1} and τ_s^{-1} are spin–orbit and spin-scattering rates, respectively, for appropriate impurities.

8.4. Finkelstein theory

Finkelstein [92] has used field-theoretical methods to generalize Eqs. (234)–(236) beyond the Hartree–Fock approximation. His results have been rederived in customary diagrammatic theory [52,40,53]. The interference processes leading to weak localization are again neglected. The theory may be regarded as first order in $1/k_F\ell$. In effect, the method consists in replacing the parameter F by a scattering amplitude γ_t for which scaling equations are derived. The equivalent of the F_o^s parameter is fixed by imposing that the compressibility remains unrenormalized, i.e., does not acquire logarithmic corrections. A second important quantity is a scaling variable z, which is analogous to the dynamical scaling exponent z which we discussed in Section 6, which gives the relative scaling of temperature (or frequency) with respect to the length scale. A very unusual feature of the theory is that z itself scales! Scaling equations are derived for γ_t and z to leading order $1/k_F\ell$. As $T \to 0$, both γ_t and z diverge. The divergence in z (see the discussion in Section 7) usually means that the momentum dependence of the fluctuations is unimportant compared to their frequency dependence. The divergence in γ_t as $T \to 0$ in such a case has been interpreted to imply divergent spatially localized magnetic fluctuations; in other words, it implies the formation of local moments [93,54]. At the same time, the scaling equations show conductivity flowing to a finite value.

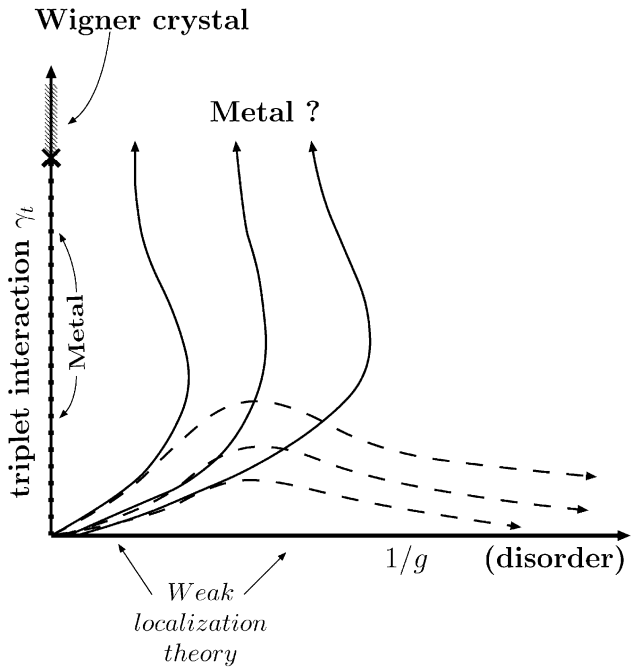

Fig. 69. Schematic renormalization group flow for the disordered interacting electron problem according to the Finkelstein theory. The dashed lines represent the effect on the solid lines on applying a magnetic-field which couples to spins alone.

The scaling trajectories of Finkelstein's theory are shown schematically in Fig. 69. While in the non-interacting theory with disorder, one always has an insulator, this theory always flows towards a metal. However, the theory cannot be trusted beyond $\gamma_t \sim 1$, as then it is uncontrolled. The theory also cannot be trusted for large disorder, $k_F \ell \sim \mathcal{O}(1)$, even for small interactions.

It is worth emphasizing that Finkelstein's theory gives an effect of the interactions in a direction opposite to the leading perturbative results. The perturbative results themselves of course are valid only for small r_s while Finkelstein theory is strictly valid only for $r_s < \mathcal{O}(1)$. One possibility is that the Finkelstein result itself is a transient and the correct theory scales back towards an insulator (the dashed lines in Fig. 69). Another possibility is that it correctly indicates (at least for some range of r_s and disorder) a strong-coupling singular Fermi liquid metallic fixed line. The new experiments discussed below can be argued to point to the latter direction.

It is hard except in very simple situations (the Kondo problem, for instance) to obtain the approach to a strong-coupling fixed point analytically. In that case, one may usually guess the nature of the fixed point and make an expansion about it to ascertain its stability. [48]

[48] Although the theory breaks down in the strong coupling regime, this situation is somewhat comparable to the hints that the weak-coupling expansion gave in the early phase of the work on the Kondo problem: these weak-coupling expansions broke down at temperatures comparable to the Kondo temperature, but did hint at the fact that the low-temperature regime was a strong coupling regime.

In making such a guess, the SFL properties towards which the Finkelstein solution flows should be kept in mind:

(i) The conductivity flows towards a finite value in the theory as $T \to 0$.
(ii) The density of single-particle states flows towards zero

$$N(\omega) \sim \omega^{\alpha} . \tag{237}$$

(iii) The magnetic susceptibility diverges at a finite length scale (the effect of a diverging z) indicating the formation of local moments.

The last point appears to be crucial. As may be seen from Eq. (244) below, the growth of the triplet scattering overrides the exchange processes which favor the insulating state. Indeed, if the triplet divergence is suppressed by an applied magnetic field, the theory reverts to the perturbative form of Eq. (225). The scale of the magnetic field for this effect is given by the temperature. The formation of localized regions of moments may be linked to the fact already discussed that the ferromagnetic state is close in energy to the paramagnetic fluid (and the crystalline states) as density is decreased. The experiments discussed below have a significant correspondence with this picture, although there are some crucial differences.

A possible strong coupling fixed point[49] is a state in which the local moments form a singlet state with a finite spin stiffness of energy of $\mathcal{O}(H_c)$ in the limit $T \to 0$. This eliminates any perturbative instability of the triplet channel about the fixed point. The state is assumed to have zero density of single-particle states at the chemical potential. This eliminates the localization singularity as well as the singularity due to the singlet channel. This state is then perturbatively stable. The conductivity of such a state can be shown to be finite. The occurrence of a characteristic scale H_c observed in the magnetoresistance experiments discussed below with $H_c \to 0$ as the metal–insulator transition in zero field as $n \to n_c$ is also in correspondence with these ideas.

8.5. Compressibility, screening length and a mechanism for metal–insulator transition

Suppose the metallic state in two dimensions is described by a fixed point hinted by the Finkelstein theory and an expansion about it. Such a description must break down near the critical r_s where a first-order transition to the Wigner transition must occur in the limit of zero disorder. General arguments suggest that the transition for finite disorder must be continuous [132].

A suggestion for the breakdown of the Finkelstein regime follows from the calculation of the correction to the compressibility due to disorder [241]. As already mentioned, no perturbative singularity is found in the compressibility due to interactions. However, the correlation energy contribution of the zero-point fluctuations of plasmons is altered due to disorder with a magnitude which also depends on r_s. The leading order contribution in powers of $(k_F \ell)^{-1}$ can be calculated for arbitrary r_s. Including this contribution, the compressibility κ may be written

[49] This paragraph is based on the unpublished work of Q. Si and C.M. Varma.

in the form

$$\frac{\kappa_0}{\kappa} = \frac{\kappa_0}{\kappa_{\text{pure}}} + 0.11 r_s^3/(\omega_0\tau) + \mathcal{O}((r_s^4)/(\omega_0\tau)^2) \,. \tag{238}$$

Here κ_{pure} is the compressibility for zero disorder, $\kappa_0 = N(0)$, and ω_0 is the Rydberg. In the Hartree–Fock approximation

$$\frac{\kappa_0}{\kappa_{\text{pure}}} = 1 - (\sqrt{2}/\pi) r_s \,. \tag{239}$$

The best available numerical calculations also give κ_0/κ varying slowly enough with r_s that the correction term (238) dominates for r_s of interest near the metal–insulator transition even for a modest disorder. For example for $\omega_0\tau \approx 10$, the disorder contribution in Eq. (238) is larger than the pure contribution for $r_s \geqslant 10$. This has an important bearing on the metal–insulator transition because the screening length s is given by

$$s/s_0 = \kappa_0/\kappa \,, \tag{240}$$

where $s_0 = a_0/2$. Strictly speaking, s is the screening length for an external immobile charge and the screening of the electron–electron interactions is modified from (238) due to vertex renormalizations. However, in this case they do not change the essential results. From Eq. (238) it follows that the screening length $s(\ell) > \ell$, the mean free path, for

$$r_s \geqslant 3(\omega_0\tau) \,. \tag{241}$$

Suppose the condition $s(\ell) > L > \ell$ is satisfied. Here L again is the size of the box for which the calculation is carried out, defined through $DL^{-2} \approx T$. The assumption of screened short-range interactions, with which perturbative corrections leading to results of Eqs. (234)–(236) are obtained, is no longer valid. In this regime, the calculations must be carried out with unscreened Coulomb interactions. The correction proportional to F in Eqs. (234)–(236) is not modified but the singlet contributions are more singular (due to the extra q^{-1} in the momentum integrals). For instance, Eq. (236) is modified to

$$\delta\sigma/\sigma = -(\sqrt{2}/\pi^2) r_s \frac{L}{\ell} \,. \tag{242}$$

This implies a crossover to strong localization. It is therefore suggested that the metallic state ceases to exist when condition (241) is satisfied.

The above line of reasoning is of particular interest because as discussed below, a sharp variation in the compressibility is indeed observed to accompany the transition from the metallic-like to insulating-like state as density is decreased (as shown in Fig. 79 below).

8.6. Experiments

Soon after the publication of the theory of weak localization, its predictions were seemingly verified in experiments on Si-MOSFETS [48,260]. The experiments measured resistivity on not very clean samples of high density with resistivity of $O(10^{-2}h/e^2)$. In a limited range of temperature, the predicted logarithmic rise in resistivity with decreasing temperature with about the right prefactor was found [41]. In view of the perturbative results of Altshuler and Aronov [14] and the knowledge that electron–electron interactions alone lead to a Wigner insulator at low

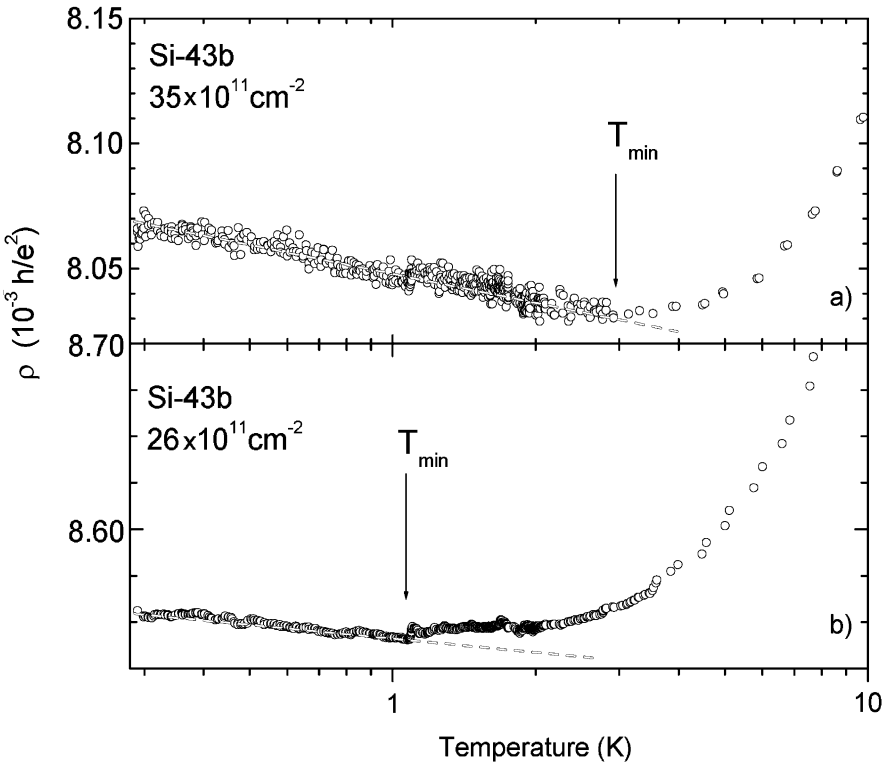

Fig. 70. Resistivity data on a fine scale for the two highest densities in Fig. 75 below, showing correspondence with the theory of weak localization at such high densities. From Pudalov et al. [216]. See text.

densities, one was led to the conviction that the metallic state does not exist in two dimensions. It was expected that samples with larger r_s will simply show logarithmic corrections to the resistivity at a higher temperature and pure samples at a lower temperature. Not too much attention was paid to Finkelstein's results which pointed to the more interesting possibility of corrections in the opposite direction.

The more recent experiments on a variety of samples on a wider range of density and of higher purity than earlier have refocused attention on the problem of disorder and interactions in two dimensions and, by implication, in three dimensions as well. Several reviews of the experiments are available [3,16,17]. We will present only a few experimental data to highlight the theoretical problems posed, and will focus on the behavior of the data as a function of temperature. The scaling of the data as a function of the electron density $n - n_c$ or field E will not be discussed; there is a considerable body of data on non-linear E-dependence (see e.g. [238] and references therein) but the significance of the data is not clear at present.

The first thing to note is that results consistent with the earlier data [48,260] are indeed obtained for high enough densities. Fig. 70 shows the resistance versus temperature in Si for $r_s \sim \mathcal{O}(1)$. The magnitude of the temperature dependence is consistent with the predictions of weak localization corrections. As we will show below in the same region of densities, the

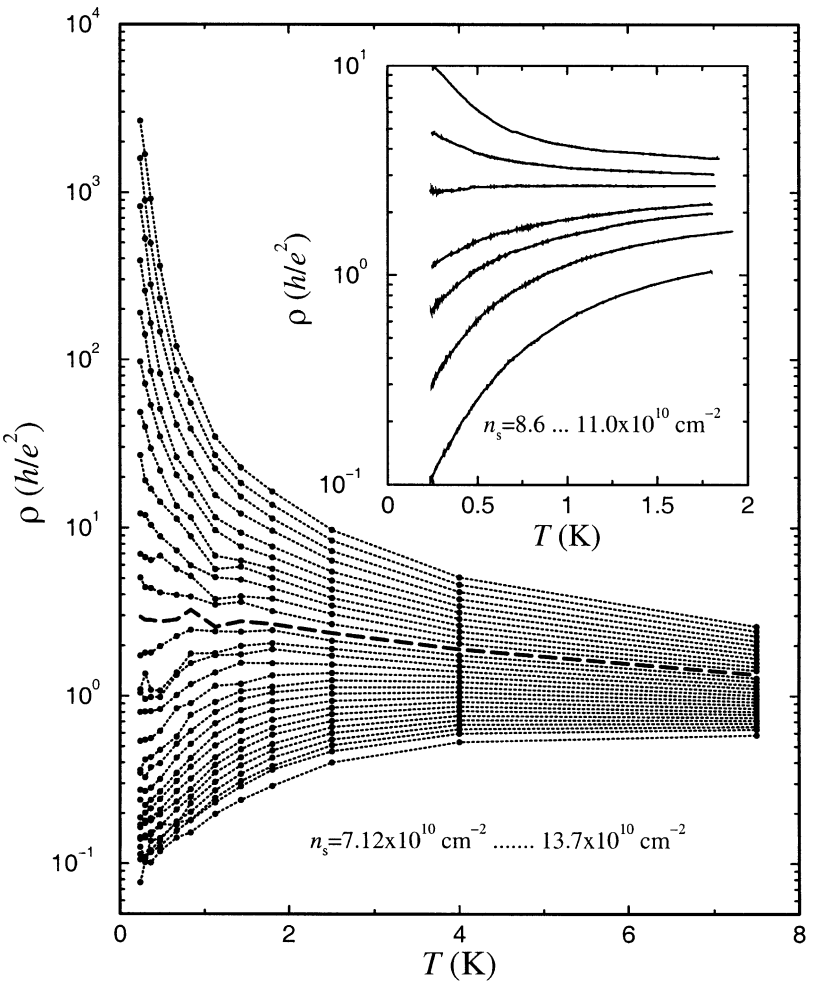

Fig. 71. Resisitivity as a function of temperature for a wide range of densities (and Fermi energy) in a disordered Si MOSFET. The inset shows accurate measurements of $\rho(T)$ close to the separatrix for another sample. From Sarachik and Kravchenko [226,3].

negative magneto-resistance predicted as the correction to weak localization, discussed above, is also observed.

Fig. 71 shows the resistivity as a function of T over a wide range of densities. Similar data from [150] over a large small of densities is shown in Fig. 72, and data over a large range of densities are plotted as a function of T/E_F in Fig.73. The resistivity clearly shows a change of sign in the curvature as a function of density at low temperatures. The resistivity at the crossover density as a function of temperature is shown down to 20 mK in the inset of Fig. 72 and is consistent with temperature independence. The true electron temperature in these samples is a question of some controversy [16,3], but more recent experiments, whose data are shown in Fig. 74, have corroborated these results by studying this issue very carefully down to 5 mK.

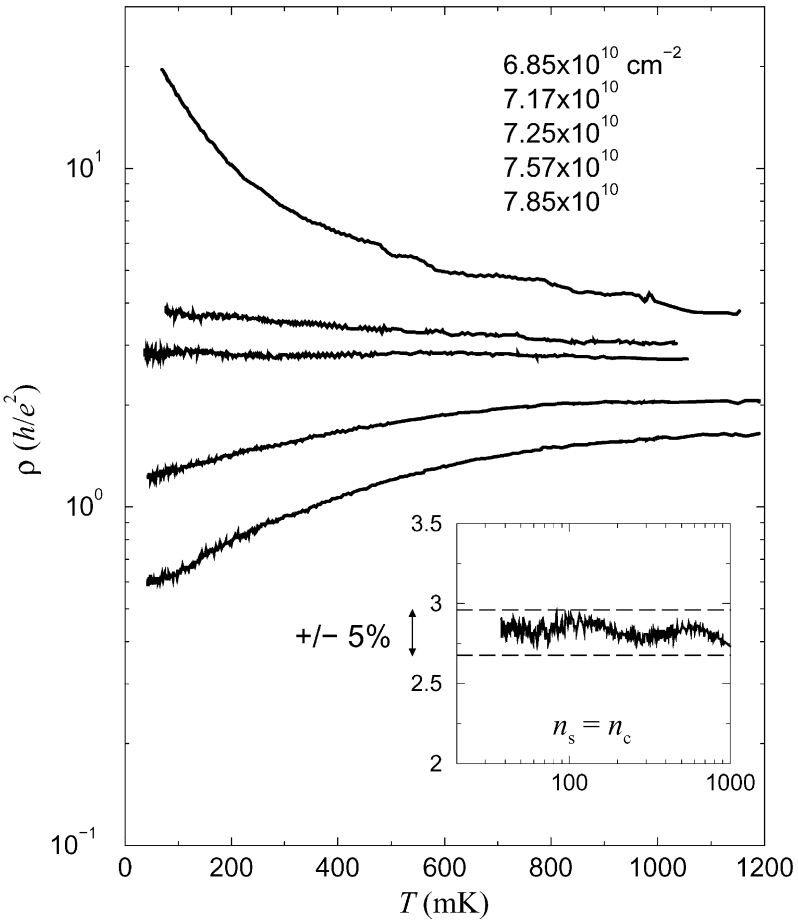

Fig. 72. Resistivity versus temperature at five different electron densities in the experiments of Kravchenko and Klapwijk [150]. The inset shows that the middle curve ($n_s = 7.25 \times 10^{10}$ cm^{-2}) changes by less than $\pm 5\%$ in the entire temperature range.

In the high-density region the resistivity does rise with decreasing temperature logarithmically, consistent with earlier measurements. The consistency of these datasets for two very different types of samples therefore gives strong evidence that these are genuine effects in both types of systems.

The data shown in Figs. 71–73 is for Si-MOSFET samples. The data for GaAs heterostructures, and Si in other geometries is qualitatively similar [120,62,63,210,119,184]. Fig. 74 shows data on high-quality gated GaAs quantum wells with densities on the metallic side of the metal–insulator "transition" taken to temperatures as low as 5 mK. The resistivity is essentially temperature independent at low temperatures. The logarithmic corrections expected from weak-localization (calculated using the measured resistivity and the theoretically expected τ_ϕ) is also shown.

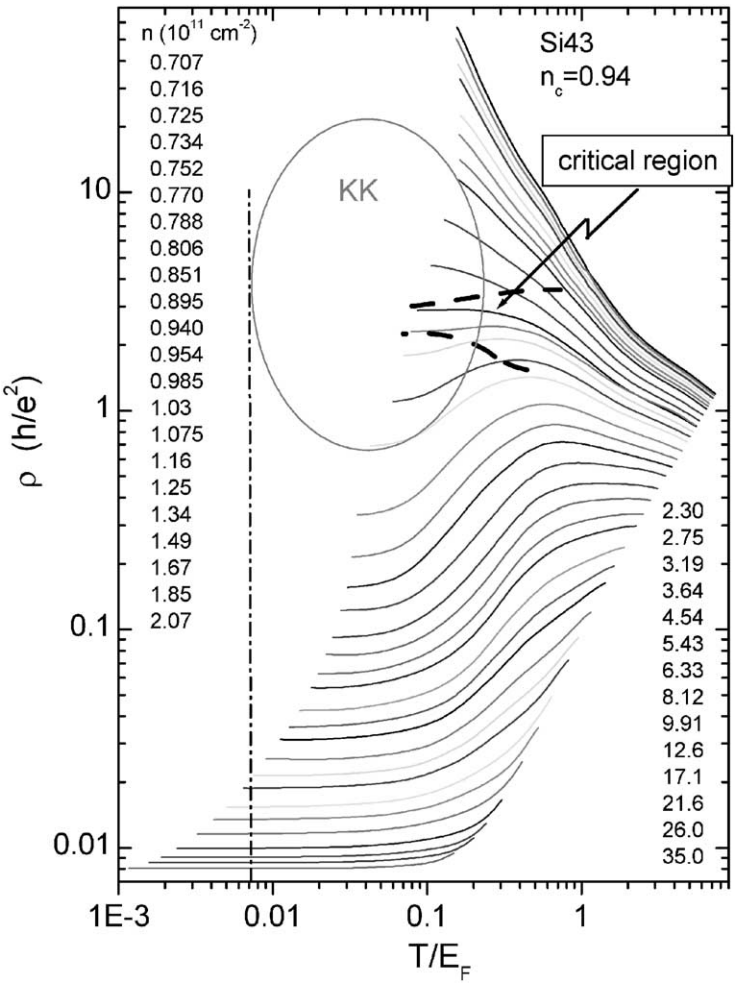

Fig. 73. Plot of the resistivity as a function of the scaled temperature T/E_F. The encircled region indicates the range of parameters explored in Fig. 72 and in [150]. The dash–dotted vertical line depicts the empirical temperature $T_Q = 0.007E_F$ below which the logarithmic temperature dependence like that of Fig. 70 sets in. From Prinz et al. [214].

8.6.1. Experiments in a parallel magnetic field

A magnetic field applied parallel to the plane couples primarily to the spin of the electrons. For small fields and for $n \gg n_c$, a positive magnetoresistance proportional to H^2 is observed as expected from perturbative calculations in the interactions. For fields such that $\mu_B H \approx E_F$, the electrons are fully polarized and the resistivity saturates as expected. The temperature dependence of the resistivity begins to become insulating-like at low temperatures with the crossover temperature increasing as n decreases [243]. This is an indication that the metallic state becomes unstable as the spins are polarized. A complete set of data is shown in Fig. 75 where resistivity versus temperature in an Si-MOSFET with density varying across n_c is shown

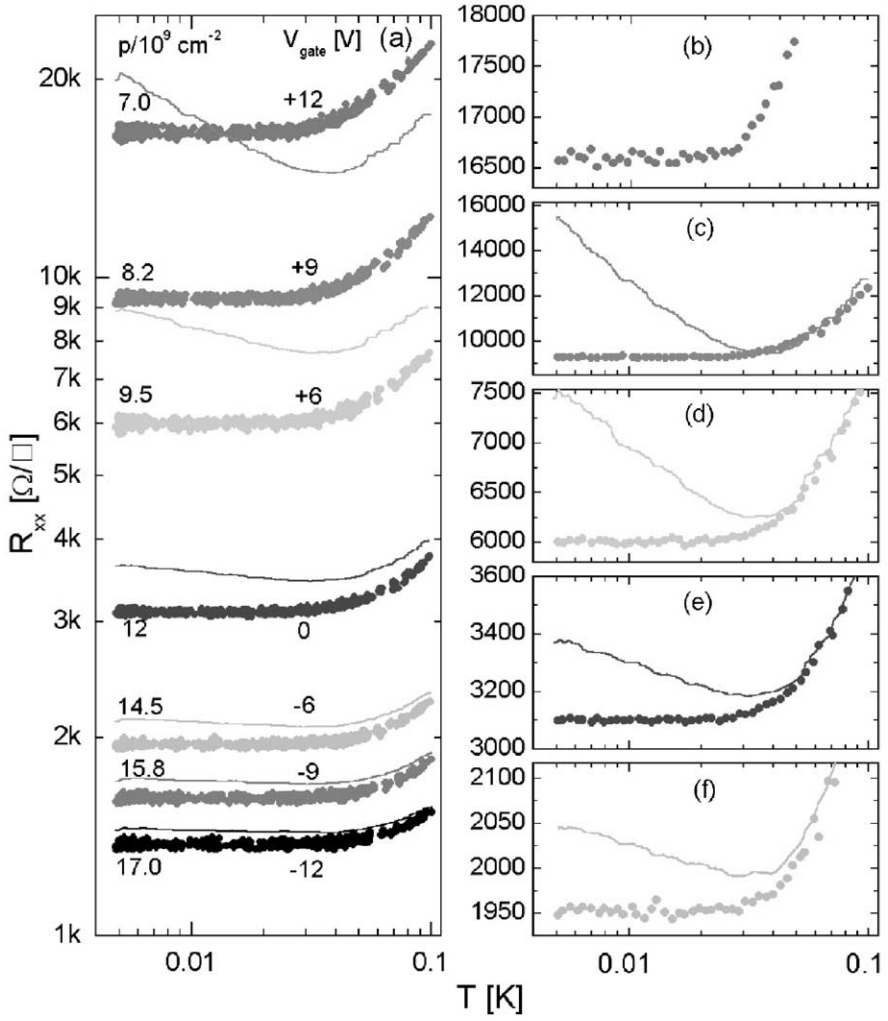

Fig. 74. (a) Temperature dependence of the longitudinal resistivity of a two-dimensional hole gas for various gate biases and associated densities in experiments on GaAs. The solid curves are estimated weak localization predictions; (b)–(f): Magnified view of the data in (a) averaged over a 5% temperature interval. The estimated weak localization prediction has been shifted to coincide with the data curve at $T = 50$ mK. From Mills et al. [184].

together with the resistivity versus magnetic field at the lowest temperature for some densities on the $n > n_c$ side. It is noteworthy that the temperature dependence of the high-field data (not shown) appears to fall on the curve of resistivity versus temperature (at $H = 0$) which the high field (low temperature) data saturates asymptotically.

The parallel magnetoresistance has been examined carefully for n close to but larger than n_c, and is shown in Figs. 76 for p-type GaAs [294].[50] It is discovered that a critical field

[50] Roughly similar results are found in Si-MOSFETS, but a unique crossover field $B_{\|}^{c}$ as in Fig. 76 is not found [223].

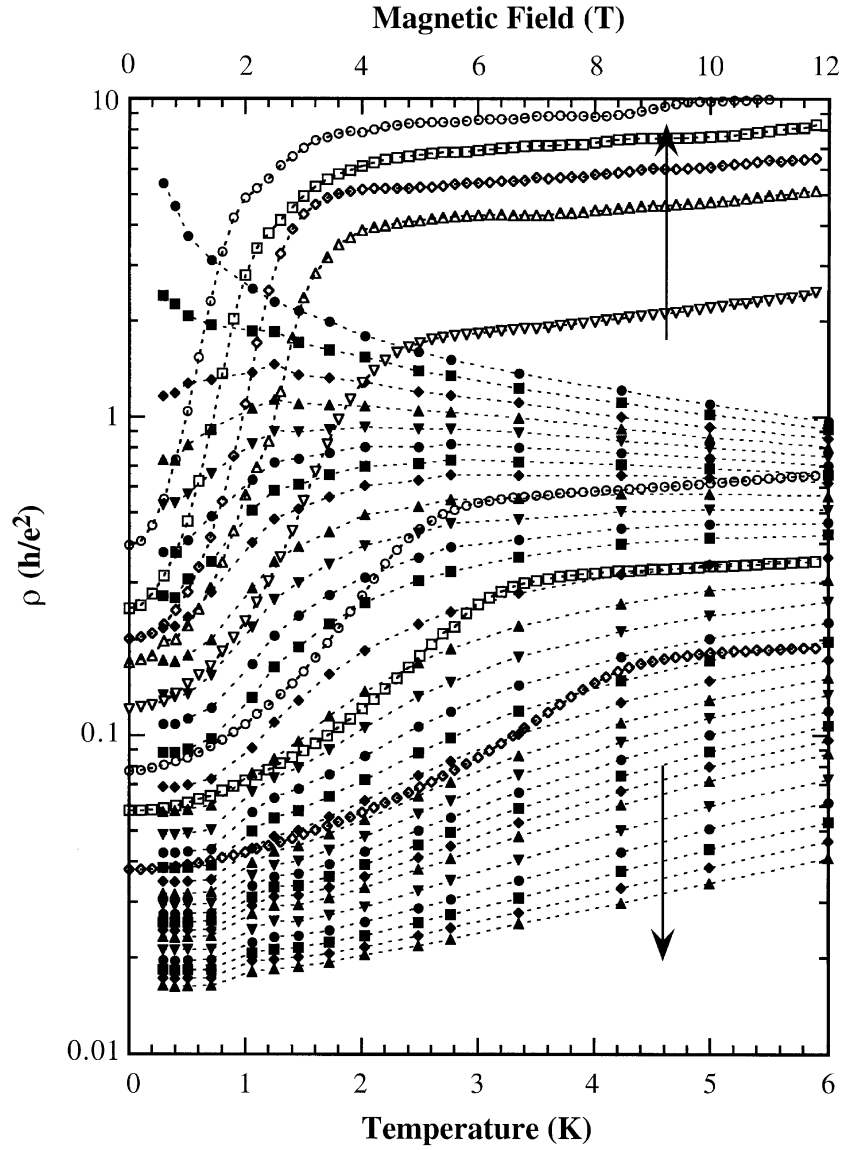

Fig. 75. Results for resistivity versus temperature and versus magnetic field applied in the plane for a few densities on either side of n_c. The magnetic field is shown on the upper axis and the data is taken at the lowest temperature for some of the densities shown in the resistivity versus temperature plots. From Pudalov et al. [215].

as a function of density $H_c(n)$ exists such that for $H < H_c(n)$ the resistivity continues to be metallic-like $\mathrm{d}\rho/\mathrm{d}T > 0$ and for $H > H_c(n)$ it is insulating like $\mathrm{d}\rho/\mathrm{d}T < 0$. The field $H_c(n)$ tends to zero as $n \to n_c$. The low-temperature data on the high fields side is puzzling and should be re-examined to ensure that the electron temperature is indeed the indicated temperature.

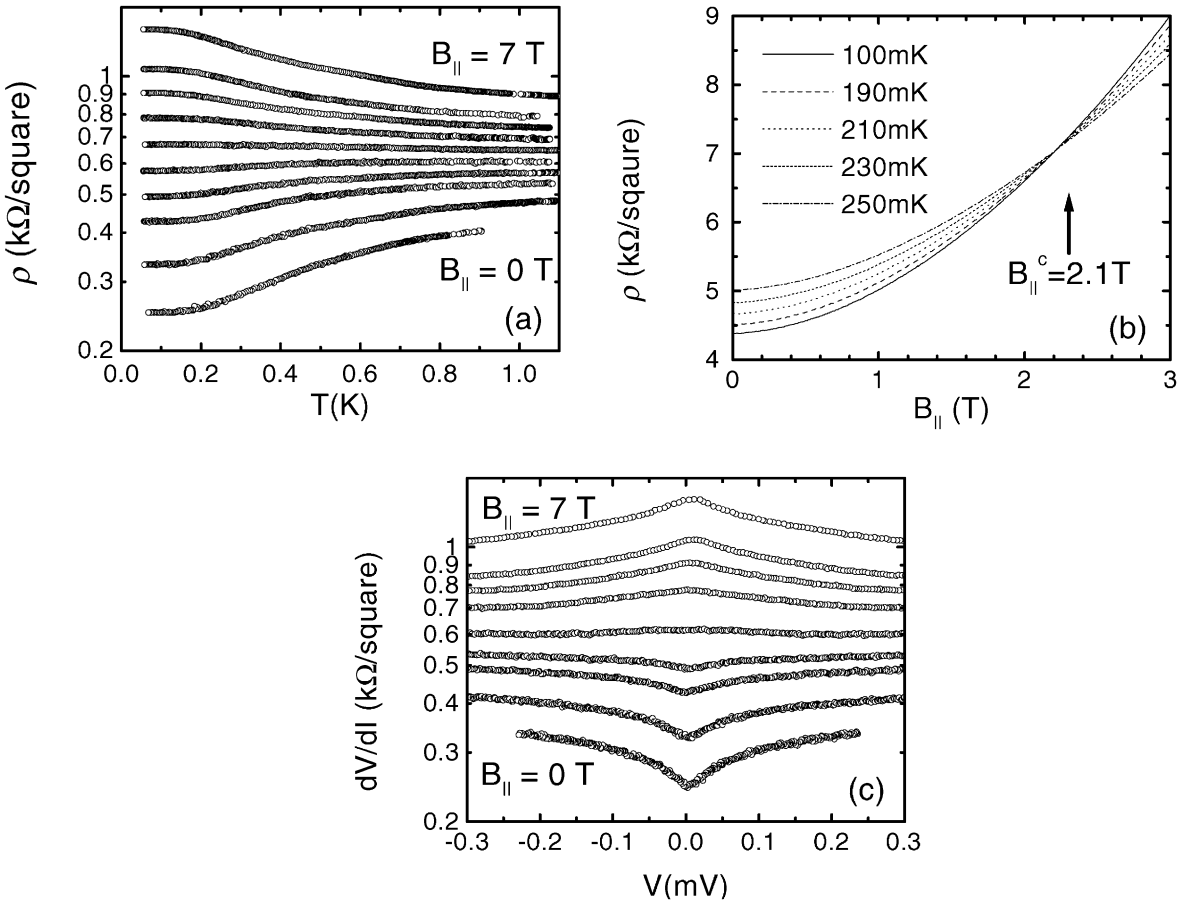

Fig. 76. Plot of the magnetoresistance. In (a) the T dependence of ρ in the zero field metallic phase is shown on a semilog plot for a hole density $3.7 \times 10^{10}\ \mathrm{cm}^{-2}$ for varying $B_{\|}$ values. As $B_{\|}$ increases from zero, the strength of the metallic behavior measured by the total change in ρ from about 1 K to 50 mK weakens progressively, and for $B_{\|} \geqslant B_c$ $\mathrm{d}\rho/\mathrm{d}T$ becomes negative (i.e., the system becomes insulating). An alternate way of demonstrating the existence of a well-defined $B_{\|}^c$ is to plot ρ against $B_{\|}$ at several different temperatures. In (b) ρ is plotted versus $B_{\|}$ at a hole density $1.5 \times 10^{10}\ \mathrm{cm}^{-2}$. $B_{\|}^c$ is read off the crossing point marked by the arrow. In (c), the differential resistivity $\mathrm{d}V/\mathrm{d}I$ measured at 50 mK across the $B_{\|}$ induced metal–insulator transition is shown at magnetic field strengths similar to those in (a). From Yoon et al. [294].

8.6.2. *Experiments in a perpendicular field*

The behavior of a resistance in all but very small perpendicular fields, is dominated by the quantum Hall effect (QHE). The connection of the quantum Hall transitions to the metal–insulator transition at $n = n_c$ and $H = 0$ is an interesting question which we will not touch on. At low fields and for $n \geqslant n_c$, outside the QHE regime, negative magnetoresistance predicted by weak-localization theory are observed. Data for $n \gg n_c$ is shown in Fig. 77 and agrees quite well with the theoretical curves as shown; similar results for n close to n_c are also reported [119]. More recent low-temperature data in GaAs heterostructures [184] is reproduced in Fig. 78 for

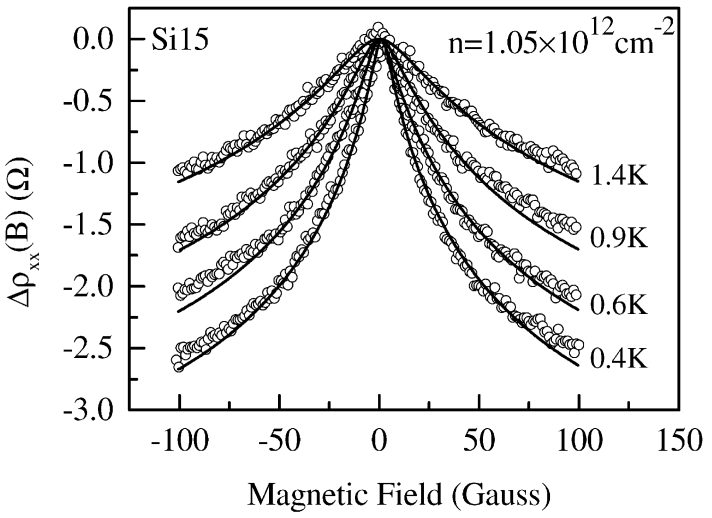

Fig. 77. Plot of the magnetoresistance. The change in the resistivity $\Delta\rho(B) = \rho_{xx}(B) - \rho_{xx}(0)$ versus magnetic field B at an electron density of 1.05×10^{12} cm^{-2} at various temperatures. The open circles denote the measurements and the full line is the best least square fit according to the single electron weak localization correction to the conductivity. From Brunthaler et al. [49].

densities $n > n_c$ but close to n_c. A magnetoresistance two orders of magnitude smaller than the weak localization theory is estimated although the width of the negative magnetoresistance region is not inconsistent with the weak-localization correction.

8.6.3. Compressibility measurements

Compressibility (κ) measurements [81,129] in the region around $n = n_c$ show a rapid change in κ^{-1} from the negative value characteristic of high r_s metallic state to positive values—see Fig. 79. These are very important measurements which show that a thermodynamic quantity has a very rapid variation near $n \approx n_c$. We have already discussed that such changes were predicted [241] to occur through perturbative corrections due to disorder in the energy of interacting electrons. Some recent ingenious measurements [130] of the local electrostatic potential show that in the region $n \approx n_c$ large-scale density fluctuations (puddles) occur with weak connections between them. Such density fluctuations become more numerous with weaker contacts between them as the density is lowered into the insulating phase. These show up in the experiments as local fluctuation in which κ^{-1} approaches 0. Completely isolated puddles (Coulomb dots) of-course must have $\kappa^{-1} = 0$.

8.7. Discussion of the experiments in light of the theory of interacting disordered electrons

In comparing the experimental results with the theory, it is necessary to separate out the effects due to "customary-physics"—for instance electron–phonon interactions, creation of ionized impurities with temperature [15], change of screening from its quantum to its classical form as a function of temperature [73] change of single-particle wavefunctions with a magnetic

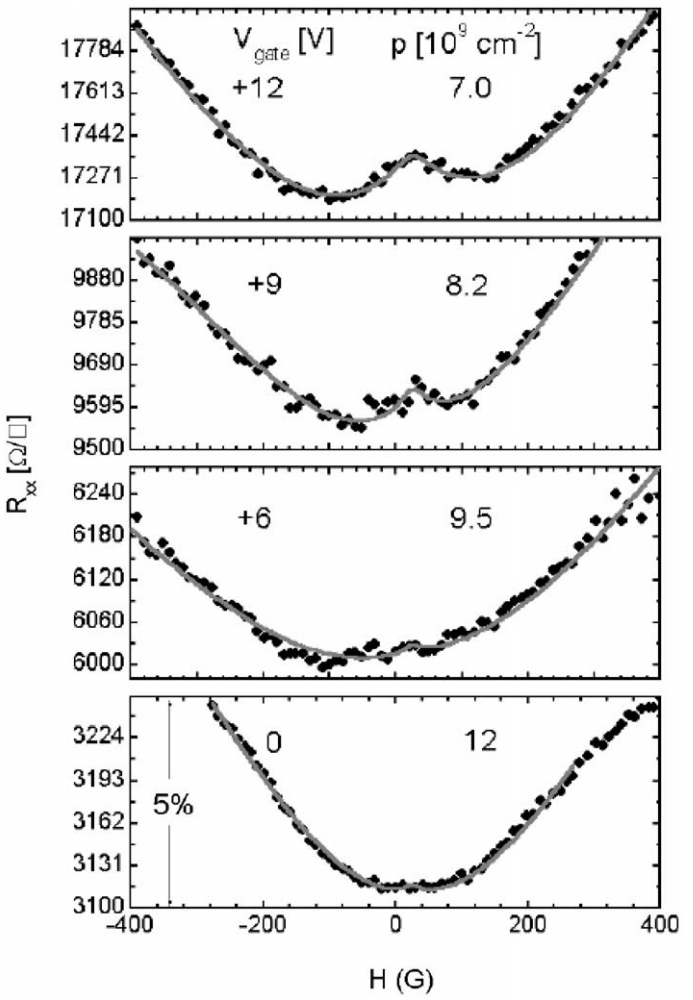

Fig. 78. Variation of the longitudinal resistance with perpendicular magnetic field for two-dimensional sample at $T = 9$ mK and at various indicated densities. The weak-localization correction is estimated to be $\mathcal{O}(10^2)$ larger than the observations at these densities. From Mills et al. [184].

fields [145], inter-valley scattering [292], etc.—from the singular effects due to impurities and interactions. The separation is at present a matter of some debate. However, it seems that the following features of the experimental data in relation to the theoretical ideas summarized in Sections 8.3, 8.4 are especially noteworthy. These must be read bearing in mind our earlier discussion that most of the interesting experiments are in a range of r_s and disorder where the theoretical problems are unresolved and only hints about the correct form of a theory are available.

- At $r_s \leqslant \mathcal{O}(1)$ and $k_F \ell \gg 1$, a logarithmic increase in resistance with decreasing T consistent with weak localization as well as with the perturbative interaction correction is observed.

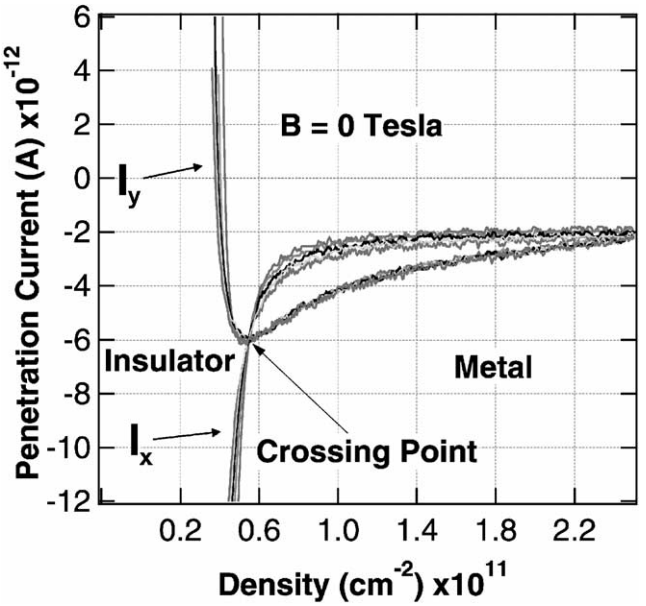

Fig. 79. Compressibility data. In this experiment, at low frequencies, I_x is directly proportional to R_x, the dissipation of the two-dimensional hole system, while I_y is proportional to the inverse compressibility. I_x and I_y are shown as a function of density for five different temperatures ranging from 0.33 to 1.28 K at an excitation frequency of 100 Hz. The crossing point of the five dissipation channel curves corresponds to the metal–insulator transition at $B = 0$. The minimum of the inverse compressibility occurs at the same hole density of 5.5×10^{10} cm^{-2}. From Dultz et al. [81].

A positive magnetoresistance consistent with the latter is also observed. Also observed is the correction to weak localization due to phase-breaking of backscattering in a perpendicular magnetic field. The latter yields sensible values and temperature dependence for the phase relaxation rate given by the theory. It appears that at high enough density, the weak localization theory supplemented by the perturbative theory of interactions is in excellent agreement with the experiments in the range of temperatures examined.

- As r_s is increased (and $k_F\ell$ decreased), the logarithmic resistance is lost in the observed temperature range, whereas weak-localization theory predicts that the coefficient of such terms (as well as the onset temperature for their occurrence) should increase. For r_s not too large, the decreased logarithmic term may be associated with the perturbative corrections (225) due to interactions.
- Upon further increasing r_s, the derivative $d\rho/dT$ becomes positive in the low-temperature region as in a metal. The magnetoresistance in a parallel field is positive $\sim H^2$ as is predicted by Finkelstein [although the variation is closer to H^2/T rather than as $(H/T)^2$] [216]. The phase-breaking correction in a perpendicular field continues to be observed. However, quite curiously the deduced τ_ϕ is larger than τ deduced from resistivity—by definition a phase-breaking rate serves as a cutoff only if $\tau_\phi < \tau$.
- In the "metallic" regime for intermediate r_s, a strongly temperature dependent contribution for $T \leqslant E_F$ is found which may be fitted to the form $\rho'(n)\exp(-E_a(n)/T)$. The magnitude of this

term rapidly decreases as the density n decreases. No accepted explanation for this contribution has been given. In Si, the change of resistivity at $n \approx 10n_c$ due to this contribution is an order of magnitude larger than in GaAs. It has been proposed [14,215] that this contribution together with the weak-localization contribution may well account for all the data in the "metallic" regime since it pushes the minimum of the resistivity below which the logarithmic temperature dependence is visible to lower temperature than the available data at lower densities.

This issue can be resolved by experiments at lower temperatures. At this point, especially in view of the consistency of the recent results of Mills et al.—see Figs. 74 and 78—with the earlier experiments, one can say that it requires an unlikely conspiracy of contributions to remove the temperature dependence over a wide range for different materials and with different degrees of disorder.

A quite different scenario also consistent with the existing data is that the logarithmic upturn in the resistivity observed in high-density samples is a transient that on further decreasing the temperature disappears to be replaced by $\mathrm{d}\rho/\mathrm{d}T \to 0$ as $T \to 0$, at least above some characteristic density which is a function of disorder. We will come back to this issue when we discuss the possible phase diagram.

- As r_s approaches r_{sc}, $\mathrm{d}\rho/\mathrm{d}T$ tends to zero (through positive values). A separatrix is observed with $\mathrm{d}\rho/\mathrm{d}T \approx 0$ over about two orders of magnitude in temperature for Si and over an order of magnitude in GaAs. For $r_s > r_{sc}$, $\mathrm{d}\rho/\mathrm{d}T$ is negative befitting an insulator. r_{sc} appears to be smaller for dirtier samples but not enough systematic data is available for drawing a functional relation.
- The electronic compressibility rapidly changes near the "transition" and rapidly becomes small on the insulating side. Its value on the insulating side is consistent with approaching zero in the limit of zero temperature. Although this is in qualitative accord with the theoretical suggestion [241], further experiments simultaneously measuring the compressibility and the conductivity at low temperatures are necessary to correlate the metal–insulator transition with the rapid variation of compressibility or the screening length. Note that it follows from the Einstein relation $\sigma = D\kappa$ that if κ is finite in the metallic state (σ finite) and zero in the insulating state ($\sigma = 0$), κ must go to zero *at the transition*. Otherwise, we would have the absurd conclusion that $D \to \infty$ at the transition.

Interesting phenomenological connections between the transport properties and formation of "puddles of electron density" of decreasing size as the metal–insulator "transition" is approached have been drawn [178]. The important question is why such behavior begins to dominate as the density is lowered to n_c. Evidence that the formation of "puddles" is a result of disorder strongly augmented by electronic correlations is available in recent measurements [130].

- Near $r_s = r_{sc}$, the resistivity as a function of temperature on the insulating side appears to be a reflection of that on the metallic side about the $\mathrm{d}\rho/\mathrm{d}T = 0$ line if the data is not considered at low temperatures [149]. Now with more complete data, we know that the resistivity flattens to zero slope at low temperatures on the "metallic" side of n_c. The most likely behavior appears to be that the resistivity approaches a finite value at low temperature on one side of n_c and an infinite value on the other. A one-parameter scaling ansatz [77] for the problem with interaction and disorder gave $\rho \to \infty$ for $n < n_c$ and $\rho \to 0$ for $n > n_c$ as $T \to 0$ and

reflection symmetry just as at any second-order transition with one scaling parameter.[51] Does this necessarily imply that multidimensional scaling is required near this transition? However, another important point to bear in mind is that since resistance does not depend on a length scale in two dimensions, it need not be a function, in particular, of the correlation length near the transition. The resistivity is allowed to be finite on one side of a metal–insulator transition and infinite on the other even though the transition may be continuous and the correlation length diverges on either side with the same exponent. The glassy nature (Coulomb glass) of the insulating state is also expected to change the critical properties.

- The resistivity at low temperatures for $n \ll n_c$ has been fitted to an activated form $\propto \exp(\Delta/T)^{\alpha}$ with $\alpha \approx 1/2$ and with $\Delta \to 0$ as $n \to n_c$. This is characteristic of a Coulomb glass [239]. Whether this is indeed the asymptotic low temperature form is not completely settled.
- The resistance at $n \approx n_c$ appears to vary from sample to sample but is within a factor of 3 of the quantum of resistance. It is worth emphasizing that n_c is close to the density expected for Wigner crystallization. With Coulomb interactions and disorder, the insulating state is indeed expected to be Wigner glass. In that case, one might expect singular frequency-dependent properties and hysteretic behavior near the transition.
- For $r_s \approx r_{sc}$ the resistance in a parallel field is especially noteworthy. In a parallel field $\mathrm{d}\rho/\mathrm{d}T$ decreases until at a field $H = H_c(n)$ it changes sign. H_c vanishes at n_c, the density where $\mathrm{d}\rho/\mathrm{d}T = 0$ for $H_{\|} = 0$. In this regime, $\rho(H, T, n)$ can be scaled as [294]

$$\rho\left(\frac{(n-n_c)}{T^{\alpha}}, \frac{(H - H_c(n-n_c))}{T^{\beta}}\right) . \tag{243}$$

This means that the transition from the metallic state to the insulating state can be driven by a magnetic field. It appears that the "metallic" state owes its existence to low-energy magnetic fluctuations which are quenched by a magnetic field. This is in line with Finkelstein theory and the flow diagram of Fig. 69 yet the existence of a scale H_c is not anticipated by the calculations of Finkelstein (nor, of course, is the mere existence of n_c). As $H_{\|}$ is further increased $\mathrm{d}\rho/\mathrm{d}T$ approaches the insulating behavior characteristic of $n > n_c$ at $H_{\|} = 0$. At a fixed temperature, the resistivity saturates for $g\mu_B H_{\|} \geqslant E_F$, i.e., for a fully polarized band.

For small perpendicular fields, negative magnetoresistance of the form of (225) continues to be observed at least for Si for $n \gg n_c$. In GaAs, this contribution at least in the range $n_c \geqslant n \geqslant 2n_c$ is negligible.

- The Hall coefficient R_H is continuous across the transition, obeying the kinetic theory result $R_H \sim 1/n$. On the "metallic" side this is not surprising. On the "insulating" side this is reminiscent of the properties of Wigner glasses [61,109].

8.8. Phase diagram and concluding remarks

It is worthwhile to try to guess the $T = 0$ phase diagram of interacting disordered electrons on the basis of the data and the available theory, inadequate though it is. A convenient set of

[51] The data also led to suggestions for a superconducting ground state on the metallic side [207], and to an anyonic state [301]!

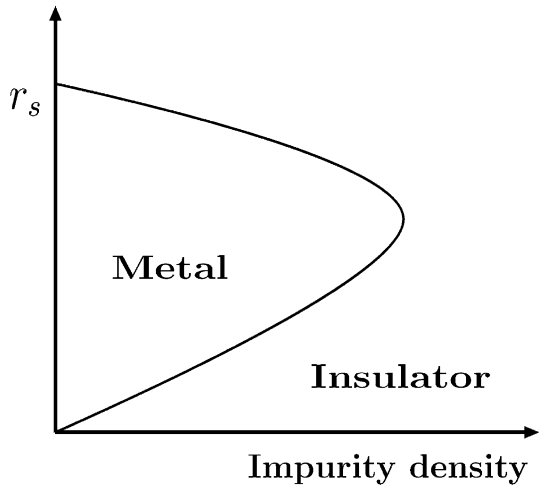

Fig. 80. A tentative phase diagram at $T = 0$ for two-dimensional disordered electrons with interactions.

axes is r_s (or $n^{-1/2}$), as it parameterizes the dimensionless interaction, and the resistance in units of h/e^2 as it parametrizes the dimensionless disorder, see Fig. 80.

Reliable theoretical results are found only along the two axes of Fig. 80. States are localized all along the horizontal axis. Localized states at $T = 0$ must be organized into one or another kind of magnetically ordered state. On the vertical axis a Fermi-liquid gives way via a first-order transition to a Wigner crystal which may have various magnetic phases.

In light of the experiments, the assumption that the entire region in Fig. 80 is an insulator made too long, has to be abandoned in all likelihood. There does appear to be a "metallic state". With disorder, a crossover to a Wigner glass must occur at large r_s. It is also clear that at high densities weak-localization theory supplemented by perturbative corrections due to interactions works quite well in the range of temperatures examined. At moderate r_s for small disorder the Finkelstein correction appears to take over and a "metallic" state takes over. The best evidence for this, paradoxically, is the magnetic field (parallel to the plane) dependence of the resistivity which appears to eliminate the "metallic" state.

Based on these considerations, the phase diagram Fig. 80 is put forth. It is surmised that the weak localization correction flows to strong localization for sufficiently strong disorder and small enough r_s, but that it gives way to a metallic state at weak-disorder and larger r_s. What determines the boundary? A possible criterion is that on one side, the Finkelstein renormalization is more important and on the other side localization due to disorder is more important. The crossover to strong localization occurs at a length scale ζ given by Eq. (219) where the resistivity doubles.

The scaling equation for the triplet interaction parameter is [92,51,157]

$$d\gamma_t/d\ln L = \pi k_F \ell (1 + 2\gamma_t)^2 \tag{244}$$

so that for small initial value γ_t^0 at $L = \ell$ one gets $\gamma_t(L) = \gamma_t^0 + (\pi k_F \ell)\ln(L/\gamma)$. As $L = \zeta$, the triplet interaction parameter $\gamma_t \approx \gamma_t^0 + 1$. The boundary between the "metallic" and the "insulating"

regions on this basis is linear at small r_s and small g^{-1}, as shown in Fig. 80. This is highly conjectural but the existence of the phase boundary at the point $r_s \to 0$ and $1/g \to 0$ is more robust.

This scenario can be tested in high density, low disorder samples by measurements of resistivity at very low temperatures. If correct in some regime of parameters near the boundary, the logarithmic weak-localization correction should appear at high temperatures and disappear at lower temperatures.

We have stressed that the "metallic state" in two-dimensions is likely to be a singular Fermi liquid with an interesting magnetic-ground state.[52] Direct or indirect measurements of the magnetic susceptibility through, for instance the magnetic field dependence of the compressibility should yield very interesting results. Also interesting would be measurements of the single-particle density of states through tunneling measurements. Further systematic and careful measurements of the compressibility are also required to correlate the transition from the "metallic" state to the increase in susceptibility.

The basic theoretical and experimental problem remains the characterization of the "metallic state" its low-temperature entropy, magnetic susceptibility, single-particle density of states, etc. The experimental and theoretical problems are many but one hopes not insurmountable.

Acknowledgements

This article is an outgrowth of lectures delivered in spring 2000 by C.M. Varma during his tenure as Lorentz Professor at the Universiteit Leiden. He wishes to thank the faculty and staff of the Physics department and the deep interest shown by the attendees of the lectures.

Special thanks are due to numerous colleagues who provided the experimental data and who explained their ideas and clarified countless issues.

ZN also wishes to take this opportunity to greatly thank his former mentor, S.A. Kivelson, for coaching in one-dimensional physics.

Finally, ZN and WvS also wish to express their thanks to Debabrata Panja, Michael Patra, Kees Storm and especially Carlo Beenakker from the Instituut-Lorentz for all their help in generating, scanning, and compressing the numerous figures.

References

[1] E. Abrahams, P.W. Anderson, D.C. Licciardo, T.V. Ramakrishnan, Scaling theory of localization: absence of quantum diffusion in two dimensions, Phys. Rev. Lett. 42 (1979) 673.

[2] E. Abrahams, C.M. Varma, What angle-resolved photoemission experiments tell about the microscopic theory for high-temperature superconductors, Proc. Nat. Acad. Sci. 97 (2000) 5714.

[3] E. Abrahams, S.V. Kravchenko, M.P. Sarachik, Metallic behavior and related phenomena in two dimensions, cond-mat/0006055, Rev. Mod. Phys. 73 (2001) 251.

[52] In this connection recent Shubnikov deHaas measurements [276] are of great interest. The results are, however, not uncontroversial, see [217].

[4] A.A. Abrikosov, L.P. Gorkov, I. Dzyaloshinskii, Methods of Quantum field Theory in Statistical Physics, Prentice-Hall, Englewood Cliffs, NJ, 1963.
[5] A.A. Abrikosov, Fundamentals of the Theory of Metals, North-Holland, Amsterdam, 1988.
[6] I. Affleck, T. Kennedy, E.H. Lieb, H. Tasaki, Rigorous results on valence-bond ground states in antiferromagnets, Phys. Rev. Lett. 59 (1987) 799.
[7] I. Affleck, A.W.W. Ludwig, H.-B. Pang, D.L. Cox, Relevance of anisotropy in the multichannel Kondo effect: comparison of conformal field theory and numerical renormalization-group results, Phys. Rev. B 45 (1992) 7918.
[8] I. Affleck, A.W.W. Ludwig, Exact critical theory of the two-impurity Kondo model, Phys. Rev. Lett. 68 (1992) 1046.
[9] I. Affleck, A.W. Ludwig, B.A. Jones, Conformal-field-theory approach to the two-impurity Kondo problem: comparison with numerical renormalization-group results, Phys. Rev. B 52 (1995) 9528.
[10] H. Alloul, Comment on "Nature of the conduction-band states in $YBa_2Cu_3O_7$ as revealed by its yttrium knight shift", Phys. Rev. Lett. 63 (1989) 689.
[11] B.L. Altshuler, A.G. Aronov, P.A. Lee, Interaction effects in disordered Fermi systems in two dimensions, Phys. Rev. Lett. 44 (1980) 1288.
[12] B.L. Altshuler, A.G. Aronov, D.E. Khmelnitskii, Suppression of localization effects by the high frequency field and the Nyquist noise, Solid State Commun. 39 (1981) 619.
[13] B.L. Altshuler, A.G. Aronov, D.E. Khmelnitskii, Effects of electron–electron collisions with small energy transfers on quantum localization, J. Phys. C 15 (1982) 7367.
[14] B.L. Altshuler, A.G. Aronov, in: A.L. Efros, M. Pollak (Eds.), Electron–Electron Interactions in Disordered Systems, Elsevier Science Publishers, New York, 1985.
[15] B.L. Altshuler, D.L. Maslov, Theory of metal–insulator transitions in gated semiconductors, Phys. Rev. Lett. 82 (1999) 145.
[16] B.L. Altshuler, D.L. Maslov, V.M. Pudalov, Metal–insulator transition in 2D: resistance in the critical region, Physica E 9 (2001) 209.
[17] B.L. Altshuler, G.W. Martin, D.L. Maslov, V.M. Pudalov, A. Prinz, G. Brunthaler, G. Bauer, Weak-localization type description of conduction in the "anomalous" metallic state, cond-mat/0008005.
[18] P.W. Anderson, Absence of diffusion in certain random lattices, Phys. Rev. 109 (1958) 1492.
[19] P.W. Anderson, Localized Magnetic States in Metals, Phys. Rev. 124 (1961) 41.
[20] P.W. Anderson, Infrared catastrophe in Fermi gases with local scattering potential, Phys. Rev. Lett. 18 (1967) 1049.
[21] P.W. Anderson, A poor man's derivation of scaling laws for the Kondo problem, J. Phys. C 3 (1970) 2436.
[22] P.W. Anderson, G. Yuval, Exact results in the Kondo problem: equivalence to a classical one-dimensional Coulomb gas, Phys. Rev. Lett. 23 (1969) 89.
[23] P.W. Anderson, G. Yuval, D.R. Hamann, Exact results in the Kondo problem II. Scaling theory, qualitatively correct solution, and some new results on one-dimensional classical statistical models, Phys. Rev. B 1 (1970) 4464.
[24] P.W. Anderson, The Theory of Superconductivity in the High T_c Cuprates, Princeton University Press, Princeton, 1997.
[25] P.W. Anderson, Mater. Res. Bull. 8 (1973) 153.
[26] T. Ando, A.B. Fowler, F. Stern, Electronic properties of two-dimensional systems, Rev. Mod. Phys. 54 (1982) 437.
[27] B. Andraka, A.M. Tsvelik, Observation of non-Fermi-liquid behavior in $U_{0.2}Y_{0.8}Pd_3$, Phys. Rev. Lett. 67 (1991) 2886.
[28] K. Andres, J.E. Graebner, H.R. Ott, $4f$-virtual-bound-state formation in $CeAl_3$ at low temperatures, Phys. Rev. Lett. 35 (1975) 1779.
[29] M.C. Aronson, M.B. Maple, R. Chau, A. Georges, A.M. Tsvelik, R. Osborn, Non-Fermi-liquid scaling in $UCu_{5-x}Pd_x$ ($x = 1, 1.5$), J. Phys.: Condens. Matter 8 (1996) 9815.
[30] M.C. Aronson, M.B. Maple, P. de Sa, R. Chau, A.M. Tsvelik, R. Osborn, Non-Fermi-liquid scaling in $UCu_{5-x}Pd_x$ ($x = 1, 1.5$), a phenomenological description, Europhys. Lett. 46 (1997) 245.
[31] A. Auerbach, Interacting Electrons and Quantum Magnetism, Springer, New York, 1994.

[32] O.M. Auslaender, A. Yacoby, R. de Picciotto, L.N. Pfeiffer, K.W. West, Experimental evidence for resonant-tunneling in a Luttinger-liquid, Phys. Rev. Lett. 84 (2000) 1756.
[33] L. Balents, M.P.A. Fisher, Weak-coupling phase diagram of two-chain Hubbard model, Phys. Rev. B 53 (1996) 12 133.
[34] L. Balents, C.M. Varma, Ferromagnetism in doped excitonic insulators, Phys. Rev. Lett. 84 (2000) 1264.
[35] B. Batlogg, C.M. Varma, The underdoped phase of cuprate superconductors, Phys. World 13 (2000) 33.
[36] V. Barzykin, L.P. Gorkov, Ferromagnetism and superstructure in $Ca_{1-x}La_xB_6$, Phys. Rev. Lett. 84 (2000) 2207.
[37] G. Baym, C. Pethick, Landau Fermi Liquid Theory, Wiley, New York, 1991.
[38] M.T. Béal-Monod, K. Maki, Renormalizability of paramagnon theories, Phys. Rev. Lett. 34 (1975) 1461.
[39] K.S. Bedell (Ed.), Strongly Correlated Electronic Materials, Addison Wesley, New York, 1989.
[40] D. Belitz, T.R. Kirkpatrick, The Anderson–Mott transition, Rev. Mod. Phys. 66 (1994) 261.
[41] G. Bergmann, Weak localization in thin films, Phys. Rep. 107 (1984) 1.
[42] O.O. Bernal, D.E. MacLaughlin, H.G. Lukefahr, B. Andraka, Copper NMR and thermodynamics of $UCu_{5-x}Pd_x$: evidence for Kondo disorder, Phys. Rev. Lett. 75 (1995) 2023.
[43] O. Betbeder-Matibet, P. Nozières, Transport equation for quasiparticles in a system of interacting fermions colliding on dilute impurities, Ann. Phys. (NY) 37 (1966) 17.
[44] B. Bogenberger, H. von Löhneysen, Tuning of non-Fermi-liquid behavior with pressure, Phys. Rev. Lett. 74 (1995) 1016.
[45] N. Bogolubov, On the theory of superfluidity, J. Phys. (USSR) XI (1947) 23.
[46] B. Bucher, P. Steiner, J. Karpinski, E. Kaldis, P. Wachter, Influence of the spin gap on the normal state transport in $YBa_2Cu_4O_8$, Phys. Rev. Lett. 70 (1993) 2012.
[47] B. Bernu, L. Candido, D.M. Ceperley, Exchange frequencies in the 2d Wigner crystal, cond-mat/0008062.
[48] D.J. Bishop, D.C. Tsui, R.C. Dynes, Nonmetallic conduction in electron inversion layers at low temperatures, Phys. Rev. Lett. 44 (1980) 1153.
[49] G. Brunthaler, A. Prinz, G. Bauer, V.M. Pudalov, E.M. Dizhur, J. Jaroszynski, P. Glod, T. Dietl, Weak localization in the 2D metallic regime of Si-MOS, Ann. Phys. (Leipzig) 8 (1999) 579.
[50] H. Castella, X. Zotos, Exact calculation of spectral properties of a particle interacting with a one dimensional fermionic system, Phys. Rev. 47 (1993) 16 186.
[51] C. Castellani, C. Di Castro, W. Metzner, Dimensional crossover from Fermi to Luttinger liquid, Phys. Rev. Lett. 72 (1994) 316.
[52] C. Castellani, C. Di Castro, P.A. Lee, M. Ma, Interaction-driven metal–insulator transitions in disordered fermion systems, Phys. Rev. B 30 (1984) 527.
[53] C. Castellani, C. Di Castro, G. Forgacs, E. Tabet, Towards a microscopic theory of the metal–insulator transition, Nucl. Phys. B 225 (1983) 441.
[54] C. Castellani, C. Di Castro, P.A. Lee, M. Ma, S. Sorella, E. Tabet, Spin fluctuations in disordered interacting electrons, Phys. Rev. B 30 (1984) 1596.
[55] A.H. Castro Neto, G. Castilla, B.A. Jones, Non-Fermi liquid behavior and Griffiths phase in f-electron compounds, Phys. Rev. Lett. 81 (1998) 3531.
[56] S. Chakravary, B.I. Halperin, D. Nelson, Low temperature behavior of two-dimensional quantum antiferromagnets, Phys. Rev. B 39 (1989) 2344.
[57] S. Chakravarty, S. Kivelson, C. Nayak, K. Voelker, Wigner glass, spin liquids, and the metal–insulator transition, Philos. Mag. B 79 (1999) 859.
[58] S. Chakravarty, R.B. Laughlin, D.K. Morr, C. Nayak, Hidden order in the cuprates, Phys. Rev. B 63 (2001) 094503.
[59] S.-W. Cheong, H.Y. Hwang, C.H. Chen, B. Batlog, L.W. Rupp, Jr., S.A. Carter, Charge-ordered states in $(La, Sr)_2NiO_4$ for hole concentrations $n_h = 1/3$ and $1/2$, Phys. Rev. B 49 (1994) 7088.
[60] Y.H. Chen, F. Wilczek, E. Witten, B.I. Halperin, Int. J. Mod. Phys. B 3 (1989) 1001.
[61] P. Chitra, T. Giamarchi, P. Le Doussal, Dynamical properties of the pinned Wigner crystal, Phys. Rev. Lett. 80 (1998) 3827.
[62] P.T. Coleridge, R.L. Williams, Y. Feng, P. Zawadzki, Metal–insulator transition at $B = 0$ in p-type SiGe, Phys. Rev. B 56 (1997) R12764.

[63] P.T. Coleridge, A.S. Sachrajda, P. Zawadski, Weak localisation, interaction effects and the metallic phase of SiGe, cond-mat/9912041.
[65] M. Combescot, P. Nozières, Infrared catastrophy and excitations in the X-ray spectra of metals, J. Phys. 32 (1971) 913.
[66] M.A. Continentino, Universal behavior in heavy fermions, Phys. Rev. B 47 (1993) 11 587.
[67] M.A. Continento, Quantum scaling in many body systems, Phys. Rep. 239 (1994) 179.
[68] J. Corson, J. Orenstein, Normal state conductivity varies as fractional power of transport lifetime in a cuprate superconductor, cond-mat/0006027.
[69] D.L. Cox, Quadrupolar Kondo effect in uranium heavy-electron materials? Phys. Rev. Lett., 59 1993 (1240).
[70] D.L. Cox, M. Jarrell, The two-channel Kondo route to non-Fermi-liquid metals, J. Phys.: Condens. Matter 8 (1996) 9825.
[71] D.L. Cox, A. Zawadowski, Exotic Kondo effects in metals: magnetic ion in a crystalline electric field and tunneling centers, Adv. Phys. 47 (1999) 599.
[72] S. Das Sarma, A. Pinczuk (Eds.), Perspectives in Quantum Hall Effects, Wiley, New York, 1997.
[73] S. Das Sarma, E.H. Hwang, Charged impurity-scattering-limited low-temperature resistivity of low-density silicon inversion layers, Phys. Rev. Lett. 83 (1999) 164.
[74] C. Dekker, Carbon nanotubes as molecular quantum wires, Phys. Today 52 (1999) 22.
[75] A. de Visser, M.J. Graf, P. Estrela, A. Amato, C. Baines, D. Andreica, F.N. Gygax, A. Schenck, Magnetic quantum critical point in UPt_3 doped with Pd, Phys. Rev. Lett. 85 (2000) 3005.
[76] R. de Picciotto, H.L. Stormer, L.N. Pfeiffer, K.W. Baldwin, K.W. West, Four-terminal resistance of a ballistic quantum wire, Nature 411 (2001) 51.
[77] V. Dobrosavljević, E. Abrahams, E. Miranda, S. Chakravarty, Scaling theory of two-dimensional metal–insulator transitions, Phys. Rev. Lett. 79 (1997) 455.
[78] S. Doniach, The Kondo lattice and weak antiferromagnetism, Physica B 91 (1977) 231.
[79] S. Doniach, S. Englesberg, Low-temperature properties of nearly ferromagnetic Fermi liquids, Phys. Rev. Lett. 17 (1966) 750.
[80] S. Doniach, E.H. Sondheimer, Green's functions for Solid State Physicists, Benjamin/Cummings, London, 1974.
[81] S.C. Dultz, H.W. Jiang, Thermodynamic signature of a two-dimensional metal–insulator transition, Phys. Rev. Lett. 84 (2000) 4689.
[82] I. Dzyaloshinskii, A.M. Polyakov, P. Wiegmann, Phys. Lett. 127A (1988) 112.
[83] V.J. Emery, in: D. Jérome, L.G. Larson (Eds.), Low-Dimensional Conductors and Superconductors, Plenum, New York, 1987, p. 47.
[84] V.J. Emery, in: J.T. Devreese, R.P. Evrard, V.E. van Doren (Eds.), Highly Conducting One-Dimensional Solids, Plenum, New York, 1979, p. 247.
[85] V.J. Emery, S. Kivelson, Mapping of the two-channel Kondo problem to a resonant-level model, Phys. Rev. B 46 (1992) 10 812.
[86] V.J. Emery, S. Kivelson, Frustrated electronic phase separation and high temperature superconductors, Physica C 209 (1993) 597.
[87] H.J. Eskes, R. Grimberg, W. van Saarloos, J. Zaanen, Quantizing charged magnetic domain walls: strings on a lattice, Phys. Rev. B 54 (1996) R724.
[88] P. Estrela, Non-Fermi liquid behavior in uranium based heavy-fermion compounds, Thesis, University of Amsterdam, 2000.
[89] P. Estrela, L.C.J. Pereira, A. de Visser, F.R. de Boer, M. Almeida, M. Godinho, J. Rebizant, J.C. Spirlet, Structural, magnetic and transport properties of single-crystalline U_2Pt_2In, J. Phys.: Condens. Matter 10 (1998) 9465.
[90] M. Fabrizio, Role of transverse hopping in a two-coupled-chains model, Phys. Rev. B 48 (1993) 15 838.
[91] A. Fetter, C. Hanna, R.B. Laughlin, The random phase approximation in the fractional-statistics gas, Phys. Rev. B 39 (1998) 9679.
[92] A.M. Finkel'stein, Influence of Coulomb interaction on the properties of disordered metals, Zh. Eksp. Teor. Fiz 84 (1983) 168 [Sov. Phys. JETP 57 (1983) 97].

[93] A.M. Finkel'stein, Weak localization and Coulomb interaction in disordered systems, Z. Phys. 56 (1984) 189.
[94] A.I. Finkelstein, Soviet Sci. Rev. (1990) 3.
[95] A.I. Finkelstein, A.I. Larkin, Two coupled chains with Tomonaga–Luttinger interactions, Phys. Rev. B 47 (1993) 10461.
[96] J.O. Fjaerstad, A. Sudbo, A. Luther, Correlation functions for a two-dimensional electron system with bosonic interactions and a square Fermi surface, Phys. Rev. B 60 (1999) 13361.
[97] M.E. Fisher, in: F.J.W. Hahne (Ed.), Critical Phenomena, Vol. 186, Lecture Notes in Physics, Springer, Berlin, 1983.
[98] M.P.A. Fisher, L.I. Glazman, Transport in a one-dimensional Luttinger liquid, in: L. Kouwenhoven, G. Schön, L. Sohn (Eds.), Mesoscopic Electron Transport, NATO ASI Series E, Kluwer, Dordrecht, 1997.
[99] L. Forro, R. Gaál, H. Berger, P. Fazekas, K. Penc, I. Készmárki, G. Mihály, Pressure induced quantum critical point and non-Fermi-liquid behavior in $BaVS_3$, Phys. Rev. Lett. 85 (2000) 1938.
[100] M. Fowler, A. Zawadowski, Scaling and the renormalization group in the Kondo effect, Solid State Commun. 9 (1971) 471.
[101] P. Fulde, J. Keller, G. Zwicknagel, Theory of heavy fermion systems, in: H. Ehrenreich, D. Turnbull (Eds.), Solid State Physics, Vol. 41, Academic Press, New York, 1988.
[102] P. Fulde, Electron Correlations in Molecules and Solids, Springer, Berlin, 1995.
[103] H. Fukuyama, Effects of mutual interactions in weakly localized regime of disordered two-dimensional systems. II. Intervalley impurity scattering, J. Phys. Soc. Japan 50 (1981) 3562.
[104] Galitski, The energy spectrum of a non-ideal fermi gas, Sov. Phys. JETP 7 (1958) 104.
[105] A. Georges, G. Kotliar, W. Krauth, M.J. Rozenberg, Dynamical mean-field theory of strongly correlated fermion systems and the limit of infinite dimensions, Rev. Mod. Phys. 68 (1996) 13.
[106] T. Giamarchi, A.J. Millis, Conductivity of a Luttinger Liquid, Phys. Rev. B 46 (1992) 9325.
[107] T. Giamarchi, C.M. Varma, A.E. Ruckenstein, P. Nozières, Singular low-energy properties of an impurity model with finite range interactions, Phys. Rev. Lett. 70 (1993) 3967.
[108] T. Giamarchi, H.J. Schulz, Anderson localization and interactions in one dimensional metals, Phys. Rev. B 37 (1988) 325.
[109] T. Giamarchi, P. Le Doussal, Phase diagrams of flux lattices with disorder, Phys. Rev. B 55 (1997) 6577.
[110] D.M. Ginsberg (Ed.), Physical Properties of High Temperature Superconductors Vol. I (1989), Vol. II (1990), Vol. III (1992), Vol. IV (1994), World Scientific, Singapore.
[111] S.M. Girvin, The quantum Hall effect: novel excitation and broken symmetries, cond-mat/9907002.
[112] H.R. Glyde, Excitations in Liquid and Solid Helium, Clarendon, Oxford, 1994.
[113] A.O. Gogolin, A.A. Nersesyan, A.M. Tsvelik, Bosonization and Strongly correlated Systems, Cambridge University Press, Cambridge, 1998.
[114] M. Grayson, D.C. Tsui, L.N. Pfeiffer, K.W. West, A.M. Chang, Continuum of chiral Luttinger liquids at the fractional quantum Hall edge, Phys. Rev. Lett. 80 (1998) 1062.
[115] F.M. Grosche, C. Pfleiderer, G.J. McMullan, G.G. Lonzarich, N.R. Bernhoeft, Critical behaviour of $ZrZn_2$, Physica B 206–207 (1995) 20.
[116] C.J. Halbroth, W. Metzner, d-Wave superconductivity and Pomeranchuk instability in the two-dimensional Hubbard model, Phys. Rev. Lett. 85 (2000) 5162.
[117] B.I. Halperin, P.C. Hohenberg, Theory of dynamic critical phenomena, Rev. Mod. Phys. 49 (1977) 435.
[118] B.I. Halperin, P.A. Lee, N. Read, Theory of the half-filled Landau level, Phys. Rev. B 47 (1993) 7312.
[119] A.R. Hamilton, M.Y. Simmons, M. Pepper, E.H. Linfeld, P.D. Rose, D.A. Ritchie, Reentrant insulator–metal transition at $B = 0$ in a two-dimensional hole gas, Phys. Rev. Lett. 82 (1999) 1542.
[120] Y. Hanein, U. Meirav, D. Shahar, C.C. Li, D.C. Tsui, H. Shtrikman, The metalliclike conductivity of a two-dimensional hole system, Phys. Rev. Lett. 80 (1998) 1288.
[121] A.B. Harris, Effects of random defects on the critical behavior of Ising models, J. Phys. C 7 (1974) 1671.
[122] S.M. Hayden, R. Doubble, G. Aeppli, T.G. Perring, E. Fawcett, Strongly enhanced magnetic excitations near the quantum critical point of $Cr_{1-x}V_x$ and why strong exchange enhancement need not imply heavy fermion behavior, Phys. Rev. Lett. 84 (2000) 999.
[123] J.A. Hertz, Quantum critical phenomena, Phys. Rev. B 14 (1976) 1165.

[124] A.C. Hewson, The Kondo Problem to Heavy Fermions, Cambridge University Press, Cambridge, 1993.
[125] S. Hikami, A.I. Larkin, Y. Nagaoka, Spin–orbit interaction and magnetoresistance in the two-dimensional random system, Progr. Theor. Phys. 63 (1980) 707.
[126] R. Hlubina, T.M. Rice, Resistivity as a function of temperature for models with hot spots on the Fermi surface, Phys. Rev. B 51 (1995) 9253.
[127] T. Holstein, R.E. Norton, P. Pincus, de Haas-van Alphen effect and the specific heat of an electron gas, Phys. Rev. B l8 (1973) 2647.
[128] A. Houghton, J.B. Marston, Bosonization and fermion liquids in dimensions greater than one, Phys. Rev. B 48 (1993) 7790.
[129] S. Ilani, A. Yacoby, D. Mahalu, H. Shtrikman, Unexpected behavior of the local compressibility near the $B=0$ metal–insulator transition, Phys. Rev. Lett. 84 (2000) 3133.
[130] S. Ilani, A. Yacoby, D. Mihalu, H. Shtrikman, Microscopic structure of the metal–insulator transition in two-dimensions, Science, submitted for publication.
[131] Y. Imry, S.-K. Ma, Random-field instability of the ordered state of continuous symmetry, Phys. Rev. Lett. 35 (1975) 1399.
[132] Y. Imry, M. Wortis, Influence of quenched impurities on first order phase transitions, Phys. Rev. B 19 (1979) 3580.
[133] Y. Imry, Introduction to Mesoscopic Physics, Oxford University Press, Oxford, 1997.
[134] L.B. Ioffe, A.I. Larkin, Gapless fermions and gauge fields in dielectrics, Phys. Rev. B 39 (1989) 8988.
[135] J. Jacklič, P. Prelovšek, Finite-temperature properties of doped antiferromagnets, Adv. Phys. 49 (2000) 1.
[136] B.A. Jones, C.M. Varma, Study of two magnetic impurities in a Fermi gas, Phys. Rev. Lett. 58 (1987) 843.
[137] B.A. Jones, C.M. Varma, J.W. Wilkins, Low-temperature properties of the two-impurity Kondo Hamiltonian, Phys. Rev. Lett. 61 (1988) 125.
[138] V. Kalmeyer, R.B. Laughlin, Equivalence of the resonating-valence-bond and quantum Hall states, Phys. Rev. Lett. 59 (1987) 2095.
[139] A. Kaminski, A.J. Mesot, H. Fretwell, J.C. Campuzano, M.R. Norman, M. Randeria, H. Ding, T. Sato, T. Takahashi, T. Mochiku, K. Kadowaki, H. Hoechst, Quasiparticles in the superconducting state of $Bis_2Sr_2CaCu_2O_8$, Phys. Rev. Lett. 84 (2000) 1788.
[140] C.L. Kane, M.P.A. Fisher, Transmission through barriers and resonant tunneling in an interacting one-dimensional electron gas, Phys. Rev. B 46 (1992) 15 233.
[141] C.L. Kane, L. Balents, M.P.A. Fisher, Coulomb interactions and mesoscopic effects in carbon nanotubes, Phys. Rev. Lett. 79 (1997) 5086.
[142] H.-Y. Kee, Effect of doping-induced disorder on T_c in cuprates, Phys. Rev. B (2001) 012506.
[143] T.S. Kim, D.L. Cox, Scaling analysis of a model Hamiltonian for Ce^{3+} impurities in a cubic metal, Phys. Rev. B 54 (1996) 6494.
[144] S.A. Kivelson, D.S. Rokshar, J.P. Sethna, Topology of the resonating valence-bond state: solitons and high T_c superconductivity, Phys. Rev. B 35 (1987) 8865.
[145] T.M. Klapwijk, S. Das Sarma, A few electrons per ion scenario for the $B=0$ metal–insulator transition in two dimensions, Solid State Commun. 110 (1999) 581.
[146] J. Kondo, Resistance minimum in dilute magnetic alloys, Progr. Theor. Phys. 32 (1964) 37.
[147] J.M. Kosterlitz, D. Thouless, Ordering, metastability and phase transitions in two-dimensional systems, J. Phys. C 6 (1973) 1181.
[148] G. Kotliar, Resonating valence bonds and d-wave superconductivity, Phys. Rev. B 37 (1988) 3664.
[149] S.V. Kravchenko, W.E. Mason, G.E. Bowker, J.E. Furneaux, V.M. Pudalov, M. D'Iorio, Scaling of an anomalous metal–insulator transition in a two-dimensional system in silicon at $B=0$, Phys. Rev. B 51 (1995) 7038.
[150] S.V. Kravchenko, T.M. Klapwijk, Metallic low-temperature resistivity in a 2D electron system over an extended temperature range, Phys. Rev. Lett. 84 (2000) 2909.
[151] H.R. Krishna-murthy, J.W. Wilkins, K.G. Wilson, Renormalization-group approach to the Anderson model of dilute magnetic alloys. I. Static properties for the symmetric case, Phys. Rev. B 21 (1980) 1003.
[152] L.D. Landau, The theory of a Fermi liquid, Zh. Eksp. Teor. Fiz. 30 (1956) 1058 [Sov. Phys. JETP 3 (1957) 920].

[153] L.D. Landau, Oscillations in a Fermi liquid, Zh. Eksp. Teor. Fiz. 32 (1957) 59 [Sov. Phys. JETP 5 (1957) 101].
[154] E.M. Lifshitz, L.P. Pitaevskii, Statistical Physics, Part 2, Pergamon, New York, 1980 (Chapter III).
[155] A.I. Larkin, V.I. Melnikov, Magnetic impurity in an almost magnetic metal, Sov. Phys. JETP 34 (1972) 656.
[156] R.B. Laughlin, The relationship between high temperature superconductors and the fractional quantum Hall effect, Science 242 (1988) 525.
[157] P.A. Lee, T.V. Ramakrishnan, Disordered electronic systems, Rev. Mod. Phys. 57 (1985) 287.
[158] P.A. Lee, Pseudogaps in underdoped cuprates, Physica C 317–318 (1999) 194.
[159] H. Lin, L. Balents, M.P.A. Fisher, Exact SO(8) Symmetry in the weakly-interacting two-leg ladder, Phys. Rev. B 58 (1998) 1794.
[160] G.G. Lonzarich, L. Taillefer, Effect of spin fluctuations on the magnetic equation of state of ferromagnetic or nearly ferromagnetic metals, J. Phys. C 18 (1985) 4339.
[161] G. Lonzarich, private communication to CMV, June 2000.
[162] J.W. Loram, K.A. Mirza, J.R. Cooper, J.L. Tallon, Superconducting and normal state energy gaps in $Y_{0.8}Ca_{0.2}Ba_2Cu_3O_{7-\delta}$ from the electronic specific heat, Physica C 282–287 (1997) 1405.
[163] A. Luther, V.J. Emery, Backward scattering in the one-dimensional electron gas, Phys. Rev. Lett. 33 (1974) 589.
[164] S.K. Ma, Modern Theory of Critical Phenomena, Benjamin Cummings, Reading, 1976.
[165] D.E. Maclaughlin, O.O. Bernal, R.H. Heffner, G.J. Nieuwenhuis, M.C. Rose, J.E. Sonier, B. Andraka, R. Chau, M.P. Maple, Glassy dynamics in non-Fermi-liquid $UCu_{5-x}Pd_x$, $x = 1.0$ and 1.5, Phys. Rev. Lett. 87 (2001) 066402.
[166] H. Maebashi, K. Miyake, C.M. Varma, Singular effects of impurities near the ferromagnetic quantum critical point, cond-mat/0109276.
[167] G.D. Mahan, Excitons in degenerate semiconductors, Phys. Rev. 153 (1967) 882.
[168] G.D. Mahan, Many-Particle Physics, Plenum, New York, 1990.
[169] M.B. Maple, R.P. Dickey, J. Herrman, M.C. de Andrade, E.J. Freeman, D.A. Gajewski, R. Chau, Single-ion scaling of the low-temperature properties of f-electron materials with non-Fermi-liquid ground states, J. Phys.: Condens. Matter 8 (1996) 9773.
[170] N.D. Mathur, F.M. Grosche, S.R. Julian, I.R. Walker, D.M. Freye, R.K.W. Haselwimmer, G.G. Lonzarich, Magnetically mediated superconductivity in heavy fermion compounds, Nature 394 (1998) 39.
[171] D.E. Maclaughlin, O.O. Bernal, H.G. Lukefahr, NMR and μSR studies of non-Fermi-liquid behavior in disordered heavy-fermion systems, J. Phys.: Condens. Matter 8 (1996) 9855.
[172] E. Manousakis, The Spin 1/2 Heisenberg antiferromagnet on a square lattice and its application to the cuprous oxides, Rev. Mod. Phys. 63 (1991) 1.
[173] J.O. Fjaerestad, J.B. Marston, Staggered orbital currents in the half-filled two-leg ladder, cond-mat/0107094.
[174] G.B. Martins, J.C. Xavier, C. Gazza, M. Vojta, E. Dagotto, Indications of spin–charge separation at short distance and stripe formation in the extended t–J model on ladders and planes, cond-mat/0007196.
[175] K. Salama, W-K. Chen, P.C.W. Chu (Eds.), Materials and Mechanisms of Superconductivity: High Temperature Superconductivity VI (Houston, 1999), North-Holland, Amsterdam, 2000, reprinted from Physica C (2000) 341–348.
[176] N. Mason, A. Kapitulnik, Dissipation effects on the superconductor–insulator transition in 2D superconductors, Phys. Rev. Lett. 82 (1999) 5341.
[177] N. Mason, A. Kapitulnik, True superconductivity in 2D "superconducting–insulating" system, Phys. Rev. B 64 (2001) 060504.
[178] Y. Meir, Percolation-type description of the metal–insulator transition in two dimensions, Phys. Rev. Lett. 83 (1999) 3506.
[179] W. Metzner, C. Di Castro, Conservation laws and correlation functions in the Luttinger liquid, Phys. Rev. B 47 (1993) 16 107.
[180] W. Metzner, D. Vollhardt, Correlated lattice fermions in $d = \infty$ dimensions, Phys. Rev. Lett. 62 (1989) 324.
[181] W. Metzner, C. Castellani, C. Di Castro, Fermi systems with strong forward scattering, Adv. Phys. 47 (1998) 317.

[182] F.P. Millikan, C.P. Umbach, R.A. Webb, Indications of a Luttinger-liquid in the fractional quantum Hall regime, Solid State Commun. 97 (1996) 309.
[183] A.J. Millis, Effect of a nonzero temperature on quantum critical points in itinerant fermion systems, Phys. Rev. B 48 (1993) 7183.
[184] A.J. Mills, et al., unpublished.
[185] E. Miranda, V. Dobrosavlijevic, G. Kotliar, Kondo disorder: a possible route towards non-Fermi-liquid behavior, J. Phys.: Condens. Matter 8 (1996) 9871.
[186] S.G. Mishra, T.V. Ramakrishnan, Temperature dependence of the spin susceptibility of nearly ferromagnetic Fermi systems, Phys. Rev. B 18 (1978) 2308.
[187] K. Miyake, S. Schmitt-Rink, C.M. Varma, Spin-fluctuation-mediated even-parity paring in heavy-fermion superconductors, Phys. Rev. B 34 (1986) 6554.
[188] R. Moessner, S.L. Sondhi, Ising models of quantum frustration, Phys. Rev. B 63 (2001) 224401.
[189] T. Moriya, A. Kawabata, Effect of spin fluctuations on itinerant electron ferromagnetism, J. Phys. Soc. Japan 34 (1973) 639.
[190] T. Moriya, A. Kawabata, Effect of spin fluctuations on itinerant electron ferromagnetism II, J. Phys. Soc. Japan 35 (1973) 669.
[191] Y. Nagaoka, Ferromagnetism in a narrow almost half-filled s band, Phys. Rev. 147 (1966) 392.
[192] N. Nagaosa, Quantum field theory in Condensed Matter Physics, Springer, Berlin, 1999.
[193] N. Nagaosa, Quantum field theory in Strongly Correlated Electronic Systems, Springer, Berlin, 1999.
[194] R. Noack, S. White, D. Scalapino, Correlations in a two-chain Hubbard model, Phys. Rev. Lett. 73 (1994) 882.
[195] P. Nozières, Interacting Fermi Systems, Benjamin, New York, 1963.
[196] P. Nozières, C. deDominicis, Singularities in the X-ray absorption and emission of metals III. One body theory exact solutions, Phys. Rev. 178 (1969) 1097.
[197] P. Nozieres, A "Fermi-liquid" description of the Kondo problem at low temperatures, J. Low Temp. Phys. 17 (1974) 31.
[198] P. Nozières, A. Blandin, Kondo effect in real metals, J. Phys. 41 (1980) 193.
[199] P. Nozières, The effect of recoil on edge singularities, J. Phys. I France 4 (1994) 1275.
[200] V. Oganesyan, S. Kivelson, E. Fradkin, Quantum theory of a nematic Fermi liquid, Phys. Rev. B 64 (2001) 195109.
[201] J. Orenstein, A.J. Millis, Advances in the physics of high temperature superconductivity, Science 288 (2000) 468.
[202] D. Orgad, Spectral functions for the Tomonaga–Luttinger and Luther–Emery liquids, Philos. Mag. B 81 (2001) 375.
[203] E. Orignac, T. Giamarchi, Effects of disorder on two strongly correlated coupled chains, Phys. Rev. B 56 (1997) 7167.
[204] I.E. Perakis, C.M. Varma, A.E. Ruckenstein, Non-Fermi-liquid states of a magnetic ion in a metal, Phys. Rev. Lett. 70 (1993) 3467.
[205] C. Pfleiderer, G.J. McMullan, G.G. Lonzarich, Pressure induced crossover of the magnetic transition from second to first order near the quantum critical point in MnSi, Physica B 206, 207 (1995) 847.
[206] C. Pfleiderer, R.H. Friend, G.G. Lonzarich, N.R. Bernhoeft, J. Flouquet, Transition from a magnetic to a nonmagnetic state as a function of pressure in MnSi, Int. J. Mod. Phys. B 7 (1993) 887.
[207] P. Phillips, Y. Wan, I. Martin, S. Knysh, D. Dalidovich, Superconductivity in a two-dimensional electron gas, Nature 395 (1998) 253.
[208] D. Pines, P. Nozieres, The Theory of Quantum Liquids, Vol. I, Addison-Wesley, New York, 1990.
[209] J. Polchinski, Low-energy dynamics of the spinon-gauge system, Nucl. Phys. B 422 (1994) 617.
[210] D. Popović, A.B. Fowler, S. Washburn, Metal–insulator transition in two dimensions: effects of disorder and magnetic field, Phys. Rev. Lett. 79 (1990) 1543.
[211] H.W.Ch. Postma, M. de Jonge, Z. Yao, C. Dekker, Electrical transport through carbon nanotube junctions created by mechanical manipulation, Phys. Rev. B 62 (2000) R10653.
[212] R. Prange, L.P. Kadanoff, Transport theory for electron–phonon interactions in metals, Phys. Rev. 134 (1964) A566.

[213] R.E. Prange, S.H. Girvin (Eds.), The Quantum Hall Effect, Springer, Berlin, 1985.
[214] A. Prinz, V.M. Pudalov, G. Brunthaler, G. Bauer, Metal–insulator transition in Si-MOS structure in: K. Hess (Ed.), Proceedings International Meeting SIMD-99, Mauri, 1999, Superlattices Microstruct., 2000, in press.
[215] V.M. Pudalov, G. Brunthaler, A. Prinz, G. Bauer, Breakdown of the anomalous two-dimensional metallic phase in a parallel magnetic field, Physica B 249–251 (1998) 697.
[216] V.M. Pudalov, G. Brunthaler, A. Prinz, G. Bauer, Maximum metallic conductivity in Si MOS structures, Phys. Rev. B 60 (1999) R2154.
[217] V.M. Pudalov, M. Gershenson, H. Kojima, N. Butch, E.M. Dizhur, G. Brunthaler, A. Prinz, G. Bauer, Fermi-liquid renormalization of the g-factor and effective mass in Si inversion layer, cond-mat/0105081.
[218] S. Rabello, Q. Si, Spectral functions in a magnetic field as a probe of spin-charge separation in a Luttinger liquid, cond-mat/0008065.
[219] D.C. Ralph, A.W.W. Ludwig, J. von Delft, R.A. Buhrman, 2-channel Kondo scaling in conductance signals from 2-level tunneling systems, Phys. Rev. Lett. 72 (1994) 1064.
[220] D.C. Ralph, A.W.W. Ludwig, J. von Delft, R.A. Buhrman, Reply to "comment on: 2-channel Kondo scaling in conductance signals from 2-level tunneling systems", Phys. Rev. Lett. 75 (1995) 770.
[221] M.Yu. Reizer, Effective electron–electron interaction in metals and superconductors, Phys. Rev. B 39 (1989) 1602.
[222] X. Rickayzen, Green's functions and Condensed Matter, Academic, London, 1980.
[223] M. Sarachik, private communication.
[224] S. Sachdev, N. Read, Metallic spin glasses, J. Phys.: Condens. Matter 8 (1996) 9723.
[225] S. Sachdev, Quantum Phase Transitions, Cambridge University Press, Cambridge, 1999.
[226] M.P. Sarachik, S.V. Kravchenko, Novel phenomena in dilute electron systems in two dimensions, Proc. Nat. Acad. USA 96 (1999) 5900.
[227] P. Schlottman, P.D. Sacramento, Multichannel Kondo problem and some applications, Adv. Phys. 42 (1993) 641.
[228] S. Schmitt-Rink, C.M. Varma, A.E. Ruckenstein, Spectral tion of holes in a quantum antiferromagnet, Phys. Rev. Lett. 60 (1998) 2793.
[229] A. Schröder, G. Aeppli, E. Bucher, R. Ramazashvili, P. Coleman, Scaling of magnetic fluctuations near a quantum phase transition, Phys. Rev. Lett. 80 (1998) 5623.
[230] A. Schröder, G. Aeppli, R. Coldea, M. Adams, O. Stockert, H.v. Lohneysen, E. Bucher, R. Ramazashvili, P. Coleman, Onset of antiferromagnetism in heavy-fermion metals, Nature 407 (2000) 351.
[232] H.J. Schulz, Phases of two coupled Luttinger liquids, Phys. Rev. B 53 (1996) 2959.
[233] H.J. Schulz, G. Cuniberti, P. Pieri, Fermi liquids and Luttinger liquids, Lecture notes of the Chia Laguna summer school, 1998 [cond-mat/9807366].
[234] A. Sengupta, Spin in a fluctuating field: the Bose(+Fermi) Kondo models, Phys. Rev. B 61 (2000) 4041.
[235] T. Senthil, M.P.A. Fisher, Fractionalization, topological order, and cuprate superconductivity, cond-mat/0008082.
[236] T. Senthil, M.P.A. Fisher, Fractionalization and confinement in the $U(1)$ and Z_2 gauge theories of strongly correlated electron systems, J. Phys. A 10 (2001) L119.
[237] R. Shankar, Renormalization-group approach to interacting fermions, Rev. Mod. Phys. 66 (1994) 129.
[238] A.A. Shashkin, S.V. Kravchenko, T.M. Klapwijk, Evolution of the metal–insulator transition in two dimensions with parallel magnetic field, cond-mat/0009180.
[239] B.I. Shklovskii, A.L. Efros, Electronic Properties of doped Semiconductors, Springer, Berlin, 1984.
[240] Q. Si, G. Kotliar, Fermi-liquid and non-Fermi-liquid phases of an extended Hubbard model in infinite dimensions, Phys. Rev. Lett. 70 (1993) 3143.
[241] Q. Si, C.M. Varma, Metal–insulator transition of disordered interacting electrons, Phys. Rev. Lett. 81 (1998) 4951.
[242] Q. Si, S. Rabello, K. Ingersent, J.L. Smith, Locally critical quantum phase transition in strongly correlated metals, Nature 413 (2001) 804.
[243] D. Simonian, S.V. Kravchenko, M.P. Sarachik, Magnetic field suppression of the conducting phase in two dimensions, Phys. Rev. Lett. 79 (1997) 2304.

[244] C. Sire, C.M. Varma, H.R. Krishnamurthy, Theory of the non-Fermi-liquid transition in the two-impurity Kondo Model, Phys. Rev. B 48 (1993) 13 833.
[245] C. Sire, C.M. Varma, A.E. Rukenstein, T. Giamarchi, Theory of the marginal-Fermi-liquid spectrum and pairing in a local copper oxide model, Phys. Rev. Lett. 72 (1994) 2478.
[246] J. Sólyom, The Fermi gas model of one-dimensional conductors, Adv. Phys. 28 (1979) 201.
[247] S.L. Sondhi, S.M. Girvin, J.P. Carini, D. Sahar, Continuous quantum phase transitions, Rev. Mod. Phys. 69 (1997) 315.
[248] S. Spielman, F. Fesler, C.B. Eom, T.H. Geballe, M.M. Fejer, A. Kapitulnik, Test of nonreciprocal circular birefringence in $YBa_2Cu_3O_7$ thin films as evidence for broken time-reversal symmetry, Phys. Rev. Lett. 65 (1990) 123.
[249] E.B. Stechel, A. Sudbo, T. Giamarchi, C.M. Varma, Pairing fluctuations in a one-dimensional copper oxide model, Phys. Rev. B 51 (1995) 553.
[250] F. Steglich, B. Buschinger, P. Gegenwart, M. Lohmann, R. Helfrich, C. Langhammer, P. Hellmann, L. Donnevert, S. Thomas, A. Link, C. Geibel, M. Lang, G. Sparn, W. Assmus, Quantum critical phenomena in undoped heavy-fermion metals, J. Phys.: Condens. Matter 8 (1996) 9909.
[251] O. Stockert, H.v. Löhneysen, A. Rosch, N. Pyka, M. Loewenhaupt, Two-dimensional fluctuations at the quantum-critical point of $CeCu_{6-x}Au_x$, Phys. Rev. Lett. 80 (1998) 5627.
[252] A. Sudbo, C.M. Varma, T. Giamarchi, E.B. Stechel, R.T. Scalettar, Flux quantization and paring in one-dimensional copper-oxide models, Phys. Rev. Lett. 70 (1993) 978.
[253] B. Tanatar, D.M. Ceperley, Ground state of the two-dimensional electron gas, Phys. Rev. B 39 (1989) 5005.
[254] C. Thessieu, J. Floquet, G. Lapertot, A.N. Stepanov, D. Jaccard, Magnetism and spin fluctuations in a weak itinerant ferromagnet: MnSi, Solid State Commun. 96 (1995) 707.
[255] D.J. Thouless, Electrons in disordered systems and the theory of localization, Phys. Rep. 13 (1974) 93.
[256] D. Thouless, Percolation and localization, in: R. Balian, R. Maynard, G. Toulouse (Eds.), Ill Condensed Matter, North-Holland, Amsterdam, 1979.
[257] J.M. Tranquada, B.J. Sternlleb, J.D. Axe, Y. Nakamura, S. Uchida, Evidence for stripe correlations of spins and holes in copper oxide superconductors, Nature 375 (1995) 561.
[258] O. Trovarelli, C. Geibel, S. Mederle, C. Langhammer, F.M. Grosche, P. Gegenwart, M. Lang, G. Sparn, F. Steglich, $YbRh_2Si_2$: Pronounced non-Fermi-liquid effects above a low-lying magnetic phase transition, Phys. Rev. Lett. 85 (2000) 626.
[259] A.M. Tsvelik, Quantum Field Theory in Condensed Matter Physics, Cambridge University Press, Cambridge, 1995.
[260] M.J. Uren, R.A. Davies, M. Pepper, The observation of interaction and localisation effects in a two-dimensional electron gas at low temperatures, J. Physica C 13 (1980) L985.
[261] T. Valla, A.V. Fedorov, P.D. Johnson, B.O. Wells, S.L. Hulbert, Q. Li, G.D. Gu, N. Khoshizuka, Evidence for quantum critical behavior in the optimally doped cuprate $Bi_2Sr_2CaCu_2O_{8+\delta}$, Science 285 (1999) 2110.
[262] T. Valla, A.V. Fedorov, P.D. Johnson, Q. Li, G.D. Gu, N. Koshizuka, Temperature dependent scattering rates at the Fermi surface of optimally doped Bi2212, Phys. Rev. Lett. 85 (2000) 828.
[263] C.M. Varma, Mixed valence compounds, Rev. Mod. Phys. 48 (1976) 219.
[264] C.M. Varma, A. Zawadowski, Scaling in an interacting two-component (valence-fluctuating) electron gas, Phys. Rev. B 32 (1985) 7399.
[265] C.M. Varma, Phenomenological Aspects of Heavy Fermions 55 (1985) 2723.
[266] C.M. Varma, S. Schmitt-Rink, E. Abrahams, Charge transfer excitation and superconductivity in "Ionic" metals, Solid State Commun. 62 (1987) 681.
[267] C.M. Varma, S. Schmitt-Rink, E. Abrahams, in: V. Kresin, S. Wolf (Eds.), Novel Mechanisms of Superconductivity, Plenum, New York, 1987.
[268] C.M. Varma, P.B. Littlewood, S. Schmitt-Rink, E. Abrahams, A.E. Ruckenstein, Phenemenology of the normal state of Cu–O high-temperature superconductors, Phys. Rev. Lett. 63 (1989) 1996.
[269] C.M. Varma, Phenomenolgical constraints on theories for high temperature superconductivity, Int. J. Mod. Phys. B 3 (1998) 2083.
[270] C.M. Varma, Non-Fermi-liquid states and pairing instability of a general model of copper oxide metals, Phys. Rev. B 55 (1997) 14 554.

[271] C.M. Varma, Only Fermi-liquids are metals, Phys. Rev. Lett. 79 (1997) 1535.
[273] C.M. Varma, Pseudogap phase and the quantum-critical point in copper-oxide metals, Phys. Rev. Lett. 83 (1999) 3538.
[274] C.M. Varma, Proposal for an experiment to test a theory of high-temperature superconductors, Phys. Rev. B 61 (2000) R3804.
[275] C.M. Varma, E. Abrahams, Effective Lorentz force due to small-angle impurity scattering: magnetotransport in high-T_c superconductors, Phys. Rev. Lett. 86 (2001) 4652.
[276] S.A. Vitkalov, M.P. Sarachik, T.M. Klapwijk, Spin polarization of two-dimensional electrons determined from Shubnikov-de Haas oscillations as a function of angle, Phys. Rev. B 64 (2001) 073101.
[277] J. Voit, One-dimensional Fermi liquids, Rep. Progr. Phys. 58 (1995) 97.
[278] J. Voit, Charge–spin separation and the spectral properties of Luttinger liquids, Phys. Rev. B 47 (1993) 6740.
[279] B.A. Volkov, Yu.V. Kopaev, A.I. Rusinov, Theory of "excitonic" ferromagnetism, Zh. Eksp. Teor. Fyz. 68 (1975) 1899 [Sov. Phys. JETP 41 (1976) 952].
[280] D. Vollhardt, High dimensions—a new approach to fermionic lattice models, Physica B 169 (1991) 277.
[281] H. von Löhneysen, T. Pietrus, G. Portisch, H.G. Schlager, A. Schröder, M. Sieck, M. Trappmann, Non-Fermi-liquid behavior in a heavy-fermion alloy at a magnetic instability, Phys. Rev. Lett. 72 (1994) 3262.
[282] H. von Löhneysen, Non-Fermi-liquid behavior in heavy-fermion systems, Physica 206 (1995) 101.
[283] H.v. Löhneysen, Non-Fermi-liquid behaviour in the heavy fermion system $CeCu_{6-x}Au_x$, J. Phys.: Condens. Matter 8 (1996) 9689.
[284] H.v. Löhneysen, A. Neubert, A. Schröder, O. Stockert, U. Tutsch, M. Loewenhaupt, A. Rosch, P. Wölfle, Magnetic order and transport in the heavy-fermion system $CeCu_{6-x}Au_x$, Eur. Phys. J. B 5 (1999) 447.
[285] H.v. Löhneysen, T. Pietrus, G. Portish, H.G. Schlager, A. Schröder, M. Sieck, T. Trappmann, Non-Fermi-liquid behavior in a heavy-fermion alloy at a magnetic instability, Phys. Rev. Lett. 72 (1994) 3262.
[286] F.J. Wegner, in: H. Nagaoka, H. Fukuyama (Eds.), Anderson Localisation, Springer, Berlin, 1982.
[287] X.G. Wen, Chiral Luttinger liquid and the edge excitations in the fractional quantum Hall states, Phys. Rev. B 41 (1990) 12 838.
[288] S.R. White, D.J. Scalapino, Density matrix renormalization group study of the striped phase in the 2D t–J model, Phys. Rev. Lett. 80 (1998) 1272.
[289] K.G. Wilson, The renormalization group: critical phenomena and the Kondo problem, Rev. Mod. Phys. 47 (1975) 773.
[290] N.S. Wingreen, B.L. Altshuler, Y. Meir, Comment on "2-channel Kondo scaling in conductance signals from 2-level tunneling systems", Phys. Rev. Lett. 75 (1995) 769.
[291] B. Wuyts, V.V. Moschalkov, Y. Bruynseraede, Resistivity and hall effect of metallic oxygen-deficient $YBa_2Cu_3O_x$ films in the normal state, Phys. Rev. B 53 (1996) 9418.
[292] Y. Yaish, O. Prus, E. Buchstab, S. Shapira, G.B. Yoseph, U. Sivan, A. Stern, Interband scattering and the "metallic phase" of two-dimensional holes in GaAs/AlGaAs, Phys. Rev. Lett. 84 (2000) 4954.
[293] H. Yasuoka, Hyperfine Interactions 105 (1997) 27.
[294] J. Yoon, C.C. Li, D. Shahar, D.C. Tsui, M. Shayegan, Parallel magnetic field induced transition in transport in the dilute two-dimensional hole system in GaAs, Phys. Rev. Lett. 84 (2000) 4421.
[295] D.R. Young, D. Hall, M.E. Torelli, Z. Fisk, J.L. Sarrao, J.D. Thompson, H.-R. Ott, S.B. Oseroff, R.G. Goodrich, R. Zysler, High-temperature weak ferromagnetism in a low-density free-electron gas, Nature 387 (1999) 2219.
[297] J. Zaanen, G. Sawatsky, J.W. Allen, Band gaps and electronic structure of transition-metal compounds, Phys. Rev. Lett. 55 (1985) 418.
[298] J. Zaanen, O. Gunnarson, Charged domain lines and the magnetism of high-T_c oxides, Phys. Rev. B 40 (1989) 7391.
[299] J. Zaanen, M. Horbach, W. van Saarloos, Charged domain-wall dynamics in doped antiferromagnets and spin fluctuations in cuprate superconductors, Phys. Rev. B 53 (1996) 8671.
[300] J. Zaanen, Order out of disorder in a gas of elastic quantum strings in $2+1$ dimensions, Phys. Rev. Lett. 84 (2000) 753.

[301] F.-C. Zhang, T.M. Rice, An anyon superconducting groundstate in Si MOSFETS? cond-mat/9708050.
[302] G. Zarand, A. Zawadowski, Theory of tunneling centers in metallic systems: role of excited states and orbital Kondo effect, Phys. Rev. Lett. 72 (1991) 542.
[303] M.E. Zhitomirsky, T.M. Rice, V.I. Anisimov, Magnetic properties: ferromagnetism in the hexaborides, Nature 402 (1999) 251.